Sensor-based formation control using a generalised rigidity framework and passivity techniques

Geoff Stacey

A thesis submitted for the degree of
Doctor of Philosophy
The Australian National University

May 2017

Except where otherwise indicated, this thesis is my own original work.

Geoff Stacey
24 May 2017

To my family.

Acknowledgments

There are, of course, many great people who have supported me during my PhD studies, and my heartfelt thanks go to every one of them. Without them, I would not be where I am today.

I wish to start by thanking my supervisor, Prof. Robert Mahony, for his continuous support and guidance. He is an excellent mentor and role model who has not only been interested in the development of my research, but also in the development of my professional skills that I am sure to use in the future. I also wish to acknowledge his assistance with financing my research.

Next, I wish to thank the rest of my advisory panel, which consists of Dr. Jochen Trumpf, Prof. Peter Corke, and Assoc. Prof. Brad Yu. In particular, this panel provided guidance during the early days of my PhD and ensured I made a good start. I also wish to give special thanks to Jochen for the numerous times he has assisted me with mathematical insight, as well as advice while Rob was unavailable.

Over the years, many wonderful people have been a part of our research group at the ANU. I am grateful to all of these people for contributing to such an excellent working environment, and I wish to give particular mention to Alex Martin, Dr. Mohammad (Behzad) Zamani, Evan Slatyer, Dr. Xiaolei (Eric) Hou, Dr. Alireza Khosravian, Moses Bangura, Juan Adarve, Dr. Viorela Ila, Dr. Chuong Nguyen, Sean O'Brien, Jean-Luc Stevens and Mina Henein who have been part of our group for a significant period of my PhD. Outside of my immediate research group, I wish to give particular acknowledgement to Dist. Prof. Brian Anderson and Zhiyong Sun for our interesting discussions concerning rigidity theory, as well as Prof. Richard Hartley for his recent tutorial sessions on Lie groups. I have also made many good friendships with members of the broader ANU community (beyond the Research School of Engineering); there are surely too many to name but I wish to express what a delight they have made the past few years.

Amongst the international research community, I wish to thank Prof. Stefano Stramigioli of the University of Twente for my visit in 2013, and Prof. Jacquelien Scherpen, Prof. Arjan van der Schaft, and Dr. Ewoud Vos of the University of Groningen for my visit in 2014. These visits were truly highlights of my PhD candidature. I greatly valued the opportunity to spend time amongst other research groups and it was a pleasure to share ideas with you. Thanks also to Prof. Tarek Hamel from the University of Nice-Sophia-Antipolis and Dr. Christian Lageman from the University of Würzburg for our interesting discussions during your visits to the ANU.

Last but not least, I owe thanks to my family and other friends in Canberra, for their continuous support throughout this journey. They have been invaluable in maintaining a healthy work-life balance that has ensured steady progress towards the completion of my thesis. I believe the secret to life is to do everything in moderation, and these people have allowed me to work when I needed to work, and relax when I needed to relax.

Abstract

The research in this thesis addresses the subject of *sensor-based formation control* for a network of autonomous agents. The task of *formation control* involves the stabilisation of the agents to a desired set of relative states, with the possible additional objective of manoeuvring the agents while maintaining this formation. Although the formation control challenge has been widely studied in the literature, many existing control strategies are based on full state information, and give little consideration to the sensor modalities available for the task. The focus of this thesis lies in the use of a generic arrangement of *partial* state measurements as can commonly be acquired by onboard sensors; for example, time-of-flight sensors can be used to measure the distances between vehicles, and onboard cameras can provide the bearing from one vehicle to each of the others. Particular aspects of the problem that are addressed in this thesis include (i) ways of modelling the formation control task, (ii) methods of analysing the system's behaviour, and (iii) the design of a formation control scheme based on generic arrangements of sensors that provide only partial position information.

A key contribution in this thesis is a generalisation of the classical notion of *rigidity*, which considers the use of distance constraints between agents in $\mathbb{R}^2$ or $\mathbb{R}^3$ to specify a rigid body (or formation). This enables the concept of rigidity to be applied to agent networks involving a variety of (possibly non-Euclidean) state-spaces, with a generic set of state constraints that may, for example, include bearings between agents as well as distances. I demonstrate that this framework is very well-suited for modelling a wide variety of formation control problems (addressing goal (i) above), and I extend several fundamental results from classical rigidity theory in order to provide significant insight for system analysis (addressing goal (ii) above). To design a formation control scheme that uses generic partial position measurements (addressing goal (iii) above), I employ a modular passivity-based approach that is developed using the bondgraph modelling formalism. I illustrate how adaptive compensation can be incorporated into this design approach in order to account for the unknown position information that is not available from the onboard sensors. Although formation control is the subject of this thesis, it should be noted that the rigidity-based and passivity-based frameworks developed here are quite general and may be applied to a wide range of other problems.

Contents

List of Figures

Chapter 1

Introduction

In this chapter, I introduce the motivation behind my research on formation control, and outline the remainder of the thesis. I begin by providing an introduction to the field in Section 1.1, which motivates the contributions of my research as summarised in Section 1.2. In Section 1.3 I list the publications in which my work has been presented. An outline of the remaining chapters is given in Section 1.4, with a summary of common notation used throughout the thesis being provided in Section 1.5.

1.1 Introduction

The topic of autonomous formation control has acquired considerable interest due to the developments of unmanned vehicles in recent years. In this scenario, the challenge is to design a control scheme that enables multiple agents (i.e. vehicles) to achieve and maintain a desired position with respect to each other (see e.g. the review papers by Chen and Wang [2005]; Anderson et al. [2008]; Oh et al. [2015]). Often, additional objectives, such as manoeuvring the formation along a desired trajectory, are also considered. There are a variety of interesting applications motivating the study of formation control. For example, Beard et al. [2001] have discussed the task of spacecraft interferometry, which requires precise regulation of agent positions to image distant stars. Ögren et al. [2004] presented a control algorithm for locating the maximum of an environmental field, such as temperature. The use of aerial vehicles to transport objects too large for a single vehicle to carry has received considerable attention by e.g. Michael et al. [2011]; Fink et al. [2011]. Recently, Vos et al. [2014] have addressed the even distribution of satellites in an orbit. The advantages of having multiple vehicles collaboratively working together in a formation are numerous, and include improved precision from measurements of the environment, redundancy in the presence of single-vehicle failures, and faster coverage of an area in exploration tasks. However, there are also many challenges that must be overcome for the successful coordination of multiple vehicles, and these have become the subject of extensive and ongoing research in the literature.

One clear consideration for formation control applications is the vehicle model. Kinematic agent models have commonly been used to simplify the problem (as seen in e.g. Das et al. [2002]; Antonelli and Chiaverini [2006]; Krick et al. [2009]), but their validity requires the vehicles to possess a sufficiently high power-to-mass ratio. Hence, it is often more appropriate to model the full dynamics as in e.g. Olfati-Saber [2006]; Franchi et al. [2012b]. Although formation control schemes commonly consider agent states in Euclidean space, for many vehicles the linear position dynamics are coupled with the vehicle's attitude (e.g. the underactuated quadrotor). Thus, such control schemes require the use of local controllers to implement the dynamics modelled for the formation controller, and rely on a separation principle for stability. A more comprehensive solution is to include attitude in the vehicle models for the formation controller, leading to states in the Special Euclidean group as addressed by e.g. Sarlette et al. [2010]; Hatanaka et al. [2012]. This approach is further motivated by the use of directional onboard sensors such as cameras, which require field-of-view limitations to be taken into account. In addition, nonholonomic constraints of the vehicles can significantly complicate the formation control algorithm. Most notably, such constraints apply to classical wheeled robots, which have seen extensive study in the formation control literature by e.g. Das et al. [2002]; Consolini et al. [2008]; Vos et al. [2016].

A second major consideration for the formation control task is the available knowledge of the vehicle states. The majority of the formation control literature implicitly assumes full state information is available for formation regulation, since the control laws proposed cannot be implemented without full state measurements. These measurements typically depend on an external tracking system, such as a global positioning system (GPS) or a motion capture system. However, such systems need a well-structured environment and can often be rendered unreliable, intermittent, or entirely unavailable in certain scenarios; e.g. underwater, in space, or in hostile locations where interference or occlusions are present. In such cases, it is more appropriate to consider the use of onboard sensors, such as cameras or time-of-flight sensors. These sensors typically only provide reliable *partial* measurements of *relative* state, such as the bearing or range to another vehicle. This introduces a question of *observability* into the formation control problem; in particular, estimates of the vehicle states with respect to a common inertial frame are often not available. This issue is widely overlooked in the existing formation control literature. One method of obtaining full relative position information is to fuse multiple onboard sensors together; however, this can become quite expensive in terms of cost, weight (which often adversely affects the vehicle dynamics), power, and computational resources. Another possibility is to employ a state observer such as the one presented by Rehbinder and Ghosh [2003], which relies on line features observed by an onboard camera, coupled with inertial measurements from an inertial measurement unit (IMU). A third alternative is to formulate the control law for each vehicle in terms of the available partial measurements of relative state, without explicitly estimating full states in a common reference frame. This strategy may be regarded as a more general case of the image-based visual servo (IBVS) control approach, where a vehicle's state is regulated by matching an image from a camera with a goal image that corresponds to the desired pose (see the tutorials Hutchinson et al. [1996]; Chaumette and Hutchinson [2006, 2007]).

Although position regulation using only partial relative state variables is quite a challenging task, it has begun to receive some attention in recent years. Cao et al. [2011] propose a *stop-and-go* strategy for kinematic agents in $\mathbb{R}^2$ with only range measurements between them. The idea is to have the agents take turns in stopping, with each moving agent making multiple range measurements of the stationary one and using triangulation to estimate its relative state in a local frame. For bearing measurements, Franchi et al. [2012a] employ two arbitrarily chosen *beacon agents* to act as reference vehicles (i.e. with special control inputs), enabling formation control of dynamic agents in $\mathbb{R}^3$. Both of these approaches exploit the particular geometrical structure of the measurement considered, and consequently, they are not easily generalisable to other sensor modalities. More recently, Zelazo et al. [2015] proposed a control scheme that uses distance measurements and two bearing measurements (available to a special agent) to estimate relative states across the network. Zhao and Zelazo [2016] have addressed formation control of kinematic agents using bearing-only measurements, without knowledge of a global reference frame. Beyond these papers, there is remarkably little literature that explicitly considers the regulation of a formation in the presence of limited relative state information. Clearly, extensions to more general sensor modalities and configurations would be of high interest for further development in the field of formation control.

There are many other aspects of the formation control problem that are of varying significance depending on the particular task at hand. As noted in the opening paragraph, it is commonly of interest to have the agents determine and track a desired trajectory whilst maintaining formation, as studied by Porfiri et al. [2007]. One may also consider the task of achieving coordinated motions that preserve the relative states of the agents, without imposing specific constraints on the relative states themselves (see e.g. the approach of Sarlette et al. [2010] concerning agent states that lie in a Lie group). A similar notion is the concept of *flocking* as described by Reynolds [1987], where agents are required to maintain a suitable distance from each other and to achieve a common velocity. This task has received attention from Olfati-Saber [2006]; Hatanaka et al. [2012]. For the purposes of both flocking and trajectory tracking, one may wish the formation itself to be flexible, particularly in order to navigate environments cluttered with obstacles, as in e.g. Das et al. [2002]; Olfati-Saber [2006]. In addition, collision avoidance between agents often needs to be explicitly enforced. Time-varying network topologies, where the available relative state information may be intermittent (due to obstructions or field-of-view limitations on the sensors), have been carefully considered by e.g. Franchi et al. [2012b]. For such cases, it is important to ensure network connectivity is maintained, as has been addressed by Ji and Egerstedt [2007]. Much of the literature proposes *decentralised* control laws, which are highly favoured for scalability of the approach. In particular, it is desirable to be able to increase the total number of agents in the formation, while preserving a fixed upper bound on the number of agents with which each agent must interact. Centralised control schemes can encounter difficulties concerning the communication or processing demands on the central agents, and commonly impose geometrical or physical constraints on the operation of the formation. A further consideration is the effect of delays in the network communications, as has been explicitly considered by Secchi et al. [2012].

With the aforementioned challenges in mind, a variety of formation control architectures have been proposed in the literature, each offering certain advantages to particular scenarios. For example, in the leader-follower approach as employed by Das et al. [2002], each vehicle regulates a direct relative state measurement to a physical leader vehicle that is guiding the formation along a trajectory. Consequently, this control scheme is a simple and natural choice when the practical constraints of physical onboard sensor measurements are of concern. However, centralising the architecture around a physical leader in this way can inhibit scalability of the formation (e.g. due to error propagation through a chain of leaders as studied in Tanner et al. [2004]) and create a point of vulnerability in the control scheme (i.e. should the leader suffer a critical failure such as a collision). An alternative is the virtual structure approach proposed by Lewis and Tan [1997], where reference trajectories for each agent are generated by considering the desired motion of a virtual structure formed by the agents (see Ren and Beard [2004a] for a decentralised approach using this framework). However, this approach typically requires the positions of the vehicles to be known in the inertial frame, since tracking a virtual reference means no physical measurement of the errors can be directly obtained. A third popular formation control strategy is the concept of behavioural control introduced by Balch and Arkin [1998]. In this approach, the overall control law is composed of multiple functions that are each designed to achieve a particular sub-task, such as formation regulation or collision avoidance. While this control scheme offers great flexibility for addressing a variety of goals, it often leads to complex stability analysis and the resulting behaviour of the system can be difficult to determine. Another perspective is to formulate formation control as a consensus problem; this approach has been reviewed by Olfati-Saber et al. [2007]; Ren et al. [2007]. For example, position regulation may be regarded as the task of achieving agreement between the vehicle positions, with each vehicle physically implementing the update law of a consensus protocol. As discussed in the review papers, the consensus framework has proven to be particularly well-suited for addressing time-varying communication topologies, and communication delays. A limitation of this approach is that it is not well-suited to other aspects of the formation control problem, such as collision avoidance.

The high degree of complexity in the formation control task means that stability analysis is often difficult to perform. Two popular approaches have emerged in the literature for overcoming this challenge. The first is to use graph-based techniques, and matrix theory, to encode the structure of the full network and to provide tools with which desirable properties, such as connectivity, can be studied and enforced. This method is widely employed in the consensus literature. Of particular interest in this approach is the concept of *rigidity*, which studies when a set of distance constraints between particular pairs of agents will be sufficient to enforce the behaviour of a rigid body across the whole formation. Thus, for a control architecture that enforces the specified distance constraints, the only permissible motions of the agents in the formation will correspond to global rotations and translations in $\mathbb{R}^d$ space.

An introduction to this approach has been presented by Anderson et al. [2008], with the concepts of *persistence* (Hendrickx et al. [2007]) and *structural persistence* (Yu et al. [2007]) enabling extensions to directed network topologies (i.e. where only one agent is trying to enforce each distance constraint). The key advantages of applying rigidity theory to formation control are that it naturally incorporates the network structure into the framework, and it explicitly specifies the distance variables to be controlled, which can assist in determining an appropriate sensor configuration. It should be noted that most techniques for regulating the specified distances still require knowledge of the full relative states.

Of particular interest to the formation control task is the notion of *infinitesimal rigidity*, which describes whether any infinitesimal deviation from a rigid formation must result in an instantaneous change in at least one of the regulated distances. This has important implications in the stability analysis of a control scheme based on enforcing those constraints, and is exploited by e.g. Oh and Ahn [2011]. Dörfler and Francis [2009] have assumed infinitesimal rigidity along with *minimal rigidity* (i.e. that the distance constraints do not overconstrain the agents), and used this to show exponential stability for a gradient-descent algorithm. Further investigation by Sun et al. [2016] has recently revealed that the requirement of minimal rigidity is not necessary to prove exponential stability of the gradient-descent approach. Another useful result is that the set of points satisfying a given infinitesimally rigid formation is a regular submanifold of the state-space. This property has enabled Krick et al. [2009] to perform stability analysis using centre manifold theory, and is also of significance for the geometrical approach used by Dörfler and Francis [2010] to study the stability or instability of equilibria in the control dynamics. Recent work by Zelazo et al. [2015] has focused on the limitation of using distance-only measurements (with two bearing measurements available to a single special agent), and proposes a formation control scheme based on preserving infinitesimal rigidity of the formation through regulation of the *rigidity eigenvalue* of the *symmetric rigidity matrix*. Meanwhile, Sun and Anderson [2015] have studied formation control for dynamic agents by extending rigidity-based analysis from the kinematic case.

Two limitations with the use of classical rigidity theory are that it is restricted to agents in $\mathbb{R}^d$, and that it only concerns the distances between agent positions, rather than other relative state constraints that might be more easily regulated by the available onboard sensors (e.g. bearings from onboard cameras). As a consequence, the notion of rigidity has been extended to bearing measurements by e.g. Franchi et al. [2012a]; Zhao and Zelazo [2016], and to agents in $\mathrm{SE}(2)$ by Zelazo et al. [2014]. However, a sufficiently general rigidity framework for many formation control scenarios has not yet been presented in the literature. In particular, it is of great practical interest to allow several different sensor modalities in the network, which need not be constrained to those of distance and direction measurements (consider, for example, the relative height between two agents as measured by onboard pressure sensors). In addition, it is commonly necessary to model agent states in the Special Euclidean group $\mathrm{SE}(3)$. Bearing measurements should typically be expressed in local coordinate frames, and onboard cameras have field-of-view constraints in practice, making the orientation of each vehicle an important state variable. Furthermore, it is not necessarily the case that all vehicles lie in the same state-space; a simple motivation for the exceptional scenario is the control of a formation involving both ground and aerial vehicles. For more advanced formation control scenarios, one may even consider constraints on the relative velocities between agents via a generalised rigidity framework. It is worth noting that a generalised concept of rigidity will not only assist with the control design of a system, but it will also provide insight into the symmetry of the system and can thus resolve the aforementioned question of observability for the available sensor measurements. The success of geometrical approaches in the formation control literature makes the generalisation of rigidity theory a highly appealing avenue for further research.

The second popular approach to formation control is to use an energy-based design that is oriented around ensuring passivity of the system, with the desired state corresponding to a global minima of the total energy function. The appeal of this technique lies in its ability to greatly simplify the stability analysis in the presence of multiple control laws corresponding to a variety of separate objectives. As a consequence, this strategy has proven particularly valuable for behavioural control schemes. Many energy-based approaches lead to modular control architectures that can be readily extended to additional considerations, such as a haptic control input from a human pilot as in Franchi et al. [2012b]. Energy-based control architectures also offer considerable flexibility via shaping of the energy functions from which the control terms are derived. They have proven particularly useful for double-integrator agent models, as seen in e.g. Leonard and Fiorelli [2001]; Franchi et al. [2012b]; Vos et al. [2016]. Formation regulation is commonly achieved by applying virtual mechanical couplings to the relative states of the agents. These couplings consist of a spring-like force based on the error in the distance between agents, and a damping term based on the relative velocity. It should be noted that although the magnitude of the force is usually derived from the *distance* error, the implementation of the resulting control term relies on full relative position information.

The use of virtual mechanical couplings provides a convenient method by which more general relative state constraints may be regulated, although to my knowledge this generalisation has not been explicitly presented in the literature, prior to the work Stacey and Mahony [2016] that forms part of the material presented in this thesis. One suitable framework for this approach is provided by van der Schaft and Maschke [2013], through the use of port-Hamiltonian theory on graphs. However, as with distance constraints, the control laws resulting from this framework will not necessarily be implementable with the available sensor measurements. One possibility for overcoming this challenge is to exploit the flexibility and modularity of the energy-based framework to incorporate adaptive compensation for the unknown state. For bearing measurements, this task is closely related to the field of image-based visual servo (IBVS) control (see Hutchinson et al. [1996]; Chaumette and Hutchinson [2006, 2007]). Passivity-based approaches to IBVS control have been presented by Fujita et al. [2007] and Mahony and Stramigioli [2012]. The application of this strategy to other sensor modalities in the context of formation control has not, to my knowledge, been considered.

In summary, formation control is a complex problem that involves the coordination of multiple agents, and in particular, the regulation of their relative states. Many aspects of this scenario have been studied extensively in the literature, for a wide variety of tasks. Common considerations include nonholonomic and dynamic vehicle models, trajectory tracking, collision avoidance, and the structure of the communication topology. However, the restriction of using *partial* relative state measurements, as are often available from onboard sensors in practice, appears to have received remarkably limited attention. Furthermore, the existing strategies for addressing this particular issue have not been sufficiently generalised to allow an arbitrary mix of appropriate sensor modalities, or vehicle state-spaces. In the existing literature, frameworks based on rigidity theory and the property of passivity have proven highly successful for distance regulation in formation control problems. The generalisation of these two approaches is therefore a highly promising avenue of research for more widely applicable solutions to the challenge of sensor-based formation control.

1.2 Contributions

The primary objective of the research in this thesis is to investigate approaches for the task of sensor-based formation control. In particular, my focus is on the direct regulation of generic partial relative state measurements, as are typically provided by onboard sensors such as cameras or time-of-flight sensors. My approaches to this problem are inspired by two major avenues of research from the literature. The first approach is to extend the classical notion of rigidity theory to include far more generic agent states and state measurements, thereby enabling geometrical arguments and techniques based on a generalised *rigidity matrix* to be employed for the stability analysis of formation control schemes. The second strategy is to apply virtual mechanical couplings to generic sensor modalities in order to obtain a highly modular passivity-based control architecture that can be easily extended to address additional considerations, such as adaptive compensation for the unknown state variables required for implementation of the control law.

The generalisation of rigidity theory is developed in the context of a symmetry of the system that is described by the action of a topological group on the combined state-space of the agents. The state of the system is subject to a number of constraints specified by fixing the values of a collection of output maps, which in practice may model the sensor modalities available for control. I regard a *formation* as the set of configurations (i.e. points) that satisfy the specified state constraints. Rigidity of a formation can then be defined as the case where all state constraints are invariant to an action of the group, and where the group action is (globally or locally) transitive on the formation. This forms an extremely general framework for rigidity theory, and I motivate this with a variety of scenarios that cannot be readily formulated with existing techniques in the literature. By studying the rigidity of a specified formation, one can resolve the question of observability: the group action precisely describes the symmetry up to which the agent states can be determined from the available sensor measurements. In the absence of a differentiable structure on the output maps, I introduce the notion of *path-rigidity* as the case where one can continuously transition between any two configurations of a globally rigid formation without breaching any state constraints. Useful characterisations of generalised rigidity and path-rigidity are provided via group-theoretic analysis.

If the symmetry is described by the action of a Lie group, and the sensor modalities possess a continuously differentiable structure, then the notion of *infinitesimal rigidity* can be naturally defined for the generalised framework. In this setting, I have proven that the generalised form of infinitesimal rigidity implies local rigidity, extending the important result by Asimow and Roth [1979] for the classical case. Furthermore, I show that an infinitesimally rigid formation consists of a collection of disjoint closed regular submanifolds of the state-space (these could theoretically be of different dimensions). This provides important structure for the analysis of many formation control schemes (see e.g. the methods employed by Krick et al. [2009]; Dörfler and Francis [2010]). I have also shown that any infinitesimally rigid formation has an open neighbourhood on which all configurations are infinitesimally rigid, which enables the structure associated with infinitesimal rigidity to be exploited in a local neighbourhood for the purposes of stability analysis. Furthermore, I have introduced a stronger notion of *robust rigidity*, which describes the case where the non-zero singular values of the output maps are bounded on an open neighbourhood of the formation. This provides important structure for stability analysis concerning non-compact formations, and enables techniques such as those employed by Sun et al. [2016] to be applied in the generalised setting. In the classical literature (e.g. Krick et al. [2009]), non-compact formations are often handled by relying on compactness of the set of *relative* states satisfying the formation; however, this approach depends on the geometry associated with the classical setting and cannot be easily extended to the generalised scenario. Robust rigidity allows exponential stability to be guaranteed, which implies boundedness of the trajectories.

I have illustrated the application of my generalised rigidity framework with two examples. The first addresses the task of network localisation, where the goal is to determine the true agent states (up to the group symmetry) using only the partial relative state measurements that are available. In the second example, I present a formation control scheme for kinematic agents. The control law is composed of two parts: the first is used to drive the agents towards a desired robustly rigid formation, while the second is used for *manoeuvring in formation*, i.e. steering the agents within the submanifold of the formation. The fact that the proposed control scheme decouples the objectives of formation regulation and steering suggests that the rigidity framework can achieve similar benefits to those of the virtual structure architecture. In both examples, the structure provided by generalised rigidity theory is exploited to achieve a solution that is applicable to an extremely general class of scenarios. The agent states may (for example) lie in the Special Euclidean group rather than Euclidean space, and an arbitrary arrangement of mixed sensor modalities can be employed (requiring only a differentiable structure on the measurements).

As an alternative to the rigidity framework, I develop a passivity-based approach to the formation control of dynamic agents in $\mathbb{R}^3$, with the aid of bondgraph diagrams. Relative to the rigidity framework, this approach aligns more closely with the highly flexible behavioural control strategy. The bondgraph modelling formalism enables an elegant representation of the energy flow between components of a port-Hamiltonian system, and ensures that the resulting design is strictly energy-consistent. This makes it an excellent tool for both the design and the analysis of the system. Formation control is achieved by applying virtual mechanical couplings directly to the available sensor measurements, using the concept of a *measurement Jacobian* to transform the control effort in the sensor space to a control input for the vehicles. Local asymptotic stability to a desired formation is ensured by a passivity-based argument, and the behaviour of the system can be adjusted by appropriate shaping of the virtual energy functions. In particular, this method can be used to avoid collisions between agents.

A shortcoming of the basic design, shared with classical passivity-based formation control algorithms (e.g. Franchi et al. [2012b]), is that implementation of the control input requires full relative position information. Such information is not typically available from the onboard sensor output and implementing the control requires a full state observer to run on each vehicle. In particular, this problem arises for the important sensor modalities of directions and distances. To resolve this challenging issue, I exploit the high modularity of the energy-based approach to incorporate adaptive compensation for the unknown state information. Adaptive control schemes for direction and distance modalities are developed separately, due to differences in the geometrical structure of the measurements. For the modified control architecture, I prove local asymptotic stability under an assumption on the structure of the sensor network, and present simulation results. It is worth emphasising that the resulting decentralised control framework allows for more general sensor configurations than those addressed by many existing approaches in the literature (e.g. Franchi et al. [2012a]; Zelazo et al. [2015]); in particular, it does not rely on the use of special agents that employ fundamentally different control schemes to the others in the network.

1.3 Publications

The research in this thesis has been presented in the following publications:

- Stacey, G.; Mahony, R.; and Corke, P., 2013. A bondgraph approach to formation control using relative state measurements. In *Proc. European Control Conf.* (Zürich, Switzerland, July 2013).

- Stacey, G. and Mahony, R., 2013. A port-Hamiltonian approach to formation control using bearing measurements and range observers. In *Proc. IEEE Conf. on Decision and Control* (Florence, Italy, December 2013).

- Stacey, G. and Mahony, R., 2016. A passivity-based approach to formation control using partial measurements of relative position. *IEEE Trans. on Automatic Control*, 61, 2 (February 2016), 538-543.

- Stacey, G.; Mahony, R.; and Trumpf, J., 2016. Generalised rigidity and path-rigidity for agent formations. In *Proc. Int. Symposium on Mathematical Theory of Networks and Systems* (Minneapolis, Minnesota, USA, July 2016).

Some material in this thesis is also contained in the following manuscript, submitted for review:

- Stacey, G. and Mahony, R., 2016. The role of symmetry in rigidity analysis: A tool for network localisation and formation control. Submitted to *IEEE Trans. on Automatic Control*.

1.4 Thesis Outline

The thesis is structured as follows. In Chapter 2, I review the formation control literature with a particular focus on the rigidity- and passivity-based approaches. In Chapter 3 I develop the generalised rigidity framework, and provide analysis of the associated topological structure as well as introducing the concept of path-rigidity. The properties of infinitesimal rigidity and robust rigidity are studied in Chapter 4, where I prove some key results for control problems concerning agent networks. This chapter is concluded by demonstrating the application of the theory to the tasks of network localisation and formation control. The passivity-based approach to formation control using virtual mechanical couplings is presented in Chapter 5. This design is primarily focused on the use of distance and inertial direction measurements, with adaptive compensation techniques being employed to account for the unknown state information. Note that the material in Chapter 5 was developed prior to that of Chapters 3 and 4 and is formulated directly with an explicit state representation rather than the more abstract rigidity-based theory. A brief conclusion is provided in Chapter 6, which includes a discussion of future work that involves the integration of theory from Chapters 3 and 4 with that of Chapter 5. Background group theory is summarised in Appendix A, and the classical notion of rigidity is reviewed in Appendix B. Port-Hamiltonian theory and the bondgraph modelling technique are described in Appendices C and D, respectively. Code used for the simulations is given in Appendix E.

1.5 Notation

To briefly clarify some standard notation; I use $\mathbb{R}$, $\mathbb{R}_{\geq 0}$, and $\mathbb{R}_{>0}$ to denote the set of real numbers, nonnegative real numbers, and positive real numbers, respectively. Let $\mathbb{R}^n$ denote the set of n-dimensional column vectors of real numbers, and $\mathbb{R}^{m \times n}$ denote the set of m-by-n matrices of real numbers (m rows and n columns). Note that

I do not consider the field of complex numbers in this thesis. All angles are given in radians.

Further notation used throughout this thesis is outlined in Table 1.2. For the purpose of the following definitions, $m, n, p, q \geq 1$ are integers, $v \in \mathbb{R}^n$ is a vector, $X \in \mathbb{R}^{m \times n}$ and $Y \in \mathbb{R}^{p \times q}$ are matrices, $\mathcal{M}$ and $\mathcal{N}$ are arbitrary smooth manifolds of finite dimension, $f : \mathcal{M} \to \mathcal{N}$, $g : \mathcal{M} \to \mathbb{R}$ and $\gamma : \mathbb{R} \to \mathcal{M}$ are smooth maps, $x \in \mathcal{M}$ is a point, $\mathcal{V} \subseteq \mathcal{U} \subseteq \mathcal{M}$ are sets, $A : \mathbb{V} \to \mathbb{W}$ is a linear operator between Euclidean spaces (assumed to be expressed as a matrix using given bases), $\delta > 0$ is a scalar constant, and **G** is a topological group. Note that this notation does not hold throughout the remainder of the thesis. Additional notes [$\cdot$] are provided below the table.

$\mathbb{S}^n$	Unit n-sphere, embedded in $\mathbb{R}^{n+1}$
T_0	Kolmogorov topology
T_1	Fréchet topology
T_2	Hausdorff topology
$I_n \in \mathbb{R}^{n \times n}$	The $n \times n$ identity matrix
$0_n \in \mathbb{R}^n$	The n-vector of zeroes
$0_{m \times n} \in \mathbb{R}^{m \times n}$	The $m \times n$ matrix of zeroes
$\\|v\\|$	Euclidean norm of a vector $v \in \mathbb{R}^n$
$\\|X\\|_F$	Frobenius norm of a matrix $X \in \mathbb{R}^{m \times n}$
$X^\top \in \mathbb{R}^{n \times m}$	Transpose of a matrix $X \in \mathbb{R}^{m \times n}$
$\bar{v}$	Homogeneous coordinates, $(v^\top, 1)^\top$, for $v \in \mathbb{R}^n$
$X \otimes Y \in \mathbb{R}^{mp \times nq}$	[i] Kronecker product of matrices X and Y
$\mathrm{O}(n)$	Orthogonal group (Section A.1)
$\mathrm{SO}(n)$	Special Orthogonal group (Section A.1)
$\mathrm{E}(n)$	Euclidean group (Section A.2)
$\mathrm{SE}(n)$	Special Euclidean group (Section A.2)
$\mathrm{S}(n)$	Similarity group (Section A.3)
$\mathrm{SS}(n)$	Special Similarity group (Section A.3)
$\mathrm{ST}(n)$	Scaled-Translations group (Section A.4)
$\mathbf{G}$	Group (Appendix A)
$\mathbf{P}_n$	Permutation group for a set of n elements
$\mathfrak{g}$	Lie algebra of a Lie group $\mathbf{G}$
$\Phi : \mathbf{G} \times \mathcal{M} \to \mathcal{M}$	(Lie) group action of a (Lie) group $\mathbf{G}$
$\iota \in \mathbf{G}$	Group identity of $\mathbf{G}$
$\operatorname{stab} \Phi_x \subseteq \mathbf{G}$	[ii] Stabiliser of Φ at x
$\mathcal{M}^\tau$	[iii] Set $\mathcal{M}$ equipped with a generic topology $\tau(\mathcal{M})$
$\mathcal{M}^\wp := \prod_{i=1}^n \mathcal{M}_i^\tau$	[iii] Product space
$\dim \mathcal{M}$	Dimension of $\mathcal{M}$
$f(\mathcal{U}) \subseteq \mathcal{N}$	Image of $\mathcal{U}$ through f
$T_x\mathcal{M}$	Tangent space of $\mathcal{M}$ at x

$\Delta_x \in T_x\mathcal{M}$	Tangent vector in $T_x\mathcal{M}$
$\dot\gamma := \frac{\mathrm{d}}{\mathrm{d}t}\gamma(t)$	Derivative of $\gamma(t)$ with respect to t
$\frac{\partial g(x)}{\partial x} := \left(\frac{\partial g(x)}{\partial x_1}, \ldots, \frac{\partial g(x)}{\partial x_m}\right) \in \mathbb{R}^{1\times m}$	Partial derivative of $g(x)$ with respect to $x := (x_1, \ldots, x_m)^\top \in \mathcal{M}$, where $m := \dim\mathcal{M}$
$\frac{\partial f(x)}{\partial x} \in \mathbb{R}^{n\times m}$	[iv] Jacobian of $f(x)$ with respect to $x \in \mathcal{M}$
$T_x^\star\mathcal{M}$	Dual space of $T_x\mathcal{M}$
$A^\star : \mathbb{W}^\star \to \mathbb{V}^\star$	Adjoint map of $A : \mathbb{V} \to \mathbb{W}$
$\mathrm{D}f(x)[\cdot] : T_x\mathcal{M} \to T_{f(x)}\mathcal{N}$	Differential of f at x
$\langle\cdot,\cdot\rangle_x : T_x\mathcal{M} \times T_x\mathcal{M} \to \mathbb{R}_{\geq 0}$	[v] Smooth, positive-definite bilinear inner product
$\Lambda_x : T_x\mathcal{M} \to T_x^\star\mathcal{M}$	[vi] Metric operator
$\nabla g(x) \in T_x\mathcal{M}$	[vi] Gradient of g at x, $\langle\nabla g(x), \Delta_x\rangle_x = \mathrm{D}g(x)[\Delta_x]$
$\operatorname{rank} A$	Rank of A
$\ker A \subseteq \mathbb{V}$	Kernel of A
$\Vert A\Vert_2$	[vii] Maximum singular value of A
$\lambda_2(A)$	[vii] Spectral gap of A
$B_\delta(x) \subseteq \mathcal{M}$	[viii] Open ball of radius δ
$\lfloor\mathcal{U}\rfloor_{\mathcal{V}} \subseteq \mathcal{U}$	[ix] Path-connected component(s) of $\mathcal{U}$ that intersect $\mathcal{V}$
$\mathbf{G}^0 \subseteq \mathbf{G}$	Connected component of the identity $\iota \in \mathbf{G}$
$\mathbf{G}^1 := \lfloor\mathbf{G}\rfloor_{\{\iota\}} \subseteq \mathbf{G}$	Path-connected component of the identity $\iota \in \mathbf{G}$
$\langle\cdot \mid \cdot\rangle : \mathbb{V} \times \mathbb{V}^\star \to \mathbb{R}$	Duality product, $\langle w \mid v\rangle := w^\top v \in \mathbb{R}$ for $v \in \mathbb{V}, w \in \mathbb{V}^\star$ (see Appendix C)

Table 1.2: Summary of notation

[i] *Kronecker product:* The Kronecker product of two matrices $X \in \mathbb{R}^{m\times n}$ and $Y \in \mathbb{R}^{p\times q}$ is defined by

$$X \otimes Y := \begin{pmatrix} x_{1,1}Y & \ldots & x_{1,n}Y \\ \vdots & \ddots & \vdots \\ x_{m,1}Y & \ldots & x_{m,n}Y \end{pmatrix} \in \mathbb{R}^{mp\times nq},$$

where $x_{i,j}$ denotes the element of X in row i and column j.

[ii] *Stabiliser of a group action:* The stabiliser is defined as the set of group elements that leave x unchanged by the group action Φ, i.e. $\operatorname{stab}\Phi_x := \{S \in \mathbf{G} \mid \Phi_x(S) = x\}$ (where $\Phi_x(S) := \Phi(S, x)$). The stabiliser is a subgroup of $\mathbf{G}$, and continuity of Φ_x implies $\operatorname{stab}\Phi_x$ is closed since $\mathcal{M}$ is Hausdorff.

[iii] *Topological Spaces:* Outside of Chapter 3, all topological spaces are assumed to

be smooth (C^∞) manifolds, and the topology superscript is omitted.

[iv] *Jacobian:* Given a map $f : \mathcal{M} \to \mathcal{N}$, the Jacobian of $f(x) = (f_1(x), \dots, f_n(x))^\top$ with respect to $x \in \mathcal{M}$ is given by

$$\frac{\partial f(x)}{\partial x} := \begin{pmatrix} \frac{\partial f_1(x)}{\partial x} \\ \vdots \\ \frac{\partial f_n(x)}{\partial x} \end{pmatrix} \in \mathbb{R}^{n \times m},$$

where $m := \dim \mathcal{M}$ and $n := \dim \mathcal{N}$.

[v] *Riemannian metric:* The family of inner products $\langle \cdot, \cdot \rangle_x$ define a Riemannian metric structure on $\mathcal{M}$.

[vi] *Metric operator:* Given a metric $\langle \cdot, \cdot \rangle_x$, fix $\Delta_x \in T_x\mathcal{M}$ and define $\Lambda_x(\Delta_x) : T_x\mathcal{M} \to \mathbb{R}$, $\Lambda_x(\Delta_x)[\Delta'_x] \mapsto \langle \Delta_x, \Delta'_x \rangle_x$. The metric operator is the mapping $\Lambda_x : T_x\mathcal{M} \to T_x^\star\mathcal{M}$ from tangent vectors $\Delta_x \in T_x\mathcal{M}$ to dual elements $\Lambda_x(\Delta_x) \in T_x^\star\mathcal{M}$. The inverse $\Lambda_x^{-1} : T_x^\star\mathcal{M} \to T_x\mathcal{M}$ is well defined and positive definite since Λ_x is positive definite. The implicit relationship $\langle \nabla g(x), \Delta_x \rangle_x = \mathrm{D}g(x)[\Delta_x]$ can be written explicitly using the operator notation $\nabla g(x) = \Lambda_x^{-1}(\mathrm{D}g(x))$. The inverse operator also defines a positive-definite inner product on the dual space $\langle \cdot, \cdot \rangle_x^\star : T_x^\star\mathcal{M} \times T_x^\star\mathcal{M} \to \mathbb{R}$, $\langle \mathrm{D}g_1(x), \mathrm{D}g_2(x) \rangle_x^\star \mapsto \mathrm{D}g_2(x)[\Lambda_x^{-1}(\mathrm{D}g_1(x))]$ for $g_1, g_2 : \mathcal{M} \to \mathbb{R}$.

[vii] *Singular values:* The left singular vectors of A are the critical points of $\langle Av, Av \rangle^\diamond$ subject to $\langle v, v \rangle = 1$, where $\langle \cdot, \cdot \rangle$ and $\langle \cdot, \cdot \rangle^\diamond$ are inner products on $\mathbb{V}$ and $\mathbb{W}$ respectively. One has $\Lambda^\diamond(Av_i) \circ A - \sigma_i^2 \Lambda(v_i) = 0$ for v_i singular vectors and σ_i singular values, where Λ and $\Lambda^\diamond$ are the metric operators associated with inner products $\langle \cdot, \cdot \rangle$ and $\langle \cdot, \cdot \rangle^\diamond$. With $n := \min\{\dim \mathbb{V}, \dim \mathbb{W}\}$, one has $\|A\|_2 := \max_{s=1,\dots,n}\{\sigma_s(A)\}$ and $\lambda_2(A) := \min_{s=1,\dots,n}\{\sigma_s(A) \mid \sigma_s(A) \neq 0\}$, where $\sigma_s(A)$ denotes the s'th singular value of A. The spectral gap λ_2 is undefined for the zero matrix.

[viii] *Open balls:* The open ball $B_\delta(x) \subseteq \mathcal{M}$ is defined with respect to the distance measure $d : \mathcal{M} \times \mathcal{M} \to \mathbb{R}_{\geq 0}$ associated with the Riemannian distance on $\mathcal{M}$, with $B_\delta(x) := \{x' \in \mathcal{M} \mid d(x, x') < \delta\}$.

[ix] *Path-connected component(s):* The set $\lfloor \mathcal{U} \rfloor_{\mathcal{V}}$ is the set of points $x \in \mathcal{U}$ for which there exists a continuous path $\gamma : [0, 1] \to \mathcal{U} \subseteq \mathcal{M}$, with $\gamma(0) = x$ and $\gamma(1) \in \mathcal{V}$.

Chapter 2

Literature Review

This chapter reviews the existing literature associated with the problem of formation control. In the process, it highlights key shortcomings of the existing techniques, and thus provides a strong motivation for the research presented in this thesis. The literature review begins in Section 2.1 with a brief summary of some popular system architectures that have been developed for formation control. In Section 2.2, I review graph-based frameworks for the formation control problem with a particular focus on the important concept of *rigidity* and its role in stability analysis. Energy-based approaches to formation control, which are particularly appealing for the consideration of dynamic agent models, are reviewed in Section 2.3.

2.1 System Architectures for Formation Control

In this section I review the classical formation control architectures that have been developed over the past couple of decades. The focus here is on the general design approaches, rather than the analysis techniques discussed in Sections 2.2 and 2.3. Specifically, I will discuss the popular architectures of *leader-follower control* (Subsection 2.1.1), *virtual structures* (Subsection 2.1.2), and *behavioural control* (Subsection 2.1.3), as well as the *consensus-based formulation* of the problem (Subsection 2.1.4). Typically, this literature assumes full state measurements of pose and velocity, although I will note some exceptions where the control approach is motivated by the particular sensors available.

Before proceeding, it is worthwhile to establish some terminology for the subsequent discussion. By *formation control*, I refer to the problem of driving the relative positions of the agents or vehicles to a desired configuration, with the possible additional task of having the formation as a whole track a desired trajectory. The term *consensus* refers to the task of having agents reach agreement about particular variables, which may be associated with the current state of the system or desirable goals. The *network topology* of a group of agents refers to the topology of the information flow between them, and is usually represented as a network graph (with nodes corresponding to agents and edges corresponding to relative state measurements or communication links between them). Finally, the concept of *flocking* is defined according to Reynolds [1987], which states that flocking is achieved when three behaviours are obeyed by each agent: collision avoidance between nearby flockmates, velocity consensus between nearby flockmates, and local attraction to a neighbourhood of nearby flockmates.

2.1.1 Leader-Follower Control

In a basic leader-follower design approach, one or more of the vehicles are designated as *leaders* and the remaining vehicles are termed *followers*. The task of the leaders is to follow the specified trajectory, whilst the followers attempt to preserve a desired position with respect to the leaders, thus keeping the vehicles moving in an intended formation. The simplicity of this approach, and the fact that each vehicle is typically only concerned with one or two other vehicles, generally results in more straightforward control design and stability analysis than for some other architectures. A drawback of this approach is the lack of a distributed network topology, i.e. the leaders are central to guiding the formation along the desired trajectory. A consequence of this is that the control schemes tend not to scale well with the number of vehicles (see Tanner et al. [2004] for some interesting analysis concerning error propagation). Furthermore, if a leader fails in some way (e.g. from a collision), then all of the vehicles following it may be unable to proceed. Another weakness in many leader-follower designs is that the leader generally does not receive feedback from the followers, meaning that scenarios could arise in which the followers are unable to track or keep up with the leader.

The leader-follower control approach has natural appeal when the vehicles are equipped with onboard cameras, since each follower simply needs to follow a leader observed in the image (at some prescribed relative state). This application has been studied for nonholonomic wheeled robots by Das et al. [2002] and Vidal et al. [2003], as well as for planes by Johnson et al. [2004]. The well-known work of Das et al. [2002] considers arrangements where each follower is guided by one or two other vehicles, which may in turn be followers guided by other leaders. It contemplates error propagation through a chain of leader-follower links, collision avoidance with obstacles in the environment, switching between different control modes or desired formations (e.g. to handle cases where a vehicle loses sight of its leader), and the communication requirements for state observation. By contrast, the work of Vidal et al. [2003] focuses primarily on the sensor model and the implementation of an image-based visual servo control scheme. Johnson et al. [2004] study two methods of using camera images to estimate the range and velocity of a leading aircraft, thus avoiding the need for communication between vehicles. The first approach involves an Extended Kalman Filter (EKF) augmented by a Neural Network (NN), while the second relies on the physical size of an observed aircraft in the image.

Many additional formation control considerations have been studied in the context of leader-follower arrangements. In Tanner et al. [2004], analysis of error propagation through a formation is performed by introducing the concept of leader-to-formation stability (LFS), which is based on input-to-state stability (ISS). The control of a formation of nonholonomic vehicles with respect to input constraints is studied by Consolini et al. [2008]. The work by Hong et al. [2008] considers dynamic agents with a single leader, and develops a distributed observer for the leader's velocity using locally available relative position measurements. Liu et al. [2008] study the controllability of a leader-follower arrangement with a time-varying network topology. In addition to the aforementioned vehicles, underactuated autonomous underwater vehicles (AUVs) subject to environmental disturbances have also received attention, see e.g. Cui et al. [2010].

2.1.2 Virtual Structure Control

A virtual structure control approach specifies a desired formation (the virtual structure) that transitions along a desired trajectory. As it does so, each agent tracks its corresponding point in the virtual structure. A significant shortcoming of this approach in practice is that it requires a measurement of the tracking error for each agent. Typically this involves measuring the agent positions in the inertial frame, since the virtual reference cannot be physically measured by the vehicle (as can be done with physical leaders). As a consequence, this approach is better suited for more structured or controlled environments where such measurements are available. A variant of the virtual structure approach uses the concept of a *virtual leader* that computes and tracks a desired reference trajectory; this can provide improved robustness relative to the case of a physical leader since it will not be subject to mechanical failures.

The idea of formation control using virtual structures was introduced by Lewis and Tan [1997], who describe an iterative process of matching the virtual structure to the vehicle formation by a measure of best-fit, and then progressing the virtual structure one time-step forward for the vehicles to track. The first step in this process serves as a form of feedback that prevents the virtual structure from escaping the formation of physical vehicles, which might otherwise fall behind due to practical constraints such as input saturation or vehicle failure. The approach is illustrated by experiments involving nonholonomic wheeled robots, with a focus on evolving the virtual structure in an appropriate manner for the nonholonomic constraints. Later developments by Ren and Beard [2004b] employ a more conventional form of feedback from the vehicles to the virtual structure, by assigning dynamics to the virtual structure that are influenced by the vehicle positions. A decentralised variation of this framework has also been presented by Ren and Beard [2004a]. Li and Liu [2008] use a desired trajectory for a virtual structure to generate desired trajectories for the individual agents, and then consider the objective of correcting relative position errors between agents in a synchronised manner. Artificial potentials and other energy-based approaches have been quite popular in conjunction with virtual leader frameworks (see e.g. Leonard and Fiorelli [2001]), and will be further discussed later in this chapter.

2.1.3 Behavioural Control

The behaviour-based approach to formation control involves defining a set of control laws (i.e. *behaviours*) that are each designed to accomplish a particular aspect of the overall task. For example, some common goals include maintaining desired relative positions, tracking a trajectory with the formation, and obstacle avoidance. The final control for each vehicle is typically derived as a weighted sum of the various behavioural components. It is important to note that behavioural control strategies generally do not involve designing for a specific intended solution; rather, the behaviour of the system (e.g. the solution trajectory) is said to *emerge* from the collection of control factors. The combination of multiple control components often makes analysis of the system difficult; consequently, energy-based analysis techniques are a natural tool of choice, since the individual energy functions corresponding to each objective can be combined to obtain a total energy function that describes the overall behaviour of the system.

An early implementation of the behavioural control strategy is studied by Balch and Arkin [1998], where the behavioural components are *move-to-goal*, *avoid-static-obstacle*, *avoid-robot*, and *noise*, the latter of which introduces a random factor to the control that helps overcome undesired local behaviour that might arise in particular cases. The experiments detail the performance of various formations that employ different references for each vehicle's desired position (e.g. with respect to a leader, or with respect to the centre of the formation). Lawton et al. [2003] approach the control problem by separating the task of regulating the relative positions from that of tracking a specified trajectory for the formation. They address control input saturation and include more detailed mathematical analysis than the earlier work. A very general behavioural control strategy has been presented by Antonelli and Chiaverini [2006], who consider arbitrary *task functions* that describe objectives as a function of the system state. Examples of task functions are provided for collision avoidance, the preservation of a rigid formation, keeping vehicles close together, and escorting a target. To implement these tasks, the pseudo-inverse of the Jacobian of the task function is used to determine a desired velocity for the agents to track. Particular consideration is given to the combination of multiple (possibly conflicting) tasks, which is handled by projecting the velocity reference from low-priority tasks onto the space of velocities permitted by more important objectives.

The behavioural control approach has been combined with a leader-follower architecture by Monteiro and Bicho [2010], who use *repellers* and *attractors* to steer key variables (such as the direction of the leader) as required for a variety of goals. The leader-follower aspect of the approach makes it suitable for implementation using onboard sensors (measuring the bearing and distance to each leader), as demonstrated by the accompanying experiments. More recently, Wang and Xin [2013] used a consensus approach to implement formation regulation and trajectory tracking in a behavioural control scheme. Two other components of the control dealt with obstacle avoidance and optimisation of the control effort with respect to a cost function. From these papers, it can be seen that the behavioural control architecture is quite flexible and indeed can often be combined with aspects of the other formation control frameworks.

2.1.4 Consensus

Many researchers have posed aspects of formation control as a *consensus* problem. In this scenario, the goal is to synchronise a particular property of each agent in a network, such as its velocity, in a decentralised manner. For formation control, the consensus problem typically involves synchronising the variable of interest (e.g. position or velocity) with a particular reference value. In achieving consensus on the vehicle positions, it is also commonly necessary to incorporate position offsets for each vehicle depending on where it should lie with respect to the rest of the formation. By integrating the consensus algorithm into the control input for the vehicles, they can be physically driven towards the common desired state. While consensus algorithms apply quite naturally to particular aspects of the formation control problem, such as arranging the agents in a desired shape, it should be noted that they often need to be combined with other strategies in order to achieve additional tasks such as collision avoidance.

The consensus literature has been reviewed by both Olfati-Saber et al. [2007] and Ren et al. [2007], with particular focus given to the formation control problem. These articles provide comparisons of various consensus strategies, and illustrate the role of graph theory in the network analysis. Numerous aspects of the problem have been addressed, with algorithms for both discrete-time and continuous-time networks, convergence analysis based on the connectivity and structure of the network, consideration of directed and/or time-varying (dynamic) network topologies, and the accommodation of communication delays. Another interesting application of consensus in the formation control setting is to decide on the trajectory of a virtual leader by which the formation is guided. This idea has been studied by Porfiri et al. [2007], where the virtual leader's trajectory is determined in real-time based on a measured vector field (associated with e.g. the temperature of the environment). Consensus algorithms are used to ensure agreement on the location of the virtual leader, as well as to maintain formation around it. A general approach for formation control concerning agents with linearised dynamics has been proposed by Li et al. [2010], with an observer-type consensus protocol based on relative measurements of the agent states. The analysis also considers the region from which consensus is achieved, and the robustness of the algorithm under external disturbances. While much of the formation control literature assumes the agent states lie in Euclidean space, Sarlette et al. [2010] have presented a general theory for the coordinated motion of agents in a Lie group. The term *coordinated motion* refers to the task of preserving the relative states between pairs of agents, and it may be left-invariant, right-invariant, or bi-invariant depending on the form of the group action. However, relative positions are not themselves driven to a specified value. The relationship between this setting and the task of achieving velocity consensus on vector spaces is studied in detail. For left-invariant coordination, the case of underactuated agents is also considered.

While many consensus approaches have found success through graph theory, other results have relied on energy-based approaches that might be more easily combined with additional strategies for tasks such as collision avoidance. An example is the study of flocking by Olfati-Saber [2006], which uses a consensus algorithm to synchronise the velocities of the agents. This work has been extended by Su et al. [2009] to allow a time-varying reference velocity, and to study the case where not all agents have knowledge of this reference.

2.2 The Role of Rigidity Theory

The classical concept of *rigidity* (Appendix B) is concerned with the case where a set of distance constraints between nodes positioned in $\mathbb{R}^2$ or $\mathbb{R}^3$ is sufficient to enforce a rigid formation; i.e. to constrain the nodes up to global translations and rotations. The subject of rigidity theory has found application in many areas of science and engineering, some of which are briefly discussed in Subsection 2.2.1. In the field of formation control, the interest in rigidity theory builds upon the model of an agent network as a graph, where the vehicles correspond to nodes and the communication topology is represented by the edges. I briefly mention some of the graph-based studies of formation control in Subsection 2.2.2, before providing a more detailed review of the application of rigidity theory in Subsection 2.2.3. In addition to the classical case of distance constraints between agents in Euclidean space, various extensions to rigidity theory are also discussed, including rigidity for bearing-based formations and consideration of *directed* constraints where only one agent regulates its distance from the other.

2.2.1 Applications of Rigidity Theory

The study of classical rigidity theory has a long history that includes a wide range of applications, such as the analysis of tensegrity frameworks (Juan and Tur [2008]) and of chemical molecules (see e.g. the collection of papers in Thorpe and Duxbury [1999]). Although this project is primarily concerned with the generalisation of rigidity theory for the purposes of formation control, it is worth briefly reviewing research for other applications where similar generalisations have proven useful.

Over the past couple of decades, the field of computer-aided design (CAD) has emerged as one application that requires more abstract notions of rigidity. The task here is to determine whether a set of constraints are sufficient to fully specify a particular arrangement of geometrical objects (e.g. points, lines, etc), and indeed whether a *realisation* fitting the specified constraints actually exists. Servatius and Whiteley [1999] have considered this problem for a combination of distance and direction constraints in the plane. An analysis approach based on group theory has been developed by Schreck and Mathis [2006] for more general constraints (such as angles and fixed points). The strategy here is to decompose the system into different types of constraints, and to separately consider the group invariance associated with each case. Recently, Gortler et al. [2013] have studied a general notion of *affine rigidity* with the perspective of groups and monoids acting on $\mathbb{R}^d$.

A related problem to formation control is that of *network localisation*, where a set of stationary agents attempt to determine their relative positions using limited sensor measurements. The literature on network localisation has been reviewed by Patwari et al. [2005]; Mao et al. [2007], and gives attention to the modelling of various sensor modalities and noise. Aspnes et al. [2006] have demonstrated the significance of rigidity theory to this field, noting that in the case of distance measurements, global rigidity is precisely the condition required for the network localisation problem to be solvable up to the symmetry of Euclidean transforms. Typically, the network localisation problem assumes the presence of a few *anchor nodes* that know their own positions in the inertial frame, thus providing a reference for the rest of the network that enables the ambiguity from this symmetry to be removed. Eren [2011] has considered an extension of the rigidity-based approach to enable the inclusion of bearing (*angle-of-arrival*) measurements in the localisation task. Another rigidity formulation for agents in $\mathrm{SE}(2)$ has been employed by Zelazo et al. [2014] to achieve unscaled relative position estimation from bearing-only measurements.

2.2.2 Graph-Based Analysis

One of the fundamental tools for the analysis of formation control schemes, including some energy-based approaches as discussed in the Section 2.3, is graph theory (Godsil and Royle [2001]). The idea is to encode the network structure as a graph representing the interactions of the agents. A key aspect of classical graph theory is that the inter-agent structure can be mapped to a matrix structure, and questions on the graph structure can be addressed by classical matrix analysis techniques. This approach is particularly common for consensus problems, as illustrated by Olfati-Saber et al. [2007]; Ren et al. [2007] and references therein. An appealing aspect of the approach is that it leads to a distributed control architecture that naturally incorporates the available relative state information between agents.

Rather than digressing into the vast number of classical graph-based results covered in the aforementioned review papers, I will presently note some more recent literature that may be of interest in the context of my project. For the practical case where the topology of the graph depends on the proximity of the agents, Ji and Egerstedt [2007] present a control strategy that guarantees connectedness is preserved, which is commonly assumed but not necessarily true for consensus algorithms. Dimarogonas and Johansson [2008] consider negative gradient control laws for formations specified by relative distances, and show that global stability can be achieved if and only if the network topology is a spanning tree (i.e. otherwise there exists a set of undesired equilibria). A consequence of this is that such control laws cannot globally stabilise rigid formations of three or more agents, since the corresponding graph must necessarily contain a cycle. To develop a globally stable control law with a directed network topology, Cortés [2009] relates the desired edge measurements to the vehicle positions via the graph Laplacian and applies the *Jacobi* *overrelaxation iteration* to drive the vehicles to a solution.

2.2.3 Rigidity-Based Formation Control

In formation control problems it is common for the desired formation to be *rigid*; i.e. one often considers a desired *virtual structure* specified by distance constraints between agents in $\mathbb{R}^2$ or $\mathbb{R}^3$, such that only global rotations or translations of the structure are permitted. Rigidity analysis, which builds upon techniques provided by graph theory, has become an increasingly popular tool that addresses such scenarios. In particular, it provides insight into whether achieving a given set of distance constraints will be sufficient (possibly in only a local region) to enforce the whole rigid structure. The graph structure underlying the rigidity framework leads to some similarities with many consensus-based approaches to formation control, and rigidity theory can also play a critical role in leader-follower control schemes since it determines how agents may respond to motions of their leaders.

A review of rigidity-based formation control approaches is provided by Anderson et al. [2008]. An important result for formations in $\mathbb{R}^2$ is Laman's theorem (Laman [1970]), which provides a combinatorial characterisation of rigid planar graphs; however, a generalisation of Laman's theorem to higher dimensions is yet to be found. Some detailed discussion of the structure associated with rigid formations, including methods of constructing them, has been presented by Eren et al. [2002]. Additionally, Olfati-Saber and Murray [2002c] have studied how rigid planar formations can be *split* into multiple rigid formations and *rejoined* into a single rigid formation, as may be necessary to negotiate obstacles. Olfati-Saber and Murray [2002b] build upon this insight to develop a decentralised controller for a directed network, based on a separation principle of coordinated rotations, coordinated translations, and shape preservation.

To properly control a rigid formation, it is important to consider whether any infinitesimal deviation from the desired formation will be observed by the distance constraints that are explicitly enforced. If this is the case, then the formation is termed *infinitesimally rigid*. This property is sufficient but not necessary for rigidity, although it will hold for almost all rigid formations of an agent network. It has proven to be of high interest for the analysis of popular gradient descent algorithms that are based on minimising a potential associated with distance errors (see e.g. Krick et al. [2009]; Oh and Ahn [2011]). In the case where the degrees of freedom in the agent states are not overconstrained, the formation possesses the stronger property of *minimal infinitesimal rigidity*, which can be used to achieve exponential stability for gradient-descent algorithms as done by Dörfler and Francis [2009]. Recent work by Sun et al. [2016] uses a similar approach, but relaxes the assumption of minimal rigidity. This is achieved by considering a subset of the state constraints, such that the formation is minimally rigid with respect to this subset. Another particularly useful result is that infinitesimal rigidity implies the set of goal configurations is a regular submanifold of the state-space. This has enabled techniques such as centre-manifold theory to be employed for stability analysis, as shown by Krick et al. [2009]. The geometrical argument constructed by Dörfler and Francis [2010] also exploits the submanifold structure of a set of equilibria to determine stability or instability. Their approach is illustrated by the example of a triangular formation enforced via a gradient control law, for which they demonstrate that the set of undesired equilibria is unstable. This enables them to conclude almost global asymptotic stability of the formation. For the practical application of rigidity theory to formation control, an important consideration is the preservation of a rigid structure under a switching graph topology, as might result from sensor limitations such as range constraints and obstacle occlusions. This issue has been addressed by Zelazo et al. [2012] using the construction of a *symmetric rigidity matrix*. The goal is achieved by ensuring that the switching graph topology induced by the agent motions does not cause the *rigidity eigenvalue* of the symmetric rigidity matrix to approach zero. Recently, Sun and Anderson [2015] have studied the relationship between the equilibria of rigid formations with single-integrator agent models and those of double-integrator agent models. The analysis models the double-integrator case as a parametrised Hamiltonian system, and leads to a result for local exponential stability. The theory is also extended to address the flocking scenario.

A particularly appealing aspect of rigidity-based formation control is that it provides a natural framework into which one can directly incorporate consideration of the available distance measurements. However, the majority of control algorithms, such as those mentioned above, cannot be implemented without full relative position measurements between *neighbouring* agents (i.e. the pairs of agents for which the relative state is directly controlled). This is quite a challenging issue to overcome and has become the focus of increasing attention in recent years. Cao et al. [2011] consider the case where *only* the distance between agents can be measured, and present a "stop-and-go" control algorithm for kinematic agents in $\mathbb{R}^2$. The idea here is to have agents take turns in stopping so that the moving agents can evaluate their relative positions by obtaining multiple distance measurements for triangulation. Recently, the task of rigidity maintenance without full relative state measurements has been considered by Zelazo et al. [2015] (extending the previously mentioned work by Zelazo et al. [2012]). In this work, only distance measurements between agents, and two additional bearing measurements available to a single agent, are required for implementation of the proposed control scheme. The bearing measurements, along with infinitesimal rigidity of the formation, enable a consensus protocol to be employed that estimates the relative positions of all agents in the network. Global estimates of the rigidity eigenvalue and the corresponding eigenvector can then be computed in a fully distributed manner. The result is a formation control scheme that permits a switching network topology as necessitated by obstacles, sensor occlusions, or range limitations.

In practice, the available sensors might not measure the distance between vehicles but may instead provide other *partial* measurements of relative position, such as the bearing measurements commonly obtained by onboard cameras. These alternative scenarios have motivated the study of other forms of rigidity in the literature, e.g. Eren [2012]; Franchi et al. [2012a]. The work of Eren [2012] builds upon earlier work by Desai [2002] to address *shape* maintenance (i.e. formation control up to scaling, rotations and translations) for kinematic nonholonomic agents in the plane. In this approach, each agent may follow either one or two leaders, which need not be common between all agents. If it follows a single leader, it regulates a desired distance l and bearing ψ; this arrangement is termed an $l - \psi$ control. Otherwise, the agent must preserve either the desired distances to each leader ($l - l$ control) or the desired bearings ($\psi - \psi$ control). Graph theory is employed to study the various network arrangements, and to accommodate changes to the network topology. The $\psi - \psi$ control arrangement is the primary focus of Eren [2012], and is built upon rigidity analysis for bearing-based formations. However, it should be noted that full relative position information for each link is required by the control implementation. This information is not required for the control algorithm proposed by Franchi et al. [2012a], who consider bearing-only formation control in $\mathbb{R}^3$ for a collection of agents equipped with onboard cameras. They designate two arbitrary agents as *beacon agents* that act as a reference for the other vehicles (i.e. with special control inputs), while the formation as a whole is guided via a haptic interface by a human pilot. The system is implemented using quadrotors and includes consideration of field-of-view constraints. The challenge of bearing-based formation control has also been studied recently by Zhao and Zelazo [2016], after establishing numerous properties of bearing rigidity. The resulting formation control scheme for kinematic agents is almost globally asymptotically stable for infinitesimally bearing-rigid formations, under a reasonable assumption on the initial agent orientations. It is worth noting that this control scheme does not require the agents to have common knowledge of a global reference frame.

The property of *persistence* (see e.g. Hendrickx et al. [2007]; Yu et al. [2007]) is closely related to rigidity and is of particular interest for formation control. The question of persistence arises when some agents are subject to constraints that they are not responsible for maintaining (or of which they are not aware), i.e. when the concept of rigidity is considered on directed graphs rather than undirected ones. The issue here is that an agent might satisfy all of the constraints it is concerned with but simultaneously make it impossible for other agents to satisfy theirs. A formation is *persistent* if it is both rigid and *constraint consistent*. Roughly speaking, the latter property ensures that if each agent continues to preserve the constraints it currently satisfies (and for which it is responsible), then all agents will be able to do so (i.e. regardless of any motion a particular agent might make while maintaining its assigned tasks). The work by Hendrickx et al. [2007] considers persistence for agents in $\mathbb{R}^2$, while that of Yu et al. [2007] addresses persistence in higher dimensions. In the latter scenario, there is an stronger concept of *structural persistence* which does not arise in the $\mathbb{R}^2$ case. This is associated with the possibility of *several* agents moving (while maintaining the constraints for which they are responsible) in such a way as to prevent the other agents from being able to preserve their constraints. A basic example of a persistent but not structurally persistent graph is one where two agents (leaders) are responsible for no constraints, and can therefore freely move away from each other, forcing the formation to fragment (this scenario cannot happen in $\mathbb{R}^2$ because a formation with two such leaders will not be persistent). The study of persistent formations is particularly relevant to the popular leader-follower control approach, since the directed maintenance of constraints is a natural component of this control architecture. For minimally persistent agent networks in $\mathbb{R}^2$, Yu et al. [2009]; Summers et al. [2011] have used linearisation techniques to present case-by-case control algorithms for particular leadership arrangements (i.e. particular allocations of responsibility for guiding the formation along its various degrees of freedom). The work by Eren [2012] on bearing formations also employs persistence analysis to motivate the study of a two-leader control architecture with an acyclic graph topology. More recently, Bayezit and Fidan [2013] have used persistence theory to generate reference trajectories that can be tracked by quadrotors and fixed-wing UAVs.

2.3 The Role of Passivity Theory

The idea in *passivity-based control* is to model the total energy present in the system, which may include *virtual energy* associated with the control law. Then, stability of the system can be achieved by designing the control law such that the total energy is strictly decreasing, with the desired system state being one of minimal energy. The following discussion of passivity-based control is motivated by two key considerations. The first is the task of *sensor-based* formation control, where the full state of the agents is not necessarily known. Passivity theory has proven to be a highly valuable tool for the sensor-based control of a single autonomous vehicle, and my research in this thesis draws inspiration from the literature reviewed in Subsection 2.3.1 concerning this subject. Secondly, for many of the formation control schemes derived from the geometrical structure provided by rigidity theory, only kinematic agent models are assumed. For many autonomous vehicles, and for more aggressive manoeuvres, a full dynamic agent model is more appropriate. Energy-based approaches are a very popular and natural way to incorporate dynamic agents into the control design and analysis, as reviewed in Subsection 2.3.2. Of particular note is the *port-Hamiltonian framework* briefly described in Appendix C.

2.3.1 State Estimation and Task-Based Control

A fundamental requirement for the control of an autonomous vehicle is knowledge of the vehicle's state. In the formation control literature, full state information is often assumed to be available (with some exceptions as noted in the preceding sections). However, in practice the state information available for each vehicle must typically be acquired by onboard sensors, which may not only suffer from noise and bias, but may also only provide *partial* state measurements (e.g. the bearing to a recognised landmark, but not the distance to it). To ensure that the control scheme can be implemented, it is clearly important to consider how the necessary information might be reliably obtained from available sensors.

A variety of state-estimation problems (involving a single vehicle) have been considered in the literature. Many of these assume measurements of linear acceleration and angular velocity are available via an onboard inertial measurement unit (IMU), which consists of accelerometers, gyrometers and magnetometers. The estimation of vehicle attitude from such measurements has been well-studied, see e.g. the filters on the Special Orthogonal group $SO(3)$ presented in Crassidis et al. [2007]; Mahony et al. [2008] and references therein.

Reliable position estimates in an inertial frame are more difficult to acquire, and usually depend on external motion capture systems or global positioning systems (GPS); thus, they require a relatively controlled environment with external infrastructure. Consequently, inertial position measurements are often unavailable underwater, in areas without a clear view to the sky (such as canyons or cities with many high-rise buildings), or in hostile environments where communication signals may be interrupted. A more practical method of deriving position estimates is to consider relative measurements to known features or landmarks. This solution has been explored by Vasconcelos et al. [2010], where state estimation on $SE(3)$ is achieved using position measurements to known landmarks as well as (possibly biased) measurements of linear and angular velocity.

Unfortunately, even the *relative* position measurements used in the approach of Vasconcelos et al. [2010] can be difficult to obtain from common onboard sensors such as cameras, which typically offer reasonable bearing information but poor distance estimates. The use of onboard cameras has found considerable popularity since they are cheap, lightweight, and offer an extraordinary amount of additional information about the environment, relative to other sensors. This has motivated extensive research concerned with the use of cameras for state estimation and autonomous control, which is generally known as the field of *visual servo control*. Two main visual servo control approaches are present in the literature, known as position-based visual servo (PBVS) control and image-based visual servo (IBVS) control, as outlined in the tutorials by Hutchinson et al. [1996]; Chaumette and Hutchinson [2006, 2007].

Position-based visual servo (PBVS) control involves estimating the full system state from visual data, for use by the control scheme. This motivates the use of *bearings* and inertial measurements for pose estimation on $SE(3)$, as considered by Baldwin et al. [2009]. Recently, Bras et al. [2015] have addressed position estimation in Euclidean space using a *single* bearing measurement and knowledge of linear velocity, assuming a persistence of excitation condition. Of course, attitude estimation on $SO(3)$ could be performed separately to obtain a full estimate of the vehicle's pose. Velocity estimates from visual and inertial information can also be obtained, as described by Cheviron et al. [2007].

Image-based visual servo (IBVS) control is an alternative that follows a task-based approach and provides inspiration for the control strategy used in this thesis. The idea is to have the desired system state specified in terms of the features in the camera's image, with the goal being to move the vehicle in such a way that the camera's image matches the specified one. The IBVS control approach has a couple of advantages; it is less computationally intensive and is typically more robust to camera calibration errors (Hutchinson et al. [1996]). One of the classical challenges met in IBVS control is the necessity of estimating the depth of the features in the image, and this problem has seen thorough investigation in the literature (see Corke and Hutchinson [2001], for example). Comport et al. [2011] have proposed a useful model of the visual servo control problem for a generalised configuration of the imaging system; that is, the case where a camera is offset from the centre of mass of the vehicle. This is achieved via the use of Plücker coordinates, which can be used to represent the line from the location of the offset camera to a point in the 3-D scene. Of particular note for my present research is the application of passivity theory to the IBVS control problem, as studied by Fujita et al. [2007] and via the bondgraph modelling approach of Mahony and Stramigioli [2012].

2.3.2 Passivity-Based Formation Control

Due to the high complexity of the formation control problem, energy-based approaches have become popular as a way of simplifying the stability analysis. In general, it can be difficult to find a suitable candidate Lyapunov function for formal stability proofs, and consequentially it is common for the control design to be specifically developed around the shaping of an appropriate virtual energy function. The control law in these approaches is given by the negative gradient of this energy function; thus, the formation is driven to a state of minimum energy that corresponds to the desired state of the system. Energy-based approaches are particularly well-suited to behavioural control strategies, since they provide a convenient way of analysing the behaviour resulting from multiple control factors.

An early energy-based approach to formation control has been presented by Leonard and Fiorelli [2001], where the coordinated rotation and translation of agents is achieved using a combination of various artificial potentials. Each artificial potential is constructed to achieve a single component of the full formation control objective; in particular, the individual potentials are used to regulate the distance between two agents, to regulate the distance between an agent and a *virtual leader* that guides the formation, or to enforce a desired velocity across the network. This framework was extended by Ögren et al. [2004] to address the task of seeking local maxima or minima in an environmental field (e.g. temperature). The idea here is to estimate the gradient of the field from the individual measurements obtained by each agent in the formation. Particular attention is given to the optimal formation of the agents for robustness to local noise in the field. Meanwhile, Olfati-Saber and Murray [2002a] have employed graph theory to define a *structural potential function* from which a control law can be derived. In this setting, rigidity analysis can be used to provide some assurance against undesired equilibria and collisions.

An extension of the basic formation control task is to guide the formation as a whole along a specified *path*. A popular formulation of this scenario involves parametrising the path and synchronising the agents' local values for the parameter. Ihle et al. [2006] present two passivity-based solutions for this scenario, one of which solely focuses on the synchronisation of the local path parameters, while the other instead uses *time* as the path parameter and corrects deviations from the resulting specified *trajectory*. The passivity framework has also been employed by Arcak [2007] to achieve coordination between a group of agents possessing a bidirectional network topology. Extensions include a discrete-time implementation and a time-varying topology. A more recent variant of this control approach, where the tasks of path-tracking in space and coordination in time are decoupled, is presented by Wang et al. [2012].

Energy-based approaches have also been applied to formations on non-Euclidean state-spaces. Sarlette et al. [2007] compare a consensus approach with an energy-based approach for the task of attitude synchronisation between agents in $SO(3)$. The advantage of the energy-based approach is that it avoids restrictions on the final angular velocity of the synchronised agents, and also leads to an implementation that does not require knowledge of the absolute angular velocities (only the relative ones). However, it relies on a fixed, undirected and connected communication topology. An energy-shaping approach is also developed by Nair and Leonard [2007] for the synchronisation of agents in $SO(3)$ and $SE(3)$, based on the method of Lagrangian reduction. Two variants of the energy-based approach for $SO(3)$ are presented in Sarlette et al. [2009]; one leads to almost global asymptotic stability while the other provides local asymptotic stability for a class of time-varying communication topologies. A passivity-based approach to the task of pose synchronisation between kinematic agents in $SE(3)$ has been presented by Hatanaka et al. [2012], with an exponential rate of convergence proven for a local neighbourhood. Extensions include achieving a common desired velocity, accounting for communication delays, allowing a time-varying network topology (which is permitted to temporarily fail the common assumption of strong connectivity), and an approach to flocking.

A popular framework for the development of passivity-based formation control is that of port-Hamiltonian theory (Duindam et al. [2009]). In this framework, nonnegative energy functions (Hamiltonians) are used to describe the energy in the various components of the system, and ports are used to model the exchange of energy between these elements as well as with the external environment. An introduction to this theory is provided in Appendix C. The merits of this approach have been strongly demonstrated by the work of Franchi et al. [2012b], where a haptic interface with a human pilot is developed to guide a formation of agents in a decentralised and passive manner. The port-Hamiltonian framework readily enables stability analysis to be performed across the various aspects of the system. Attention is given to formation regulation, stability with respect to the control input from the human, collision avoidance between vehicles and the environment, and the allowance of a time-varying network topology as may be induced by obstructions to the onboard relative state sensors. The latter is a particularly non-trivial problem since establishing control links between vehicles introduces energy to the system. It is addressed by monitoring reserves of available energy across the agents in the network, which are typically recharged through the dissipation of energy by the control terms. Further extensions have been presented by Secchi et al. [2012] in order to accommodate non-negligible delays between the control interface and the agents, as well as between pairs of agents.

The use of virtual mechanical couplings to regulate the relative positions of agents is a well-established technique that can be naturally represented in the port-Hamiltonian framework. This approach has been employed by Vos et al. [2014] to obtain an evenly-spaced deployment of satellites around an orbit, and by Vos et al. [2016] to achieve formation control for a line of nonholonomic agents tracking a constant reference heading and velocity. This work benefits from the theory of *canonical transforms* for port-Hamiltonian systems, as developed by Fujimoto and Sugie [2001]; Fujimoto et al. [2003]. A possible extension of the classical virtual coupling approach is to passively vary the parameters of the virtual springs over time, using the theory for variable springs outlined in Stramigioli and Duindam [2001]. Among other objectives, this could be used to produce a time-varying formation, although I am not aware of any work that specifically applies this extension to formation control scenarios. It is also worth mentioning the general theory for port-Hamiltonian systems on graphs developed by van der Schaft and Maschke [2013], from which a basic formation control architecture using virtual couplings can be derived.

Note that none of the energy-based approaches in the aforementioned formation control literature are directly applicable to the case where only *partial* relative position information is available between pairs of agents. I am not aware of any literature that addresses this shortcoming with a passivity-based framework.

2.4 Conclusions from the Literature

Two decades ago, growing interest in the coordination of multiple autonomous vehicles led to a number of new formation control schemes being proposed in the literature (see Lewis and Tan [1997]; Balch and Arkin [1998]; Leonard and Fiorelli [2001]; Das et al. [2002]). Several of these earlier works also accommodated nonholonomic agent models, as motivated by the wheeled ground vehicles available at the time. As the field developed, researchers turned more attention to communication architectures such as the one proposed by Beard et al. [2001]. In 2003, Murray et al. [2003] identified networked systems as a key subject for future control applications, and this may have contributed the popularity of consensus-based approaches to formation control as reviewed by Olfati-Saber et al. [2007]; Ren et al. [2007], which enable particular attention to be given to the communication topology. Approaches based on rigidity theory also built upon the graph-based framework of consensus algorithms, as reviewed by Anderson et al. [2008].

While much of the research in autonomous control up to this point had focussed on vehicles in either Euclidean space or $\mathrm{SE}(2)$, further technological developments soon motivated the consideration of more complex agent models in $\mathrm{SE}(3)$. For example, the quadrotor (shown in Figure 2.1) is an underactuated aerial vehicle for which horizontal translations are achieved via attitude control (i.e. setting the direction of thrust from the rotors). As a consequence, the task of *state-estimation* (as considered by Vasconcelos et al. [2010]) required renewed attention for the autonomous control of single vehicles, with a particular need to focus on the use of cheap, lightweight sensors. At the same time, improvements in computational capabilities made vision

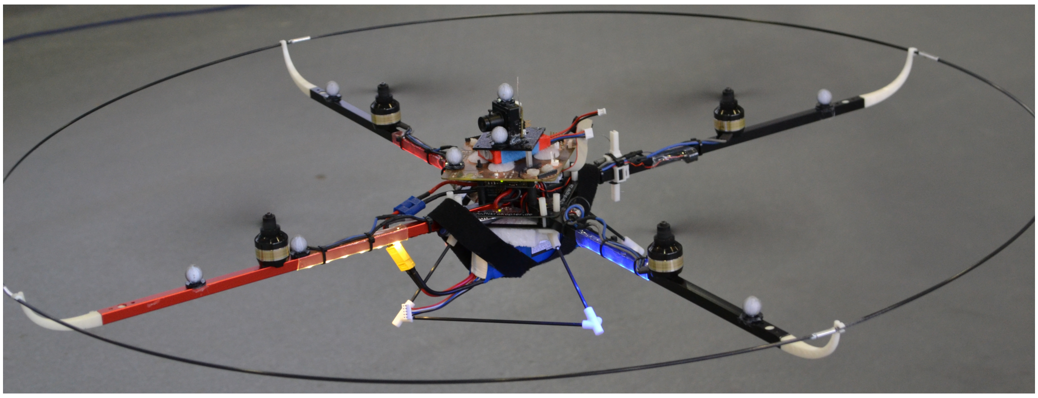

Figure 2.1: A quadrotor vehicle from the ANU Computer Vision and Robotics Lab.

processing algorithms more feasible, setting the scene for the widespread use of on-board cameras. As a result, techniques from the field of image-based visual servo (IBVS) control (summarised by Hutchinson et al. [1996]; Chaumette and Hutchinson [2006, 2007]) transitioned from early applications concerning robotic manipulators to the autonomous control of aerial vehicles. New passivity-based approaches to IBVS control, such as those of Fujita et al. [2007]; Mahony and Stramigioli [2012], are of particular note.

In recent years, formation control schemes have been extended to agents in three-dimensional space, with sensor limitations now being recognised as a significant aspect of the problem (previously, vehicles in the plane had a greater capacity to carry onboard sensors and the state-estimation problem for such vehicles is less difficult). Rigidity theory has continued to play a critical role in the field, since it provides a natural tool for regulating full relative positions in Euclidean space using measurements of the *distances* between agents (see e.g. Zelazo et al. [2015]). Extensions of rigidity theory have enabled similar approaches using *bearing* measurements as are typically obtained from onboard cameras (see e.g. Franchi et al. [2012a]); however, general agent state-models (including combinations of agents in *different* state-spaces) and general sensor arrangements (involving multiple different sensor modalities) are yet to be addressed. Meanwhile, passivity-based techniques have emerged as an alternative that is well-suited for *dynamic* agent models, as considered by Franchi et al. [2012b]. A current issue for passivity-based approaches to formation control is that they do not accommodate limitations in the knowledge of the agent states.

Today, formation control remains a very active research subject in the literature. The above discussion highlights a particular need to address the subject of *sensor-based* formation control, and thus motivates the research presented in this thesis. In particular, my contributions build upon the aforementioned work by extending rigidity theory to far more general system models (involving arbitrary agent states and sensor configurations), and by developing a passivity-based framework that requires only *partial* relative position information as is commonly provided by onboard sensors.

Chapter 3

Generalised Rigidity Theory

This chapter considers a generalisation of the classical rigidity theory presented in Appendix B. In particular, the generalised framework accommodates agents that lie in arbitrary (non-Euclidean) state-spaces, and permits generic state constraints in the form of a fixed value for an output map from the system state. The formulation is developed with respect to a symmetry of the system that is described by the action of a topological group. A primary focus of the work in this chapter is to illustrate how a formation of agents may be modelled within this generalised rigidity framework. I also introduce the notion of *path-rigidity*, which describes the case where the set of states permitted by the constraints is path-connected. This property ensures that one can continuously transition between any two such states without breaching the state constraints. The material in this chapter draws from the publication Stacey et al. [2016].

3.1 Introduction

Classical rigidity theory (as described by Jackson [2007]) studies whether a given set of distance constraints between nodes in $\mathbb{R}^2$ or $\mathbb{R}^3$ is sufficient to enforce rigid-body behaviour of the nodes (i.e. such that only global translations and rotations are possible without breaching the constraints). This classical concept of rigidity has proven useful in a wide range of applications, from the analysis of tensegrity frameworks (see Juan and Tur [2008]) to the study of chemical molecules (see e.g. the collection of papers in Thorpe and Duxbury [1999]).

More recently, rigidity theory has found application to the tasks of network localisation as demonstrated by Aspnes et al. [2006], and formation control as studied by e.g. Olfati-Saber and Murray [2002c]; Anderson et al. [2008]; Krick et al. [2009]. In these settings, the state constraints on the agent network often correspond to values measured by the available sensor modalities. Rigidity theory can be used to provide insight into the observability of the system state; specifically, it describes the symmetry up to which the full state can be determined. The fact that the state constraints may take forms other than distances is a particularly interesting aspect of these applications, and this observation has motivated several reformulations of the classical notion of rigidity. For example, the use of bearings has been considered by

Eren [2011] in the context of network localisation, and by Franchi et al. [2012a]; Zhao and Zelazo [2016] for the task of formation control. A further complication is that the agent states commonly consist of orientation as well as position, motivating the formulation of rigidity by Zelazo et al. [2014] for agents in $SE(2)$. More advanced scenarios may involve several different types of constraints (imposed by a variety of available sensor modalities), or agents that lie in different state-spaces (e.g. where aerial vehicles are in coordination with ground vehicles). Rather than reformulate rigidity theory on a case-by-case basis for each situation, it is clearly desirable to develop a more general rigidity framework that can readily accommodate a much broader class of scenarios.

Classical rigidity analysis is typically performed with respect to a network graph (see e.g. Laman [1970]; Asimow and Roth [1978, 1979]; Connelly [2005]); however, the generalisation of this framework to accommodate mixed agent states and constraints, as well as constraints involving more than two agents, is not straightforward. A more general notion of rigidity can be defined with respect to a symmetry described by the action of a topological group. Schreck and Mathis [2006] have applied this interpretation in the context of computer-aided design (CAD) to consider the rigidity of systems with multiple types of constraint. More recently, the notion of *affine rigidity* has been studied by Gortler et al. [2013] using the action of monoids on Euclidean space. Aside from these works, the formulation and analysis of rigidity with respect to group symmetries has received somewhat limited attention in the literature, and a sufficiently general framework for network localisation and formation control applications is yet to be presented.

In this chapter, I develop a highly generalised rigidity framework that readily accommodates agents in differing state-spaces and with various types of state constraints. The basic formulation is constructed using tools from topology and group theory, both of which are studied in Singh [2013]. Specifically, I characterise rigidity as a type of symmetry associated with the action of a topological group on the full state-space of the system. I use the term *formation* to refer to the set of agent states that satisfy a given collection of state constraints. A formation is termed *rigid* (in either a local or global region) if all agent configurations satisfying the constraints lie in the orbit of this group action. Within this framework, I introduce the notion of *path-rigidity*, which describes the case where one can transition between any two configurations of a globally rigid formation without breaking the constraints. I characterise this property with a useful group theoretic result. Aside from offering useful global structure, path-rigidity is of particular interest in the case of non-differentiable sensor modalities, for which theory from infinitesimal rigidity (see Chapter 4, and also Asimow and Roth [1979]) cannot be applied.

The remainder of this chapter is as follows. In Section 3.2, I formalise the structure of an agent network and introduce the notions of symmetry that will be used to describe rigidity. The generalised definition of rigidity is presented and studied in Section 3.3. In Section 3.4 I introduce the notion of *path-rigidity*, and provide a simple characterisation of this property using group-theoretic analysis. A brief conclusion for the chapter is given in Section 3.5.

3.2 System Model and Symmetries

In this section I formalise the structure associated with the agent networks considered in this chapter. The model of the system is presented in Subsection 3.2.1 along with several motivating examples, while Subsection 3.2.2 discusses the associated symmetry that is described by the action of a topological group. This will lead to a formal definition of generalised rigidity in the next section.

3.2.1 Agent Networks and Formations

Consider a system with a state x that lies in a set $\mathcal{M}$. Assume $\mathcal{M}$ is equipped with a Hausdorff topology $\tau(\mathcal{M})$, and let $\mathcal{M}^\tau := (\mathcal{M}, \tau(\mathcal{M}))$ denote the resulting topological space. Throughout this chapter, I will commonly suppose the full state $x \in \mathcal{M}^\tau$ is constructed from the individual states of N agents, with agent i having state x_i in a topological space $\mathcal{M}_i^\tau$. However, it should be noted that this structure is not required for the main development. Although it is very common to consider a product space $\mathcal{M}^\wp := \prod_{i=1}^N \mathcal{M}_i^\tau$ (Example 3.2.1), I do not assume this scenario. The generality of this formulation is motivated by Examples 3.2.2 and 3.2.3.

Example 3.2.1. A simple and very common scenario is where each agent x_i lies in a Hausdorff topological space $\mathcal{M}_i^\tau$, and the full state-space possesses the product structure $\mathcal{M}^\wp := \prod_{i=1}^N \mathcal{M}_i^\tau$. In this case, the state-space $\mathcal{M}^\wp$ inherits the Hausdorff topology from the individual state-spaces $\mathcal{M}_i^\tau$. Many other desirable properties, such as differentiability of the state-spaces, can also be inherited in this way. ⋄

Example 3.2.2. The consideration of other constructions for $\mathcal{M}^\tau$ is motivated by the scenario where vehicles share a physical state-space. Suppose that $\mathcal{M}_i^\tau = \mathcal{M}_j^\tau$ for all $i, j \in \{1, \dots, N\}$, with $\tau(\mathcal{M}_i)$ a Hausdorff topology. In this case, states where $x_i = x_j$ for some $i, j \in \{1, \dots, N\}$ are not physically feasible since this corresponds to a collision between the vehicles. Such situations are also problematic for certain sensor modalities; for example, range measurements (see Example 3.2.9) become nonsmooth at such points, and direction-based measurements (Example 3.2.12) become ill-defined at these points. Therefore, it can be appropriate to exclude such points from rigidity analysis by considering the set $\mathcal{M}^\tau := \mathcal{M}^\wp \setminus \mathcal{W}$, where $\mathcal{W} := \{x \in \mathcal{M}^\wp \mid x_i = x_j\}$. Since $\mathcal{M}^\tau$ is an open subset of $\mathcal{M}^\wp$, it can be given the induced topology of the product space. More formally, a set $\mathcal{U} \subseteq \mathcal{M}^\tau$ is open if and only if it is open as a subset $\mathcal{U} \subseteq \mathcal{M}^\wp$. Note that subspaces of $\mathcal{M}^\wp$ will inherit the Hausdorff structure. It should also be noted that $\mathcal{M}^\tau$ is *not* a product space; each vehicle can occupy any position in the common state-space $\mathcal{M}_i^\tau$, but its position imposes a constraint on those of the other vehicles. ⋄

An interesting motivation for the generality of the proposed framework is given by the case where agents are *interchangeable*; that is, where one is not concerned with which particular agent occupies each position. This scenario arises, for example, in the subject of *flocking* as defined by Reynolds [1987] and studied by Olfati-Saber

[2006]. To the best of my knowledge, this problem has not previously been considered from a topological perspective, although some very interesting topological structure is involved. For example, the state-space of the full agent network is not the product space $\mathcal{M}^{\wp}$ of the individual agent state-spaces, as in Example 3.2.1, but is instead the *quotient* of this product space by permutations of the agents, as discussed in Example 3.2.3, below. The proposed rigidity framework is well-suited to modelling and analysing such scenarios, and I will address some related considerations via several other examples and remarks throughout this chapter.

Example 3.2.3. Suppose that all agents lie in the same Hausdorff topological space, i.e. that $\mathcal{M}_i^\tau = \mathcal{M}_j^\tau$ for all $i, j \in \{1, \ldots, N\}$, and that we wish the agents to be *interchangeable*. Thus, two states $\tilde{x}, \tilde{x}'$ in the product space $\mathcal{M}^{\wp}$ are equivalent if $\tilde{x}'$ can be obtained from $\tilde{x}$ by switching the positions of the agents (or by reassigning the agent indexes). To model this scenario, let $\mathbf{P}_N$ denote the group of permutations of N elements. The action on an N-tuple $\tilde{x} = (x_1, \ldots, x_N) \in \mathcal{M}^{\wp}$ by a permutation $\sigma \in \mathbf{P}_N$ is defined by $\sigma(\tilde{x}) := (\sigma_1(\tilde{x}), \ldots, \sigma_N(\tilde{x}))$, with $\sigma_i(\tilde{x}) := x_j$ for some $j \in \{1, \ldots, N\}$ and each j appearing exactly once in the list. With interchangeable agents, the true system state lies in the quotient space $\mathcal{M}^\tau := \mathcal{M}^{\wp} / \sim$, where $\tilde{x} \sim \tilde{x}' \Leftrightarrow \exists \sigma \in \mathbf{P}_N : \tilde{x}' = \sigma(\tilde{x})$ defines an equivalence relation for $\tilde{x}, \tilde{x}' \in \mathcal{M}^{\wp}$. The equivalence relation $\sim$ imposes a natural quotient topology on the full state-space $\mathcal{M}^\tau$; specifically, I employ the *final topology* of the natural projection $\pi : \mathcal{M}^{\wp} \to \mathcal{M}^\tau$ (i.e. a set $\mathcal{U} \subseteq \mathcal{M}^\tau$ is open if and only if the pre-image $\pi^{-1}(\mathcal{U}) \subseteq \mathcal{M}^{\wp}$ is open). Note that this construction ensures that π is an open map. Furthermore, the equivalence relation $\sim$ is closed in $\mathcal{M}^{\wp} \times \mathcal{M}^{\wp}$ since it is the product of $\mathcal{M}^{\wp}$ with a finite number of singletons corresponding to the permutations of the agents. By [Singh, 2013, Proposition 7.1.6], these conditions are sufficient to conclude that the quotient space $\mathcal{M}^\tau$ is Hausdorff. ◇

Remark 3.2.4. In many practical applications, it is desirable for the state-space to be smooth. If the state-space is the quotient of a smooth manifold by a smooth, free, and proper action of a Lie group, then smoothness is ensured by the quotient manifold theorem [Lee, 2013, Theorem 21.10] (see also [Lee, 2013, Theorem 21.13] for the case where this group is discrete). Further insight for a discrete Lie group is provided via [Lee, 2013, Lemma 21.11], which offers sufficient and necessary conditions for the group action to be proper. In particular, for the case of agent permutations as in Example 3.2.3, smoothness of $\mathcal{M}^\tau$ can be obtained by excluding points where two or more agents are co-located, as in Example 3.2.2 (in fact, this is necessary for the action to be free as well as proper). ◇

The full state of the system is measured via an output map $h : \mathcal{M}^\tau \to \mathcal{Y}$, which will be used to specify constraints that define a formation. Note that for the most general formulation of rigidity, a topology on the output space $\mathcal{Y}$ is not required. However, for many applications the topology $\tau(\mathcal{Y})$ of $\mathcal{Y}$ is an important consideration for system analysis, and for such cases in this chapter I will denote the relevant topological space by $\mathcal{Y}^\tau$. A specific output value of a given state $x \in \mathcal{M}^\tau$ is denoted by

$$y := h(x) \in \mathcal{Y}.$$

As outlined in Remark 3.2.5, the map h will typically be composed of a set of M functions corresponding to the sensor modalities available to the agents. Therefore, in the following examples and remarks I will commonly consider a measurement y_k from a sensor modality $h_k : \mathcal{M}^\tau \to \mathcal{Y}_k$.

Remark 3.2.5. Suppose we have a set of M *sensor modalities*, each described by a map $h_k : \mathcal{M}^\tau \to \mathcal{Y}_k$ with a *state measurement* $y_k := h_k(x)$ in a *measurement space* $\mathcal{Y}_k$. Typically, the full output map will possess the product structure, i.e. $y := h(x) := (h_1(x), \ldots, h_M(x)) \in \mathcal{Y}$, where $\mathcal{Y} := \prod_{k=1}^{M} \mathcal{Y}_k$. However, for the general development I will allow non-product topologies on $\mathcal{Y}$ as motivated later by Example 3.2.24. Note that the individual sensor modalities h_k, and the measurement spaces $\mathcal{Y}_k$, need not be the same for all k. It is also commonly the case that a sensor modality h_k will not depend upon the full state $x \in \mathcal{M}^\tau$, but will instead be a function of only two agent states x_i and x_j in a product space $\mathcal{M}^\wp$. ◇

Remark 3.2.6. Although a topology on $\mathcal{Y}$ (or $\mathcal{Y}_k$) is not strictly required for the formal definition of rigidity, it is often highly desirable for $h(x)$ to be continuous, or even differentiable. This structure can play an important role in the analysis of the system, particularly for applications such as formation control (see Subsection 4.4.2). Throughout this chapter, I will assume the topology $\tau(\mathcal{Y}_k)$ on each measurement space is at least T_0 (Kolmogorov). It is worth noting that some common sensor modalities (e.g. directions, see Example 3.2.12) are not continuous under any finer topology. This observation motivates careful consideration of the topology associated with examples and discussions in the sequel. It is also helpful to note that the T_0 property will be inherited by the product space $\mathcal{Y}^\wp$. ◇

Remark 3.2.7. It should be noted that for the purposes of rigidity we are not interested in the availability of the measurement y_k to particular agents in the system. While this is an important consideration for many applications, such as formation control, the property of rigidity is only concerned with whether certain constraints $y_k = \mathring{y}_k$ are satisfied. An interesting extension is the concept of *persistence*, where only one agent is aware of each constraint (as considered by Hendrickx et al. [2007]; Yu et al. [2007] for the classical case); however, this avenue of research is not pursued in this thesis. ◇

Remark 3.2.8. Although this work regards $h_k(x)$ as a sensor modality, it may alternatively be interpreted as a *task function* that measures the system state with respect to a goal. Antonelli and Chiaverini [2006] present some interesting examples of task functions, as well as a control strategy based on the inverse kinematics described by these functions. ◇

Below, I present numerous examples of sensor modalities that are of interest to network localisation and formation control tasks. Some of these possess interesting topological structures that are not readily addressed by less general frameworks, and several will be employed in later examples.

Example 3.2.9. Suppose the full state $x \in \mathcal{M}^{\wp}$ of a system possesses the product structure as in Example 3.2.1. Consider two agents i and j with states $x_i, x_j \in \mathbb{R}^d$ (with $d \geq 1$). A *range* or *distance* measurement between these agents is given by

$$y_k := h_k(x_i, x_j) := \|x_i - x_j\| \in \mathbb{R}_{\geq 0},$$

where $\|\cdot\|$ denotes the Euclidean norm of a vector and $\mathbb{R}_{\geq 0}$ denotes the set of non-negative real numbers. $\diamond$

Example 3.2.10. Suppose the full state[1] $X \in \mathcal{M}^{\wp}$ of a system possesses the product structure, and consider two agents with states $X_i, X_j \in \mathrm{SE}(3)$ in the Special Euclidean group of dimension 3. The matrix representation for these states is

$$X_i := \begin{pmatrix} R_i & \xi_i \\ 0_3^\top & 1 \end{pmatrix}. \tag{3.1}$$

Here, $R_i \in \mathrm{SO}(3)$ is a 3×3 rotation matrix (i.e. an orthogonal matrix of determinant 1), $\xi_i \in \mathbb{R}^3$ is a position vector, and 0_3 is the 3-vector for which all entries are zero. Let $y_j^0 \in \mathbb{R}^3$ be a point fixed with respect to agent j (typically the origin). A *position* measurement of y_j^0 expressed in the body-fixed frame of agent i is described by

$$\bar{y}_k := \overline{h_k(X_i, X_j)} := X_i X_j^{-1} \bar{y}_j^0, \tag{3.2}$$

where $\bar{v} := (v^\top, 1)^\top$ denotes a vector v expressed in homogeneous coordinates. $\diamond$

Example 3.2.11. Suppose the state-space $\mathcal{M}^{\wp}$ of a system is equipped with the product structure, and consider two agents with states $X_i, X_j \in \mathrm{SE}(3)$ as in (3.1). For this case, a *bearing* measurement in the *body-fixed frame* of agent i is described by

$$y_k := h_k(X_i, X_j) := \begin{cases} R_i \frac{\xi_j - \xi_i}{\|\xi_j - \xi_i\|} \in \mathbb{S}^2 & \xi_i \neq \xi_j \\ \aleph & \text{otherwise,} \end{cases}$$

where $\mathbb{S}^2$ denotes the unit sphere and $\aleph$ is an exceptional point. Note that, since this measurement does not depend upon the orientation R_j of agent j, it can be similarly applied for an agent state $x_j \in \mathbb{R}^3$.

The measurement space for the bearing measurement is given by $\mathcal{Y}_k := \{\mathbb{S}^2 \cup \{\aleph\}\}$. This can be assigned the T_0 topology $\tau(\mathcal{Y}_k) := \{\tau(\mathbb{S}^2), \{\mathbb{S}^2 \cup \{\aleph\}\}\}$, which makes $h_k(X_i, X_j)$ continuous. It is worth noting that this is the final topology of $\mathcal{Y}_k$ with respect to $h_k(X_i, X_j)$; i.e. there is no finer topology for which $h_k(X_i, X_j)$ is continuous. To see this, observe that the pre-image $h_k^{-1}(\aleph) \subseteq \mathrm{SE}(3) \times \mathrm{SE}(3)$ consists of all points where $\xi_i = \xi_j$ (with R_i and R_j arbitrary), which is closed and not open. This implies that $\{\aleph\}$ cannot be an open subset of $\mathcal{Y}_k^\tau$ (in particular, $h_k(X_i, X_j)$ is not continuous for $\tau(\mathcal{Y}_k) := \{\tau(\mathbb{S}^2), \{\aleph\}\}$). Furthermore, observe that for any open neighbourhood $\mathcal{U}_{h_k^{-1}(\aleph)}$ of $h_k^{-1}(\aleph)$, the image $h_k(\mathcal{U}_{h_k^{-1}(\aleph)})$ is $\mathcal{Y}_k$. $\diamond$

[1] In this chapter I will use capitals to indicate states that are expressed in matrix form.

Bearing measurements are often obtained from onboard cameras, which do not typically provide good depth information. In the case where the vehicle's attitude is known (as may be achieved using an inertial measurement unit), bearing measurements can be de-rotated into the inertial frame to obtain an *inertial direction measurement* as modelled in the following example.

Example 3.2.12. Consider a system with a product structure on the full state-space $\mathcal{M}^{\wp}$. An *inertial direction* measurement between two agents with states $x_i, x_j \in \mathbb{R}^3$ is given by

$$y_k := h_k(x_i, x_j) := \frac{(x_j - x_i)}{\|x_j - x_i\|} \in \mathbb{S}^2$$

if $x_i \neq x_j$, and $y_k := h_k(x_i, x_j) := \aleph$ otherwise. The measurement space $\mathcal{Y}_k^{\tau}$ is identical to that of bearing measurements, given in Example 3.2.12. $\diamond$

Remark 3.2.13. The T_0 topology of the measurement space in Examples 3.2.11 and 3.2.12 can be problematic for analysis. In particular, the lack of a differentiable structure on $\mathcal{Y}_k^{\tau}$ prevents an interpretation of infinitesimal rigidity (see Section 4.2) for this scenario. However, in the case where co-located agents are not of interest (e.g. for the purposes of developing a controller that avoids collisions between agents), the problematic states for which $y_k = \aleph$ can be removed in the manner described by Example 3.2.2. The resulting (local) output space will then possess the desired structure. $\diamond$

Measurements of the angles formed between agents are another practical sensor modality that does not rely on knowledge of the inertial frame. They are a classical example of a measurement that depends on more than two agent states.

Example 3.2.14. Suppose the state-space $\mathcal{M}^{\wp}$ of a system is equipped with the product structure, and consider an agent $x_p \in \mathbb{R}^3$ that measures the angle between two other agents $x_i, x_j \in \mathbb{R}^3$. Such a measurement is described by

$$\begin{aligned} y_k &:= h_k(x_p, x_i, x_j) \\ &:= \begin{cases} \cos^{-1}\left(\frac{(x_i - x_p)^\top (x_j - x_p)}{\|x_i - x_p\|\|x_j - x_p\|}\right) \in \mathbb{S}^1/\sim & x_p \neq x_i, x_p \neq x_j \\ \aleph & \text{otherwise,} \end{cases} \end{aligned}$$

where $\aleph$ denotes an exceptional point and $\theta_1 \sim \theta_2 \Leftrightarrow \theta_1 = \pm\theta_2$ defines an equivalence relation for $\theta_1, \theta_2 \in [-\pi, \pi)$. In this case, the measurement space is $\mathcal{Y}_k := \{(\mathbb{S}^1/\sim) \cup \{\aleph\}\}$ and it can be given the T_0 topology $\tau(\mathcal{Y}_k) := \{\tau(\mathbb{S}^1/\sim), \{(\mathbb{S}^1/\sim) \cup \{\aleph\}\}\}$ (cf. the similar scenario in Example 3.2.11). $\diamond$

One interesting possibility that has received very little attention in the formation control literature is a sensor modality that cannot distinguish between the agents it observes (although the regulation of constraints based on such cases has received some attention in flocking algorithms, e.g. Olfati-Saber [2006]). Sensor modalities of this form can be readily modelled with the proposed framework.

Example 3.2.15. Consider a state-space $\mathcal{M}^{\wp}$ equipped with the product topology, and suppose an agent p with state $x_p \in \mathbb{R}^3$ is equipped with a sensor that can detect the range to $N-1$ other agents $x_i \in \mathbb{R}^3$, without distinguishing which agent corresponds to each distance. Such a sensor modality can be modelled by the mapping

$$h_k(x) := \{\|x_i - x_p\|\}_{i \neq p} \in \mathcal{Y}_k^{\tau}.$$

Here, the measurement space is defined by $\mathcal{Y}_k^{\tau} := \mathbb{R}_{\geq 0}^{N-1} / \sim_{y_k}$, where $\tilde{y}_k \sim_{y_k} \tilde{y}_k' \Leftrightarrow \exists \sigma \in \mathbf{P}_{N-1} : \tilde{y}_k' = \sigma(\tilde{y}_k)$ defines the equivalence relation (for $\tilde{y}_k, \tilde{y}_k' \in \mathbb{R}_{\geq 0}^{N-1}$). ◇

The interest in some sensor modalities may not be primarily motivated by physical sensors, but may instead be concerned with developing an appropriate model for a particular application. For example, constraints on the system imposed by the requirement of collision avoidance need only ensure that the closest pair of agents satisfy a minimum safety distance.

Example 3.2.16. Suppose a state-space $\mathcal{M}^{\wp}$ is equipped with the product topology, and consider a collection of N agents with states $x_i \in \mathbb{R}^3$. The smallest distance between any two agents is given by

$$y_k := h_k(x) := \min_{i,j \in \{1,\ldots,N\}} \|x_i - x_j\| \in \mathbb{R}_{\geq 0}. \qquad \diamond$$

I now formalise the structure of a *generalised agent network* for my study of rigidity.

Definition 3.2.17. A *generalised agent network* is described by $\mathcal{N} := (\mathcal{M}^{\tau}, \mathcal{Y}, h)$, where $h : \mathcal{M}^{\tau} \to \mathcal{Y}$ is the output map from the Hausdorff topological state-space $\mathcal{M}^{\tau}$ to the output space $\mathcal{Y}$. ◇

Remark 3.2.18. Although this generalised notion does not involve a graph structure, it accommodates a similar interpretation of a network to the classical case (c.f. Definition B.9) under appropriate constructions of h and $\mathcal{M}^{\tau}$, as discussed in the prior examples and remarks. The classical graph structure used in many formation control problems does not readily accommodate certain possibilities allowed by the generalised framework, such as having agents in different state-spaces and measurements involving more than two agents. However, it should be acknowledged that graph-based techniques may still be of value for analysis in the generalised setting. For example, one promising avenue for future research is to consider the use of graph automorphisms to describe agent permutations. In more specific scenarios, graphs may also continue to play an important role in algorithms for constructing rigid agent networks (e.g. in a manner similar to the Henneberg construction for the classical case, as outlined in Anderson et al. [2008]). ◇

For convenience, I will simply use the term *agent network* to refer to the generalised definition in the sequel. For the discussion of agent networks, I introduce the following terminology.

Definition 3.2.19. A *configuration* of an agent network $\mathcal{N} := (\mathcal{M}^\tau, \mathcal{Y}, h)$ specifies a fixed state $x \in \mathcal{M}^\tau$. $\diamond$

Remark 3.2.20. The popular notion of a *framework* (Jackson [2007]; Krick et al. [2009]) from classical rigidity theory (see Definition B.12) can be generalised to an agent network $\mathcal{N} := (\mathcal{M}^\tau, \mathcal{Y}, h)$ along with a configuration $x \in \mathcal{M}^\tau$. However, I find that this terminology is of limited value in the discussion of formations, and will not use it in this thesis. $\diamond$

Definition 3.2.21. For a given agent network $\mathcal{N} := (\mathcal{M}^\tau, \mathcal{Y}, h)$, two configurations $x, x' \in \mathcal{M}^\tau$ are *equivalent* (Jackson [2007]; Zelazo et al. [2015]) or *indistinguishable* if $y = h(x) = h(x') = y'$. $\diamond$

A major advantage of the rigidity framework developed in this thesis is that it accommodates a broad range of scenarios that cannot be represented in existing formulations. For example, state-dependent network topologies can be readily modelled as described in Remark 3.2.22, while interchangeable agents can be modelled as discussed in Remark 3.2.23.

Remark 3.2.22. In many practical scenarios, the availability of a measurement depends upon the state of the agents. For example, many onboard sensors have a limited field of view, which might be restricted by orientation (e.g. for an onboard camera), occlusions, or range. In order to model such situations, one can augment a measurement space $\tilde{\mathcal{Y}}_k$ with an additional point $\aleph$ (i.e. use $\mathcal{Y}_k := \tilde{\mathcal{Y}}_k \cup \{\aleph\}$) that is used to indicate when the measurement is not available. This provides an alternative to using time-varying graphs for modelling state-dependent or time-varying network topologies. The knowledge that a measurement is unavailable can itself be useful information for specifying or determining a particular configuration. $\diamond$

Remark 3.2.23. Consider the case of interchangeable agents as presented in Example 3.2.3, and let $\sim$ denote the equivalence relation of agent permutations. Let $\tilde{h} : \mathcal{M}^\wp \to \mathcal{Y}^\tau$ be a continuous sensor modality, and suppose that $\tilde{x} \sim \tilde{x}'$ implies the configurations $\tilde{x}, \tilde{x}' \in \mathcal{M}^\wp$ are indistinguishable, i.e. that $\tilde{h}(\tilde{x}) = \tilde{h}(\tilde{x}')$. Denote $\pi : \mathcal{M}^\wp \to \mathcal{M}^\tau$ as the natural projection to the quotient space $\mathcal{M}^\wp / \sim$. By the universal property of quotient spaces, there must exist a unique continuous map $h : \mathcal{M}^\tau \to \mathcal{Y}^\tau$ such that $\tilde{h} = h \circ \pi$. Therefore, the case of interchangeable agents can be represented in the proposed framework using the continuous output map h. $\diamond$

The insight from Remark 3.2.23 enables one to model functionally identical agents as interchangeable, as illustrated by the following example. This is an appealing consideration for scenarios concerned with efficient trajectory planning for a formation of autonomous vehicles.

Example 3.2.24. Consider a collection of four agents with states $x_i \in \mathbb{R}^2$, and suppose the full state-space $\mathcal{M}^\wp$ possesses the product topology. Suppose agents 1 and 2 are each equipped with a range sensor that does not distinguish between other agents, as in Example 3.2.15. This arrangement is shown in Figure 3.1, with the

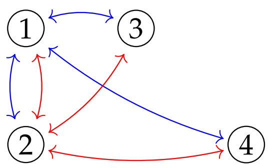

Figure 3.1: Network configuration for Example 3.2.24. Distances in blue are measured by y_1, and those in red are measured by y_2.

distances measured by y_1 shown in blue and those measured by y_2 shown in red. Due to the quotient structure on the measurement spaces $\mathcal{Y}_k$, agents 3 and 4 will be indistinguishable, and can therefore be regarded as interchangeable (Remark 3.2.23). To see this, observe that the set of blue distances will be unaffected by switching the agent positions, as will the set of red distances. Assuming a product topology $\mathcal{Y}^\wp := \mathcal{Y}_1 \times \mathcal{Y}_2$ for the measurement space, agents 1 and 2 are *not* indistinguishable since each measurement y_k is associated with a particular agent (i.e. if the positions of agents 1 and 2 are swapped, the sets of red and blue distances in Figure 3.1 will also switch). However, since agents 1 and 2 are functionally identical, it may be desirable to regard them as interchangeable. This can be achieved by defining another equivalence relation $(y_1, y_2) \sim_y (y_2, y_1)$ on $\mathcal{Y}^\wp$ (independent of the equivalence relation on each $\mathcal{Y}_k$ described in Example 3.2.15), and using the measurement space $\mathcal{Y}^\tau := \mathcal{Y}^\wp / \sim_y$. Now, agents 1 and 2 can be regarded as an interchangeable pair, and agents 3 and 4 can be regarded as a second interchangeable pair, with the output map h being well-defined on the corresponding quotient space $\mathcal{M}^\tau := \mathcal{M}^\wp / \sim$. By this method, one can model a complex network of several different types of agents, with the agents that are functionally identical being regarded as interchangeable. ◇

The following definition formalises the concept of an agent formation, for which I will define generalised rigidity.

Definition 3.2.25. For a given agent network $\mathcal{N} := (\mathcal{M}^\tau, \mathcal{Y}, h)$ on a Hausdorff topological space $\mathcal{M}^\tau$, a *formation* $\mathcal{F}(\mathring{y})$ is defined as the set of configurations $x \in \mathcal{M}^\tau$ such that $h(x) = \mathring{y}$. That is,

$$\mathcal{F}(\mathring{y}) := \{x \in \mathcal{M}^\tau \mid y = h(x) = \mathring{y}\}. \qquad \diamond$$

Conceptually, a configuration is a fixed agent state $x \in \mathcal{M}^\tau$ of the system, while a formation is the set of configurations in the pre-image of a fixed output $\mathring{y} \in \mathcal{Y}$. Alternatively, $\mathcal{F}(\mathring{y})$ may be regarded as the set of configurations that are equivalent to some reference configuration $\mathring{x} \in \mathcal{M}^\tau$ that generates the reference measurement $\mathring{y} = h(\mathring{x})$. Note that it is possible that a particular specification $\mathring{y}$ is not realisable, in which case the corresponding formation $\mathcal{F}(\mathring{y})$ is the null set.

3.2.2 Equivariance and Congruence

The generalised definition of rigidity presented in this thesis is associated with a natural symmetry of a formation. Let $\mathbf{G}$ be a Hausdorff topological group[2] with a continuous group action $\Phi : \mathbf{G} \times \mathcal{M}^\tau \to \mathcal{M}^\tau$. For this thesis, I will work with left group actions, but this choice is arbitrary for the theory. A brief review of group theory, as well as a summary of the groups used in this thesis, is provided in Appendix A.

Remark 3.2.26. It is quite common for the group $\mathbf{G}$ to act on the individual agent states independently, i.e. to have a continuous group action $\phi_i : \mathbf{G} \times \mathcal{M}_i^\tau \to \mathcal{M}_i^\tau$ defined for each agent i. In this case, the group action Φ on the full state-space can be naturally constructed by taking the product of the individual group actions ϕ_i. However, for this work I will allow more general structure where Φ cannot be decomposed into individual group actions, in order to enable numerous other possibilities. For example, this structure is required for the symmetry to allow permutations of the agent positions, or to reflect an agent's location through a line between two others. $\diamond$

There are two types of invariance that can be of interest for the generalised formulation of rigidity. The first of these is as follows.

Definition 3.2.27. An output map $h(x)$ is termed *invariant* with respect to a continuous group action Φ of a Hausdorff topological group $\mathbf{G}$ if $h(x) = h(\Phi(S, x))$ for all $S \in \mathbf{G}$ and all $x \in \mathcal{M}^\tau$. $\diamond$

Example 3.2.28. Consider a collection of agents with states $x_i \in \mathbb{R}^3$, where the full state-space $\mathcal{M}^\wp$ has the product structure. A rigid-body transformation, with an optional reflection, can be defined by

$$\Phi((Q, \xi), x) := (Qx_1 + \xi, \dots, Qx_N + \xi).$$

Here, $Q \in \mathrm{O}(3)$ is an orthogonal matrix and $\xi \in \mathbb{R}^3$. Note that the same element $S = (Q, \xi) \in \mathrm{E}(3)$ is applied to each individual state x_i. Given a range measurement h_k between agents i and j (as in Example 3.2.9), one has

$$\begin{aligned} h_k(\phi_i(S, x_i), \phi_j(S, x_j)) &= \|\phi_i(S, x_i) - \phi_j(S, x_j)\| \\ &= \|Qx_i + \xi - Qx_j - \xi\| \\ &= \|x_i - x_j\| \\ &= h_k(x_i, x_j). \end{aligned}$$

This confirms the well-known fact that distances are invariant to rigid-body transformations and reflections. $\diamond$

[2]A topological group is Hausdorff ([Singh, 2013, Proposition 12.1.6]) and Tychonoff ([Singh, 2013, Theorem 12.1.7]) if and only if it is a Kolmogorov (T_0) space.

Example 3.2.29. Consider a collection of agents with states $X_i \in \mathrm{SE}(3)$, where the full state-space $\mathcal{M}^{\wp}$ has the product structure. A rigid-body transformation of the agent states is applied via left multiplication by the Lie-group SE(3), i.e.

$$\Phi(S, X) := (SX_1, \ldots, SX_N),$$

where $S \in \mathrm{SE}(3)$. For a relative position measurement as in Example 3.2, this transform gives (in homogeneous coordinates)

$$\begin{aligned}\overline{h_k(\phi_i(S, X_i), \phi_j(S, X_j))} &= (X_i^{-1} S^{-1} S X_j)\bar{y}_k^0 \\ &= (X_i^{-1} X_j)\bar{y}_k^0 \\ &= \overline{h_k(X_i, X_j)}.\end{aligned}$$

◇

Example 3.2.30. Consider the angle sensor modality presented in Example 3.2.14, for agents in $\mathbb{R}^3$. Let $S := (Q, \xi, \rho) \in \mathrm{S}(3)$ be an element of the *Similarity group* S(3) described in Appendix A.3, where $Q \in \mathrm{O}(3)$ is a rotation with a possible reflection, $\xi \in \mathbb{R}^3$ is a translation, and $\rho \in \mathbb{R}_{>0}$ is a scaling factor. The group action on an agent state $x_i \in \mathbb{R}^3$ is defined by $\phi_i(S, x_i) := \rho(Qx_i + \xi)$. Noting that $\phi_p(S, x_p) = \phi_i(S, x_i)$ whenever $x_p = x_i$, it follows that $h_k(\Phi(S, x)) = \aleph$ if $h_k(x) = \aleph$. It remains to check the case where $x_p \neq x_i$ and $x_p \neq x_j$:

$$\begin{aligned}&h_k(\phi_p(S, x_p), \phi_i(S, x_i), \phi_j(S, x_j)) \\ &\quad := \cos^{-1}\left(\frac{(\rho(Qx_i + \xi) - \rho(Qx_p + \xi))^\top(\rho(Qx_j + \xi) - \rho(Qx_p + \xi))}{\|\rho(Qx_i + \xi) - \rho(Qx_p + \xi)\|\|\rho(Qx_j + \xi) - \rho(Qx_p + \xi)\|}\right) \\ &\quad = \cos^{-1}\left(\frac{(x_i - x_p)^\top(x_j - x_p)}{\|x_i - x_p\|\|x_j - x_p\|}\right) \\ &\quad = h(x_p, x_i, x_j).\end{aligned}$$

Here, I have used the fact that $Q^\top Q = I_3$, where I_3 denotes the 3×3 identity matrix. This demonstrates that angle sensor modalities are invariant to global translations, rotations, scaling, and reflections. ◇

Example 3.2.31. Consider the case of a body-fixed-frame bearing between agents $X_i, X_j \in \mathrm{SE}(3)$, as in Example 3.2.11. Let ϕ_i denote the group action of the Special Similarity group SS(3), as defined in Appendix A.3. For a group element $S := (Q, \xi, \rho) \in \mathrm{SS}(3)$, one has (assuming $\xi_i \neq \xi_j$)

$$\begin{aligned}h_k(\phi_i(S, X_i), \phi_j(S, X_j)) &= h_k((QR_i, \rho(Q\xi_i + \xi)), (QR_j, \rho(Q\xi_j + \xi))) \\ &= (QR_i)^\top \frac{(\rho(Q\xi_j + \xi) - \rho(Q\xi_i + \xi))}{\|\rho(Q\xi_j + \xi) - \rho(Q\xi_i + \xi)\|} \\ &= R_i^\top \frac{(\xi_j - \xi_i)}{\|\xi_j - \xi_i\|} = h_k(X_i, X_j).\end{aligned}$$

Thus, body-fixed-frame bearings are invariant to the action of SS(3). ⋄

Unlike bearings in the body-fixed frame, inertial direction measurements are not invariant to rotations, as shown in the following example.

Example 3.2.32. Consider an inertial direction measurement (Example 3.2.12) between two agents with states $x_i, x_j \in \mathbb{R}^3$. Let ϕ_i denote the group action of the Similarity group S(3), as defined in Appendix A.3, and let $S := (Q, \xi, \rho) \in \mathrm{S}(3)$ be a group element. Then, assuming $x_i \neq x_j$,

$$\begin{aligned} h_k(\phi_i(S, x_i), \phi_j(S, x_j)) &:= \frac{(\rho(Qx_j + \xi) - \rho(Qx_i + \xi))}{\|\rho(Qx_j + \xi) - \rho(Qx_i + \xi)\|} \\ &= \frac{Q(x_j - x_i)}{\|x_j - x_i\|} \\ &= Qh_k(x_i, x_j). \end{aligned} \tag{3.3}$$

Thus, the sensor modality of inertial directions is *not* invariant with respect to the action of S(3); specifically, it is not invariant to the rotations or reflections described by $Q \in \mathrm{O}(3)$. However, it is easily seen from (3.3) that inertial directions are invariant to global translations $\xi \in \mathbb{R}^3$ and global scaling $\rho \in \mathbb{R}_{>0}$; hence, this sensor modality is invariant with respect to the group of scaled-translations, ST(3) (Appendix A.4). ⋄

In practice, full invariance of the output map h as described in Definition 3.2.27 may be stronger than required for an appropriate interpretation of rigidity. Instead, it may be sufficient for the invariance property to hold only at a specific output value $\mathring{y}$ that defines a formation. For such cases, I provide the following definition.

Definition 3.2.33. An output value $\mathring{y}$ of an output map $h(x)$ is termed *invariant* with respect to a continuous group action Φ of a Hausdorff topological group $\mathbf{G}$ if, for all $x \in \mathcal{M}^\tau$ such that $h(x) = \mathring{y}$, it holds that $h(\Phi(S, x)) = \mathring{y}$ for all $S \in \mathbf{G}$. ⋄

Clearly, if an output map is invariant with respect to a group action Φ, then all output values derived from that map will also be invariant. To illustrate the distinction between Definition 3.2.27 and Definition 3.2.33, I revisit Example 3.2.32.

Example 3.2.34. Consider the case of inertial direction measurements between agents in $\mathbb{R}^3$, as in Example 3.2.32, and recall that they are not invariant to the rotations and reflections of the Similarity group S(3). However, as was the case for the angle sensor modality studied in Example 3.2.30, the particular measurement $\mathring{y}_k = \aleph$ *is* invariant with respect to the group action of S(3). Furthermore, it can be seen from (3.3) that a fixed inertial direction measurement $\mathring{y}_k \in \mathbb{S}^2$ is invariant with respect to rotations about the axis of that measurement. For example, a direction measurement parallel to the x-axis will be invariant to rotations about the x-axis. ⋄

Remark 3.2.35. Consider a Hausdorff topological group $\mathbf{G}$ and a continuous group action $\check{\Phi} : \mathbf{G} \times \mathcal{M}^\wp \to \mathcal{M}^\wp$. Suppose we are interested in a state-space given by the quotient $\mathcal{M}^\tau := \mathcal{M}^\wp / \sim$ for some equivalence relation $\sim$ (see Example 3.2.3).

Since the natural projection $\pi : \mathcal{M}^{\wp} \to \mathcal{M}^{\tau}$ is continuous, the map $\tilde{\Phi} := \pi \circ \check{\Phi}$ is also continuous. Furthermore, analogously to the case in Remark 3.2.23, suppose that $\tilde{x} \sim \tilde{x}'$ (where $\tilde{x}, \tilde{x}' \in \mathcal{M}^{\wp}$) implies $\tilde{\Phi}(S, \tilde{x}) = \tilde{\Phi}(S, \tilde{x}')$ for all $S \in \mathbf{G}$. Then, the universal property of quotient spaces ensures there exists a unique continuous map $\Phi : \mathbf{G} \times \mathcal{M}^{\tau} \to \mathcal{M}^{\tau}$ such that $\Phi(S, \pi(\tilde{x})) := \tilde{\Phi}(S, \tilde{x})$. It is straightforward to verify that this map is a continuous group action on $\mathcal{M}^{\tau}$ as required by the rigidity framework. $\diamond$

Remark 3.2.36. Consider a Hausdorff topological group $\mathbf{G}$ and a continuous group action $\tilde{\Phi} : \mathbf{G} \times \tilde{\mathcal{M}}^{\tau} \to \tilde{\mathcal{M}}^{\tau}$. Suppose we are interested in a state-space $\mathcal{M}^{\tau} := \tilde{\mathcal{M}}^{\tau} \setminus \mathcal{W}$, where $\mathcal{W} \subseteq \tilde{\mathcal{M}}^{\tau}$ is an exceptional set (see Example 3.2.2). Assume that the orbits of $\mathbf{G}$ that intersect $\mathcal{W}$ are contained in $\mathcal{W}$, or equivalently that $\tilde{\Phi}(S, x) \in \mathcal{M}^{\tau}$ for all $S \in \mathbf{G}$ and all $x \in \mathcal{M}^{\tau}$. This condition is commonly satisfied in practice; in particular, it is guaranteed in the typical case where the group action acts on each agent state $x_i \in \mathcal{M}_i^{\tau}$ in the same way, with $\mathcal{W}$ being the set of points where two agent states coincide (as in Example 3.2.2). Under this assumption, the induced group action $\Phi : \mathbf{G} \times \mathcal{M}^{\tau} \to \mathcal{M}^{\tau}, \Phi(S, x) \mapsto \tilde{\Phi}(S, x)$ is an appropriate group action on the desired state-space. $\diamond$

The property of rigidity is associated with the symmetries of the formation. The two notions of invariance provided in Definitions 3.2.27 and 3.2.33 lead to two classes of symmetry.

Definition 3.2.37. Let $\mathcal{N} := (\mathcal{M}^{\tau}, \mathcal{Y}, h)$ be an agent network on a Hausdorff topological space $\mathcal{M}^{\tau}$, let $\mathcal{F}(\mathring{y})$ be a formation of the agent network $\mathcal{N}$, and let $\mathbf{G}$ be a Hausdorff topological group with a continuous group action $\Phi : \mathbf{G} \times \mathcal{M}^{\tau} \to \mathcal{M}^{\tau}$.

(i) If the output map $h(x)$ is invariant with respect to Φ, then the *agent network* $\mathcal{N}$ is *equivariant* with respect to Φ.

(ii) If a fixed output value $\mathring{y}$ is invariant with respect to Φ, then the *formation* $\mathcal{F}(\mathring{y})$ is *equivariant* with respect to Φ. $\diamond$

It is clear that if an agent network is equivariant with respect to a group action Φ, then every formation of that agent network is equivariant. I emphasise that equivariance requires invariance with respect to the same group action across all sensor modalities (or measurements) k in the network (or formation). Although the study of rigidity presented in this chapter allows equivariant *formations* (Definition 3.2.37 (ii)), the additional structure of equivariant *agent networks* (Definition 3.2.37 (i)) will be required in the next chapter.

The final notion used for the formal definition of rigidity is a generalised form of congruence (Jackson [2007]).

Definition 3.2.38. Two configurations $x, x' \in \mathcal{M}^{\tau}$ of an agent network are *congruent* with respect to a continuous group action $\Phi : \mathbf{G} \times \mathcal{M}^{\tau} \to \mathcal{M}^{\tau}$ of a Hausdorff topological group $\mathbf{G}$ if there exists a transform $S \in \mathbf{G}$ such that $\Phi(S, x) = x'$. $\diamond$

3.3 Generalised Rigidity

In this section I define and analyse the generalised notion of rigidity. The formal definition is presented in Subsection 3.3.1 along with some illustrative examples, while basic analysis is provided in Subsection 3.3.2.

3.3.1 Defining Rigidity

Generalised rigidity is defined with respect to the symmetry of a group action, using the concepts of equivariance and congruence introduced in Subsection 3.2.2.

Definition 3.3.1. (**Generalised rigidity**) Let $x \in \mathcal{M}^\tau$ be a configuration of an agent network $\mathcal{N} := (\mathcal{M}^\tau, \mathcal{Y}, h)$, and suppose the measurement $\mathring{y} := h(x)$ is invariant with respect to a continuous group action $\Phi : \mathbf{G} \times \mathcal{M}^\tau \to \mathcal{M}^\tau$ of a Hausdorff topological group $\mathbf{G}$. The configuration x is *locally rigid* with respect to Φ if there exists an open neighbourhood $\mathcal{U}_x \subseteq \mathcal{M}^\tau$ of x such that all configurations $x' \in (\mathcal{F}(\mathring{y}) \cap \mathcal{U}_x)$ are congruent. That is, there exists $S \in \mathbf{G}$ such that $\Phi(S, x) = x'$. If this holds with $\mathcal{U}_x = \mathcal{M}^\tau$, then x is *globally rigid* with respect to Φ. $\diamond$

Definition 3.3.1 defines rigidity for a *configuration* $x \in \mathcal{M}^\tau$ of an agent network $\mathcal{N}$ (or a formation $\mathcal{F}(h(x))$), as is commonly done in the literature (see e.g. Asimow and Roth [1978]; Jackson [2007]; Krick et al. [2009]). In this thesis, I am often concerned with the notion of rigidity for a given *formation* of the agent network; hence, I also introduce the following definition.

Definition 3.3.2. Let $\mathcal{F}(\mathring{y})$ be a formation that is equivariant with respect to a continuous group action $\Phi : \mathbf{G} \times \mathcal{M}^\tau \to \mathcal{M}^\tau$ of a Hausdorff topological group $\mathbf{G}$. The formation $\mathcal{F}(\mathring{y})$ is *locally rigid* or *globally rigid* with respect to Φ if all configurations $x \in \mathcal{F}(\mathring{y})$ are locally rigid or globally rigid, respectively. $\diamond$

Note that by definition, global rigidity is a special case of local rigidity. In this chapter I will primarily focus on globally rigid formations, with a brief discussion concerning locally rigid formations at the end of Subsection 3.3.2. The relationship between locally rigid configurations and locally rigid formations will be considered with the aid of additional structure in Chapter 4. Observe that *global* rigidity of a formation $\mathcal{F}(\mathring{y})$ is equivalent to global rigidity of a configuration $\mathring{x} \in \mathcal{F}(\mathring{y})$. The intuition behind the property of global rigidity is as follows: invariance of $\mathring{y} := h(\mathring{x})$ ensures the orbit $\Phi_{\mathring{x}}(\mathbf{G})$ lies in the formation $\mathcal{F}(\mathring{y})$, while congruence ensures that $\mathcal{F}(\mathring{y}) \subseteq \Phi_{\mathring{x}}(\mathbf{G})$. Hence, the group action is transitive on the set of valid configurations, and the formation $\mathcal{F}(\mathring{y})$ possesses the structure of a homogeneous space. This insight is explored further in the next subsection. In the remainder of the present subsection, I provide several examples illustrating the generalised rigidity framework.

Example 3.3.3. Consider four agents in $\mathbb{R}^2$ for which the full state-space has the product topology, and suppose there are nonzero distance constraints (Example 3.2.9) specified between all agent pairs (i.e. $M = 6$). This formation $\mathcal{F}(\mathring{y})$ is globally rigid with respect to the natural group action of $E(2)$. However, unless the specified formation is collinear, then it will only be *locally* rigid with respect to the action of $SE(2)$, because the neighbourhood $\mathcal{U}_x$ about any configuration $x \in \mathcal{F}(\mathring{y})$ must be small enough not to include a reflected configuration. Note that if the specified formation is collinear, then it will be *globally* rigid with respect to $SE(2)$ because in this case any reflection can be equivalently achieved by a rotation followed by a translation.

The formation will not be rigid with respect to the natural group actions of $S(2)$, $SS(2)$ or $ST(2)$ (as defined in Appendix A), because distance measurements are not invariant to scaling. It will also fail to be rigid with respect to translations, because a rotation of a configuration will lie outside of the group orbit, but still preserve all distance constraints. $\diamond$

The following example illustrates the flexibility of allowing different agent states and sensor modalities. In particular, cases where the agents lie in different state-spaces may correspond to scenarios involving several different types of vehicles.

Example 3.3.4. Consider four agents in the plane with nonzero distance constraints between them, as in Example 3.3.3. Suppose we add a fifth agent with state $X_5 := (R_5, \xi_5) \in SE(2)$ (where $R_5 \in SO(2)$ describes the agent's orientation and $\xi_5 \in \mathbb{R}^2$ is its position in the plane), and that this agent measures the bearing to each other agent $i \in \{1, \ldots, 4\}$ in its local body-fixed-frame. That is,

$$y_k = h_k(X_5, x_i) := \frac{R_5^\top (x_i - \xi_5)}{\|x_i - \xi_5\|} \in S^1$$

for $i \in \{1, \ldots, 4\}$, assuming the agents are not co-located (recall that we can exclude such points as in Example 3.2.2). Observe that an element of the group $SE(2)$ can act independently on each agent state in a natural manner (see Appendix A), even though the agents lie in two different state-spaces ($\mathbb{R}^2$ and $SE(2)$). Note also that all sensor modalities (distances and body-fixed-frame bearings) are invariant to the resulting transform of the full state-space (see Examples 3.2.28 and 3.2.31). The scenario considered here is illustrated in Figure 3.2(a), with red lines representing distance constraints and blue arrows representing bearing constraints. The reference frame for agent 5 is also shown.

To study rigidity of the formation $\mathcal{F}(h(\mathring{x}))$ generated by a reference configuration $\mathring{x}$, first recall from Example 3.3.3 that agents 1 to 4 are constrained to $E(2)$ transforms by the distance constraints. I therefore consider where X_5 may be positioned with respect to the other four. Note that a single bearing (e.g. from ξ_5 to x_1) does not constrain the position of ξ_5 at all, since the orientation R_5 can be adjusted as necessary. However, a *pair* of bearings (y_a, y_b) from agent 5 to two other agents will require the position ξ_5 to satisfy the (signed) *angle* $\alpha(y_a, y_b)$ between the two bearings; consequently, the position of ξ_5 will be constrained to an arc as shown in Figure 3.2(b). With four bearings, there are three angle constraints corresponding to agent pairs

$\{1,2\}$, $\{2,3\}$, and $\{3,4\}$. Any configuration satisfying all constraints must lie on an intersection of the three corresponding arcs; in particular, this condition will be satisfied at $\mathring{x}$. To avoid special cases, I will make the following additional assumptions about $\mathring{x}$:

(i) no three agents are collinear.

(ii) there is no circle that has ξ_5 and three other agent positions on its circumference.

Condition (ii) ensures arcs involving a common agent (e.g. $\{1,2\}$ and $\{2,3\}$) can only intersect in at most one place. As a consequence, all three arcs will only have one common intersection, at the position of agent 5 in the reference state $\mathring{x}$. The orientation R_5 is then fixed by any individual bearing. One may therefore conclude that the (arbitrary) configuration $\mathring{x} \in \mathcal{F}(\mathring{y})$ is locally rigid under action by SE(2).

To determine *global* rigidity of $\mathring{x}$, it remains to consider where ξ_5 may be positioned with respect to a reflection of the other four agents. Observe that if the position ξ_5 is reflected through the line between two other agents, as shown in Figure 3.2(c), the (signed) angle $\alpha(y_a, y_b)$ is preserved only if the orientation R_5 is also reflected. However, this reflection of the coordinate frame will break the convention of a right-hand frame (see Appendix A.1); from this insight one may conclude that the position ξ_5 cannot be reflected with the rest of the formation. It remains to verify that the reflection of agents 1 to 4 does not permit ξ_5 to be positioned elsewhere. Suppose, without loss of generality, that agents 1 to 4 are reflected through the line between agents 1 and 2. It is clear from the above discussion that ξ_5 must remain on the same arc between agents 1 and 2 regardless of the reflection. However, since the agents are not collinear, the arcs corresponding to agent pairs $\{2,3\}$ and $\{3,4\}$ will move as a result of the reflection and they will no longer have a common point of intersection. It follows that the formation $\mathring{x}$ is *globally* rigid with respect to the action of SE(2). $\diamond$

It should be noted that *global* rigidity remains, by nature, a difficult property to determine in general, although insight from the group symmetry may assist substantially in the analysis, as seen in the previous example. Below is a more complex example involving onboard sensors that do not distinguish between other agents. This is a realistic consideration that may arise due to sensor limitations or as part of the problem formulation (for example, the task of flocking as considered by Olfati-Saber [2006] does not specify relations between specific agents). I will return to this example during the discussion of path-rigidity in Section 3.4.

Example 3.3.5. Consider a network of four agents in $\mathbb{R}^2$, and let h_1 be a measurement of the distances from agent 1 to each of the other agents, without distinguishing between them (as in Example 3.2.15). Suppose agents 2, 3 and 4 can observe the angles (as in Example 3.2.14) between each pair of other agents, again without distinguishing between them (i.e. each agent obtains an unordered 3-tuple of the angles formed by each pair of other agents). Let the measurements $h_2, h_3, h_4 \in [0, \pi]$ be the *maximum*

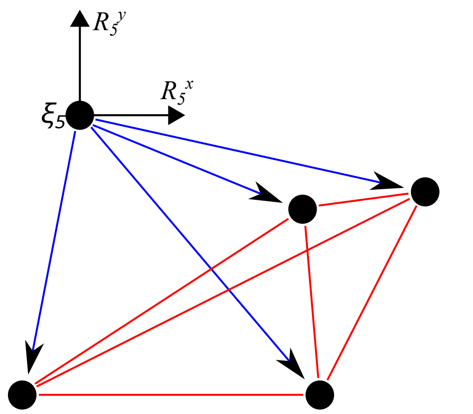

(a) A generic agent configuration for Example 3.3.4.

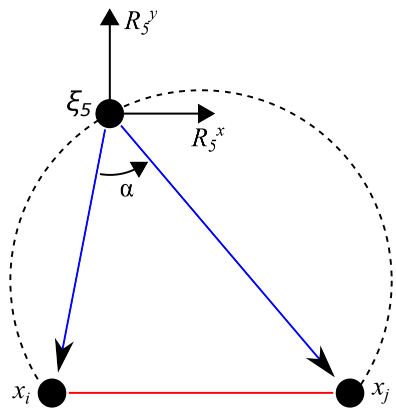

(b) The signed angle α between two bearing constraints (to agents x_i and x_j) restricts ξ_5 to an arc (dotted line) that passes from x_i to x_j.

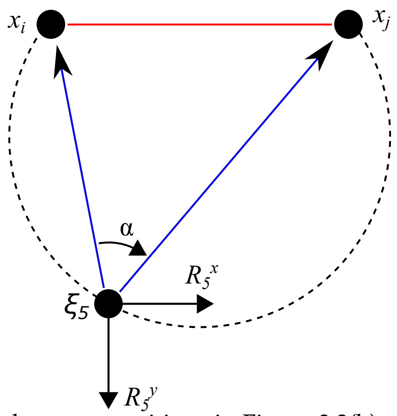

(c) If the agent positions in Figure 3.2(b) are reflected, the bearing constraints can only be satisfied with a reflected reference frame, meaning $X_5 \notin \mathrm{SE}(2)$.

Figure 3.2: Diagrams illustrating the analysis in Example 3.3.4. The dots represent agent positions, with ξ_5 labelled and the x and y axes of the orientation R_5 denoted by R_5^x and R_5^y, respectively. Solid red lines indicate distance constraints, while blue arrows indicate bearing constraints.

angles observed by each of these agents. For simplicity, I will assume that no agents are co-located.

Suppose the state-space has the product topology, $\mathcal{M}^{\wp} := (\mathbb{R}^2)^4$. A rectangular formation can be specified by

$$\mathring{y} = (\lfloor(a, b, c)\rfloor, (\pi/2), (\pi/2), (\pi/2)), \tag{3.4}$$

where angles are expressed in radians and $\lfloor(a, b, c)\rfloor$ denotes the equivalence class obtained by permutations of specified nonzero distances $a, b, c \in \mathbb{R}_{>0}$. Note that these distances are assumed to satisfy the constraint $c^2 = a^2 + b^2$. A diagram of such a formation is given in Figure 3.3.

It is readily observed that the constraints (3.4) enforce a quadrilateral for which all interior angles are $\pi/2$ radians. In particular, if one agent were inside the triangle formed by the other three, then only *one* of the outer three agents could measure a maximum angle of $\pi/2$. It is then clear that the two shortest distances in $\mathring{y}_1$ are the lengths of two adjacent sides of the rectangle. The fact that the formation is a rectangle of fixed dimensions implies that the specified formation is locally rigid with respect to the natural action of E(2) (to which both distances and angles are invariant; see Examples 3.2.28 and 3.2.30). It is not globally rigid with respect to such transforms since agents 2, 3, and 4 can have their positions arbitrarily switched without breaking the formation (I elaborate on this point further in Example 3.4.11).

Now suppose we wish to regard agents 2, 3 and 4 as interchangeable. To do this, all sensor modalities must be invariant to permutations of these agents (see Remark 3.2.23) in order for the output map to be well-defined on the quotient space $\mathcal{M}^\tau := \mathcal{M}^\wp / \sim$ (where $\sim$ is the equivalence relation described by permutations of the agents as in Example 3.2.3). This issue can be resolved following the insight from Example 3.2.24; that is, let $\tilde{h} := (h_1, \lfloor (h_2, h_3, h_4) \rfloor)$ where $\lfloor (h_2, h_3, h_4) \rfloor$ is an unordered 3-tuple. The output map $\tilde{h}$, along with the natural group action $\tilde{\Phi}$ of E(2) on $\mathbb{R}^2$, induce well-defined maps h and Φ on the quotient space $\mathcal{M}^\tau$. Note that (in this case) the change to the output map does not affect the earlier rigidity analysis performed on the product space. Since switching the positions of agents 2, 3 or 4 results in an equivalent state, the formation will now be *globally* rigid with respect to rigid-body transforms (see Example 3.4.11, later, for further insight here). ◇

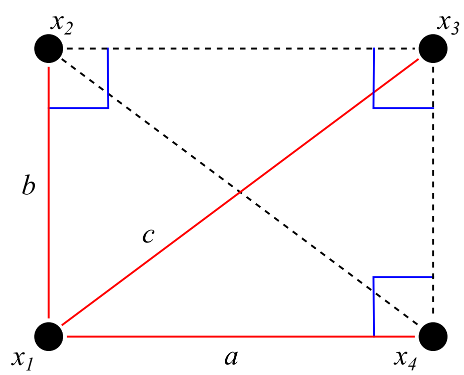

Figure 3.3: Diagram of a rectangular formation (in $\mathbb{R}^2$) satisfying the constraints specified in Example 3.3.5. Distance constraints (a, b, and c) associated with h_1 are shown in red, while the constraints on the maximum angles observed by agents 2, 3, and 4 are shown in blue (all right-angles). Dotted lines are only for reference.

The next example illustrates a scenario where one might be interested in invariant *measurements* rather than invariant *sensor modalities*; i.e. where only the *formation* is equivariant (as described in Part (ii) of Definition 3.2.37) rather than the agent network.

Example 3.3.6. Consider the case where two agents are constrained to the x-y plane with a specified distance between them. Suppose a third agent with state $x_3 \in \mathbb{R}^3$ measures the relative height (i.e. the z-component of the relative position) and the inertial direction (Example 3.2.12) to the first agent, with the objective of being positioned at a specified distance directly above it. Although the directional sensor modality is not invariant to rotations, the desired measurement $\mathring{y}_k = (0, 0, -1)^\top$ is invariant to rotations about the z-axis. Since the first two agents lie in the plane, it is sensible to consider rigidity of this formation with respect to the action of $\mathrm{E}(2)$, with the group acting in the x-y plane on the state $x_3 \in \mathbb{R}^3$. It is straightforward to verify that this formation will be globally rigid with respect to such transformations. $\diamond$

3.3.2 Rigidity Analysis

In this subsection, I present some basic results concerning the structure of globally rigid and locally rigid formations. In the previous subsection, I noted that the definition of global rigidity implies that the formation $\mathcal{F}(\mathring{y})$ has the structure of a homogeneous space. I will begin with some elaboration on this insight.

Let $\operatorname{stab}\Phi_x := \{S \in \mathbf{G} \mid \Phi(S, x) = x\} \subseteq \mathbf{G}$ denote the *stabiliser* of a point $x \in \mathcal{M}^\tau$, i.e. the set of transformations in $\mathbf{G}$ that leave x unchanged by the group action. It is well-known and easily verified that this is a subgroup of $\mathbf{G}$. Observe that $\operatorname{stab}\Phi_x$ is the pre-image of a singleton set under the continuous map $\Phi_x(S) := \Phi(S, x)$. Since $\mathcal{M}^\tau$ is a T_1 topological space (a necessary condition for it to be Hausdorff), this implies that $\operatorname{stab}\Phi_x$ is closed. It follows that the quotient space $\mathbf{G}/\operatorname{stab}\Phi_x$ is Hausdorff (see [Singh, 2013, Proposition 7.1.6, and note also Proposition 12.3.1]). I now present the main result for this section, which considers some well-known characteristics of homogeneous spaces in the context of globally rigid formations.

Theorem 3.3.7. *Let $\mathcal{F}(\mathring{y})$ be a formation and let $\mathbf{G}$ be a Hausdorff topological group with a continuous group action $\Phi : \mathbf{G} \times \mathcal{M}^\tau \to \mathcal{M}^\tau$. Then, the following hold:*

(i) If $\mathcal{F}(\mathring{y})$ is globally rigid, then all stabilisers $\operatorname{stab}\Phi_{\mathring{x}}$ with $\mathring{x} \in \mathcal{F}(\mathring{y})$ are homeomorphic. More specifically, for all $\mathring{x}, \mathring{x}' \in \mathcal{F}(\mathring{y})$, there exists $S \in \mathbf{G}$ such that $\operatorname{stab}\Phi_{\mathring{x}'} = S \cdot \operatorname{stab}\Phi_{\mathring{x}} \cdot S^{-1}$.

(ii) The formation $\mathcal{F}(\mathring{y})$ is globally rigid with respect to Φ if and only if there exists some reference state $\mathring{x} \in \mathcal{F}(\mathring{y})$ such that the mapping

$$\Psi_{\mathring{x}} : \mathbf{G}/\operatorname{stab}\Phi_{\mathring{x}} \to \mathcal{M}^\tau, \Psi_{\mathring{x}}(S \cdot \operatorname{stab}\Phi_{\mathring{x}}) := \Phi_{\mathring{x}}(S) \tag{3.5}$$

is continuous and bijective onto $\mathcal{F}(\mathring{y})$, where $S \in \mathbf{G}$ (see Figure 3.4).

(iii) If the formation $\mathcal{F}(\mathring{y})$ is globally rigid with respect to Φ, then the map $\Psi_{\mathring{x}} : \mathbf{G}/\operatorname{stab}\Phi_{\mathring{x}} \to \mathcal{M}^\tau$ in (3.5) is a homeomorphism if and only if the map $\Phi_{\mathring{x}} : \mathbf{G} \to \mathcal{M}^\tau$ is open.

Proof To show (i), I note that there exists $S \in \mathbf{G}$ such that $\Phi(S, \mathring{x}) = \mathring{x}'$ since $\mathcal{F}(\mathring{y})$ is globally rigid. For any $S' \in \operatorname{stab}\Phi_{\mathring{x}'}$, one has $\Phi(S', \mathring{x}') = \mathring{x}'$ and therefore $\Phi(S^{-1} \cdot S' \cdot S, \mathring{x}) = \Phi(S^{-1}, \mathring{x}') = \Phi(S^{-1} \cdot S, \mathring{x}) = \mathring{x}$. This implies that $\operatorname{stab}\Phi_{\mathring{x}'} \subseteq S \cdot \operatorname{stab}\Phi_{\mathring{x}} \cdot S^{-1}$.

The analogous argument with $\Phi(S^{-1}, \mathring{x}') = \mathring{x}$ shows that the relation can be reversed, so the two sets are equal. Note that the group operation $(\cdot)$ is a homeomorphism in either of its arguments.

For (ii), the forward implication is well-known [Singh, 2013, p. 352] in the context of orbit spaces. For the reverse implication, observe that since $\Psi_{\mathring{x}}$ is bijective, then for any $x, x' \in \mathcal{F}(\mathring{y})$ there exist $S \cdot \operatorname{stab} \Phi_{\mathring{x}}, S' \cdot \operatorname{stab} \Phi_{\mathring{x}} \in (\mathbf{G} / \operatorname{stab} \Phi_{\mathring{x}})$ such that $\Psi_{\mathring{x}}(S \cdot \operatorname{stab} \Phi_{\mathring{x}}) = \Phi_{\mathring{x}}(S) = x$ and $\Psi_{\mathring{x}}(S' \cdot \operatorname{stab} \Phi_{\mathring{x}}) = \Phi_{\mathring{x}}(S') = x'$. Thus, one has $\Phi(S' \cdot S^{-1}, x) = \Phi(S', \mathring{x}) = x'$. The formation $\mathcal{F}(\mathring{y})$ is equivariant since it is the image of $\Psi_{\mathring{x}}$ (see Figure 3.4). It follows that $\mathcal{F}(\mathring{y})$ is globally rigid.

The result (iii) is easily seen from Figure 3.4 by noting that the canonical projection π is continuous and open. ■

$$\begin{tikzcd}
\mathbf{G} \arrow[d, "\pi"'] \arrow[dr, "\Phi_{\mathring{x}}"] & \\
\mathbf{G} / \operatorname{stab} \Phi_{\mathring{x}} \arrow[r, "\Psi_{\mathring{x}}"'] & \mathcal{F}(\mathring{y})
\end{tikzcd}$$

Figure 3.4: Mappings between spaces for a globally rigid formation $\mathcal{F}(\mathring{y})$. Here, π is the canonical projection, and the diagram commutes.

Example 3.3.8. The key insight from Theorem 3.3.7 can be illustrated by revisiting Example 3.3.3, where four agents in the plane have nonzero distance constraints between all pairs. Assume for this example that the agents are not collinear. In this case, the stabiliser of any point $\mathring{x} \in \mathcal{F}(\mathring{y})$ is the identity of $\mathrm{E}(2)$, and hence Φ itself is a continuous bijection onto $\mathcal{F}(\mathring{y})$. Now, if we instead suppose that the agent states lie in $\mathbb{R}^3$, then the formation is globally rigid with respect to $\mathrm{E}(3)$. However, in this case the stabiliser of $\mathring{x} \in \mathcal{F}(\mathring{y})$ will include any reflection combined with the $\mathrm{SE}(3)$ action that reverts the change induced by that reflection (a trivial case is a reflection through the plane of the four agents, which leaves their positions unchanged). Theorem 3.3.7 states that these stabilisers are homeomorphic for all configurations of $\mathcal{F}(\mathring{y})$. Note that the existence of an $\mathrm{SE}(3)$ transform that reverts the reflection is a consequence of the formation being planar. If the fourth agent were positioned outside the plane of the other three, then no $\mathrm{SE}(3)$ transform following a reflection would be able to return the fourth agent to the original "side" of the plane (note that this plane is fixed to the other three agents, not to the inertial reference frame). In this case, the stabiliser of any configuration $\mathring{x} \in \mathcal{F}(\mathring{y})$ would again be the identity. ◇

In the remainder of this section, I briefly consider the structure of locally rigid formations and configurations, and draw comparisons with the global case. The following lemma is concerned with the orbits $\Phi_{\mathring{x}_a}(\mathbf{G}) \subseteq \mathcal{M}^\tau$ of indexed configurations $\mathring{x}_a \in \mathcal{F}(\mathring{y})$.

Lemma 3.3.9. *Let $\mathcal{F}(\mathring{y})$ be a formation that is locally rigid with respect to a continuous group action $\Phi : \mathbf{G} \times \mathcal{M}^\tau \to \mathcal{M}^\tau$ of a Hausdorff topological group $\mathbf{G}$. Then, there exists a* *collection of open sets* $\{\mathcal{U}_{a\in\mathcal{I}}\} \subseteq \mathcal{M}^\tau$ *that covers* $\mathcal{F}(\mathring{y})$ *(where* $\mathcal{I}$ *is an index set), such that* $\mathcal{F}_a(\mathring{y}) := \mathcal{F}(\mathring{y}) \cap \mathcal{U}_a = \Phi_{\mathring{x}_a}(\mathbf{G})$ *for each* $a \in \mathcal{I}$*, with* $\mathring{x}_a \in \mathcal{F}_a(\mathring{y})$*.*

Proof Local rigidity implies that each $x \in \mathcal{F}_a(\mathring{y})$ has an open neighbourhood $\mathcal{U}_x \in \mathcal{M}^\tau$ such that all configurations $x' \in \mathcal{F}(\mathring{y}) \cap \mathcal{U}_x$ are congruent. Let $\mathcal{U}_a := \cup_{x\in\Phi_{\mathring{x}_a}(\mathbf{G})}\mathcal{U}_x$ be the union of these such neighbourhoods. The result then follows from the easily verified fact that congruence is an equivalence relation. ■

Definition 3.3.10. Let $\mathcal{F}(\mathring{y})$ be a formation that is equivariant with respect to a continuous group action $\Phi : \mathbf{G} \times \mathcal{M}^\tau \to \mathcal{M}^\tau$ of a Hausdorff topological group $\mathbf{G}$. An orbit $\Phi_{\mathring{x}}(\mathbf{G}) \subseteq \mathcal{F}(\mathring{y})$ of a configuration $\mathring{x} \in \mathcal{F}(\mathring{y})$ is termed a *rigid component* of $\mathcal{F}(\mathring{y})$ if all configurations $x \in \Phi_{\mathring{x}}(\mathbf{G})$ are locally rigid with respect to Φ. ◇

Lemma 3.3.9 provides insight into the relation between local rigidity and global rigidity. Specifically, a globally rigid formation consists of only one rigid component, while a locally rigid formation consists of multiple rigid components that have disjoint open neighbourhoods. Since any rigid component $\mathcal{F}_a(\mathring{y})$ of a locally rigid formation is a homogeneous space, one can conclude that the results of Theorem 3.3.7 apply in a local open neighbourhood $\mathcal{U}_a$ of $\mathcal{F}_a(\mathring{y})$.

Although it is not strictly required for the definition of rigidity presented in this chapter, it is often desirable for the full output map h to be invariant to Φ (Definition 3.2.27), rather than just a specific output value $\mathring{y}$ (Definition 3.2.33). With such structure, any configuration in the orbit of a locally rigid configuration will also be locally rigid.

Theorem 3.3.11. *Let* $\mathcal{F}(\mathring{y})$ *be a formation of an agent network* $\mathcal{N} := (\mathcal{M}^\tau, \mathcal{Y}, h)$*, and suppose that* $\mathcal{N}$ *is equivariant with respect to a continuous group action* $\Phi : \mathbf{G} \times \mathcal{M}^\tau \to \mathcal{M}^\tau$ *of a Hausdorff topological group* $\mathbf{G}$*. Let* $\mathring{x} \in \mathcal{F}(\mathring{y})$ *be a configuration that is locally rigid with respect* Φ*. Then, all configurations* $x \in \Phi_{\mathring{x}}(\mathbf{G})$ *are locally rigid with respect to* Φ*.*

Proof The result follows by noting that the bijective map $\Phi_S : \mathcal{M}^\tau \to \mathcal{M}^\tau, \Phi_S(x') \mapsto \Phi(S, x')$ has a continuous inverse $\Phi_{S^{-1}}$, and is therefore a homeomorphism. Specifically, let $\mathcal{U}_{\mathring{x}}$ be an open neighbourhood of $\mathring{x}$ such that all configurations $x \in \mathcal{F}(\mathring{y}) \cap \mathcal{U}_{\mathring{x}}$ are congruent. For any $S \in \mathbf{G}$, $\Phi_S(\mathcal{U}_{\mathring{x}})$ is an open neighbourhood of $\Phi_S(\mathring{x})$. Furthermore, the equivariance of $\mathcal{N}$ implies $h(\Phi_S(x')) = h(x')$ for any $x' \in \mathcal{U}_{\mathring{x}}$. Thus, for $x \in \mathcal{F}(\mathring{y}) \cap \mathcal{U}_{\mathring{x}}$ one has $\Phi_S(x) \in \mathcal{F}(\mathring{y})$, and $\Phi_S(x)$ is congruent to $\Phi_S(\mathring{x})$ since congruence is an equivalence relation. For $x' \notin \mathcal{F}(\mathring{y})$, one has $\Phi_S(x') \notin \mathcal{F}(\mathring{y})$. Therefore, $\Phi_S(\mathring{x})$ is locally rigid with respect to Φ. ■

Theorem 3.3.11 reveals that if $\mathcal{N}$ is equivariant with respect to Φ, then the existence of a locally rigid configuration $\mathring{x} \in \mathcal{F}(\mathring{y})$ implies there is at least one rigid component $\Phi_{\mathring{x}}(\mathbf{G})$. It should be observed that this does not imply the full formation $\mathcal{F}(\mathring{y})$ is locally rigid; there may be equivalent configurations that do not lie in $\Phi_{\mathring{x}}(\mathbf{G})$ and that are not locally rigid. The characterisation of the set of all rigid components for a general formation remains a difficult global problem for which the present theory offers no general solution; this challenge is made more difficult by the generality allowed in the output map h. However, it is worth noting that in many practical applications the local structure about a single rigid component is of primary interest.

3.4 Path-Rigidity

In this section I introduce the notion of *path-rigidity*, defined in Subsection 3.4.1. This is a stronger property than global rigidity and can be used to study the existence of trajectories between different configurations of a given formation, such that the formation constraints are preserved along the trajectory. In Subsection 3.4.2, I depart from the rigidity framework to derive a group theoretic result for homogeneous spaces, which is then employed to provide a useful characterisation of path-rigidity in Subsection 3.4.3.

3.4.1 Defining Path-Rigidity

Path-rigidity describes the case where one can transition between any two configurations of the formation using a continuous path that preserves all state constraints. In the classical literature, agent motions are typically considered via the notion of *infinitesimal rigidity*, as studied in Chapter 4. However, for the generalised rigidity framework, the notion of path-rigidity is motivated by the fact that a differentiable structure may not be present in some scenarios (in particular, the output map h may not be differentiable). The formal definition of path-rigidity is based on the notion of continuous congruence, defined as follows.

Definition 3.4.1. For a given agent network $\mathcal{N} := (\mathcal{M}^\tau, \mathcal{Y}, h)$ and a Hausdorff topological group $\mathbf{G}$ with continuous group action $\Phi : \mathbf{G} \times \mathcal{M}^\tau \to \mathcal{M}^\tau$, two configurations $x, x' \in \mathcal{M}^\tau$ of $\mathcal{N}$ are *continuously congruent* with respect to Φ if there exists a continuous parametrised function $\sigma(t) : [0,1] \to \mathbf{G}$ such that $\sigma(0) = \iota$ (where $\iota \in \mathbf{G}$ denotes the identity) and $\Phi(\sigma(1), x) = x'$. ◇

Definition 3.4.2. (**Path-rigidity**) Let $\mathcal{F}(\mathring{y})$ be a formation that is equivariant with respect to a continuous group action $\Phi : \mathbf{G} \times \mathcal{M}^\tau \to \mathcal{M}^\tau$ of a Hausdorff topological group $\mathbf{G}$. The formation $\mathcal{F}(\mathring{y})$ is *path-rigid* with respect to Φ if all configurations $x, x' \in \mathcal{F}(\mathring{y})$ are continuously congruent. ◇

It is clear from the definition that path-rigidity implies global rigidity. The following lemma provides a simple topological characterisation of path-rigidity.

Lemma 3.4.3. *Let* $\mathbf{G}$ *be a Hausdorff topological group with a continuous group action* $\Phi : \mathbf{G} \times \mathcal{M}^\tau \to \mathcal{M}^\tau$*. Then, a globally rigid formation* $\mathcal{F}(\mathring{y})$ *is path-rigid with respect to* Φ *if and only if, for any configuration* $\mathring{x} \in \mathcal{F}(\mathring{y})$*, the quotient* $\mathbf{G}/\operatorname{stab}\Phi_{\mathring{x}}$ *is path-connected.*

Proof The forward implication follows by projecting the path in $\mathbf{G}$ onto $\mathbf{G}/\operatorname{stab}\Phi_{\mathring{x}}$ (cf. Figure 3.4). For the reverse implication, recall from Theorem 3.3.7 that the stabilisers of each $\mathring{x} \in \mathcal{F}(\mathring{y})$ intersect the same number of path-connected components (since the group operation $(\cdot)$ is a homeomorphism), and that $\Psi_{\mathring{x}} : \mathbf{G}/\operatorname{stab}\Phi_{\mathring{x}} \to \mathcal{F}(\mathring{y})$ is a continuous bijection. Since the quotient $\mathbf{G}/\operatorname{stab}\Phi_{\mathring{x}}$ is path-connected, for any two points $x, x' \in \mathcal{F}(\mathring{y})$ there exists a continuous path $\sigma : [0,1] \to \mathbf{G}/\operatorname{stab}\Phi_{\mathring{x}}$

such that $\Psi_{\hat{x}} \circ \sigma$ is a continuous path from x to x'. By the universal property of quotients, σ lifts to a continuous path $\tilde{\sigma} : [0,1] \to \mathbf{G}$, which will have $\tilde{\sigma}(0) = \iota \in \mathbf{G}$ and $\Phi(\tilde{\sigma}(1), x) = x'$. ■

For further insight into path-rigidity, I will rely on group theory concerning the structure of $\mathbf{G}$, as studied in the next subsection.

3.4.2 Group Theoretic Analysis

In this subsection, I will present a group-theoretic result (see Theorem 3.4.7) that leads to a useful characterisation of path-rigidity in Subsection 3.4.3. The derivation of Theorem 3.4.7 requires several concepts and existing results from the literature, in addition to some preliminary analysis.

Given a Hausdorff topological group $\mathbf{G}$, let $\mathbf{G}^0$ denote the connected component (Singh [2013]) of the identity $\iota \in \mathbf{G}$. It is well-known that connected components are always closed ([Singh, 2013, Proposition 3.2.2]). Similarly, let $\mathbf{G}^1$ be the path-connected component (Singh [2013]) of the identity $\iota \in \mathbf{G}$, and note that $\mathbf{G}^1 \subseteq \mathbf{G}^0$. It is straightforward to show that both $\mathbf{G}^0$ and $\mathbf{G}^1$ are normal subgroups of $\mathbf{G}$ ([Singh, 2013, Proposition 12.2.4, Exercise 21 from Section 12.2]).

The analysis in this subsection concerns the quotient space $\mathbf{G}/\mathbf{H}$ formed with a closed subgroup $\mathbf{H} \subseteq \mathbf{G}$. Recall that $\mathbf{H}$ being closed is necessary and sufficient for this quotient to be Hausdorff ([Singh, 2013, Proposition 7.1.6 with Proposition 12.3.1]). To simplify the analysis, I will suppose that $\mathbf{G}/\mathbf{H}$ is path-connected if it is connected. The following proposition provides a useful sufficient condition for this assumption to hold.

Proposition 3.4.4. *Let $\mathbf{G}$ be a Hausdorff topological group with a closed subgroup $\mathbf{H} \subseteq \mathbf{G}$, and suppose that the quotient $\mathbf{G}/\mathbf{H}$ is connected. Then, $\mathbf{G}/\mathbf{H}$ is path-connected if the path-connected component $\mathbf{G}^1$ of the identity is open in $\mathbf{G}$.*

Proof The coset $G \cdot \mathbf{G}^1$ (with $G \in \mathbf{G}$) is an open, path-connected component of $\mathbf{G}$ since left multiplication by G is a homeomorphism. Since $G \in G \cdot \mathbf{G}^1$, every path-connected component of $\mathbf{G}$ is of this form. In particular, they are all open, and as a consequence they are all closed. It follows that all connected components of $\mathbf{G}$ are path-connected.

Note that the canonical projection $\pi : \mathbf{G} \to \mathbf{G}/\mathbf{H}$ is a continuous and open surjection ([Singh, 2013, Proposition 12.3.1]). It follows from the continuity of π that the image of a path-connected component is path-connected ([Singh, 2013, Proposition 3.3.5]). Also note that if two (or more) path-connected subspaces (in $\mathbf{G}/\mathbf{H}$) share a point, their union is path-connected ([Singh, 2013, Corollary 3.3.3]).

Now suppose, for a contradiction, that $\mathbf{G}/\mathbf{H}$ is not path-connected. There must then exist two complementary collections $\{\mathbf{G}_{a\in\mathcal{I}}\}$ and $\{\mathbf{G}_{b\in\mathcal{I}}\}$ of (path-)connected components of $\mathbf{G}$ whose images (under π) are disjoint (here, $\mathcal{I}$ denotes an index set). Since π is open these images are open, and since π is a surjection these images form a partition of $\mathbf{G}/\mathbf{H}$. This would imply that $\mathbf{G}/\mathbf{H}$ is not connected, which contradicts the assumption of the proposition. ■

The requirement that $\mathbf{G}/\mathbf{H}$ be path-connected if it is connected may seem a little obscure in practice, and therefore I will adopt the more convenient assumption that $\mathbf{G}^1$ is open for the sequel. I am not aware of any practical scenario where this distinction is relevant, but all following results will hold for the more general condition if required. A particularly common case for which Proposition 3.4.4 applies is where $\mathbf{G}$ is locally path-connected (as defined in Singh [2013]). The fact that $\mathbf{G}^1$ is open for this case is given by Corollary 3.4.7 of Singh [2013].

In the following proposition I study the relationship between the connected components of a group $\mathbf{G}$ and those of a closed subgroup $\mathbf{H}$.

Proposition 3.4.5. *Let $\mathbf{G}$ be a Hausdorff topological group and $\mathbf{H} \subseteq \mathbf{G}$ a closed subgroup. Let $\mathbf{G}^0$ and $\mathbf{H}^0$ be the connected components of the identities in $\mathbf{G}$ and $\mathbf{H}$, respectively. Then the subgroup $\mathbf{H} \cap \mathbf{G}^0 \subseteq \mathbf{H}$ is normal in $\mathbf{H}$ and the group homomorphism*

$$\alpha : \mathbf{H}/\mathbf{H}^0 \to \mathbf{H}/(\mathbf{H} \cap \mathbf{G}^0), H \cdot \mathbf{H}^0 \mapsto H \cdot (\mathbf{H} \cap \mathbf{G}^0)$$

is well-defined and surjective for $H \in \mathbf{H}$. Furthermore, the group homomorphism

$$\beta : \mathbf{H}/(\mathbf{H} \cap \mathbf{G}^0) \to \mathbf{G}/\mathbf{G}^0, H \cdot (\mathbf{H} \cap \mathbf{G}^0) \mapsto H \cdot \mathbf{G}^0 \tag{3.6}$$

is well-defined and injective.

Proof Note that $H \cdot (\mathbf{H} \cap \mathbf{G}^0) \cdot H^{-1} \subseteq H \cdot \mathbf{H} \cdot H^{-1} \subseteq \mathbf{H}$ since $\mathbf{H}$ is a group and $H \cdot (\mathbf{H} \cap \mathbf{G}^0) \cdot H^{-1} \subseteq H \cdot \mathbf{G}^0 \cdot H^{-1} \subseteq \mathbf{G}^0$ since $\mathbf{G}^0$ is normal in $\mathbf{G}$. It follows that $H \cdot (\mathbf{H} \cap \mathbf{G}^0) \cdot H^{-1} \subseteq \mathbf{H} \cap \mathbf{G}^0$ and so $\mathbf{H} \cap \mathbf{G}^0$ is normal in $\mathbf{H}$.

Let $H_1, H_2 \in \mathbf{H}$ with $H_1 \cdot \mathbf{H}^0 = H_2 \cdot \mathbf{H}^0$. Then there exists $H_3 \in \mathbf{H}^0$ such that $H_1 = H_2 \cdot H_3$. Since $\mathbf{H}^0$ is connected and contains the identity element of $\mathbf{H}$ and $\mathbf{G}$, one has $\mathbf{H}^0 \subseteq \mathbf{G}^0$ and hence $H_3 \in \mathbf{H} \cap \mathbf{G}^0$. Therefore $H_1 \cdot (\mathbf{H} \cap \mathbf{G}^0) = H_2 \cdot (\mathbf{H} \cap \mathbf{G}^0)$ and so α is well-defined. It is surjective since $\mathbf{H}^0 \subseteq \mathbf{H} \cap \mathbf{G}^0$.

Now consider $H_1, H_2 \in \mathbf{H}$ with $H_1 \cdot (\mathbf{H} \cap \mathbf{G}^0) = H_2 \cdot (\mathbf{H} \cap \mathbf{G}^0)$. Then there exists $H_3 \in \mathbf{H} \cap \mathbf{G}^0$ with $H_1 = H_2 \cdot H_3$. Since $H_3 \in \mathbf{G}^0$, this implies that $\beta(H_1 \cdot (\mathbf{H} \cap \mathbf{G}^0)) = H_1 \cdot \mathbf{G}^0 = H_2 \cdot \mathbf{G}^0 = \beta(H_2 \cdot (\mathbf{H} \cap \mathbf{G}^0))$ and so β is well-defined.

Finally, let $H_1, H_2 \in \mathbf{H}$ with $\beta(H_1 \cdot (\mathbf{H} \cap \mathbf{G}^0)) = H_1 \cdot \mathbf{G}^0 = H_2 \cdot \mathbf{G}^0 = \beta(H_2 \cdot (\mathbf{H} \cap \mathbf{G}^0))$. Then there exists $H_3 \in \mathbf{G}^0$ such that $H_1 = H_2 \cdot H_3$. This implies that $H_3 = H_2^{-1} \cdot H_1 \in \mathbf{H}$ and hence that $H_3 \in \mathbf{H} \cap \mathbf{G}^0$. It follows that $H_1 \cdot (\mathbf{H} \cap \mathbf{G}^0) = H_2 \cdot (\mathbf{H} \cap \mathbf{G}^0)$ and therefore β is injective. ∎

For the main result of this subsection, the notion of the *component group* is also of interest.

Definition 3.4.6. Let $\mathbf{G}$ be a Hausdorff topological group and let $\mathbf{G}^0$ be the connected component of the identity. The *component group* of $\mathbf{G}$ is defined as $\pi_0(\mathbf{G}) := \mathbf{G}/\mathbf{G}^0$. ◇

Given a subgroup $\mathbf{H} \subseteq \mathbf{G}$, one can define a homomorphism on the component groups by

$$\pi_0^{\mathrm{id}} : \pi_0(\mathbf{H}) \to \pi_0(\mathbf{G}), H \cdot \mathbf{H}^0 \mapsto \mathrm{id}(H) \cdot \mathbf{G}^0, \tag{3.7}$$

where id : $\mathbf{H} \hookrightarrow \mathbf{G}, H \mapsto H$ denotes the inclusion group homomorphism.

I conclude this subsection with the following theorem.

Theorem 3.4.7. *Let $\mathbf{G}$ be a Hausdorff topological group, let $\mathbf{H}$ be a closed subgroup of $\mathbf{G}$, and let $\mathbf{G}^0$ and $\mathbf{H}^0$ be the connected components of the identities in $\mathbf{G}$ and $\mathbf{H}$, respectively. Assume the path-connected component $\mathbf{G}^1$ of the identity in $\mathbf{G}$ is open. Then the following are equivalent:*

(i) The homogeneous space $\mathbf{G}/\mathbf{H}$ is connected.

(ii) The subgroup $\mathbf{H}$ contains an element from every connected component of $\mathbf{G}$.

(iii) The homomorphism π_0^{id} (3.7) *of component groups is surjective.*

(iv) The homomorphism β (3.6) *is an isomorphism.*

(v) For every $G \in \mathbf{G}$ there exist $H \in \mathbf{H}$ and $G^0 \in \mathbf{G}^0$ such that $G = H \cdot G^0$.

Proof The proof is given as a sequence of implications and equivalences.

(i) $\Rightarrow$ (ii): By Proposition 3.4.4, $\mathbf{G}/\mathbf{H}$ is path-connected. Let $\sigma : [0,1] \to \mathbf{G}/\mathbf{H}$ be a continuous path connecting $\iota \cdot \mathbf{H}$ to any $G \cdot \mathbf{H}$ in $\mathbf{G}/\mathbf{H}$. By the universal property of quotients, the path σ lifts to a continuous path $\tilde{\sigma} : [0,1] \to \mathbf{G}$ such that $\sigma = \pi \circ \tilde{\sigma}$, where $\pi : \mathbf{G} \to \mathbf{G}/\mathbf{H}$ is the canonical projection. By design, the path $\tilde{\sigma}$ connects some element $\iota \cdot H_1 = H_1 \in \mathbf{H} \subseteq \mathbf{G}$ to some element $G \cdot H_2 \in \mathbf{G}$, where $H_2 \in \mathbf{H}$. It follows that $\tilde{\sigma} \cdot H_2^{-1}$ is a continuous path connecting $H_1 \cdot H_2^{-1} \in \mathbf{H} \subseteq \mathbf{G}$ to $G \in \mathbf{G}_1 \subseteq \mathbf{G}$, where $\mathbf{G}_1$ is the path-connected component of G. This implies that $H_1 \cdot H_2^{-1} \in \mathbf{G}_1 \cap \mathbf{H}$. Since G is arbitrary, every path-connected component $\mathbf{G}_1$ contains an element of $\mathbf{H}$.

(ii) $\Rightarrow$ (i): Let $\mathbf{G}_1$, $\mathbf{G}_2$ be two path-connected components of $\mathbf{G}$ (I allow $\mathbf{G}_1 = \mathbf{G}_2$), with $G_1 \in \mathbf{G}_1$ and $G_2 \in \mathbf{G}_2$. Pick $H_1 \in \mathbf{G}_1 \cap \mathbf{H}$ and $H_2 \in \mathbf{G}_2 \cap \mathbf{H}$. The map $\gamma : \mathbf{G} \to \mathbf{G}$, $G \mapsto G \cdot (H_1^{-1} \cdot H_2)$ is a homeomorphism, so the image of $\mathbf{G}_1$ is a path-connected component of $\mathbf{G}$. Since $H_2 = H_1 \cdot (H_1^{-1} \cdot H_2) = \gamma(H_1)$, one has $\gamma(\mathbf{G}_1) = \mathbf{G}_2$. In particular, $\gamma(G_1) = G_1 \cdot (H_1^{-1} \cdot H_2) \in \mathbf{G}_2$ and hence there is a continuous path $\tilde{\sigma} : [0,1] \to \mathbf{G}$ connecting $G_1 \cdot (H_1^{-1} \cdot H_2)$ to G_2. Let $\pi : \mathbf{G} \to \mathbf{G}/\mathbf{H}$ be the canonical projection, and then $\sigma := \pi \circ \tilde{\sigma}$ is a continuous path connecting $G_1 \cdot \mathbf{H}$ to $G_2 \cdot \mathbf{H}$ in $\mathbf{G}/\mathbf{H}$. Since G_1 and G_2 are arbitrary, the quotient $\mathbf{G}/\mathbf{H}$ is path-connected.

(ii) $\Rightarrow$ (iii): For any $G \in \mathbf{G}$ there exists $H \in \mathbf{H}$ with $H \in G \cdot \mathbf{G}^0$. This implies that $\pi_0^{\mathrm{id}}(H \cdot \mathbf{H}^0) = H \cdot \mathbf{G}^0 = G \cdot \mathbf{G}^0$, and since $G \in \mathbf{G}$ is arbitrary this means that π_0^{id} is surjective.

(iii) $\Rightarrow$ (ii): For any $G \in \mathbf{G}$ there exists $H \in \mathbf{H}$ such that $G \cdot \mathbf{G}^0 = H \cdot \mathbf{G}^0 = \pi_0^{\mathrm{id}}(H \cdot \mathbf{H}^0)$. In particular, $H \in G \cdot \mathbf{G}^0$. Since $G \in \mathbf{G}$ is arbitrary, for every connected component $G \cdot \mathbf{G}^0$ there exists $H \in \mathbf{H}$ with $H \in G \cdot \mathbf{G}^0$.

(iii) $\Leftrightarrow$ (iv): By definition the homomorphism π_0^{id} factors as $\pi_0^{\mathrm{id}} = \beta \circ \alpha$ with α surjective. Hence, π_0^{id} is surjective if and only if β surjective. Since β is always injective, this is the case if and only if β is an isomorphism.

(iv) $\Rightarrow$ (v): For any $G \in \mathbf{G}$ there exists $H \in \mathbf{H}$ such that $G \cdot \mathbf{G}^0 = \beta(H \cdot (\mathbf{H} \cap \mathbf{G}^0)) = H \cdot \mathbf{G}^0$. Hence, there exists $G^0 \in \mathbf{G}^0$ such that $G = H \cdot G^0$.

(v) $\Rightarrow$ (iv): For any $G \in \mathbf{G}$ there exists $H \in \mathbf{H}$ and $G^0 \in \mathbf{G}^0$ such that $G = H \cdot G^0$. This implies $G \cdot \mathbf{G}^0 = H \cdot \mathbf{G}^0 = \beta(H \cdot (\mathbf{H} \cap \mathbf{G}^0))$. Since $G \in \mathbf{G}$ is arbitrary, β is surjective and hence an isomorphism. ■

3.4.3 Analysis of Path-Rigidity

In this subsection I return to the rigidity framework and provide further analysis of path-rigidity. In particular, I combine the insight from Theorem 3.4.7 with Lemma 3.4.3 to derive a group-theoretic characterisation of this property.

Corollary 3.4.8 presents the main result for this subsection, which follows from Theorem 3.4.7 by considering $\mathbf{H} = \operatorname{stab} \Phi_{\mathring{x}}$.

Corollary 3.4.8. *Let* $\mathbf{G}$ *be a Hausdorff topological group with a continuous group action* $\Phi : \mathbf{G} \times \mathcal{M}^\tau \to \mathcal{M}^\tau$*. Assume the path-connected component* $\mathbf{G}^1$ *of the identity in* $\mathbf{G}$ *is open. Then, a globally rigid formation* $\mathcal{F}(\mathring{y})$ *is path-rigid with respect to* Φ *if and only if the stabiliser of any configuration* $\mathring{x} \in \mathcal{F}(\mathring{y})$ *contains at least one element from every (path-)connected component of* $\mathbf{G}$*.*

Proof By Theorem 3.4.7, the quotient $\mathbf{G}/\operatorname{stab} \Phi_{\mathring{x}}$ is path-connected if and only if $\operatorname{stab} \Phi_{\mathring{x}}$ contains an element from every (path-)connected component of $\mathbf{G}$. The result follows from Lemma 3.4.3. ■

The application of this result is demonstrated by the following examples.

Example 3.4.9. Recall the scenario described in Example 3.3.6, where the formation is a triangle perpendicular to the x-y plane, to which two of the agents are constrained. It was established that this formation is globally rigid with respect to $\mathrm{E}(2)$ transforms. However, it is not difficult to see that it is actually globally rigid with respect to $\mathrm{SE}(2)$ transforms, since any reflection can be equivalently achieved by the combination of a rotation and a translation. Since $\mathrm{SE}(2)$ is a path-connected group, it follows that the formation is path-rigid. Corollary 3.4.8 provides a more elegant way of observing this: for the action of $\mathrm{E}(2)$ on any configuration of the formation, the stabiliser will contain a reflection through the plane containing the triangle. Since this stabiliser includes a point from both (path-)connected components of $\mathrm{E}(2)$, one can conclude that the formation is path-rigid. ◇

A helpful feature of Corollary 3.4.8 is that the stabiliser only needs to be considered for a single configuration of the formation. I believe this corollary is of particular appeal in more complex scenarios involving non-product topologies on the state-space, as in the following examples.

Example 3.4.10. Consider four agents in $\mathbb{R}^3$, with the full state-space possessing the product topology. Suppose the distance between each pair of agents (i.e. $M = 6$) is constrained to a value of 2. This specifies a triangular pyramid formation that is globally rigid with respect to the action of $\mathrm{E}(3)$. The formation is not path-rigid, because the stabiliser only includes the identity (specifically, a reflection through a plane containing three agents will move the fourth agent to the other side of that plane, and no $\mathrm{SE}(3)$ transform will be able to revert this change).

Now suppose that we wish to regard agents 1 and 2 as interchangeable (see Remark 3.2.23 and Example 3.2.24). To enable this, suppose we quotient the measurement space by the equivalence relation $\tilde{y} \sim_y \tilde{y}' \Leftrightarrow \exists \sigma \in \mathbf{P}_6 : \tilde{y}' = \sigma(\tilde{y})$ for $\tilde{y}, \tilde{y}' \in \mathcal{Y}^{\wp}$, i.e. let $\mathcal{Y}^{\tau} := \mathcal{Y}^{\wp} / \sim_y$. The state-space can then defined by $\mathcal{M}^{\tau} := \mathcal{M}^{\wp} / \sim_x$, where $(x_1, x_2, x_3, x_4) \sim_x (x_2, x_1, x_3, x_4)$. Clearly, the specified formation is still a triangular pyramid that is globally rigid with respect to the group action of $\mathrm{E}(3)$. Now consider a configuration of the formation where $x_1 = (-1, 0, 0)^{\top}$ and $x_2 = (1, 0, 0)^{\top}$, which ensures that both x_3 and x_4 must lie in the y-z plane. A reflection through this plane will therefore only switch the positions of agents 1 and 2. Since these are interchangeable, such a reflection is an element of the stabiliser. Consequently, one can conclude from Corollary 3.4.8 that the formation is path-rigid. $\diamond$

Example 3.4.11. Recall the scenario considered in Example 3.3.5, where a rectangular formation is specified for four agents using sensor modalities that do not distinguish between agents. With a product topology on the state-space, it was established that the formation is locally rigid with respect to the action of $\mathrm{E}(2)$. For global rigidity, the group action must additionally include permutations of agents 2, 3 and 4; thus, the formation is globally rigid with respect to the group action of $\mathbf{P}_3 \times \mathrm{E}(2)$ given by $\Phi((\sigma, S), x) := \tilde{\sigma}(\Phi^{\mathrm{E}}_S(x))$, where Φ^{E}_S is the standard Euclidean transform acting on the individual agent states and $\tilde{\sigma}(x) := (x_1, \sigma_1(x_2, x_3, x_4), \sigma_2(x_2, x_3, x_4), \sigma_3(x_2, x_3, x_4))$ for $\sigma \in \mathbf{P}_3$. The group $\mathbf{P}_3 \times \mathrm{E}(2)$ has 12 path-connected components, and it is clear that for an arbitrary rectangle, those involving a permutation of the agents will not intersect the stabiliser, meaning that the formation is not path-rigid.

Now suppose the state-space has the quotient topology $\mathcal{M}^{\tau} := \mathcal{M}^{\wp} / \sim$ as considered in the latter part of Example 3.3.5 (where $\sim$ denotes the equivalence relation obtained by permutations of agents 2, 3 and 4). The quotient topology means transforms that only apply a permutation of the agents will lie in the stabiliser; however, a reflection of the rectangle will change whether its longer side lies clockwise or anticlockwise from agent 1. Thus, components of the group that include a Euclidean reflection do not intersect the stabiliser and the formation is still not path-rigid. However, in the special case where the formation is a square (i.e. $a = b$ in (3.4)), any reflection can be combined with a de-rotation and translation such that an equivalent square results from the transform. The fact that this changes the order of the agents around the perimeter of the square has no consequence since the state-space is factored by agent permutations, and it follows from Corollary 3.4.8 that the formation will be path-rigid. $\diamond$

3.5 Conclusions and Future Work

In this chapter I have presented a generalised framework for the concept of rigidity, suitable for a very broad class of state-spaces and state constraints. The generality of this new framework enables it to address a variety of interesting scenarios that are not readily accommodated by existing techniques in the literature; for example, one may consider vehicles in different state-spaces (e.g. aerial vehicles in formation with ground vehicles), vehicles using different sensor modalities, and vehicles that are interchangeable due to functional equivalence. The formulation of rigidity is developed with respect to a symmetry described by the action of a group; specifically, a formation is *globally rigid* if all configurations satisfying the constraints are contained in the orbit of the group action. This group-theoretic perspective of rigidity plays a key role in achieving the generality of the framework; by contrast, the common graph-based approaches in the existing literature are not easily extended to situations where the nodes (or edges) may differ in structure. To aid global analysis of rigid formations in this generalised framework, I have introduced the notion of *path-rigidity*, where one can transition between any two configurations of a globally rigid formation without breaching any of the state constraints. I have characterised this property with a simple group-theoretic result involving the stabiliser of any configuration in a globally rigid formation.

For future work, it may be of interest to perform further analysis on the path-connected components of a globally rigid formation that is not path-rigid. This might be achieved by considering a local version of Theorem 3.4.8. One can begin by considering the path-connected components of the group that intersect the stabiliser of a configuration in a globally rigid formation. If these path-connected components form a subgroup $\mathbf{H}$ of $\mathbf{G}$, and the formation is a regular submanifold of $\mathcal{M}^\tau$ (see the next chapter for sufficient conditions for this), then it is clear that an analogous result to Theorem 3.4.8 can be applied with $\mathbf{H}$. Thus, a natural objective for further analysis is to relax these conditions.

The insight concerning path-rigidity is likely to be of particular interest for trajectory planning applications. For example, consider a collection of interchangeable vehicles for which a desired formation has been specified, along with a desired final configuration within the formation. The first task of the trajectory planner would be to determine the path-connected component of the formation that contains the desired state. Then, it can direct the vehicles towards a nearby configuration in this path-connected component, and proceed to guide the formation along the group orbit towards the final state.

The rigidity framework developed in this chapter is extremely general, and it is my hope that there are many other applications for which it may prove useful. However, it should be acknowledged that this generality comes at the cost of analysis techniques that may rely upon additional structure. Adaptations of this framework for particular applications, and the consequences of additional structural assumptions, is a clear avenue for future research on this notion of rigidity. A primary example of this is provided by the application of formation control, where the property of *infinitesimal rigidity* and the associated analytical tools are of key interest. This particular extension of the rigidity framework is explored in detail in the next chapter.

Chapter 4

Generalised Infinitesimal Rigidity

In this chapter I build upon the generalised rigidity framework developed in Chapter 3 to study a generalised notion of *infinitesimal rigidity*. To define this property, I assume the output map from the system state is smooth, and that the symmetry associated with the system is described by the Lie group action of a Lie group. Infinitesimal rigidity can then be naturally defined as the case where the Lie algebra captures all infinitesimal deviations from a configuration that do not instantaneously change the output value of the system's state. I show that several fundamental properties of infinitesimal rigidity in the classical setting can be extended to the generalised framework, and I introduce a new notion of *robust rigidity* that is of interest for scenarios involving non-compact formations (this property is guaranteed for the classical case). The theory developed in this chapter is demonstrated through application to network localisation and formation control tasks in a highly abstract setting, involving arbitrary agent state-spaces and sensor modalities. The material presented here draws from Stacey and Mahony [2016], submitted for publication.

4.1 Introduction

In classical rigidity theory, the property of *infinitesimal rigidity* describes whether infinitesimal variations of the agents are constrained to rigid-body motions. This concept has emerged as a key tool for the analysis of agent networks. An important result is that infinitesimal rigidity implies local rigidity, as shown by Asimow and Roth [1979]. Furthermore, if one configuration of an agent network is infinitesimally rigid, then all *generic* or *regular* configurations are infinitesimally rigid (see Asimow and Roth [1979] or Appendix B). A consequence of this is that the set of infinitesimally rigid configurations must be open. Thus, the study of infinitesimal rigidity provides valuable insight for the stability analysis of network localisation tasks (as in Aspnes et al. [2006]) and of formation control schemes (see e.g. Anderson et al. [2008]; Krick et al. [2009]; Oh and Ahn [2011]; Zelazo et al. [2015]) in a local neighbourhood of a given infinitesimally rigid formation.

An appealing aspect of the structure associated with infinitesimal rigidity is that it ensures the set of configurations satisfying the constraints corresponds to a regular submanifold of the full state-space (Asimow and Roth [1978]). This has enabled the application of centre-manifold theory as utilised by Krick et al. [2009], and other geometrical approaches such as that of Dörfler and Francis [2010]. Alternatively, stability analysis may rely on the stronger property of *minimal infinitesimal rigidity*, where the number of constraints are minimised in order to remove undesired equilibria from the control system. With this property, exponential convergence to a desired configuration can be readily demonstrated using Lyapunov-based techniques, as in Dörfler and Francis [2009]. Recent work by Sun et al. [2016] has used a similar approach, but relaxed the requirement of minimal rigidity. This is achieved by considering a subset of the state constraints, with respect to which the formation is then minimally rigid. While the notion of infinitesimal rigidity is typically concerned with distance constraints between agents in Euclidean space, it has been extended to some specific non-classical scenarios in the literature (e.g. the case of bearing measurements between agents in $SE(2)$ addressed by Zelazo et al. [2014]). However, to my knowledge there remains no sufficiently general framework for the application of infinitesimal rigidity theory to cases involving arbitrary and mixed state-spaces and state constraints, as are commonly encountered in the tasks of network localisation and formation control.

In this chapter, I incorporate a generalised notion of *infinitesimal rigidity* into the generalised rigidity framework developed in Chapter 3. Although this theory is primarily developed with network localisation and formation control problems in mind, it should be noted that it is not specific to such applications. For this work I assume a differentiable structure on the state-spaces and the sensor modalities, and the stronger form of invariance described in Definition 3.2.27; i.e. that the full *output map* is invariant with respect to the group action rather than just a specific *output value*. With this structure, I define infinitesimal rigidity as the case where the Lie algebra of the system's symmetry describes (via the differential of the group action) all infinitesimal deviations from a configuration that do not result in an instantaneous change in the output value. I prove that in the generalised case, an infinitesimally rigid formation is composed of multiple regular submanifolds of the state-space that may be of differing dimensions. In addition, I show that the set of infinitesimally rigid configurations is open. This extends the aforementioned fundamental results from the classical setting in Asimow and Roth [1978, 1979], which have been of critical value for rigidity applications. I also introduce a new concept of *robust rigidity*, which is associated with the structure of the output map in an open neighbourhood of a non-compact formation. I provide a useful characterisation of this property in terms of the symmetry of the group action, and note that it is guaranteed for the classical distance-only scenario. The significance of these results is demonstrated with two example applications, concerning the tasks of network localisation and formation control with kinematic agents. The generality of the rigidity framework enables solutions to these problems to be developed in an extremely abstract setting that has not been fully addressed by existing approaches in the literature.

Following the present introduction, Section 4.2 describes the additional structural assumptions required for the theory developed in this chapter (relative to the slightly more general formulation of rigidity in Chapter 3), before proceeding to the extension of *infinitesimal rigidity* to the generalised setting. The new concept of *robust rigidity* is presented in Section 4.3. Section 4.4 presents two case studies, illustrating applications of the theory to network localisation and formation control problems. Concluding remarks are given in Section 3.5.

4.2 Infinitesimal Rigidity

This section studies the concept of *infinitesimal rigidity* in the generalised framework. The notion of infinitesimal rigidity requires the output map h to be differentiable (at least in the region of interest) and assumes the symmetry of the formation to be described by the action of a Lie group $\mathbf{G}$. Infinitesimal rigidity is defined as the case where all infinitesimal motions of the agents, such that the formation constraints are preserved, are associated with an element of the Lie algebra $\mathfrak{g}$ of $\mathbf{G}$. In the classical case (see Appendix B), the property of infinitesimal rigidity is determined by the rank of the *rigidity matrix*. For the generalised case, the rigidity matrix is essentially a Jacobian that describes how the measurements change with respect to infinitesimal variations of the agent states (in local coordinates). This enables the generalised form of infinitesimal rigidity to be studied in a similar manner to the classical case, as discussed in Remark 4.2.3 and Example 4.2.9.

The property of infinitesimal rigidity is defined for the generalised setting in Subsection 4.2.1. In Subsection 4.2.2 I extend several well-known results for the classical case to the generalised scenario. In particular, given a formation $\mathcal{F}(\mathring{y})$ that is infinitesimally rigid with respect to a group action Φ, I show that $\mathcal{F}(\mathring{y})$ is also locally rigid with respect to Φ, that each rigid component (Definition 3.3.10) of $\mathcal{F}(\mathring{y})$ is a closed regular submanifold of the state-space[1] $\mathcal{M}$, and that there is an open neighbourhood about $\mathcal{F}(\mathring{y})$ on which all configurations are infinitesimally rigid with respect to Φ. Some basic examples concerning infinitesimal rigidity are provided in Subsection 4.2.3.

4.2.1 Defining Infinitesimal Rigidity

For the study of infinitesimal rigidity, some additional structure is assumed throughout this chapter, relative to that required in Chapter 3. Firstly, the state-space $\mathcal{M}$ and output space $\mathcal{Y}$ are assumed to be smooth (C^∞) finite-dimensional Riemannian manifolds, and the output map $h : \mathcal{M} \to \mathcal{Y}$ is also assumed to be smooth. Note that points for which this structure fails to hold can be excluded in the manner demonstrated by Example 3.2.2 and Remark 3.2.36. I will suppose that $\mathbf{G}$ is a Lie group with Lie algebra $\mathfrak{g}$ and a Lie group action $\Phi : \mathbf{G} \times \mathcal{M} \to \mathcal{M}$. Finally, I will assume that the full output map h is invariant in the sense of Definition 3.2.27, rather than allowing the weaker condition where a specific output value is invariant (Definition 3.2.33). That

[1]Different topologies on the state-space $\mathcal{M}$ and the output space $\mathcal{Y}$ will not be considered in this chapter; consequently, I will omit the superscripts indicating the associated topology throughout this chapter.

is, I assume the agent network $\mathcal{N}$ is equivariant with respect to Φ (Part (i) of Definition 3.2.37), rather than only assuming the formation $\mathcal{F}(\mathring{y})$ is equivariant (Part (ii) of Definition 3.2.37). This assumption provides desirable structure for control applications (the symmetry will not be altered by perturbations from the desired formation), and is necessary for the proofs of many substantial results in this chapter.

Definition 4.2.1. Let $\mathcal{N} := (\mathcal{M}, \mathcal{Y}, h)$ be an agent network, with $\mathcal{M}$ and $\mathcal{Y}$ being smooth finite-dimensional Riemannian manifolds and h a smooth map. A (first-order) *infinitesimal variation* of a configuration $x \in \mathcal{M}$ is a tangent vector $\Delta_x \in T_x\mathcal{M}$. A (first-order) *infinitesimal motion* (Hendrickson [1992]; Zelazo et al. [2015]) is an infinitesimal variation $\Delta_x \in T_x\mathcal{M}$ such that

$$\mathrm{D}h(x)[\Delta_x] = 0. \tag{4.1}$$

$\diamond$

The intuition here is that infinitesimal motions from the configuration x do not instantaneously change the output value $y = h(x)$. For a curve $x(t)$ with $\dot{x}(0) = \Delta_x$, an infinitesimal motion from the formation $\mathcal{F}(h(x(0)))$ satisfies

$$\frac{\mathrm{d}}{\mathrm{d}t}y(0) = \mathrm{D}h(x(0))[\dot{x}(0)] = \mathrm{D}h(x(0))[\Delta_x] = 0.$$

Motions of this nature may be thought of as "moving in formation"; that is, moving the configuration x while preserving the formation constraints. The generalised notion of infinitesimal rigidity can now be presented.

Definition 4.2.2. (**Infinitesimal rigidity**) Let $\mathcal{N} := (\mathcal{M}, \mathcal{Y}, h)$ be an agent network, with $\mathcal{M}$ and $\mathcal{Y}$ being smooth finite-dimensional Riemannian manifolds and h a smooth map. Suppose $\mathcal{N}$ is equivariant with respect to a Lie group action $\Phi : \mathbf{G} \times \mathcal{M} \to \mathcal{M}$ of a Lie group $\mathbf{G}$ with Lie algebra $\mathfrak{g}$. A configuration $x \in \mathcal{M}$ is *infinitesimally rigid* (with respect to Φ) if, for all infinitesimal motions $\Delta_x \in T_x\mathcal{M}$ (4.1), there exists $u \in \mathfrak{g}$ such that $\Delta_x = \mathrm{D}\Phi_x(\iota)[u]$ (where ι is the identity in $\mathbf{G}$ and $\Phi_x(S) := \Phi(S, x)$). A formation $\mathcal{F}(\mathring{y})$ of $\mathcal{N}$ is *infinitesimally rigid* with respect to Φ if all configurations $x \in \mathcal{F}(\mathring{y})$ are infinitesimally rigid. $\diamond$

Remark 4.2.3. (**Local coordinates**) It is often useful to define a local coordinate map in an open neighbourhood $\mathcal{U}_{\mathring{x}}$ of a given configuration $\mathring{x} \in \mathcal{F}(\mathring{y})$. Let $q := \theta_{\mathring{x}}(x)$ denote the local coordinates of a configuration $x \in \mathcal{U}_{\mathring{x}}$ described by the smooth coordinate transform $\theta_{\mathring{x}} : \mathcal{U}_{\mathring{x}} \to \mathbb{R}^n$, where $n := \dim \mathcal{M}$ and $\theta_{\mathring{x}}(\mathring{x}) := 0$. Similarly, let $p := \varphi_{\mathring{y}}(y) \in \mathbb{R}^m$ denote the local coordinates of a point y in a local open neighbourhood $\mathcal{U}_{\mathring{y}} \subseteq \mathcal{Y}$ of $\mathring{y}$ (with $m := \dim \mathcal{Y}$ and $\varphi_{\mathring{y}}(\mathring{y}) := 0$). Define the *generalised rigidity matrix* as $J_{\mathring{x}}(q) := \mathrm{d}/\mathrm{d}q\ \varphi_{\mathring{y}}(h(\theta_{\mathring{x}}^{-1}(q)))$, i.e. the derivative of the map $\varphi_{\mathring{y}} \circ h \circ \theta_{\mathring{x}}^{-1}$ with respect to q (on the set $\theta_{\mathring{x}}(h^{-1}(\mathcal{U}_{\mathring{y}}) \cap \mathcal{U}_{\mathring{x}})$). In these coordinates, the infinitesimal motions (4.1) are described by

$$\Delta_p := J_{\mathring{x}}(q)\Delta_q = 0, \tag{4.2}$$

where $\Delta_q \in \mathbb{R}^n$ and $\Delta_p \in \mathbb{R}^m$ denote tangent vectors of $x \in \mathcal{M}$ and $h(x) \in \mathcal{Y}$, respectively. The Jacobian $J_{\mathring{x}}(q)$ is analogous to the classical rigidity matrix described in Appendix B, as discussed in Example 4.2.9. In coordinate-free language, the linear map defined by the differential $\mathrm{D}h(x)[\cdot] : T_x\mathcal{M} \to T_{h(x)}\mathcal{Y}$ is the natural generalisation of the rigidity matrix. $\diamond$

Define a subspace $\mathbb{V}(x) \subset T_x\mathcal{M}$ by

$$\mathbb{V}(x) := \operatorname{span}\{\mathrm{D}\Phi_x(\iota)[u] \mid u \in \mathfrak{g}\}, \tag{4.3}$$

i.e. $\mathbb{V}(x)$ is the image of $\mathfrak{g}$ under the tangent mapping $\mathrm{D}\Phi_x(\iota)$. In the following lemma I use this construction to present a useful equivalent characterisation of infinitesimally rigid configurations.

Lemma 4.2.4. *Let $\mathcal{N} := (\mathcal{M}, \mathcal{Y}, h)$ be an agent network, with $\mathcal{M}$ and $\mathcal{Y}$ being smooth finite-dimensional Riemannian manifolds and h a smooth map. Suppose $\mathcal{N}$ is equivariant with respect to a Lie group action $\Phi : \mathbf{G} \times \mathcal{M} \to \mathcal{M}$ of a Lie group $\mathbf{G}$ with Lie algebra $\mathfrak{g}$. Then,*

(i) for all $x \in \mathcal{M}$, $\mathbb{V}(x) \subseteq \ker \mathrm{D}h(x)$.

(ii) a configuration $x \in \mathcal{M}$ is infinitesimally rigid with respect to Φ if and only if $\mathbb{V}(x) = \ker \mathrm{D}h(x)$.

Proof To see (i), first observe that $\mathrm{D}\Phi_x(\iota)$ is surjective on $\mathbb{V}(x)$ by definition (4.3). Equivariance of $\mathcal{N}$ with respect to Φ implies that $h(\Phi_x(S(t))) = \mathring{y}$ is constant for all curves $S(t) \in \mathbf{G}$ with $S(0) = \iota$. Therefore, $\frac{\mathrm{d}}{\mathrm{d}t}\mathring{y} = 0 = (\mathrm{D}h(x) \circ \mathrm{D}\Phi_x(\iota))[\dot{S}(0)] = \mathrm{D}h(x)[v]$ for $\dot{S}(0) \in \mathfrak{g}$ arbitrary and $v = \mathrm{D}\Phi_x(\iota)[\dot{S}(0)] \in \mathbb{V}(x)$.

Statement (ii) follows directly from the definition of infinitesimal rigidity (Definition 4.2.2). ■

4.2.2 Analysis of Infinitesimal Rigidity

The analysis of infinitesimal rigidity provided in this subsection establishes several important structural properties for control applications. I begin by showing that all configurations in the orbit of an infinitesimally rigid configuration $\mathring{x}$ are also infinitesimally rigid (this result is analogous to that of Theorem 3.3.11 for locally rigid configurations). This fact greatly simplifies the task of determining infinitesimal rigidity for a given formation, as has been noted by e.g. Krick et al. [2009] for the classical case.

Theorem 4.2.5. *Let $\mathcal{F}(\mathring{y})$ be a formation of an agent network $\mathcal{N} := (\mathcal{M}, \mathcal{Y}, h)$, with $\mathcal{M}$ and $\mathcal{Y}$ being smooth finite-dimensional Riemannian manifolds and h a smooth map. Suppose that $\mathcal{N}$ is equivariant with respect to a Lie group action $\Phi : \mathbf{G} \times \mathcal{M} \to \mathcal{M}$ of a Lie group $\mathbf{G}$, and that a configuration $\mathring{x} \in \mathcal{F}(\mathring{y})$ is infinitesimally rigid with respect to Φ. Then, all configurations $x \in \Phi_{\mathring{x}}(\mathbf{G})$ are infinitesimally rigid with respect to Φ.*

Proof Let $x \in \Phi_{\mathring{x}}(\mathbf{G})$ be arbitrary and let $S \in \mathbf{G}$ be such that $x = \Phi_S(\mathring{x})$ (where $\Phi_S(\mathring{x}) := \Phi(S, \mathring{x})$). The invariance of h ensures $h(x') = h(\Phi_S(x'))$ for all $x' \in \mathcal{M}$. Therefore,

$$\begin{aligned} \mathrm{D}h(\mathring{x}) &= \mathrm{D}(h \circ \Phi_S)(\mathring{x}) \\ &= \mathrm{D}h(\Phi_S(\mathring{x})) \circ \mathrm{D}\Phi_S(\mathring{x}). \end{aligned} \tag{4.4}$$

Note that Φ_S is a diffeomorphism with inverse $\Phi_{S^{-1}}$. It follows that for any $\Delta_x \in \ker \mathrm{D}h(x)$, one has

$$0 = \mathrm{D}h(x)[\Delta_x] = \mathrm{D}h(\mathring{x}) \circ \mathrm{D}\Phi_{S^{-1}}(x)[\Delta_x]$$

and hence $\mathrm{D}\Phi_{S^{-1}}(x)[\Delta_x] \in \ker \mathrm{D}h(\mathring{x})$.

Recall from Lemma 4.2.4 that $\ker \mathrm{D}h(\mathring{x}) = \mathbb{V}(\mathring{x})$; therefore, there exists $u \in \mathfrak{g}$ such that $\mathrm{D}\Phi_{S^{-1}}(x)[\Delta_x] = \mathrm{D}\Phi_{\mathring{x}}(\iota)[u]$ (4.3). Then,

$$\begin{aligned} \Delta_x &= \mathrm{D}\Phi_S(\mathring{x}) \circ \mathrm{D}\Phi_{S^{-1}}(x)[\Delta_x] \\ &= \mathrm{D}\Phi_S(\mathring{x}) \circ \mathrm{D}\Phi_{\mathring{x}}(\iota)[u] \\ &= \mathrm{D}(\Phi_S \circ \Phi_{\mathring{x}})(\iota)[u] \\ &= \mathrm{D}\Phi_x(\iota)[u] \in \mathbb{V}(x). \end{aligned}$$

Hence, $\ker \mathrm{D}h(x) \subseteq \mathbb{V}(x)$ and by Lemma 4.2.4 it follows that x is infinitesimally rigid. ■

In the classical case, infinitesimal rigidity of a configuration plays a key role in rigidity analysis, primarily because it is a sufficient condition for local rigidity (Asimow and Roth [1979]). In addition, an infinitesimally rigid formation is a regular submanifold of the full state-space (Asimow and Roth [1978]; Krick et al. [2009]). This observation has enabled stability analysis of formation control algorithms to be performed using techniques such as centre manifold theory (see Krick et al. [2009]). The following theorem extends both of these important results to the generalised scenario.

Theorem 4.2.6. *Let $\mathcal{F}(\mathring{y})$ be a formation of an agent network $\mathcal{N} := (\mathcal{M}, \mathcal{Y}, h)$, and suppose it is infinitesimally rigid with respect to a Lie group action Φ of a Lie group $\mathbf{G}$. Then, the formation $\mathcal{F}(\mathring{y})$ is locally rigid with respect to Φ, and each rigid component (Definition 3.3.10) of $\mathcal{F}(\mathring{y})$ is a closed regular submanifold of $\mathcal{M}$.*

Proof Let $\mathring{x} \in \mathcal{F}(\mathring{y})$ be an arbitrary point and note that the orbit $\Phi_{\mathring{x}}(\mathbf{G})$ is a subset of $\mathcal{F}(\mathring{y})$ since the network is equivariant. The image $\Psi_{\mathring{x}}(\mathbf{G}/\operatorname{stab}\Phi_{\mathring{x}})$ (where $\Psi_{\mathring{x}}$ is defined as in (3.5)) is a homogeneous space with constant dimension

$$\kappa := \dim \mathbb{V}(\mathring{x}) = \dim \mathbf{G} - \dim \operatorname{stab} \Phi_{\mathring{x}}.$$

The map $\Psi_{\mathring{x}}$ is a bijective immersion, and hence $\Psi_{\mathring{x}}(\mathbf{G}/\operatorname{stab}\Phi_{\mathring{x}})$ is an immersed submanifold [Absil et al., 2008, pp. 24-25, note also Proposition 3.4.5].

Let $x \in \Phi_{\mathring{x}}(\mathbf{G})$ and let $\mathcal{U}_x \subseteq \mathcal{M}$ be an open neighbourhood of x. Let $\theta_x(x') := (q_1, \dots, q_\kappa, q_{\kappa+1}, \dots, q_n) \in \mathbb{R}^n$ (where $n := \dim \mathcal{M}$) define local coordinates on $\mathcal{U}_x$, with $\theta_x(x) = 0$ and such that $q_i = 0$ for $i \in \{\kappa+1, \dots, n\}$ if $\theta_x^{-1}(q) \in \lfloor \Phi_x(\mathbf{G}) \cap \mathcal{U}_x \rfloor_{\{x\}}$ (here, $\lfloor \mathcal{U} \rfloor_{\mathcal{V}}$ denotes the path-connected components of $\mathcal{U}$ that intersect $\mathcal{V}$, as described in Part [ix] of Subsection 1.5). Define $J(q) := \mathrm{d}/\mathrm{d}q \; \varphi_{\mathring{y}}(h(\theta_x^{-1}(q)))$ (see Remark 4.2.3). Recall from Part (ii) of Lemma 4.2.4 that $\mathbb{V}(x) = \ker \mathrm{D}h(x)$ for all $x \in \mathcal{F}(\mathring{y})$. Hence, the matrix $J(q)$ has rank $r := n - \kappa$, and contains a full-rank $r \times r$ submatrix $J_\perp(q)$ (constructed by removing linearly dependent rows and columns of $J(q)$). The continuity of $J(q)$ ensures that $J_\perp(q)$ remains full rank in an open neighbourhood $\mathcal{V}_x \subset \mathbb{R}^n$ of 0. Let $\mathcal{U}'_x = \mathcal{U}_x \cap \theta_x^{-1}(\mathcal{V}_x)$ and note that $\mathcal{U}'_x$ is open. It follows that for any $q \in \mathcal{V}_x$ with a coordinate $q_i \neq 0$ for $i \in \{\kappa+1, \dots, n\}$, one has $h(\theta_x^{-1}(q)) \neq \mathring{y}$ and therefore $\theta_x^{-1}(q) \notin \mathcal{F}(\mathring{y})$. In particular, the set $\mathcal{F}(\mathring{y}) \cap \mathcal{U}'_x$ is a path-connected regular submanifold of $\mathcal{U}'_x$. Let

$$\mathcal{U}_{\Phi_{\mathring{x}}} = \cup_{x \in \Phi_{\mathring{x}}(\mathbf{G})} \mathcal{U}'_x$$

and note that $\mathcal{U}_{\Phi_{\mathring{x}}}$ is an open set such that $\mathcal{F}(\mathring{y}) \cap \mathcal{U}_{\Phi_{\mathring{x}}} = \Phi_{\mathring{x}}(\mathbf{G})$. It follows firstly that $\mathcal{F}(\mathring{y})$ is locally rigid with respect to Φ. Secondly, noting that the formation $\mathcal{F}(\mathring{y})$ is closed since it is the continuous pre-image of a point in a T_1 topological space, it follows that each rigid component is a closed regular submanifold of $\mathcal{M}$ [Absil et al., 2008, Proposition 3.3.2]. ■

I emphasise that proving the rigid components are closed relies on infinitesimal rigidity of the full *formation*, not just infinitesimal rigidity of a given component. It should also be noted that although each rigid component of $\mathcal{F}(\mathring{y})$ is a closed regular submanifold, they need not have the same dimension. The dimension of a particular rigid component will depend on the dimension of the stabiliser of the group action at any configuration in that component.

The final result in this subsection states that any infinitesimally rigid formation has an open neighbourhood on which all configurations are infinitesimally rigid. This provides important structure for stability analysis in applications such as network localisation and formation control.

Theorem 4.2.7. *Let $\mathcal{N} := (\mathcal{M}, \mathcal{Y}, h)$ be an agent network, where $\mathcal{M}$ and $\mathcal{Y}$ are smooth finite-dimensional Riemannian manifolds and h is a smooth map. Suppose that a configuration $\mathring{x} \in \mathcal{M}$ is infinitesimally rigid with respect to a Lie group action Φ of a Lie group $\mathbf{G}$. Then, there exists an open neighbourhood $\mathcal{U}_{\Phi_{\mathring{x}}} \subseteq \mathcal{M}$ of the orbit $\Phi_{\mathring{x}}(\mathbf{G})$ such that, for all configurations $x \in \mathcal{U}_{\Phi_{\mathring{x}}}$, one has* $\dim \operatorname{stab} \Phi_x = \dim \operatorname{stab} \Phi_{\mathring{x}}$ *and x is infinitesimally rigid with respect to Φ.*

Proof A straightforward application of Theorem 4.2.5 ensures all configurations in the orbit $\Phi_{\mathring{x}}(\mathbf{G})$ are infinitesimally rigid. For any infinitesimally rigid configuration $x' \in \Phi_{\mathring{x}}(\mathbf{G})$, Lemma B.21 in Appendix B implies there exists an open neighbourhood $\mathcal{U}^h_{x'} \subseteq \mathcal{M}$ such that $\operatorname{rank} \mathrm{D}h(x) \geq \operatorname{rank} \mathrm{D}h(x')$ for all $x \in \mathcal{U}^h_{x'}$. Define the graph of the group action as $\Gamma : \mathbf{G} \times \mathcal{M} \to \mathcal{M} \times \mathcal{M}, \Gamma(S, x) \mapsto (\Phi(S, x), x)$. Then (using local vectorised coordinates)

$$\mathrm{D}\Gamma(\iota, x) = \begin{pmatrix} \mathrm{D}\Phi_x(\iota) & \mathrm{D}\Phi_\iota(x) \\ 0 & I_n \end{pmatrix},$$

where $n := \dim \mathcal{M}$ and 0 is a zero matrix of appropriate dimensions. By Lemma B.21 in Appendix B there exists an open neighbourhood $\mathcal{U}_{x'}^{\Phi}$ of x' such that

$$\operatorname{rank} \mathrm{D}\Phi_x(\iota) + n = \operatorname{rank} \mathrm{D}\Gamma(\iota, x) \geq \operatorname{rank} \mathrm{D}\Gamma(\iota, x') = \operatorname{rank} \mathrm{D}\Phi_{x'}(\iota) + n$$

for all $x \in \mathcal{U}_{x'}^{\Phi}$. Hence, $\operatorname{rank} \mathrm{D}\Phi_x(\iota) \geq \operatorname{rank} \mathrm{D}\Phi_{x'}(\iota)$ on this neighbourhood. By Lemma 4.2.4, equivariance of $\mathcal{N}$ implies $\dim \mathbb{V}(x) = \operatorname{rank} \mathrm{D}\Phi_x(\iota) \leq \dim \ker \mathrm{D}h(x) = n - \operatorname{rank} \mathrm{D}h(x)$, with equality holding at $x = x'$. It follows that $\operatorname{rank} \mathrm{D}\Phi_x(\iota) = \dim \ker \mathrm{D}h(x)$ for $x \in \mathcal{U}_{x'}^{h} \cap \mathcal{U}_{x'}^{\Phi}$. Since $x' \in \Phi_{\mathring{x}}(\mathbf{G})$ is arbitrary, all configurations are infinitesimally rigid in an open neighbourhood $\mathcal{U}_{\Phi_{\mathring{x}}} := \cup_{x' \in \Phi_{\mathring{x}}(\mathbf{G})} (\mathcal{U}_{x'}^{h} \cap \mathcal{U}_{x'}^{\Phi})$ of the orbit $\Phi_{\mathring{x}}(\mathbf{G})$. ■

Remark 4.2.8. In classical rigidity, if any *regular* (Asimow and Roth [1979]) or *generic* (Anderson et al. [2008]) configuration x is infinitesimally rigid (under the constraints $h(x)$), then *all* regular configurations will be infinitesimally rigid (Asimow and Roth [1979]). Furthermore, no other configurations will be infinitesimally rigid. In this case, the agent network is said to be *generically rigid*. An important consequence of this property is that the set of infinitesimally rigid configurations must be open and its complement must have Lebesque measure zero (Asimow and Roth [1979]).

Theorem 4.2.7 provides similar insight in the generalised setting, for a *local neighbourhood* of any given infinitesimally rigid configuration. To extend the notion of generic rigidity to a *global* property in the generalised framework, the global structure of both the group action Φ and the output map h must be taken into account. Consider the set of configurations $x \in \mathcal{M}$ for which $\dim \operatorname{stab} \Phi_x$ is minimised on $\mathcal{M}$, and for which $\operatorname{rank} \mathrm{D}h(x)$ is maximised on $\mathcal{M}$. Assume that this set is nonempty. It is trivial to see that if any configuration in this set is infinitesimally rigid, then they must all be so; furthermore, a simple dimensionality argument reveals that no other configurations may be infinitesimally rigid in this case (note that the set of other configurations need not have Lebesque measure zero, as was true for the classical scenario). In order to avoid the awkward term *generalised generic rigidity*, I propose the term *regular rigidity* for this property. ◇

4.2.3 Discussion and Examples

In this subsection I present several examples concerning generalised infinitesimal rigidity. I begin by considering the classical case of distance measurements and the relatively straightforward case of inertial direction measurements.

Example 4.2.9. Consider a network of agents in $\mathbb{R}^3$ with only distance constraints (Example 3.2.9) between them. Let $\mathcal{F}(\mathring{y})$ be a formation specified by fixed values

$\mathring{y}_k \in \mathbb{R}$ for the *squared* distances between agents, i.e.

$$h_k(x_i, x_j) := (x_i - x_j)^\top (x_i - x_j) = \mathring{y}_k. \tag{4.5}$$

The use of the distance squared ensures the output map is differentiable on the full state-space $\mathbb{R}^{3\times N}$ and is often considered in the classical literature (Jackson [2007]). The differential of (4.5) is

$$\mathrm{D}h_k(x_i, x_j)[\Delta_i, \Delta_j] = (x_i - x_j)^\top (\Delta_i - \Delta_j) = 0, \tag{4.6}$$

where $\Delta_i \in T_{x_i}\mathcal{M}_i$ denotes a tangent vector at the state x_i of agent i. The infinitesimal motions (Definition 4.2.1) of the system are the tangent vectors $\Delta_x = (\Delta_1^\top, \ldots, \Delta_N^\top)^\top \in \mathrm{T}_x\mathcal{M}$ such that (4.6) holds for all $k \in \{1, \ldots, M\}$. In the classical literature, infinitesimal rigidity is defined as the case where the only such solutions correspond to a common rigid-body motion applied to each agent's position (Zelazo et al. [2015]). The $M \times 3N$ *rigidity matrix* $J(x)$ from the classical literature (Jackson [2007]; Anderson et al. [2008]) is a block matrix for which the (k, i)'th 1×3 block entry is given by $(x_i - x_j)^\top$, the (k, j)'th block is given by $(x_j - x_i)^\top$, and all other entries (i.e. where the measurement k does not depend on agent i) are zero. Using this construction, the set of equations (4.6) can be expressed in matrix form as $J(x)\Delta_x = 0$, with stacked coordinates $x = (x_1^\top, \ldots, x_N^\top)^\top$ providing Euclidean (local) coordinates on the whole space. It is easily verified that the classical rigidity matrix $J(x)$ is a specialisation of $\mathrm{D}h(x)$, which can be computed using local coordinates as discussed in Remark 4.2.3. In particular, the collection of all M equations given by (4.6) is equivalent to the expression (4.1). Thus, the classical notion of infinitesimal rigidity is a specialisation of the present development. $\diamond$

Example 4.2.10. Suppose we have inertial direction measurements between agents with states $x_i \in \mathbb{R}^3$, as in (Example 3.2.12). Note that in order to ensure the required differentiability of $h(x)$, I will exclude configurations where $x_i = x_j$ (for some $i, j \in \{1, \ldots, N\}$) from the state-space as discussed in Example 3.2.2 and Remark 3.2.36. The differential of the output map in this case is,

$$\begin{aligned}\mathrm{D}h_k(x_i, x_j)[\Delta_i, \Delta_j] &= \left(\frac{1}{\|x_j - x_i\|} I_3 - \frac{(x_j - x_i)(x_j - x_i)^\top}{\|x_j - x_i\|^3}\right)(\Delta_j - \Delta_i) \\ &= \frac{1}{\|x_j - x_i\|}(I_3 - y_k y_k^\top)(\Delta_j - \Delta_i),\end{aligned} \tag{4.7}$$

where $\Delta_i \in T_{x_i}\mathcal{M}_i$ denotes a tangent vector at x_i. Hence, the (k, i)'th block entry of $J(x) = \mathrm{D}h(x)$ in (4.1) is

$$\frac{\chi_k^i}{\|x_i - x_j\|}(I_3 - y_k y_k^\top) \in \mathbb{R}^{3\times 3}.$$

Here, χ_k^i is 1 or -1 depending on whether x_i is the first or second argument of $h_k(x_i, x_j)$. As in Example 4.2.9, the set of equations described by (4.7) can be expressed in matrix form as $\mathrm{D}h(x)[\Delta_x] = 0$, stacking the agent positions in $\mathbb{R}^3$ to obtain

Euclidean local coordinates for the system state. Note that by Part (i) of Lemma 4.2.4, the matrix $\mathrm{D}h(x)$ will inherit the invariance of the direction measurements. That is, motions corresponding to global translations or scaling (Example 3.2.32) must lie in the kernel of $\mathrm{D}h(x)$. ◇

Example 4.2.11. The generalised framework allows $h(x)$ to consist of multiple sensor modalities. For a basic example of this case, consider the agent network illustrated in Figure 4.1. Here, the agents lie in $\mathbb{R}^3$ space, the red lines indicate distance constraints, and the blue arrows indicate direction constraints. The rigidity matrix for this scenario is given by

$$\mathrm{D}h(x) = \begin{pmatrix} (x_1 - x_3)^\top & 0 & (x_3 - x_1)^\top \\ 0 & (x_2 - x_3)^\top & (x_3 - x_2)^\top \\ f(x_2, x_1) & -f(x_2, x_1) & 0 \\ 0 & -f(x_2, x_3) & f(x_2, x_3) \end{pmatrix},$$

where

$$f(x_i, x_j) = \frac{1}{\|x_j - x_i\|} I_3 - \frac{(x_j - x_i)(x_j - x_i)^\top}{\|x_j - x_i\|^3}. \tag{4.8}$$

The top two lines of this matrix are expressed using 1×3 blocks and correspond to the distance measurements. The bottom two lines are expressed using 3×3 blocks that correspond to the direction measurements. Each block of three columns in the matrix corresponds to the state of one of the agents in the network. By using distance and direction constraints together, invariance to both rotations and scaling can be removed, leaving the full output map invariant to only translations. ◇

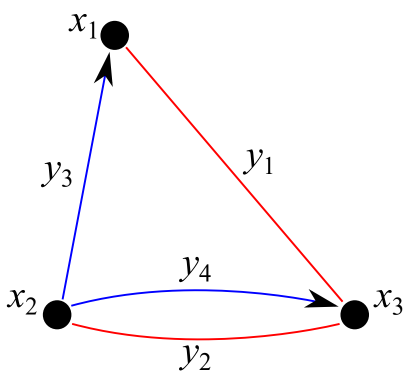

Figure 4.1: The agent network for Example 4.2.11. The dots represent agent positions in $\mathbb{R}^3$, the red lines indicate distance constraints between pairs of agents, and the blue arrows indicate direction constraints between pairs of agents.

In some cases, expressing the states x_i or the measurements y_k in vector form may obscure the natural matrix structure associated with these variables (e.g. when $Y_k \in \mathrm{SE}(3)$). The following examples show that sometimes, this matrix structure can be preserved for the analysis of infinitesimal rigidity by exploiting the fact that we are only interested in when $\mathrm{D}h(x) = 0$.

Example 4.2.12. Consider agents with states $X_i \in \mathrm{SE}(3)$, and a sensor modality $h_k(X_i, X_j) := X_i^{-1} X_j$ that measures the full relative state. In this case, it is necessary to vectorise the output $Y_k = h_k(X_i, X_j)$ in order to obtain the form in (4.2), which may complicate the analysis. However, by setting the differential of $h_k(X_i, X_j)$ to a zero matrix $\Delta_{Y_k} \in T_{Y_k}\mathcal{Y}_k$, one obtains

$$\begin{aligned} 0 = \Delta_{Y_k} &= -X_i^{-1}\Delta_{X_i} X_i^{-1} X_j + X_i^{-1}\Delta_{X_j} \\ &= -\Delta_{X_i} X_i^{-1} + \Delta_{X_j} X_j^{-1}. \end{aligned}$$

Infinitesimal motions of the system can therefore be expressed as

$$\Delta'_X J(X) = 0,$$

where $\Delta'_X := (\Delta_{X_1}, \ldots, \Delta_{X_N})$ and $J(X)$ is a $4N \times 4M$ matrix with the (i,k)'th 4×4 block entry given by $\chi_k^i X_i^{-1}$ (or $\chi_k^j X_j^{-1}$) if edge k connects to agent i (or j) and zero otherwise (with the sign χ_k^i depending on the direction of the measurement). ◇

Example 4.2.13. Extending the prior example concerning agent states $X_i \in \mathrm{SE}(3)$, suppose that only the relative position (in the body-fixed frame) is measured. That is, suppose (using homogeneous coordinates as defined in Section 1.5)

$$\overline{h_k(X_i, X_j)} := X_i^{-1} X_j \bar{y}_j^0,$$

where $\bar{y}_j^0$ is stationary with respect to X_j (see Example 3.2). Setting $\Delta_{\bar{y}_k} = 0$ gives

$$\begin{aligned} 0 = \Delta_{\bar{y}_k} &= -(X_i^{-1}\Delta_{X_i} X_i^{-1} X_j + X_i^{-1}\Delta_{X_j})\bar{y}_j^0 \\ &= -\Delta_{X_i}\bar{y}_k + \Delta_{X_j}\bar{y}_j^0 \\ &= \Delta'_X J(X), \end{aligned}$$

where $\Delta'_X := (\Delta_{X_1}, \ldots, \Delta_{X_N})$. In this case, the (i,k)'th 4×1 block element of $J(X)$ is $\chi_k^i \bar{y}_j^0$ expressed with respect to X_i (or X_j) if edge k connects to agent i (or j), and 0 otherwise. ◇

4.3 Robust Rigidity

In this section, I introduce a new concept of *robust rigidity* that characterises the behaviour of the output map on non-compact formations. In Subsection 4.3.1, robust rigidity is defined as the case where the nonzero singular values of $\mathrm{D}h(x)$ are upper and lower bounded in an open neighbourhood of the formation; in particular, these bounds are invariant to translations along the group orbit. This implies that for any deviation of the agents from the formation, the resulting changes in the output value will be bounded. Although the formal definition of robust rigidity is associated with the output map, my analysis in Subsection 4.3.2 reveals that this property can be characterised entirely in terms of the system's symmetry. With this insight, some simple examples are considered in Subsection 4.3.3. In particular, it is shown that robust rigidity is always obtained for formations that are rigid in the classical sense; i.e., it applies for any rigid formation that consists only of distance constraints between agents in Euclidean space (see Example 4.3.3). The significance of robust rigidity for the purposes of stability analysis will be illustrated in the next section.

4.3.1 Defining Robust Rigidity

Robust rigidity is a stronger property than infinitesimal rigidity of a formation. According to Theorem 4.2.7, the rank of the output map, $r := \operatorname{rank} \mathrm{D}h(x)$, is constant in an open neighbourhood of each rigid component $\Phi_{\mathring{x}}(\mathbf{G}) \in \mathcal{F}(\mathring{y})$ of the formation (note, however, that the rank of each rigid component need not necessarily be the same). For the definition of robust rigidity, I use $\lfloor h^{-1}(B_\delta(\mathring{y})) \rfloor_{\mathcal{F}(\mathring{y})}$ to denote the path-connected components of $h^{-1}(B_\delta(\mathring{y}))$ that intersect $\mathcal{F}(\mathring{y})$, as described in the notation section (Subsection 1.5). I also use $\|\mathrm{D}h(x)\|_2$ to denote the maximum singular value of $\mathrm{D}h(x)$ (2-norm) and $\lambda_2(\mathrm{D}h(x))$ to denote the minimum non-zero singular value of $\mathrm{D}h(x)$ (spectral gap). Note that these singular values are dependent upon the Riemannian metrics defined for $\mathcal{M}$ and $\mathcal{Y}$ (see the discussion in Part [vii] of Section 1.5).

Definition 4.3.1. (**Robust rigidity**) Let $\mathcal{N} := (\mathcal{M}, \mathcal{Y}, h)$ be an agent network, with $\mathcal{M}$ and $\mathcal{Y}$ being smooth finite-dimensional Riemannian manifolds and h a smooth map. Suppose that a formation $\mathcal{F}(\mathring{y})$ of $\mathcal{N}$ is infinitesimally rigid with respect to a Lie group action $\Phi : \mathbf{G} \times \mathcal{M} \to \mathcal{M}$ of a Lie group $\mathbf{G}$. The formation $\mathcal{F}(\mathring{y})$ is *robustly rigid* with respect to Φ if, for some $\delta > 0$ (possibly infinity), there exist uniform bounds $\overline{\epsilon}(\delta) > \underline{\epsilon}(\delta) > 0$ such that for any $x \in \lfloor h^{-1}(B_\delta(\mathring{y})) \rfloor_{\mathcal{F}(\mathring{y})}$ then

$$\underline{\epsilon}(\delta) \le \lambda_2(\mathrm{D}h(x)) \le \|\mathrm{D}h(x)\|_2 \le \overline{\epsilon}(\delta). \tag{4.9}$$

$\diamond$

To better understand this property, consider an open neighbourhood $\mathcal{U}_{\mathring{x}}$ of a configuration $\mathring{x} \in \mathcal{F}(\mathring{y})$, on which all configurations are infinitesimally rigid (Theorem 4.2.7). If this neighbourhood has compact closure, then it is clear that the non-zero singular values of $\mathrm{D}h(x)$ are bounded for $x \in \mathcal{U}(\mathring{x})$. Robust rigidity then ensures that such bounds exist for the full orbits contained in $\Phi(\mathbf{G}, \mathcal{U}_{\mathring{x}})$. Further analysis and insight concerning this property is provided in the following subsections.

4.3.2 Analysis of Robust Rigidity

In this subsection I characterise robust rigidity in terms of the symmetry described by the group action. This provides further insight to the structure associated with robust rigidity, as well as enabling a straightforward method of determining robust rigidity in practice.

Theorem 4.3.2. *Let $\mathcal{F}(\mathring{y})$ be a formation of an agent network $\mathcal{N} := (\mathcal{M}, \mathcal{Y}, h)$ that is infinitesimally rigid with respect to a Lie group action Φ of a Lie group $\mathbf{G}$, and suppose that $\mathcal{F}(\mathring{y})$ has finitely many rigid components (Definition 3.3.10). The formation $\mathcal{F}(\mathring{y})$ is robustly rigid with respect to Φ if and only if there exists $\delta > 0$ such that, for every $x \in \lfloor h^{-1}(B_\delta(\mathring{y})) \rfloor_{\mathcal{F}(\mathring{y})}$, there exist $\overline{\mu}(x) > \underline{\mu}(x) > 0$ such that for all $S \in \mathbf{G}$*

$$\underline{\mu}(x) \leq \underline{\sigma}(\mathrm{D}\Phi_S(x)) \leq \overline{\sigma}(\mathrm{D}\Phi_S(x)) \leq \overline{\mu}(x). \tag{4.10}$$

Here, $\overline{\sigma}$ (resp. $\underline{\sigma}$) denotes the maximum (resp. minimum) singular value of $\mathrm{D}\Phi_S(x)$.

Moreover, δ can be chosen such that all configurations $x \in \lfloor h^{-1}(B_\delta(\mathring{y})) \rfloor_{\mathcal{F}(\mathring{y})}$ are infinitesimally rigid with respect to Φ.

Proof For the forward implication, consider an arbitrary configuration $\mathring{x}_a \in \mathcal{F}(\mathring{y})$ where $\mathring{x}_a$ denotes an element of the a'th rigid component. Let $\mathcal{U}_{\mathring{x}_a} \subseteq \mathcal{M}$ be an open neighbourhood with compact closure[2] such that all configurations $x \in \mathcal{U}_{\mathring{x}_a}$ are infinitesimally rigid (Theorem 4.2.7). Observe that the image $\Phi(\mathbf{G}, \mathcal{U}_{\mathring{x}_a})$ is an open neighbourhood of the orbit $\Phi_{\mathring{x}_a}(\mathbf{G})$ since $\Phi_S : \mathcal{M} \to \mathcal{M}$ is a diffeomorphism. Furthermore, all configurations $x \in \Phi(\mathbf{G}, \mathcal{U}_{\mathring{x}_a})$ are infinitesimally rigid by Theorem 4.2.5. Choose $\delta_a, \bar{\delta}_a$ with $0 < \delta_a < \bar{\delta}_a$ such that $B_{\delta_a}(\mathring{x}_a) \subset B_{\bar{\delta}_a}(\mathring{x}_a) \subseteq \mathcal{U}_{\mathring{x}_a}$, and define $\delta'_a = \inf\{d(h(x), \mathring{y}) \mid x \in \Phi(\mathbf{G}, B_{\bar{\delta}_a}(\mathring{x}_a)) \setminus \Phi(\mathbf{G}, B_{\delta_a}(\mathring{x}_a))\}$ where $d : \mathcal{Y} \times \mathcal{Y} \to \mathbb{R}_{\geq 0}$ denotes a distance measure on $\mathcal{Y}$. Note that invariance of h ensures δ'_a is nonzero. It follows that

$$\left\lfloor h^{-1}(B_{\delta'_a}(\mathring{y})) \right\rfloor_{\Phi(\mathbf{G}, \mathring{x}_a))} \subseteq \Phi(\mathbf{G}, \mathcal{U}_{\mathring{x}_a}). \tag{4.11}$$

Robust rigidity implies that there exists $\delta > 0$ for which the bounds (4.9) hold for all $x \in \lfloor h^{-1}(B_\delta(\mathring{y})) \rfloor_{\mathcal{F}(\mathring{y})}$. Choose $\delta' = \min\{\delta, \delta'_1, \ldots, \delta'_P\}$, where P denotes the number of rigid components of $\mathcal{F}(\mathring{y})$. For all $x' \in \mathcal{U}_{\mathring{x}_a} \cap h^{-1}(B_{\delta'}(\mathring{y}))$ then $\Phi(S, x') \in \lfloor h^{-1}(B_{\delta'}(\mathring{y})) \rfloor_{\mathcal{F}(\mathring{y})}$; from (4.4) and classical singular value properties [Horn and Johnson, 1991, Theorem 3.3.16],

$$\begin{aligned} \underline{\sigma}(\mathrm{D}\Phi_S(x')) &\geq \|\mathrm{D}h(\Phi_S(x'))\|_2^{-1} \lambda_2(\mathrm{D}h(x')) \\ &\geq \frac{\underline{\epsilon}}{\overline{\epsilon}}, \end{aligned}$$

for all $S \in \mathbf{G}$. Similarly,

$$\begin{aligned} \|(\mathrm{D}h(\Phi_S(x')))^\dagger \circ \mathrm{D}h(\Phi_S(x')) \circ \mathrm{D}\Phi_S(x')\|_2 &\leq \|(\mathrm{D}h(\Phi_S(x')))^\dagger\|_2 \|\mathrm{D}h(x')\|_2 \\ &\leq \frac{\overline{\epsilon}}{\underline{\epsilon}} \end{aligned}$$

[2]Note that although $\mathcal{M}$ is not complete (the set of infeasible points are open boundaries in $\mathcal{M}$), it is always possible to restrict to an open set around $\mathcal{F}(\mathring{y})$ that excludes the infeasible points, and is paracompact.

for all $S \in \mathbf{G}$ (where $A^\dagger$ denotes the pseudoinverse of a matrix A). This completes the proof for the forward implication as well as the final statement of the theorem.

For the reverse implication, let $\mathring{x}_a \in \mathcal{F}(\mathring{y})$ be an element of the a'th rigid component, and let $\mathcal{U}_{\mathring{x}_a}$ be an open neighbourhood of $\mathring{x}_a$ with compact closure, on which all configurations are infinitesimally rigid (Theorem 4.2.7). Define

$$\overline{\epsilon}_{\mathring{x}_a} := \sup_{x' \in \mathcal{U}_{\mathring{x}_a}} \|\mathrm{D}h(x')\|_2, \qquad \underline{\epsilon}_{\mathring{x}_a} := \inf_{x' \in \mathcal{U}_{\mathring{x}_a}} \lambda_2(\mathrm{D}h(x')).$$

Thus, for any $x' \in \mathcal{U}_{\mathring{x}_a}$ then

$$0 < \underline{\epsilon}_{\mathring{x}_a} \leq \lambda_2(\mathrm{D}h(x'))_2 \leq \|\mathrm{D}h(x')\|_2 \leq \overline{\epsilon}_{\mathring{x}_a} < \infty$$

where the first and final inequalities follow from the properties of infinitesimal rigidity along with continuity of singular values of continuous operators and compactness of the closure of $\mathcal{U}_{\mathring{x}_a}$. Define

$$\overline{\mu}_{\mathring{x}_a} := \sup_{x' \in \mathcal{U}_{\mathring{x}_a}} \overline{\mu}(x'), \qquad \underline{\mu}_{\mathring{x}_a} := \inf_{x' \in \mathcal{U}_{\mathring{x}_a}} \underline{\mu}(x')$$

from (4.10) and note that $\overline{\mu}_{\mathring{x}_a} \geq \underline{\mu}_{\mathring{x}_a} > 0$ since the closure of $\mathcal{U}_{\mathring{x}_a}$ is compact.

The map $\Phi_S : \mathcal{M} \to \mathcal{M}$ is a diffeomorphism and $\mathrm{D}\Phi_S(x)$ is full rank. It follows that $\Phi_S(\mathcal{U}_{\mathring{x}_a})$ is an open neighbourhood of $\Phi_S(\mathring{x}_a)$, with $\Phi(\mathbf{G}, \mathcal{U}_{\mathring{x}_a})$ an open neighbourhood of the rigid component $\Phi_{\mathring{x}_a}(\mathbf{G})$. For $x' \in \mathcal{U}_{\mathring{x}_a}$, one has from (4.4) and the properties of singular values [Horn and Johnson, 1991, Theorem 3.3.16] that

$$\begin{aligned}\|\mathrm{D}h(\Phi_S(x'))\|_2 &\leq \|\mathrm{D}h(x')\|_2 \overline{\sigma}((\mathrm{D}\Phi_S(x'))^{-1}) \\ &\leq \|\mathrm{D}h(x')\|_2 \frac{1}{\underline{\sigma}(\mathrm{D}\Phi_S(x'))},\end{aligned}$$

for all $S \in \mathbf{G}$. Similarly,

$$\begin{aligned}\lambda_2(\mathrm{D}h(\Phi_S(x'))) &\geq \lambda_2(\mathrm{D}h(x'))(\overline{\sigma}(\mathrm{D}\Phi_S(x')))^{-1} \\ &\geq \lambda_2(\mathrm{D}h(x')) \frac{1}{\overline{\sigma}(\mathrm{D}\Phi_S(x'))}\end{aligned}$$

for all $S \in \mathbf{G}$. It follows that

$$\underline{\epsilon}_a := \frac{\underline{\epsilon}_{\mathring{x}_a}}{\overline{\mu}_{\mathring{x}_a}} \leq \lambda_2(\mathrm{D}h(\Phi_S(x'))) \leq \|\mathrm{D}h(\Phi_S(x'))\|_2 \leq \frac{\overline{\epsilon}_{\mathring{x}_a}}{\underline{\mu}_{\mathring{x}_a}} =: \overline{\epsilon}_a.$$

Define $\delta'_a > 0$ in the same manner as for (4.11). Choose $\delta' = \min\{\delta'_1, \ldots, \delta'_P\}$ and note that

$$\Big\lfloor h^{-1}(B_{\delta'}(\mathring{y})) \Big\rfloor_{\mathcal{F}(\mathring{y})} \subseteq \cup_{i=1}^{P} \Phi(\mathbf{G}, \mathcal{U}_{\mathring{x}_a}),$$

on which (4.9) holds with

$$\overline{\epsilon}(\delta') = \max\{\overline{\epsilon}_a\}, \qquad \underline{\epsilon}(\delta') = \min\{\underline{\epsilon}_a\}.$$

This completes the proof. ∎

Theorem 4.3.2 describes a class of symmetries for which all infinitesimally rigid formations will be robustly rigid. In particular, observe that robust rigidity implies the group action $\Phi_S(x)$ does not map any two nearby points $x, x' \in \mathcal{M}$ to become arbitrarily close or arbitrarily far apart, as $\|S\|_{\mathbf{G}} \to \infty$ for some norm $\|\cdot\|_{\mathbf{G}}$ on $\mathbf{G}$.

4.3.3 Discussion and Examples

The property of robust rigidity is illustrated further in the examples below. I begin by showing that for the classical scenario involving only distance constraints, all infinitesimally rigid formations are robustly rigid.

Example 4.3.3. Consider an agent network $\mathcal{N} := (\mathcal{M}, \mathcal{Y}, h)$, where h consists only of distance constraints between agents in $\mathbb{R}^3$ (Example 3.2.9). Let $\Phi_S(x)$ denote a rigid-body transform of the full state $x \in \mathcal{M}$, where $S := (Q, \xi) \in \mathrm{SE}(3)$ consists of a rotation $Q \in \mathrm{O}(3)$ (including a possible reflection) and a translation $\xi \in \mathbb{R}^3$. Then, for an individual agent state $x_i \in \mathbb{R}^3$,

$$\mathrm{D}\phi_{iS}(x_i) = \frac{\mathrm{d}(Qx_i + \xi)}{\mathrm{d}x_i} = Q.$$

Since the singular values of Q are always equal to 1, it follows that the singular values of $\mathrm{D}h(\Phi_S(x))$ are unchanged by the group element S. By Theorem 4.3.2, this implies that all infinitesimally rigid formations of the agent network will be robustly rigid. ◇

Example 4.3.4. Consider an agent network $\mathcal{N} := (\mathcal{M}, \mathcal{Y}, h)$, where h consists only of inertial direction constraints between agents in $\mathbb{R}^3$ (Example 3.2.12). Let $\Phi_S(x)$ denote a transform of the full state $x \in \mathcal{M}$ that consists of scaling $\rho > 0$ and a translation $\xi \in \mathbb{R}^3$ (i.e. $S := (\rho, \xi) \in \mathrm{ST}(3)$). In this case,

$$\mathrm{D}\phi_{iS}(x_i) = \frac{\mathrm{d}(\rho(x_i + \xi))}{\mathrm{d}x_i} = \rho I_3,$$

and one can observe that the bounds on the singular values of $\mathrm{D}\Phi_S(x)$ will scale by ρ. Since ρ may be arbitrarily small or large, it follows from Theorem 4.3.2 that the formations of this agent network will not be robustly rigid. This analysis reflects the fact that if the agents are arbitrarily close together, then a small deviation in the agent states can cause a large change in the associated direction measurement. Similarly, if the agents are a large distance apart, then deviations in the agent states will only cause a small change in the direction. ◇

A point of particular interest from Theorem 4.3.2 is that robust rigidity is determined only by the symmetry of the agent network and not the specific arrangement of the available sensor modalities. Consequently, infinitesimally rigid formations of the agent network in Example 4.3.4 can be made robustly rigid with respect to global translations by simply adding any non-zero distance constraint between any pair of agents.

4.4 Applications

My study of rigidity theory in this chapter has been motivated by the tasks of network localisation and formation control. In this section, I demonstrate how this rigidity framework can be employed to develop conceptually simple and highly general solutions to these problems. The task of network localisation is considered in Subsection 4.4.1, while the task of formation control is addressed in Subsection 4.4.2.

4.4.1 Application I: Network Localisation

The goal in network localisation problems is to determine the true state of an agent network using partial measurements of the relative states. A key observation for this scenario is that there is, by definition, insufficient information to distinguish between equivalent configurations. Rigidity of the formation is therefore of high interest because it determines the symmetry up to which the full state can be determined. For network localisation problems, it is common to assume the presence of several *anchor nodes* that have a known state in the inertial frame (see e.g. Mao et al. [2007]; Eren [2011]). These nodes act as references for the remainder of the network, and enable the symmetry of the system to be broken.

Consider an agent network $\mathcal{N} := (\mathcal{M}, \mathcal{Y}, h)$ that is equivariant with respect to a Lie group action Φ of a Lie group $\mathbf{G}$. Suppose the system has a stationary true state $\mathring{x} \in \mathcal{M}$ such that the formation $\mathcal{F}(\mathring{y})$ is robustly rigid with respect to Φ, where $\mathring{y} := h(\mathring{x})$. Then, there exists an open neighbourhood $\mathcal{U}$ of $\mathcal{F}(\mathring{y})$ such that all configurations $\hat{x} \in \mathcal{U}$ are infinitesimally rigid. The goal of the network localisation problem is to determine, up to the symmetry described by Φ, the true state of the system. More precisely, given any initial estimate $\hat{x} \in \mathcal{U}$ of the true state, we wish $\hat{x}(t) \to \Phi_{\mathring{x}}(\mathbf{G})$. To achieve this, let $V_{\mathring{y}} : \mathcal{Y} \to \mathbb{R}_{\geq 0}$ be a positive-definite cost function on the output space $\mathcal{Y}$, such that $V_{\mathring{y}}(\mathring{y}) = 0$ and the Hessian $\mathrm{D}^2 V_{\mathring{y}}(\mathring{y})$ at $\mathring{y}$ has full rank. A typical example would be a norm or distance measure on the output space $\mathcal{Y}$ that is centred at $\mathring{y}$. Using the Riemannian metric structure $\langle \cdot, \cdot \rangle_x : T_x\mathcal{M} \times T_x\mathcal{M} \to \mathbb{R}_{\geq 0}$ on $\mathcal{M}$, a simple gradient-descent approach can be employed for the time-evolution of the estimate (here, ∇ denotes the gradient of a function as described in Section 1.5):

$$\dot{\hat{x}} := -\nabla \left(V_{\mathring{y}} \circ h \right) (\hat{x}). \tag{4.12}$$

Local convergence of this estimate to the true state (up to the invariance described by Φ) is given by the following theorem.

Theorem 4.4.1. *Consider a formation $\mathcal{F}(\mathring{y})$ of an agent network $\mathcal{N} := (\mathcal{M}, \mathcal{Y}, h)$, where $\mathring{x} \in \mathcal{M}$ denotes the stationary true configuration of the agents and $\mathring{y} := h(\mathring{x})$. Suppose that $\mathcal{F}(\mathring{y})$ is robustly rigid with respect to a Lie group action Φ of a Lie group $\mathbf{G}$. Then, there exists an open neighbourhood $\mathcal{U} \subseteq \mathcal{M}$ of $\mathcal{F}(\mathring{y})$ such that, for all initial estimates $\hat{x} \in \mathcal{U}$, the update law* (4.12) *ensures $\hat{x}(t)$ converges exponentially to a point $x_\infty \in \mathcal{F}(\mathring{y})$ as $t \to \infty$.*

Remark 4.4.2. A key part of this theorem statement is that the estimate converges to a *limit point* in the formation $\mathcal{F}(\mathring{y})$ and does not diverge to infinity. The property of robust rigidity plays a critical role in proving this claim. $\diamond$

Proof Since $\mathcal{F}(\mathring{y})$ is robustly rigid, there exists a $\delta_0 > 0$ such that for every $x \in \lfloor h^{-1}(B_{\delta_0}(\mathring{y}))\rfloor_{\mathcal{F}(\mathring{y})}$, there exist $\overline{\mu}(x) > \underline{\mu}(x) > 0$ such that (4.10) holds (Theorem 4.3.2). Since $V_{\mathring{y}}(y)$ is positive-definite with full-rank Hessian at $\mathring{y}$, there exists $\delta' > 0$ such that $V_{\mathring{y}}^{-1}([0,\delta')) \subseteq B_{\delta_0}(\mathring{y})$, with full-rank Hessian on this set. With this construction,

$$\mathcal{U}' := \left\lfloor h^{-1}(V_{\mathring{y}}^{-1}([0,\delta')))\right\rfloor_{\mathcal{F}(\mathring{y})} \subseteq \left\lfloor h^{-1}(B_{\delta_0}(\mathring{y}))\right\rfloor_{\mathcal{F}(\mathring{y})}$$

is a *sublevel* set of $V_{\mathring{y}} \circ h$. Note for later that $\delta' > 0$ can be chosen arbitrarily small. Furthermore, robust rigidity implies infinitesimal rigidity, which ensures the only critical points of $V_{\mathring{y}} \circ h : \mathcal{M} \to \mathbb{R}$ in $\mathcal{U}'$ are characterised by $h(\hat{x}) := \mathring{y}$ (i.e. points in $\mathcal{F}(\mathring{y})$).

Since the rank of $\mathrm{D}h(\hat{x})$ is constant on $\mathcal{U}'$, h is a subimmersion [Abraham et al., 1988, Definition 3.5.15, note also Proposition 3.5.16] on this neighbourhood. The Fibration Theorem [Abraham et al., 1988, Theorem 3.5.18] implies there exist an open sub-neighbourhood $\mathcal{U}_{\mathring{x}} \subseteq \mathcal{U}'$ of $\mathring{x}$ and an open neighbourhood $\mathcal{U}_{h(\mathring{x})} \subseteq \mathcal{Y}$ of $h(\mathring{x})$, along with a submanifold $\bar{\mathcal{X}} \subseteq \mathcal{M}$ with $\mathring{x} \in \bar{\mathcal{X}}$, such that $h(\mathcal{U}_{\mathring{x}})$ is a submanifold of $\mathcal{Y}$ and h locally induces a diffeomorphism $h_{\mathcal{X}} : \mathcal{X} \to \mathcal{Z}$ from $\mathcal{X} := h^{-1}(\mathcal{U}_{h(\mathring{x})}) \cap \bar{\mathcal{X}} \cap \mathcal{U}_{\mathring{x}}$ to $\mathcal{Z} := h(\mathcal{U}_{\mathring{x}}) \cap \mathcal{U}_{h(\mathring{x})}$. Note that $h(\mathcal{X}) = h(\Phi_S(\mathcal{X})) = \mathcal{Z}$ for all $S \in \mathbf{G}$ by invariance. Since $\mathcal{X}$ is transverse to $\Phi_{\mathring{x}}(\mathbf{G})$ and $V_{\mathring{y}}$ is positive definite, one can always find a positive $\delta < \delta'$ such that $h(h^{-1}(V_{\mathring{y}}^{-1}([0,\delta)))) \subseteq \mathcal{Z}$. Let $\bar{V}_{\mathring{y}}$ denote the restriction of $V_{\mathring{y}}$ to the domain $\mathcal{Z}$. Define $\mathcal{U} := \left\lfloor h^{-1}(\bar{V}_{\mathring{y}}^{-1}([0,\delta)))\right\rfloor_{\mathcal{F}(\mathring{y})} \subseteq \mathcal{U}'$ and note that $\mathcal{U}$ is an open sublevel set of $\bar{V}_{\mathring{y}} \circ h$.

Consider $\bar{V}_{\mathring{y}} \circ h$ as a candidate Lyapunov function. The time-derivative of $\bar{V}_{\mathring{y}} \circ h$ is

$$\begin{aligned}
\frac{\mathrm{d}}{\mathrm{d}t}\left(\bar{V}_{\mathring{y}} \circ h\right)(\hat{x}) &= \mathrm{D}(\bar{V}_{\mathring{y}} \circ h)(\hat{x})[\dot{\hat{x}}] \\
&= \langle \nabla(\bar{V}_{\mathring{y}} \circ h)(\hat{x}), \dot{\hat{x}} \rangle_{\hat{x}} \\
&= -\langle \nabla(\bar{V}_{\mathring{y}} \circ h)(\hat{x}), \nabla(\bar{V}_{\mathring{y}} \circ h)(\hat{x}) \rangle_{\hat{x}} \\
&\leq 0,
\end{aligned} \tag{4.13}$$

with equality holding only at the critical points of $\bar{V}_{\mathring{y}} \circ h$. Since the control law (4.12) is locally Lipschitz, there exists $t_1 > 0$ such that a unique trajectory exists for $t \in [0, t_1]$ [Khalil, 2002, Theorem 3.1]. While the trajectory exists, (4.13) shows that $\hat{x}$

is constrained to $\mathcal{U}$.

Continuing from (4.13), and employing the notation for the metric operator described in Section 1.5,

$$\begin{aligned} \mathrm{D}(\bar{V}_{\mathring{y}} \circ h)(\hat{x})[\dot{\hat{x}}] &= -\mathrm{D}(\bar{V}_{\mathring{y}} \circ h)(\hat{x}) \left[\Lambda_{\hat{x}}^{-1} \left(\mathrm{D}(\bar{V}_{\mathring{y}} \circ h)(\hat{x})\right)\right] \\ &= -\mathrm{D}\bar{V}_{\mathring{y}}(h(\hat{x})) \circ \mathrm{D}h(\hat{x}) \left[\Lambda_{\hat{x}}^{-1} \left(\mathrm{D}h(\hat{x})^\star \circ \mathrm{D}\bar{V}_{\mathring{y}}(h(\hat{x}))\right)\right] \\ &= -\mathrm{D}\bar{V}_{\mathring{y}}(h(\hat{x})) \left[\mathrm{D}h(\hat{x}) \circ \Lambda_{\hat{x}}^{-1} \circ \mathrm{D}h(\hat{x})^\star \left[\mathrm{D}\bar{V}_{\mathring{y}}(h(\hat{x}))\right]\right]. \end{aligned} \tag{4.14}$$

Consider the operator

$$\mathrm{D}h(\hat{x}) \circ \Lambda_{\hat{x}}^{-1} \circ \mathrm{D}h(\hat{x})^\star : T^\star_{h(x)}\mathcal{Z} \times T^\star_{h(x)}\mathcal{Z} \to \mathbb{R}, \tag{4.15}$$

which is the symmetric bilinear inner product on $T^\star_{h(\hat{x})}\mathcal{Z}$, defined by (4.14), obtained by pushing forward $\Lambda_{\hat{x}}^{-1}$ by $\mathrm{D}h(\hat{x})$. By construction, $\mathrm{D}h(\hat{x})$ is a full-rank map from $\mathcal{U}$ onto $T_{h(\hat{x})}\mathcal{Z}$, and robust rigidity ensures the singular values of $\mathrm{D}h(\hat{x})$ have a positive lower bound for $\hat{x} \in \mathcal{U}$ (i.e. independent of translations of $\hat{x}$ along the group orbit). Combining this with the bounds on the singular values of $\Lambda_{\hat{x}}^{-1}$ for $\hat{x} \in \mathcal{M}$, it follows that $\mathrm{D}h(\hat{x}) \circ \Lambda_{\hat{x}}^{-1} \circ \mathrm{D}h(\hat{x})^\star$ is full rank with a positive lower bound c_0 on the eigenvalues. Using this bound to continue the computation from (4.13) and (4.14), and recalling Part [vi] of Section 1.5, one has

$$\begin{aligned} \frac{\mathrm{d}}{\mathrm{d}t}(\bar{V}_{\mathring{y}} \circ h)(\hat{x}) &= \mathrm{D}(\bar{V}_{\mathring{y}} \circ h)(\hat{x})[\dot{\hat{x}}] \\ &\leq -c_0 \langle \mathrm{D}\bar{V}_{\mathring{y}}(h(\hat{x})), \mathrm{D}\bar{V}_{\mathring{y}}(h(\hat{x})) \rangle^{\diamond\star}_{h(\hat{x})} \\ &\leq -c_0 c_1 \bar{V}_{\mathring{y}} \circ h(\hat{x}), \end{aligned} \tag{4.16}$$

where $\langle \cdot, \cdot \rangle^{\diamond\star}_{h(\hat{x})}$ denotes the inner product on $T^\star_{h(\hat{x})}\mathcal{Z}$ associated with the operator (4.15) and

$$c_1 := \inf_{\hat{x} \in \mathcal{U} \setminus h^{-1}(\mathring{y})} \frac{\langle \mathrm{D}\bar{V}_{\mathring{y}}(h(\hat{x})), \mathrm{D}\bar{V}_{\mathring{y}}(h(\hat{x})) \rangle^{\diamond\star}_{h(\hat{x})}}{\bar{V}_{\mathring{y}}(h(\hat{x}))}.$$

Note that $c_1 > 0$ is well defined and strictly positive since the function $\bar{V}_{\mathring{y}}$ is positive-definite around $\mathring{y}$ with full-rank Hessian.

From (4.16), $(V_{\mathring{y}} \circ h)(\hat{x}(t)) \to 0$ exponentially for $\hat{x} \in \mathcal{U}$. By (4.12), this ensures $\|\dot{\hat{x}}\| < \alpha e^{-\beta t}$ for some $\alpha, \beta > 0$. It follows that the length $L_{\hat{x}}(t) := \int_0^t \|\dot{\hat{x}}\| \mathrm{d}t < \int_0^t \alpha e^{-\beta t} \mathrm{d}t = (\alpha/\beta)(1 - e^{-\beta t})$; i.e. the total length of the trajectory is finite ($L_{\hat{x}}(\infty) < \alpha/\beta$), and compact. It follows that trajectories exist for all time and $\lim_{t \to \infty} \hat{x}(t)$ exists, i.e. $\hat{x}(t)$ converges to a point x_∞. Condition (4.14) ensures that $x_\infty \in \mathcal{F}(\mathring{y})$ and this concludes the proof. ■

Remark 4.4.3. Suppose that $\mathring{y}, h(\hat{x}) \in \mathcal{Y}$ share a common coordinate frame, as is guaranteed (for example) if a global coordinate system can be defined for $\mathcal{Y}$. In this case, one can employ the simple cost function $V_{\mathring{y}}(h(\hat{x})) := \frac{1}{2}(h(\hat{x}) - \mathring{y})^\top (h(\hat{x}) - \mathring{y})$, for which the differential is $\mathrm{D}V_{\mathring{y}}(h(\hat{x})) = h(\hat{x}) - \mathring{y}$. ◇

Remark 4.4.4. In many cases, the state-space $\mathcal{M}$ is a product of the individual state-spaces $\mathcal{M}_i$, and the metric operator $\Lambda_{\hat{x}}$ for the point $\hat{x}$ will be a block diagonal matrix. In this scenario, the state estimate $\hat{x}_i$ for an individual agent is derived from (4.12) (see also Part [vi] of Section 1.5) as

$$\dot{\hat{x}}_i = -\Lambda_{\hat{x}_i}^{-1} \left(\sum_{k=1}^{M} \frac{\partial V_{\mathring{y}}(\hat{y})}{\partial \hat{y}_k} \circ \frac{\partial h_k(\hat{x})}{\partial \hat{x}_i} \right),$$

where $\hat{y} := h(\hat{x})$ and $\hat{y}_k := h_k(\hat{x})$. Note that $\partial h_k(\hat{x})/\partial \hat{x}_i$ will be nonzero only for sensor modalities involving agent i. This suggests that a distributed implementation is possible for appropriate functions $V_{\mathring{y}}$ (i.e. functions such that $\partial V_{\mathring{y}}(\hat{y})/\partial \hat{y}_k$ also depends solely on measurements available to agent i). $\diamond$

It is worth noting that the update law (4.12) can also be applied, in an entirely analogous manner, to the task of regulating a given formation. Consider an agent network $\mathcal{N} := (\mathcal{M}, \mathcal{Y}, h)$ and suppose that $\mathring{y}$ specifies a desired formation $\mathcal{F}(\mathring{y})$ for the agents. If the true state $x \in \mathcal{M}$ of the agents is known, the approach in (4.12) can be used to drive the agents towards $\mathcal{F}(\mathring{y})$ as stated in the following corollary. Note that I will elaborate on this result in the next subsection, in order to direct a network of agents to a specified *configuration*.

Corollary 4.4.5. *Consider a desired formation $\mathcal{F}(\mathring{y})$ of an agent network $\mathcal{N} := (\mathcal{M}, \mathcal{Y}, h)$, and assume that the true agent states $x \in \mathcal{M}$ are known. Suppose that $\mathcal{F}(\mathring{y})$ is robustly rigid with respect to a Lie group action Φ of a Lie group* $\mathbf{G}$. *Let $V_{\mathring{y}} : \mathcal{Y} \to \mathbb{R}_{\geq 0}$ be a positive-definite cost function with minimum at $\mathring{y}$, and with full-rank Hessian* $\mathrm{D}^2 V_{\mathring{y}}(\mathring{y})$ *at $\mathring{y}$. Then, there exists an open neighbourhood $\mathcal{U} \subseteq \mathcal{M}$ of $\mathcal{F}(\mathring{y})$ such that, for all initial states $x \in \mathcal{U}$, the control law $\dot{x} := -\nabla \left(V_{\mathring{y}} \circ h\right)(x)$ ensures $x(t)$ converges exponentially to a point $x_\infty \in \mathcal{F}(\mathring{y})$ as $t \to \infty$.*

Remark 4.4.6. The property of robust rigidity plays a key role in the above analysis because it guarantees a positive lower bound on the spectral gap $\lambda_2(\mathrm{D}h)$. This provides a core characteristic for the output map h in the case of non-compact formations. In the classical setting, the issue of non-compactness arises from the invariance of distance measurements to global translations. It is commonly addressed by considering the behaviour of the agents with respect to the geometrical centre of the formation, as in Krick et al. [2009], which enables global translations to be factored out of the analysis. However, it is important to realise that this approach relies on the Euclidean structure of the full state-space, and consequently cannot be directly extended to more generic scenarios. Robust rigidity provides a way to overcome this issue in the generalised setting and allows one to show that the trajectories do not traverse indefinitely along the symmetry of the system. $\diamond$

Remark 4.4.7. The property of *minimal rigidity* in the classical setting is defined as the case where a locally rigid formation has the fewest number of distance constraints required for rigidity (Dörfler and Francis [2009]). In the generalised setting, it makes more sense to consider this property with regard to *degrees of freedom* rather than the

M individual constraints, which may differ in form. This interpretation leads to the notion of *minimal infinitesimal rigidity*, defined as the case where the image of $\mathrm{D}h(\mathring{x})$ is surjective onto the tangent space $T_{h(\mathring{x})}\mathcal{Y}$ (where $\mathring{x} \in \mathcal{M}$ is an infinitesimally rigid configuration). An appealing aspect of this property is that it ensures any desired infinitesimal deviation of an output measurement $\mathring{y} = h(\mathring{x}) \in \mathcal{Y}$ can be achieved by some infinitesimal variation of $\mathring{x}$.

In the classical case of distance-only constraints, minimal rigidity combined with infinitesimal rigidity has been used to prove exponential stability for control schemes based on gradient-descent approaches (see Dörfler and Francis [2009]). The above theory not only extends the classical setting to a far more generalised scenario, but it also relaxes the requirement of *minimal* rigidity to that of *robust* rigidity, which is guaranteed for classical formations consisting of only distance constraints (Example 4.3.3). The key insight that enables this to be achieved in the above analysis is the observation that a subset of the formation constraints enforces minimal infinitesimal rigidity with respect to a submanifold $\mathcal{Z}$ of $\mathcal{Y}$. That is, for local analysis one need only be concerned with a subset of independent constraints. This approach may be regarded as a generalisation of the one independently developed in the very recent paper by Sun et al. [2016], which concerns the classical case of only distance constraints.

It should be noted that the requirement of *minimal* rigidity (in the classical setting) has also been relaxed via other methods, such as the approach of Krick et al. [2009] based on centre manifold theory. It is observed by Krick et al. [2009] that although minimal rigidity is not strictly required, it is likely to improve the performance of the control scheme by increasing the region of convergence. This is because minimal rigidity implies there are fewer control terms derived from different measurements, which may cancel and thus introduce undesired equilibria to the system. $\diamond$

4.4.2 Application II: Formation Control

In the previous subsection, I considered the regulation of the state $x(t) \in \mathcal{M}$ of an agent network $\mathcal{N} := (\mathcal{M}, \mathcal{Y}, h)$ towards a specified formation $\mathcal{F}(\mathring{y}) \in \mathcal{M}$. I will now consider the task of manoeuvring the agents towards a specified *configuration* $\mathring{x} \in \mathcal{F}(\mathring{y})$. Suppose that the agents are already stabilised to the formation $\mathcal{F}(\mathring{y})$ (as may be achieved by the approach in Corollary 4.4.5, for example), and that we wish to transition the agents towards the configuration $\mathring{x}$ without breaking the state constraints $\mathring{y}$. For this scenario, I will assume that $\mathcal{F}(\mathring{y})$ is infinitesimally rigid and *path-rigid* (Definition 3.4.2) with respect to a Lie group action Φ of a Lie group $\mathbf{G}$. Path-rigidity is necessary in order to ensure that it is possible for the agents to manoeuvre between the initial configuration $x(0) \in \mathcal{F}(\mathring{y})$ and the goal configuration $\mathring{x} \in \mathcal{F}(\mathring{y})$ while preserving the state constraints. It also implies that $\mathcal{F}(\mathring{y})$ is globally rigid (alternatively, one may observe via Theorem 4.2.6 that any path-connected infinitesimally rigid formation must be globally rigid); thus, $\mathcal{F}(\mathring{y})$ consists of a single group orbit and is a regular submanifold of $\mathcal{M}$ (Theorem 4.2.6).

For this task, I consider a simple kinematic agent model and specify a velocity input for the agents that is constrained to the subspace $\mathbb{V}(x)$ (4.3); i.e. the image of the Lie algebra $\mathfrak{g}$ through the differential $\mathrm{D}\Phi_x(\iota)$. Note that infinitesimal rigidity ensures that such an input will preserve the state constraints.

Assuming the true state $x(t) \in \mathcal{F}(\mathring{y})$ is known, the control input for the agents can be specified using a suitable smooth positive-definite cost function $\mathcal{L}_{\mathring{x}} : \mathcal{M} \to \mathbb{R}_{\geq 0}$. Specifically, let

$$\dot{x} := -\mathrm{D}\Phi_x(\iota)[\nabla(\mathcal{L}_{\mathring{x}} \circ \Phi_x)(\iota)]. \tag{4.17}$$

Note that the gradient $\nabla(\mathcal{L}_{\mathring{x}} \circ \Phi_x)(\iota)$ is defined using an inner product $\langle \cdot, \cdot \rangle_\iota$ on $\mathfrak{g}$, but does not depend on the specification of a Riemannian metric for all of $\mathbf{G}$.

Theorem 4.4.8. *Consider a formation $\mathcal{F}(\mathring{y})$ of an agent network $\mathcal{N} := (\mathcal{M}, \mathcal{Y}, h)$, and suppose $\mathcal{F}(\mathring{y})$ is infinitesimally rigid and path-rigid (Definition 3.4.2) with respect to a Lie group action Φ of a Lie group $\mathbf{G}$. Let $\mathring{x} \in \mathcal{F}(\mathring{y})$ denote a desired configuration for the agents. Then, there exists an open neighbourhood $\mathcal{U} \subseteq \mathcal{M}$ of $\mathring{x}$ such that, for all initial configurations $x(0) \in \mathcal{U} \cap \mathcal{F}(\mathring{y})$, the kinematic control input* (4.17) *ensures $x(t) \to \mathring{x}$ as $t \to \infty$, with $x(t)$ remaining in $\mathcal{F}(\mathring{y})$.*

Proof Since $\mathcal{F}(\mathring{y})$ is path-rigid, it is globally rigid and hence consists of a single orbit $\Phi_{\mathring{x}}(\mathbf{G})$. Recalling Theorem 4.2.6, infinitesimal rigidity then implies that $\mathcal{F}(\mathring{y})$ is a regular submanifold of $\mathcal{M}$. Observe that the control input (4.17) lies in the tangent space of $\mathcal{F}(\mathring{y})$ and thus trajectories of the system are constrained to $\mathcal{F}(\mathring{y})$.

Stability of the system is shown using $\mathcal{L}_{\mathring{x}}(x)$ as a candidate Lyapunov function. Observe that there exists an open neighbourhood $\mathcal{U}_{\mathring{x}} \subseteq \mathcal{F}(\mathring{y})$ of $\mathring{x}$, with compact closure, that is a sublevel set of $\mathcal{L}_{\mathring{x}}(x)$ and for which the only critical point in $\mathcal{U}_{\mathring{x}}$ is where $x = \mathring{x}$ (note also that an open set $\mathcal{U} \subseteq \mathcal{M}$ exists such that $\mathcal{U}_{\mathring{x}} = \mathcal{U} \cap \mathcal{F}(\mathring{y})$). For a configuration $x(t) \in \mathcal{U}_{\mathring{x}}$, the time-derivative of $\mathcal{L}_{\mathring{x}}(x)$ is given by

$$\begin{aligned}
\frac{\mathrm{d}}{\mathrm{d}t}\mathcal{L}_{\mathring{x}}(x) &= \mathrm{D}\mathcal{L}_{\mathring{x}}(x)[\dot{x}] \\
&= -\mathrm{D}\mathcal{L}_{\mathring{x}}(x) \circ \mathrm{D}\Phi_x(\iota)[\nabla(\mathcal{L}_{\mathring{x}} \circ \Phi_x)(\iota)] \\
&= -\langle \nabla(\mathcal{L}_{\mathring{x}} \circ \Phi_x)(\iota), \nabla(\mathcal{L}_{\mathring{x}} \circ \Phi_x)(\iota) \rangle_\iota \\
&\leq 0,
\end{aligned}$$

with equality holding only when $x = \mathring{x}$. It follows that $\mathcal{L}_{\mathring{x}}(x)$ is upper bounded by its initial value, and consequently that any trajectory with initial state $x(0) \in \mathcal{U}_{\mathring{x}}$ is constrained to $\mathcal{U}_{\mathring{x}}$ for all time. Application of Lyapunov's method then shows that $\mathcal{L}_{\mathring{x}}(x) \to 0$ and therefore $x(t) \to \mathring{x}$ as required. ∎

Remark 4.4.9. The steering control for an individual agent i is found by the elements of (4.17) corresponding to the coordinates of x_i, i.e.

$$\dot{x}_i = -\left.\frac{\partial \Phi_{x_i}(S)}{\partial S}\right|_{S=\iota} \circ \Lambda_\iota^{-1} \left(\sum_{i=1}^{N} \frac{\partial \mathcal{L}_{\mathring{x}}(x)}{\partial x_i} \circ \left.\frac{\partial \Phi_{x_i}(S)}{\partial S}\right|_{S=\iota} \right)$$

where Λ_ι denotes the metric operator on $\mathfrak{g}$ (see Part [vi] of Section 1.5). The gradient is the element of the Lie algebra that minimises the cost function across the full agent network; this is reflected in the fact that the sum is taken over all agents. Managing agreement on this gradient vector in a distributed manner is a subject for future research; it may be achieved via standard consensus techniques or it may be sufficient to have each agent estimate the gradient vector from a limited number of neighbours (exploiting the relatively low dimension of the Lie algebra). Mapping the gradient vector through $\mathrm{D}\Phi_x(\iota)$ is equivalent to simply moving each individual vehicle according to the group transform. $\diamond$

For the practical application of Theorem 4.4.8, it is necessary to stabilise the agents to the formation $\mathcal{F}(\mathring{y})$ while simultaneously manoeuvring them towards $\mathring{x}$. Combining Corollary 4.4.5 with Theorem 4.4.8 leads to the control law

$$\dot{x} = v_1 + v_2, \tag{4.18}$$

where

$$\begin{aligned} v_1 &:= -\nabla \left(V_{\mathring{y}} \circ h \right) (x), \\ v_2 &:= -\mathrm{D}\Phi_x(\iota)[\nabla(\mathcal{L}_{\mathring{x}} \circ \Phi_x)(\iota)]. \end{aligned}$$

Thus, the control objective is achieved by decomposing the problem into two components: the first control term drives the agents towards the desired formation $\mathcal{F}(\mathring{y})$, and the second directs the agents towards a desired configuration while preserving their present formation. Stability analysis of the resulting control scheme is readily performed in a local neighbourhood of $\mathring{x}$ on which all configurations are infinitesimally rigid (recall that Theorem 4.2.7 ensures such a neighbourhood exists). Observe that

$$\langle v_1, v_2 \rangle_x = -\mathrm{D}V_{\mathring{y}}(h(x)) \circ \mathrm{D}h(x)[v_2] = 0,$$

since $v_2 \in \mathbb{V}(x)$ lies in the kernel of $\ker \mathrm{D}h(x)$. That is, the two control terms v_1 and v_2 are orthogonal with respect to the Riemannian metric $\langle \cdot, \cdot \rangle_x$ on $\mathcal{M}$. It follows that v_2 does not disrupt the exponential convergence of the system to $\mathcal{F}(\mathring{y})$ (the result from the calculations (4.13), (4.14), (4.16) still holds), at which point Theorem 4.4.8 can be applied to show that $x(t)$ converges to $\mathring{x}$.

An appealing aspect of this approach is that it explicitly separates the task of regulating the formation (converging to $\mathcal{F}(\mathring{y})$) from that of manoeuvring in formation towards a desired configuration $\mathring{x} \in \mathcal{F}(\mathring{y})$. These two tasks are commonly identified as independent objectives in behavioural control approaches to formation control (see e.g. Lawton et al. [2003]), and can also be naturally expressed in the virtual structure framework (i.e. where the virtual structure is a configuration that moves in the submanifold of the formation). The approach outlined above is also likely to enable straightforward extensions to address cases where the desired configuration, or even the specification $\mathring{y}$ of the formation, are time-varying. Note that the behaviour of the system can be adjusted by suitable shaping of the cost functions $V_{\mathring{y}}$ and $\mathcal{L}_{\mathring{x}}$.

4.5 Conclusions and Future Work

In this chapter I have extended the classical notion of *infinitesimal rigidity* to the generalised framework introduced in Chapter 3. Several fundamental results by Asimow and Roth [1978, 1979] have also been extended to this more general setting. Together, these results show that an infinitesimally rigid formation is a regular submanifold of the state space, with an open neighbourhood on which all configurations are also infinitesimally rigid. This insight is critical for network localisation and formation control problems, providing structure for local convergence analysis and allowing the task of manoeuvring in formation to be resolved as a control problem in a submanifold. In addition to this analysis, I have introduced a new notion of *robust rigidity* that captures important structural properties from the classical case for scenarios involving non-compact formations. The significance of these results has been illustrated through the applications of network localisation and formation control, both of which commonly involve more complex agent networks than are addressed by classical rigidity theory.

A limitation of the results presented in this chapter is that they do not allow one to easily consider the transition between orbits in a local neighbourhood of the formation. For this purpose, it would be of great interest to construct a fibre bundle structure on a local neighbourhood of the formation. Suppose the base-space is a formation $\mathcal{F}(\mathring{y})$, and let us consider the transverse submanifold $\mathcal{X}$ used in the proof of Theorem 4.4.1 as a candidate fibre. It is clear that a local neighbourhood around each point in the formation will possess the structure obtained by the product of these two submanifolds (recall Theorem 4.2.7 and observe that each nearby orbit will intersect the transverse submanifold $\mathcal{X}$ at precisely one point). It remains to define a suitable projection map $\pi : \Phi(\mathbf{G}, \mathcal{X}) \to \mathcal{F}(\mathring{y})$. For a point $x \in \mathcal{X}$, one can specify $\pi(x) := \mathring{x}$ where $\mathring{x} \in \mathcal{F}(\mathring{y}) \cap \mathcal{X}$. For a point $x' \notin \mathcal{X}$, an intuitive idea is to find the group element $S \in \mathbf{G}$ such that $x' \in \Phi_S(\mathcal{X})$, and to define the projection as $\pi(x') := \Phi_S(\mathring{x})$. However, although the stabilisers of the points in $\mathcal{X}$ are homeomorphic, they need not be identical. Thus, it appears that additional structure is necessary for the projection π to be well-defined. Some insight for this problem is provided by the work of Duistermaat and Kolk [2000], who introduced the concept of a *slice*; this is essentially a transverse submanifold $\mathcal{X}$ for which the stabiliser of each point $x \in \mathcal{X}$ is the same. It is proven that for a *proper* group action, a slice always exists [Duistermaat and Kolk, 2000, Theorem 2.3.3]. The necessity of this condition in the present setting is a subject for further investigation. It should be emphasised that a fibre-bundle structure would play a significant role in the analysis of the system, since it would enable one to interpret the fibre $\mathcal{X}$ as a *shape-space* on which convergence to a specified formation can be studied.

The proposed algorithm for network localisation is able to determine the system state up to the symmetry described by the group action. Many network localisation strategies rely on the presence of *anchor nodes* (see e.g. Mao et al. [2007]; Eren [2011]) in order to reference the configuration with respect to an inertial frame. In the proposed framework, the information associated with these anchor nodes may simply be modelled as measurements of the agent states in the inertial frame. Thus, it is likely that the theory in this chapter could provide valuable insight for the arrangement of anchor nodes in generalised settings.

Chapter 5

Passivity-Based Formation Control

In this chapter I develop a passivity-based approach to the task of driving dynamic vehicles in $\mathbb{R}^3$ space to a desired static formation, using generic partial measurements of relative position. The control framework is developed using the elegant bondgraph modelling formalism outlined in Appendix D, leading to a highly modular design that employs virtual mechanical couplings on the available sensor measurements. For the cases of direction and distance measurements, I incorporate adaptive compensation into the control scheme to handle the unknown component of the relative positions. I prove local asymptotic stability of the desired formation, and illustrate the system's behaviour with simulation results. The work in this chapter draws from the papers Stacey et al. [2013]; Stacey and Mahony [2013, 2016].

5.1 Introduction

The task of formation control between autonomous vehicles has received considerable attention in recent years (see e.g. Ren and Beard [2004a]; Chen and Wang [2005]; Mastellone et al. [2008]; Turpin et al. [2012]; Oh et al. [2015]). Energy-based approaches developed around the concepts of artificial potentials (Leonard and Fiorelli [2001]; Vos et al. [2016]) and passivity (Hatanaka et al. [2012]; Franchi et al. [2012b]) have found particular appeal, due to their ability to simplify the control design and stability analysis of complex systems. A general theoretical framework concerning port-Hamiltonian systems on graphs, developed by van der Schaft and Maschke [2013], can also be used to derive a similar formation control architecture.

It is important to observe that much of the existing literature on formation control relies upon the availability of full relative position information between pairs of agents. While such information can be provided in well-structured environments through the use of an external tracking system, such as a motion-capture system or a global positioning system (GPS), many scenarios impose limitations on the use of such infrastructure that can render this information unreliable or entirely unavailable (e.g. signal occlusions or hostile interference). Hence, it is often more appropriate to consider the use of *partial* relative position measurements (such as distances or directions) as can commonly be acquired by onboard sensors (e.g. time-of-flight sensors or onboard cameras, respectively). The restriction to such partial relative position measurements makes the formation control problem significantly more challenging, and this case has received remarkably limited attention in the literature (see e.g. Johnson et al. [2004]; Cao et al. [2011]; Franchi et al. [2012a]; Zelazo et al. [2015]; Zhao and Zelazo [2016]). The proposed solutions typically involve exploiting the particular geometrical structure of a certain sensor modality, and cannot be readily extended to other types of measurements, or to more general sensor configurations. For example, the bearing-based controller proposed by Franchi et al. [2012a] relies on nominating two *beacon agents* that act as references for the remainder of the formation. For distance-based position estimation, Cao et al. [2011] use a *stop-and-go* strategy that requires kinematic agents to take turns in stopping, while the moving agents obtain multiple distance measurements for triangulation in a local coordinate frame. Recently, Zelazo et al. [2015] have employed rigidity theory to achieve distance-based formation control while ensuring the formation remains rigid; the idea in this work is to estimate the full relative positions of the vehicles by exploiting a special agent for which two bearing measurements are also available. A notion of bearing rigidity has also been developed and employed for the task of bearing-based formation control by Zhao and Zelazo [2016].

The task of position regulation using bearing measurements is well-studied in the image-based visual servo (IBVS) control literature (see the tutorials Hutchinson et al. [1996]; Chaumette and Hutchinson [2006, 2007]). A passivity-based approach to target tracking using visual information has been presented by Fujita et al. [2007]. A similar strategy for IBVS control is developed by Mahony and Stramigioli [2012] using the elegant bondgraph modelling framework (see Appendix D). The extension of these energy-based approaches to other partial relative position measurements, and to the task of formation control, has not been further investigated to the best of my knowledge.

In this chapter, I use the bondgraph modelling framework to develop a passivity-based formation control architecture for dynamic agents in $\mathbb{R}^3$, with a particular focus on the use of generic *partial* measurements of the relative positions between agents. This forms a strong contrast with much of the formation control literature, which typically requires full information of relative positions. Furthermore, the control architecture enables far more general sensor configurations involving multiple sensor modalities, whereas many existing formation control schemes in the literature typically focus on a single type of relative position measurement. The approach draws inspiration from the techniques used in the IBVS control literature (most notably, from the work by Mahony and Stramigioli [2012]), and involves generalising the *image Jacobian* to a *measurement Jacobian* for an arbitrary sensor modality. This enables the use of virtual mechanical couplings, similar to those considered by Leonard and Fiorelli [2001]; Vos et al. [2016], to be applied directly to the sensor measurements, with the measurement Jacobian transforming the resulting control force into the state-space of the agents. In the particularly important cases of direction and distance sensor modalities, the measurement Jacobians depend upon unknown relative state information (i.e. the complementary measurements of distance and direction, respectively). I address this issue by incorporating adaptive compensation into the bondgraph modelling framework, with the designs for direction and distance measurements considered separately due to differences in the geometrical structure of these sensor modalities. The adaptive compensation accounts for the energy associated with the error in the applied control input (compared to the ideal control input determined by the true state), and thus ensures that passivity of the system is strictly preserved. This design is proven to be locally asymptotically stable to the desired formation. The adaptive compensation approach is in contrast to the more common strategy of using an observer to estimate the unknown state, and relying on a separation principle to preserve the stability of the system. The drawback to the alternative observer-based approach is that the observer may introduce energy to the system during its transient, thus breaching the passivity of the system and making formal stability analysis difficult to perform. Simulation results for the proposed control scheme are also presented.

The formation control problem considered in this chapter is formulated in Section 5.2. In Section 5.3 I construct and analyse the basic control architecture for generic sensor modalities. To address implementation issues that arise for direction and distance measurements (associated with the structure of the available measurements), separate adaptive control designs for these two important sensor modalities are developed in Section 5.4. A summary of the chapter is provided in Section 5.5.

5.2 Vehicle and Sensor Models

In this section I formulate the formation control problem considered in the remainder of the chapter. I begin by establishing the vehicle model in Subsection 5.2.1, and a description of the sensor model follows in Subsection 5.2.2. In Subsection 5.2.3 I introduce the basic network structure and formalise the formation control task.

5.2.1 Vehicle Model

This chapter addresses the task of driving a group of N vehicles towards a desired formation. Each vehicle i is modelled as a fully-actuated point-mass system with position $\xi_i \in \mathbb{R}^3$ and mass $c_i^m > 0$. The i'th vehicle has kinetic energy given by

$$T_i(\dot{\xi}_i) := \frac{1}{2} c_i^m \|\dot{\xi}_i\|^2,$$

and potential energy described by

$$U_i(\xi_i) := c_i^m g \xi_i^z.$$

Here, g is the constant acceleration due to gravity, and $\xi_i^z > 0$ is the vehicle's height above ground level. The Hamiltonian

$$H_i^{\text{mech}}(\xi_i, \dot{\xi}_i) := T_i(\dot{\xi}_i) + U_i(\xi_i) \tag{5.1}$$

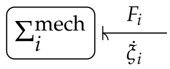

Figure 5.1: Bondgraph notation for the mechanical subsystem of vehicle i. The power port is associated with the implemented control force F_i and the resulting velocity $\dot{\xi}_i$.

is a non-negative function that describes the total mechanical energy of the i'th vehicle. The dynamics of the vehicle under a control force $F_i \in \mathbb{R}^3$ are modelled by (Goldstein [1980])

$$F_i - c_i^m g\vec{e}_3 = c_i^m \ddot{\xi}_i, \tag{5.2}$$

where $\vec{e}_3$ denotes a unit vector in the vertical (upwards) direction.

The implemented control force consists of three components as follows:

$$F_i := -F_i^{\text{comp}} - D_i\dot{\xi}_i + \tau_i. \tag{5.3}$$

Here,

$$F_i^{\text{comp}} := -\frac{\partial U_i}{\partial \xi_i} = -c_i^m g\vec{e}_3$$

is a compensation term used to counteract the effect of gravity[1], and $D_i > 0$ is a positive-definite coefficient for the damping applied to the vehicle. Note that this coefficient may include both physical and virtual damping (i.e. artificial damping applied by the control). The control input τ_i remains to be designed such that the vehicles converge to a desired formation.

Throughout this chapter I will derive insight to the formation control architecture with the aid of the bondgraph modelling formalism (for further details on the bondgraph notation, see Appendix D or Borutzky [2006]). To model the i'th vehicle, I begin with the component in Figure 5.1 that represents the mechanical part of the system, i.e. the dynamics described by (5.2) with energy (5.1). While this component could be modelled in further detail, doing so will provide limited additional insight for the control design. The mechanical subsystem takes the implemented control force F_i as an input, and provides the vehicle's velocity $\dot{\xi}_i$ as an output. This is represented in the diagram by the placement of the causality bar on the left end of the power bond (i.e. the end attached to the mechanical component). The power through this bond is expressed by $\langle F_i \mid \dot{\xi}_i \rangle := F_i^\top \dot{\xi}_i$. Note that the half-arrow indicates positive power flow is in the direction *towards* the mechanical subsystem.

The model of the vehicle's full system, which consists of the mechanical component (5.2) and the control input (5.3), is represented in Figure 5.2. In the remainder of this chapter, the vehicle's system will be denoted as indicated on the right hand side of this figure. In the bondgraph diagram, the decomposition of the control input F_i given in (5.3) is represented using a 1-junction. The resistive element R_i represents the dissipation of energy due to the damping D_i, while the storage element C_i^{comp}

[1]The use of $-F_i^{\text{comp}}$ in (5.3) rather than defining a positive term is to make the definition consistent with the conventional one used in the bondgraph notation, seen later in Figure 5.2.

contains the energy used to drive the gravity compensation. This energy is described by the Hamiltonian

$$H_i^{\text{comp}}(\xi_i) := -U_i(\xi_i) = -c_i^m g\vec{e}_3.$$

Although the energy should technically be positive definite, the above definition is suitable for the purposes in this chapter. Specifically, this is because the energy stored in $H_i^{\text{comp}}(\xi_i)$ cancels with the gravitational potential $U_i(\xi_i)$ in (5.1), meaning that the total energy in the vehicle's system is that of the kinetic energy function $T_i(\dot{\xi}_i) \geq 0$. The bond to the right of the 1-junction, associated with the control input τ_i, will be used to exchange power between the vehicle and the remainder of the network. Note that the bondgraph diagram affirms that the vehicle's system is *passive* with respect to the control input τ_i and the velocity output $\dot{\xi}_i$. To see this, observe from the diagram that the total energy in the vehicle's model is the kinetic energy $T_i(\dot{\xi}_i) \geq 0$, and that the only energy exchange with the environment is the positive energy dissipation via the element R_i. This clarity of the system's passivity is a key motivation for the bondgraph modelling framework.

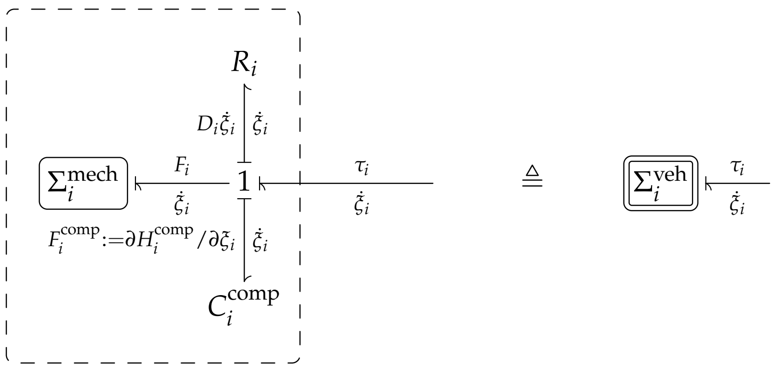

Figure 5.2: Bondgraph model of a single vehicle in the formation control problem. The rightmost bond is the power port through which the formation control input τ_i is applied. The vehicle's system in the dashed box will later be denoted as shown on the right.

In this chapter, I am only concerned with controlling the position of each vehicle in the formation, as is commonly considered in the literature (see e.g. Franchi et al. [2012b]). In particular, I do not regulate the vehicle attitudes as part of the formation control task. This leaves them unconstrained for use in a hierarchical control architecture as in Hua et al. [2013]. In practice, such an architecture will be required for the local control of underactuated vehicles (e.g. quadrotors) in order to implement the linear point-mass dynamics modelled in (5.2). It is also worth noting that the attitude of each vehicle can typically be obtained from IMU data (see e.g. Mahony et al. [2008]). This information can be exploited to de-rotate all state measurements into the inertial frame, and for simplicity I will therefore express measurements with respect to this frame rather than the body-fixed frames of the vehicles.

5.2.2 Sensor Model

Suppose there are M virtual *links* between pairs of vehicles, with each link k being associated with the relative position

$$\zeta_k := \xi_i - \xi_j \in \mathbb{R}^3 \tag{5.4}$$

of a vehicle i with respect to a vehicle j. A particularly important aspect of the formation control problem I consider in this chapter is that only *partial measurements* y_k of the relative positions ζ_k are available. I will assume that these measurements can be freely communicated between the two vehicles associated with them (i.e. vehicles i and j). If multiple readings are available, as might be the case if there is a sensor on each vehicle, then a consensus algorithm can be employed to ensure agreement on the accepted measurement y_k. Consequently, the measurement y_k is assumed to be mutually determined by vehicles i and j, and I will adopt the notational convention that $i < j$ for all links $k = (i, j)$ to avoid duplicate measurements or ambiguity in (5.4).

Formally, I define a partial measurement y_k of the relative position ζ_k by a smooth map $y_k : \mathbb{R}^3 \setminus \mathcal{W}_k \to \mathcal{Y}_k$, where $\mathcal{Y}_k$ denotes a smooth manifold termed the *output space* and $\mathcal{W}_k$ is an *exceptional set* consisting of non-regular points in $\mathbb{R}^3$ to which the output map cannot be smoothly extended. The partial measurements of distance and direction are of particular practical interest, since they are naturally obtained by common forms of onboard sensors, and I will primarily focus on these measurements in this chapter.

A *distance* measurement is defined by

$$y_k = r_k := \|\zeta_k\| \in \mathbb{R}_{>0}, \tag{5.5}$$

where the output space $\mathcal{Y}_k = \mathbb{R}_{>0}$ is the set of positive real numbers and the exceptional set consists of a single point $\zeta_k = 0$, at which the output map is nonsmooth. For a *direction* measurement, one has

$$y_k = s_k := \frac{\zeta_k}{\|\zeta_k\|} \in \mathbb{S}^2, \tag{5.6}$$

where the output space $\mathcal{Y}_k = \mathbb{S}^2$ is the unit sphere and the exceptional set again consists of the point $\zeta_k = 0$, at which the direction is undefined. Observe that for physical vehicles, the case where $\zeta_k = 0$ corresponds to a collision. Any practical control scheme should include safeguards to ensure that closed-loop trajectories never pass through such points, and it is therefore natural to exclude these points from the theoretical framework for formation control.

It is convenient to develop the theory in this chapter using an embedding of the output space $\mathcal{Y}_k$ into a *sensor space* $\mathbb{R}^m$, where $m \geq 1$ is a sufficiently high dimension. For example, the embedding of a distance measurement r_k is simply the open set $\mathbb{R}_{>0} = \{x \in \mathbb{R} \mid x > 0\}$ embedded in $\mathbb{R}$. For a direction measurement s_k, the embedding is that of the unit sphere $\mathbb{S}^2 = \{(x, y, z)^\top \mid x, y, z \in \mathbb{R}, x^2 + y^2 + z^2 = 1\}$

in $\mathbb{R}^3$. The embedding of $\mathcal{Y}_k$ in $\mathbb{R}^m$ induces a natural geometry on the output space that will be of use in the sequel.

Define the *measurement Jacobian* as the $m \times 3$ matrix

$$L_{y_k}(\zeta_k) := \frac{\partial y_k}{\partial \zeta_k}(\zeta_k). \tag{5.7}$$

The time-evolution of a measurement y_k is then described by

$$\dot{y}_k := L_{y_k}\dot{\zeta}_k. \tag{5.8}$$

For a distance measurement $r_k \in \mathbb{R}_{>0}$, the time-derivative is

$$\begin{aligned} \dot{r}_k &:= \frac{\mathrm{d}}{\mathrm{d}t}(\zeta_k^\top \zeta_k)^{\frac{1}{2}} = \frac{\zeta_k^\top \dot{\zeta}_k}{(\zeta_k^\top \zeta_k)^{\frac{1}{2}}} \\ &= s_k^\top \dot{\zeta}_k, \end{aligned}$$

and the *distance Jacobian* is therefore (cf. Example 4.2.9)

$$L_{r_k} = s_k^\top \in \mathbb{R}^{1\times 3}. \tag{5.9}$$

Similarly, the time-derivative of a direction measurement $s_k \in \mathbb{S}^2$ is

$$\begin{aligned} \dot{s}_k &:= \frac{\mathrm{d}}{\mathrm{d}t}\frac{\zeta_k}{r_k} = \frac{\dot{\zeta}_k}{r_k} - \frac{\dot{r}_k \zeta_k}{r_k^2} \\ &= \frac{1}{r_k}(I_3 - s_k s_k^\top)\dot{\zeta}_k, \end{aligned}$$

and hence the *image Jacobian* is defined by (cf. Example 4.2.10)

$$L_{s_k} := \frac{1}{r_k}(I_3 - s_k s_k^\top) \in \mathbb{R}^{3\times 3}. \tag{5.10}$$

The concept of the image Jacobian L_{s_k} is well-established in the IBVS control literature (see e.g. Hutchinson et al. [1996], and the image *interaction matrix* in Chaumette and Hutchinson [2006, 2007]). Note that the formulation presented in this chapter is slightly different to the classical construction; specifically, I consider a bearing in the embedded sphere rather than expressing it in the 2-D coordinate frame of a camera image. The use of the sphere has been motivated by Corke and Mahony [2009] (although this work used the coordinates of colatitude and azimuth angles rather than Cartesian coordinates).

5.2.3 Specification of the Formation Control Task

Let $\mathring{y}_k$ be a set of parameters that specify the desired static formation for the vehicles in terms of the available sensor measurements y_k. The goal of the formation controller developed in this chapter is to ensure all errors

$$\tilde{y}_k := y_k - \mathring{y}_k \tag{5.11}$$

approach zero. Note that the natural sensor error defined in (5.11) relies on the Euclidean structure of the sensor embedding space.

It is convenient to introduce some notation from graph theory to represent the measurement interconnections between vehicles. Let $\mathcal{G} := (\mathcal{V}, \mathcal{E})$ be an undirected network graph, with $\mathcal{V}$ being a set of N vertices and $\mathcal{E}$ being a set of M edges between pairs of vertices in $\mathcal{V}$. Each vertex $i \in \mathcal{V}$ corresponds to a vehicle in the network and each edge $k = (i, j) \in \mathcal{E}$ corresponds to a sensor measurement. Note that the graph $\mathcal{G}$ does not contain any self edges (i.e. where $k = (i, i)$), but it may contain multiple edges between a single pair of vehicles if each edge is associated with a different sensor modality. The use of an *undirected* graph is motivated by the earlier assumption that the measurements y_k are mutual between vehicles i and j. The *neighbours* of a vertex i are the vertices $j \neq i$ that are connected directly to vertex i by at least one edge k. The notation $\mathcal{E}_i$ will be used to refer to the set of edges attached to vertex i.

The formation control input for the i'th vehicle is defined as

$$\tau_i := \sum_{k \in \mathcal{E}_i} \chi^i_k \epsilon_k. \tag{5.12}$$

Here, the control force $\epsilon_k \in \mathbb{R}^3$ is derived from a virtual mechanical coupling in link k, based on the available measurement y_k. The sign constant χ^i_k is set to $+1$ if link k connects to a vehicle of lower index than i, and -1 if it connects to a vehicle of higher index. As a consequence of this sign change, the two vehicles joined by a link k will experience equal but opposite virtual forces ϵ_k from the formation control scheme. The detailed specification of the control force ϵ_k is the focus of the remainder of this chapter.

The bondgraph model representing the construction of the control input τ_i is shown in Figure 5.3. The bonds on the right-hand side of the diagram will connect to the virtual mechanical coupling associated with the sensor measurement y_k, for each link $k \in \mathcal{E}_i$ that connects to a neighbour of vehicle i. Note that the orientation of the half-arrow on each of these bonds represents the sign coefficient χ^i_k.

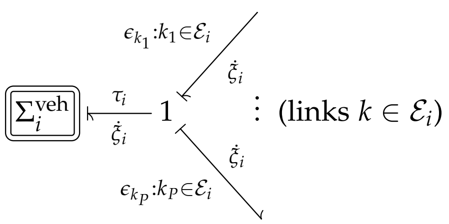

Figure 5.3: Bondgraph model showing the construction of τ_i given by (5.12).

5.3 Control using Virtual Mechanical Couplings

In this section I develop a generic sensor-based control scheme for the formation control task formulated in Section 5.2. The control input is derived from virtual mechanical couplings placed on the available sensor measurements, and is presented in Subsection 5.3.1. Analysis proving local asymptotic stability of the proposed control scheme is given in Subsection 5.3.2. Subsection 5.3.3 provides some discussion of the control design and the stability result, along with simulations.

5.3.1 Controller Model

For the task of sensor-based formation control, I derive a control term ϵ_k based on a generic partial relative position measurement y_k. The control effort is driven by a virtual mechanical coupling on the error $\tilde{y}_k$ given in (5.11). To specify the energy associated with this virtual coupling, I propose the spring-like Hamiltonian function

$$H_k^{\mathrm{vmc}}(y_k) := \frac{1}{2}\tilde{y}_k^\top c_k^{\mathrm{vmc}} \tilde{y}_k, \tag{5.13}$$

where $c_k^{\mathrm{vmc}} > 0$ is a constant. The power exchanged with this energy function consists of a flow $\dot{\tilde{y}}_k = \dot{y}_k$ (since $\mathring{y}_k$ is constant) and an effort e_k^{vmc} given by (Duindam et al. [2009])

$$e_k^{\mathrm{vmc}} := \mathbb{P}'_{y_k}\left(\frac{\partial H_k^{\mathrm{vmc}}}{\partial y_k}\right) = c_k^{\mathrm{vmc}}\mathbb{P}'_{y_k}(\tilde{y}_k). \tag{5.14}$$

Here, $\mathbb{P}'_{y_k}(\cdot)$ denotes the projection onto the embedded tangent space $T_{y_k}\mathcal{Y}_k$ associated with taking the differential on $\mathcal{Y}_k$ [Absil et al., 2008, Proposition 5.3.2]. For a direction measurement s_k, this projection is $\mathbb{P}'_{s_k} := (I_3 - s_k s_k^\top)$, while for a distance measurement r_k it is simply the identity. To verify that the resulting power exchange is energy-consistent, observe that

$$\begin{aligned} \frac{\mathrm{d}}{\mathrm{d}t}H_k^{\mathrm{vmc}} &:= \frac{\partial H_k^{\mathrm{vmc}}(y_k)}{\partial y_k}\dot{y}_k = \mathbb{P}'_{y_k}\left(\frac{\partial H_k^{\mathrm{vmc}}(y_k)}{\partial y_k}\right)\dot{y}_k \\ &= \langle e_k^{\mathrm{vmc}} \mid \dot{y}_k\rangle, \end{aligned} \tag{5.15}$$

since $\mathbb{P}'_{y_k}(\cdot)$ projects onto $T_{y_k}\mathcal{Y}_k$ and $\dot{y}_k \in T_{y_k}\mathcal{Y}_k$. It is important to note that the effort (5.14) and power exchange (5.15) are expressed in accordance with the bondgraph convention of defining power as positive when it flows *into* the energy storage element. The effort applied *by* the virtual spring to the remainder of the system will be $-e_k^{\mathrm{vmc}}$, which corresponds to a negative proportional term as is commonly employed in control schemes. I will consistently use this convention for the direction of positive power throughout this chapter.

To improve the system response, I include a virtual damping term

$$d_k^{\mathrm{vmc}} := D_k^{\mathrm{vmc}}\dot{y}_k$$

in the virtual mechanical coupling, where $D_k^{\mathrm{vmc}} > 0$ is a damping coefficient. As with the effort e_k^{vmc}, the damping term d_k^{vmc} is expressed with positive power being in the direction towards the dissipative element, and the actual damping force exerted on the system will be $-d_k^{\text{vmc}}$. The total virtual effort associated with the virtual coupling is now given by

$$\gamma_k := e_k^{\text{vmc}} + d_k^{\text{vmc}}. \tag{5.16}$$

Note that the effort (5.16) lies in the tangent space of the measurement space $\mathcal{Y}_k$, not the state-space of the vehicles. The negative of this effort, i.e. $-\gamma_k$, may be interpreted as the effort that should be applied to the measurement y_k in order to drive it towards the desired value $\mathring{y}_k$. In order to obtain a control force $\epsilon_k \in \mathbb{R}^3$ that can be applied to the vehicles, it is necessary to transform the virtual force γ_k using the measurement Jacobian (5.7). Therefore, I set

$$\epsilon_k := L_{y_k}^{\top} \gamma_k, \tag{5.17}$$

which is passed to vehicles i and j as described by (5.12).

The total power supplied by the virtual mechanical coupling may be computed as

$$\begin{aligned} \langle \gamma_k \mid \dot{y}_k \rangle &= \langle \gamma_k \mid L_{y_k} \dot{\zeta}_k \rangle = \langle L_{y_k}^{\top} \gamma_k \mid \dot{\zeta}_k \rangle \\ &= \langle \epsilon_k \mid \dot{\xi}_i \rangle - \langle \epsilon_k \mid \dot{\xi}_j \rangle. \end{aligned} \tag{5.18}$$

Here, each of the two terms on the right hand side represents the power exchanged with one of the connected passive vehicles, and it follows that the proposed control scheme is energy-consistent.

The control architecture based on the virtual mechanical coupling is modelled by the bondgraph diagram in Figure 5.4. The storage element C_k^{vmc} contains the energy described by the Hamiltonian H_k^{vmc} (5.13) used to drive the control, while the energy dissipation through the virtual damping is represented by the resistive element R_k^{vmc}. The upper-central 1-junction shows that the virtual effort γ_k (5.16) is composed of the efforts associated with the virtual spring and damper. The MTF is a modulated transformer that implements the dual relationships (5.8) and (5.17), with the measurement Jacobian L_{y_k} provided as an input signal as indicated by the normal arrow into the MTF symbol. The bondgraph notation enforces this dual relationship in order to ensure an energy-consistent interconnection through the MTF, i.e. the expression for ϵ_k (5.17) is determined directly by the sensor kinematics (5.8). The 0-junction defines the relative velocity $\dot{\zeta}_k$, using the relative orientation of the two lower bonds to encode a difference between the individual vehicle velocities $\dot{\xi}_i$ and $\dot{\xi}_j$. These bond orientations enforce the application of equal and opposite control efforts $-\epsilon_k$ (vehicle i) and ϵ_k (vehicle j) to the two vehicles, thus encoding the χ_k^i function in (5.12).

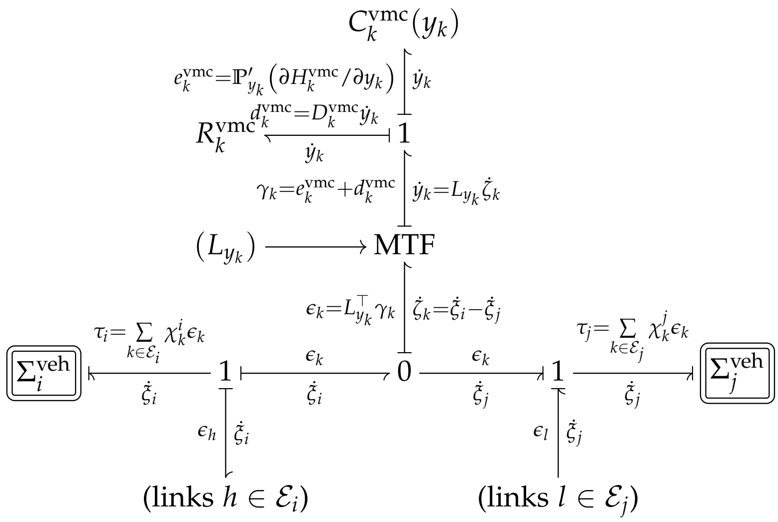

Figure 5.4: Bondgraph model of a control link between two vehicles, given a partial relative position measurement y_k. Note the difference in the relative orientation of the energy bonds going to each vehicle's subsystem. The relative orientations of the links h and l may vary.

5.3.2 Stability Analysis

Before proceeding to the stability analysis of the control scheme developed in Subsection 5.3.1, I provide the following summary of the scenario, which includes some additional notation involving the stacking of variables in the system.

Scenario 5.3.1. Consider a connected network of N vehicles with M links between them. The i'th vehicle has a state $(\xi_i, \dot{\xi}_i)$ and dynamics described by (5.2) and (5.3). The set of all links is denoted $\mathcal{E}$, and the set of links attached to vehicle i is denoted $\mathcal{E}_i$. Suppose that each link $k \in \mathcal{E}$ is associated with a partial measurement $y_k(\zeta_k)$ of the relative position (5.4), and that these measurements are well-defined and smooth for $\zeta_k \in \mathbb{R}^3 \setminus \{0\}$. Let $\mathring{y}_k$ denote a target stationary value for the partial relative position measurement y_k, with the error denoted by $\tilde{y}_k$ as in (5.11). The control input τ_i for each vehicle is described by (5.12), (5.16) and (5.17). Denote $\xi := (\xi_1^\top, \ldots, \xi_N^\top)^\top$ and $\tau := (\tau_1^\top, \ldots, \tau_N^\top)^\top$. Let $\zeta := (\zeta_1^\top, \ldots, \zeta_M^\top)^\top$ and define y, $\mathring{y}$ and $\tilde{y}$ analogously. Denote $Z := \{\zeta \mid \tilde{y}(\zeta) = 0\}$ as the set of desired relative positions, with $\Xi := \{\xi \mid \zeta(\xi) \in Z\} \subset \mathbb{R}^{3\times N}$. ◇

The stability analysis will rely on the passivity of the full system. The bondgraph model of the system shows that the total energy is given by

$$H^{\text{total}}(\xi, \dot{\xi}) = \sum_{i=1}^{N} T_i(\dot{\xi}) + H^{\text{vmc}}(\zeta(\xi)), \tag{5.19}$$

where

$$H^{\mathrm{vmc}}(\zeta) := \sum_{k=1}^{M} H_k^{\mathrm{vmc}}(y_k(\zeta_k)).$$

The bondgraph formalism guarantees that the system is modelled in an energy-consistent manner. Hence, the time-derivative of the total energy function can be found simply by summing the dissipative terms, i.e.

$$\frac{\mathrm{d}}{\mathrm{d}t} H^{\mathrm{total}} := -\sum_{i=1}^{N} \dot{\xi}_i^\top D_i \dot{\xi}_i - \sum_{k=1}^{M} \dot{y}_k^\top D_k^{\mathrm{vmc}} \dot{y}_k. \tag{5.20}$$

For the stability result presented in this subsection, I employ an assumption that ensures the system variables remain well-defined in a local region on which the trajectories evolve.

Assumption 5.3.2. Assume there exist $\kappa_1, b_1 > 0$ such that $H^{\mathrm{vmc}}(\zeta_k) < \kappa_1$ implies

$$\inf_{\mu \in \mathcal{W}} \|\zeta - \mu\| > b_1,$$

where

$$\mathcal{W} := \cup_{k=1}^{M} \{\zeta \in \mathbb{R}^3 \mid \zeta_k = 0 \text{ for some } k\}. \qquad \diamond$$

Theorem 5.3.3. *Consider Scenario 5.3.1, with the full state given by $(\xi, \dot{\xi})$ and with the total energy H^{total} in the system being described by* (5.19)*. Assume that all measurement Jacobians L_{y_k}* (5.7) *are known, and that the set Z is nonempty and compact. Suppose that Assumption 5.3.2 holds.*

Then, there exists an open set $\mathcal{A} \subset (\mathbb{R}^{3N}, \mathbb{R}^{3N})$ about $(\Xi, 0)$ such that $(\xi, \dot{\xi}) \to (\Xi, 0)$, for all initial conditions $(\xi(0), \dot{\xi}(0)) \in \mathcal{A}$.

Proof The full system is dissipative, with the total Hamiltonian (5.19) having time-derivative (5.20). Since H^{total} is non-increasing, it is bounded by its initial value. This places an upper bound on all $\dot{\xi}_i$, and it follows that solutions exist for all time. Assumption 5.3.2 implies that the energy $H^{\mathrm{vmc}}(\zeta)$ in the virtual mechanical couplings is well-defined and smooth in an open region about Z, and by invariance this is also true in an open region about Ξ. One can therefore define a positive constant $\kappa_2 \leq \kappa_1$ such that the set $\mathcal{Z} := \{\zeta \in \mathbb{R}^3 \mid H^{\mathrm{vmc}}(\zeta) < \kappa_2\}$ is compact, and such that the only critical points of $H^{\mathrm{vmc}}(\zeta(\xi))$ at which $\zeta(\xi) \in \mathcal{Z}$ are those in Ξ. Define $\mathcal{A}$ as the set of points in $(\mathbb{R}^{3N}, \mathbb{R}^{3N})$ such that $H^{\mathrm{total}} < \kappa_2$, and note that $\mathcal{A}$ is forward invariant due to (5.20). I now constrain the analysis to the system's evolution in $\mathcal{A}$.

Note that $\|L_{y_k}\|_F$ (where $\|\cdot\|_F$ denotes the Frobenius norm of a matrix) is upper bounded since $\zeta(\xi) \in \mathcal{Z}$ is bounded. It is straightforward to verify that all control forces, and hence all $\ddot{\xi}_i$, are also bounded on $\mathcal{A}$ (recall Assumption 5.3.2). This implies that $\ddot{H}^{\mathrm{total}}$ is bounded and that $\dot{H}^{\mathrm{total}}$ is uniformly continuous. Barbalat's lemma [Khalil, 2002, Lemma 8.2] shows that $\dot{H}^{\mathrm{total}}$ converges to zero. It follows that

$\dot{\xi} \to 0$, and hence that $d_k^{\mathrm{vmc}} \to 0$ and $\gamma_k \to e_k$. Since the control signals are smooth and bounded (the time derivative of τ is a function of bounded variables with all denominators bounded away from zero), it follows that $(\mathrm{d}^3/\mathrm{d}t^3)\xi$ is also bounded and hence that $\ddot{\xi}$ is uniformly continuous. A second application of Barbalat's lemma shows that $\ddot{\xi} \to 0$. From (5.2) and (5.3), this implies that $\tau \to 0$. Observe that $\chi_k^i = -(\partial\zeta_k/\partial\xi_i)$ and

$$L_{y_k} = \frac{\partial y_k}{\partial \zeta_k} = \frac{\partial y_k}{\partial \zeta_k}\mathbb{P}'_{y_k}.$$

From (5.12), and recalling that $d_k^{\mathrm{vmc}} \to 0$, one then has

$$\begin{aligned}
\lim_{t\to\infty} \tau_i &= \lim_{t\to\infty} \sum_{k\in\mathcal{E}_i} \chi_k^i \epsilon_k \\
&= -\lim_{t\to\infty} \left(\sum_{k\in\mathcal{E}_i} \frac{\partial\zeta_k}{\partial\xi_i}\frac{\partial y_k}{\partial\zeta_k}^{\top} \mathbb{P}'_{y_k} \left(\frac{\partial H_k^{\mathrm{vmc}}}{\partial y_k} \right) \right) - \lim_{t\to\infty} \left(\sum_{k\in\mathcal{E}_i} \frac{\partial\zeta_k}{\partial\xi_i}\frac{\partial y_k}{\partial\zeta_k}^{\top} d_k^{\mathrm{vmc}} \right) \\
&= -\lim_{t\to\infty} \frac{\partial}{\partial\xi_i} \sum_{k\in\mathcal{E}_i} H_k^{\mathrm{vmc}}.
\end{aligned}$$

Consequently, $\tau \to 0$ implies that

$$\lim_{t\to\infty} \frac{\partial}{\partial\xi} H^{\mathrm{vmc}}(\zeta(\xi)) = 0.$$

By invariance, it follows that ξ converges to the set of critical points of $H^{\mathrm{vmc}}(\zeta(\xi))$ for trajectories in $\mathcal{A}$. Therefore, $(\xi, \dot{\xi}) \to (\Xi, 0)$ for all initial conditions in $\mathcal{A}$. ■

Remark 5.3.4. The result in Theorem 5.3.3 assumes that Z is compact. It should be noted that such structure is commonly required for stability analysis in the formation control literature (see e.g. Krick et al. [2009]). Typically, it is a suitable assumption since it ensures the constraints $\mathring{y}_k$ do not permit the vehicles to be an arbitrarily large distance apart. This prevents the possibility of the vehicles minimising H_k^{vmc} by diverging to infinity. ◇

Remark 5.3.5. Note that Theorem 5.3.3 says nothing about the convergence of the system to a *point* within the set $(\Xi, 0)$. A formation defined in terms of relative measurements is not located in space, and without additional control terms it may continue to drift indefinitely. Similarly, if only direction measurements are used then the formation's scale will be uncontrolled, due to the resulting invariance in the Hamiltonian. Such behaviour is a fundamental property of the symmetry of the formation control problem rather than a consequence of the proposed design methodology. ◇

5.3.3 Discussion and Simulations

In this subsection I present simulation results illustrating typical performance of the proposed control architecture. I also discuss the possibility of implementing collision avoidance by appropriate shaping of the Hamiltonians.

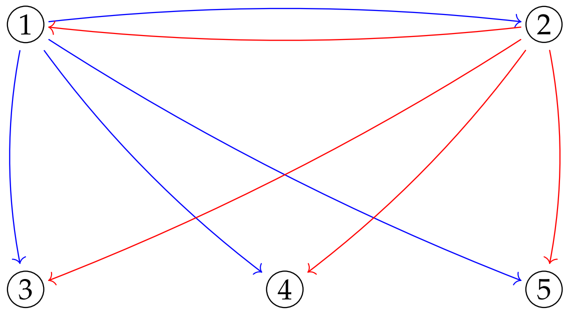

Figure 5.5: Network topology for the simulation. Blue arrows indicate direction measurements obtained by vehicle 1, while red arrows indicate distance measurements obtained by vehicle 2.

Consider the control task of achieving and maintaining a desired formation consisting of five fully-actuated dynamic vehicles in $\mathbb{R}^3$, using knowledge of their relative positions. Note that this problem formulation (namely, the exclusive use of *relative* position constraints) prevents the formation from being directed to a desired position in the inertial frame; consequently, the goal position of each vehicle is specified relative to vehicle 1 as follows: $\mathring{\xi}_1 = (0,0,0)^\top$, $\mathring{\xi}_2 = (3,0,0)$, $\mathring{\xi}_3 = (3,5,0)^\top$, $\mathring{\xi}_4 = (0,5,0)^\top$, $\mathring{\xi}_5 = (0,0,5)^\top$. Suppose the goal formation is regulated using a desired direction from vehicle 1 to each other vehicle, and a desired distance between vehicle 2 and each other vehicle. The network topology for this arrangement is illustrated by the network graph in Figure 5.5. Note that these measurements are sufficient to fully describe the desired formation up to global translations.

This scenario has been simulated forty times (using the Matlab code supplied in Appendix E), with the position of each vehicle being randomly initialised within 3 units of its place in a goal configuration (i.e. the initial error in the relative position of any two vehicles may be up to 6 units). A typical result is illustrated in Figures 5.6 and 5.7. Figure 5.6(a) shows the positions of the vehicles, beginning at the points marked with asterisks and moving towards those marked with circles (which lie in the goal formation). The total energy in the system over time is plotted in Figure 5.6(b), and converges to zero as expected. Figure 5.7(a) shows the magnitude of the error in each direction link over time (using the $\mathbb{R}^3$ embedding of the sphere $\mathbb{S}^2$), while the distance errors are plotted in Figure 5.7(b). Convergence to the specified formation is readily observed, despite a large initial error in the relative position of vehicles 1 and 2, with respect to which all other positions are regulated (in particular, the initial direction s_1 is nearly π radians from the desired value).

A drawback of the direct implementation of the proposed control architecture is that the control force ϵ_k (5.17) from the virtual mechanical coupling may still require full measurement of ζ_k in order to implement the measurement Jacobian L_{y_k}. For example, the distance Jacobian is the transpose of the unknown direction s_k, while the image Jacobian is scaled by the inverse of the unknown distance r_k. It should be noted that this issue does not arise for all sensor modalities; for example, if pressure

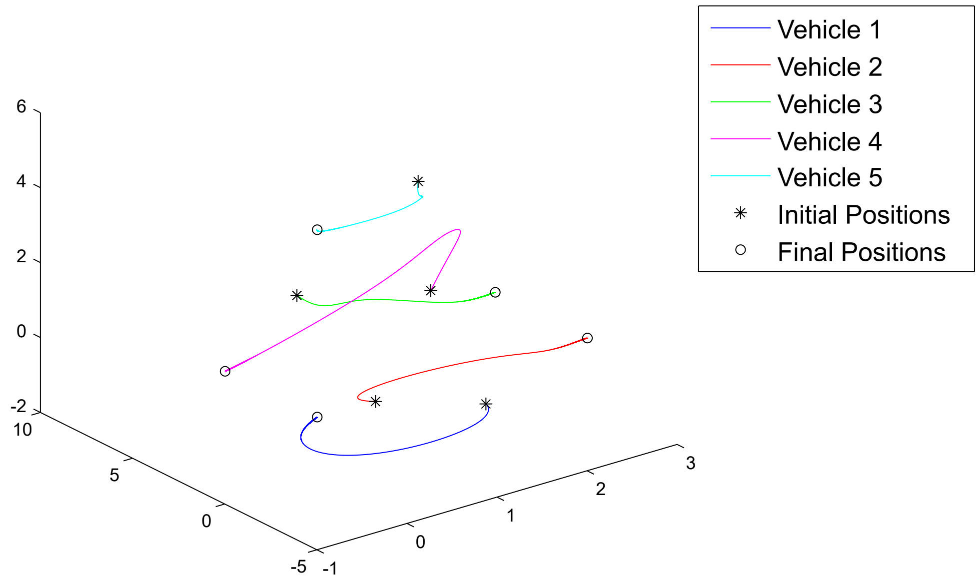

(a) The positions of each vehicle in the network, starting at the points marked with asterisks and ending at those marked with circles.

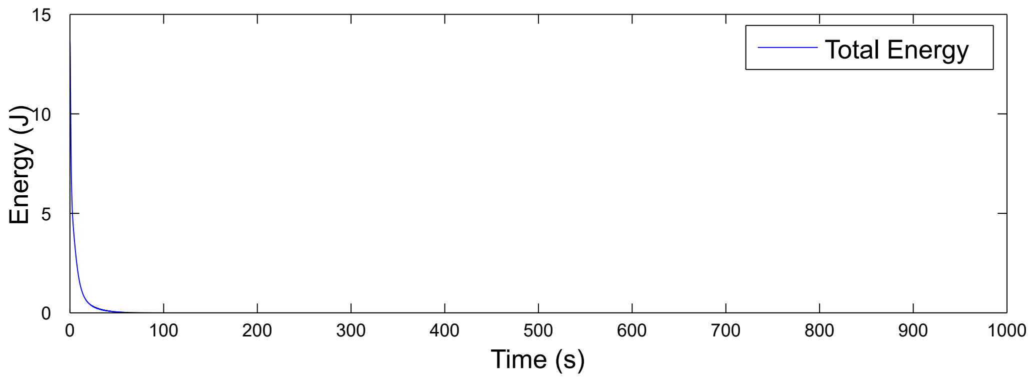

(b) Plot of the total energy in the network.

Figure 5.6: Simulation results for the proposed passivity-based formation control scheme, with full knowledge of the measurement Jacobians. The goal formation is achieved by regulating directions from vehicle 1 and distances from vehicle 2.

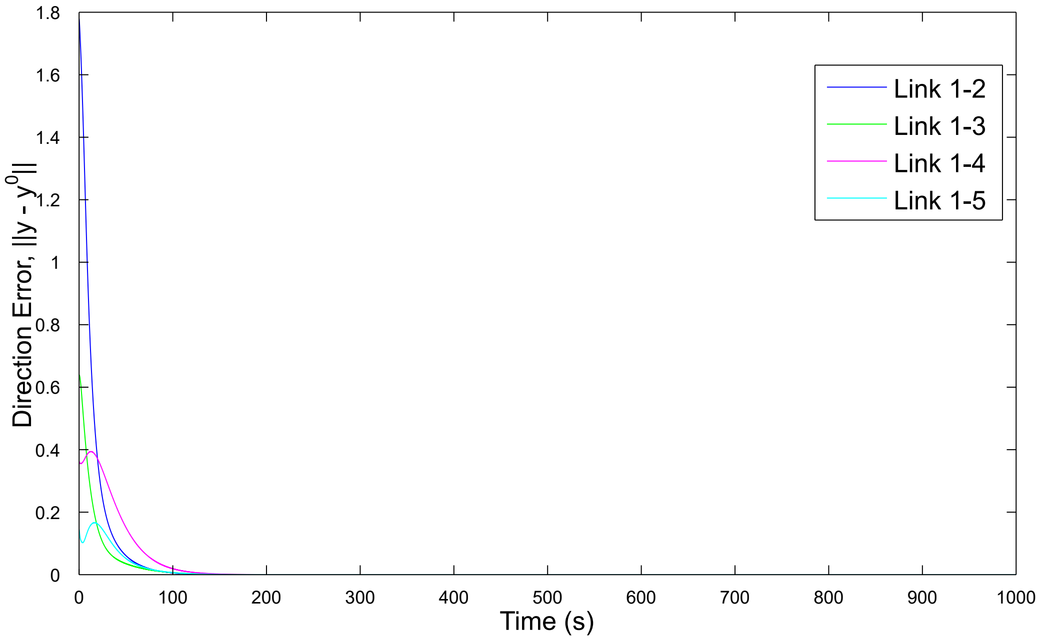

(a) Plot of the error in the regulated directions between vehicles.

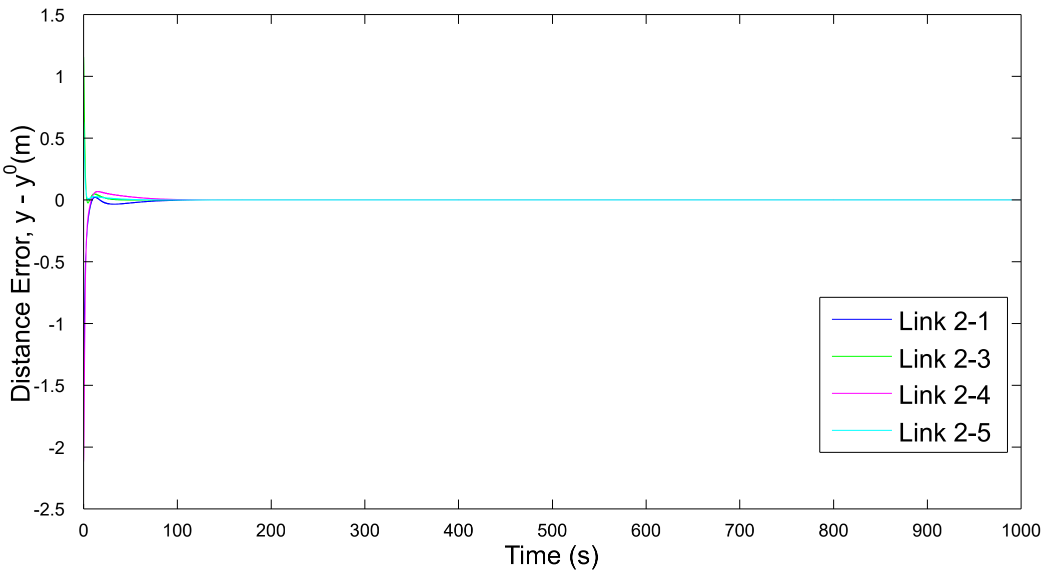

(b) Plot of the error in the regulated distances between vehicles.

Figure 5.7: Simulation results for the proposed passivity-based formation control scheme, with full knowledge of the measurement Jacobians. The goal formation is achieved by regulating directions from vehicle 1 and distances from vehicle 2. Here, the goal measurement $\mathring{y}$ is written y^0.

sensors are used to determine relative height, the measurement Jacobian will simply be $\vec{e}_3^\top = (0, 0, 1)$. In Section 5.4, I present modifications for the proposed control to adaptively compensate for the unknown information in the key cases of distance and direction measurements.

In many practical scenarios, it is desirable to adjust the behaviour of the system in order to enforce additional objectives, such as collision avoidance between vehicles. The modular energy-based approach provides two convenient methods by which this can be achieved, often without requiring substantial reassessment of the system's stability. One approach involves careful shaping of the existing energy Hamiltonians. While the Hamiltonian function in (5.13) is chosen for its simplicity and generality, one may, for example, consider the following Hamiltonian for a distance measurement:

$$H_k^{\text{vmc}}(r_k) := \frac{c_k^{\text{vmc}} \tilde{r}_k^2}{r_k}.$$

With this choice, the energy is zero when $r_k = \mathring{r}_k$, and it approaches infinity as $r_k \to 0$ (i.e. the vehicles collide) or $r_k \to \infty$ (i.e. the formation expands). The control effort in the sensor space is then given by

$$e_k^{\text{vmc}} := \frac{\partial H_k^{\text{vmc}}}{\partial r_k} = c_k^{\text{vmc}} \left(\frac{2 r_k \tilde{r}_k - \tilde{r}_k^2}{r_k^2} \right) = c_k^{\text{vmc}} \left(\frac{r_k^2 - \mathring{r}_k^2}{r_k^2} \right).$$

It should be noted that in general, such a link can only be used to enforce collision avoidance between two vehicles for which a distance measurement is available. However, if the desired formation specified by $\mathring{y}$ is rigid, then it is straightforward to see that such a link may be used to indirectly enforce collision avoidance between all vehicles, if the total energy available in the system applies a sufficiently small bound on the errors in the other links.

Another possibility for collision avoidance is to design a new energy-based control term and to inject it into the bondgraph framework (e.g. by introducing a new measurement link at the 1-junction in Figure 5.3). This approach is motivated by observing that in real world scenarios, onboard cameras are a particularly appealing lightweight sensor modality, and consequently the majority of relative position measurements are likely to be directions. While a good estimate of relative distance cannot generally be obtained from a single onboard camera, the camera may still be of assistance for the purpose of collision avoidance. In a local neighbourhood of a vehicle, a vision system can use the size of a nearby observed target to acquire a reasonable estimate of the target's distance. For example, Johnson et al. [2004] consider estimating the distance to a plane from the length of its wingspan in an image. In this case, the associated Hamiltonian can be carefully shaped such that it has negligible effect whenever the vehicles are a safe distance apart, but becomes active as a collision avoidance algorithm when the vehicles approach each other and reasonable distance estimation becomes available.

5.4 Adaptive Compensation for Direction and Distance Measurements

The implementation of the control term ϵ_k in (5.17) requires knowledge of the measurement Jacobian L_{y_k} defined in (5.7). In the important cases of direction and distance measurements, this Jacobian will not generally be known. In this section, I address this issue for these measurements separately (with direction measurements considered in Subsection 5.4.1 and distance measurements in Subsection 5.4.2), by incorporating adaptive compensation into the design from Section 5.3 to account for the unknown state information. Stability analysis of the modified control architecture is provided in Subsection 5.4.3, with simulations and discussion given in Subsection 5.4.4.

5.4.1 Control using Direction Measurements

In the case of a direction measurement s_k (5.6), the image Jacobian L_{s_k} (5.10) used in the control term ϵ_k (5.17) depends on the generally unknown distance r_k (5.5). To resolve this, I introduce an adaptive dynamic state $\hat{r}_k \in \mathbb{R}_{>0}$ and the *implementable* image Jacobian

$$\hat{L}_{s_k} := \frac{1}{\hat{r}_k}(I_3 - s_k s_k^\top). \tag{5.21}$$

I now propose the control term

$$\epsilon_k := \hat{L}_{s_k}\gamma_k, \tag{5.22}$$

instead of the one given in (5.17). An important point to note here is that with this control term, the power supplied by the virtual mechanical coupling will not match that associated with the control input to the vehicles, i.e. the result (5.18) no longer holds (assuming $\hat{r}_k \neq r_k$). This is due to the fact that the true flow $\dot{s}_k$ of the direction measurement depends on the true distance r_k, whereas the control term depends on the adaptive variable. Indeed, the structure required by the bondgraph notation for the MTF element in Figure 5.4 is not satisfied (see Appendix D).

To address this issue, I design dynamics for the adaptive variable $\hat{r}_k$ such that the energy discrepancy introduced by the error

$$\check{r}_k := \hat{r}_k - r_k$$

is precisely accounted for. Define

$$\alpha_k := \frac{r_k}{\hat{r}_k}\gamma_k,$$

and note that $\epsilon_k = \hat{L}_{s_k}^\top\gamma_k = L_{s_k}^\top\alpha_k$. Consequently, $\langle \alpha_k \mid \dot{s}_k\rangle = \langle \epsilon_k \mid \dot{\zeta}_k\rangle$, i.e. α_k is the control effort in the sensor space that matches the power drawn by the implemented control term ϵ_k defined in (5.22). Therefore, the discrepancy between the power drawn for the implemented control and the power supplied by the virtual mechanical coupling is given by $\langle -\beta_k \mid \dot{s}_k \rangle$, where

$$\beta_k := \alpha_k - \gamma_k = -\frac{\check{r}_k}{\hat{r}_k}\gamma_k.$$

To account for the power associated with β_k, I define the Hamiltonian

$$H_k^{\mathrm{ac}} := \frac{1}{2} c_k^{\mathrm{ac}} \check{r}_k^2.$$

The power exchanged with this Hamiltonian consists of an effort

$$e_k^{\mathrm{ac}} := \frac{\partial H_k^{\mathrm{ac}}}{\partial \check{r}_k} = c_k^{\mathrm{ac}} \check{r}_k,$$

and a flow $\dot{\check{r}}_k$ (Duindam et al. [2009]). Let

$$A_k := -\frac{\gamma_k^\top}{c_k^{\mathrm{ac}} \hat{r}_k} \in \mathbb{R}^{1\times 3}$$

denote the transform such that $\beta_k = A_k^\top e_k^{\mathrm{ac}}$, and let the dynamics of $\hat{r}_k$ be specified by

$$\dot{\hat{r}}_k = \dot{r}_k + A_k \dot{s}_k. \tag{5.23}$$

With this choice, $\dot{\check{r}}_k = A_k \dot{s}_k$ and therefore

$$\begin{aligned}\langle \beta_k \mid \dot{s}_k \rangle &= \langle A_k^\top e_k^{\mathrm{ac}} \mid \dot{s}_k \rangle = \langle e_k^{\mathrm{ac}} \mid A_k \dot{s}_k \rangle \\ &= \langle e_k^{\mathrm{ac}} \mid \dot{\check{r}}_k \rangle,\end{aligned}$$

which verifies that the power supplied by H_k^{ac} will match that drawn or dissipated due to the discrepancy β_k.

It is worth briefly considering the implementation of the modified control architecture. The value of $\dot{s}_k$ used in (5.23) is assumed to be available by numerical differentiation of the sensor measurement s_k. Observe that $\dot{r}_k = s_k^\top \dot{\zeta}_k$, and hence that the dynamics (5.23) can be computed if each vehicle is also able to estimate and communicate its velocity. In practice, this might be estimated by integration of the linear acceleration obtained from an onboard IMU, or by an optic flow algorithm with an onboard camera. I emphasise that the energy stored in H_k^{ac} does not need to be estimated in order to implement the proposed control. The construction of the control architecture is such that this Hamiltonian will possess (and supply) only a finite quantity of energy, even though the amount available is not known. Consequently, passivity of the overall system is preserved regardless of the error $\check{r}_k$. Such a property is not true in general for a classical observer-control design for nonlinear systems.

In Figure 5.8, I present a bondgraph model of the control link between two vehicles i and j, using the modified control architecture for a direction measurement.

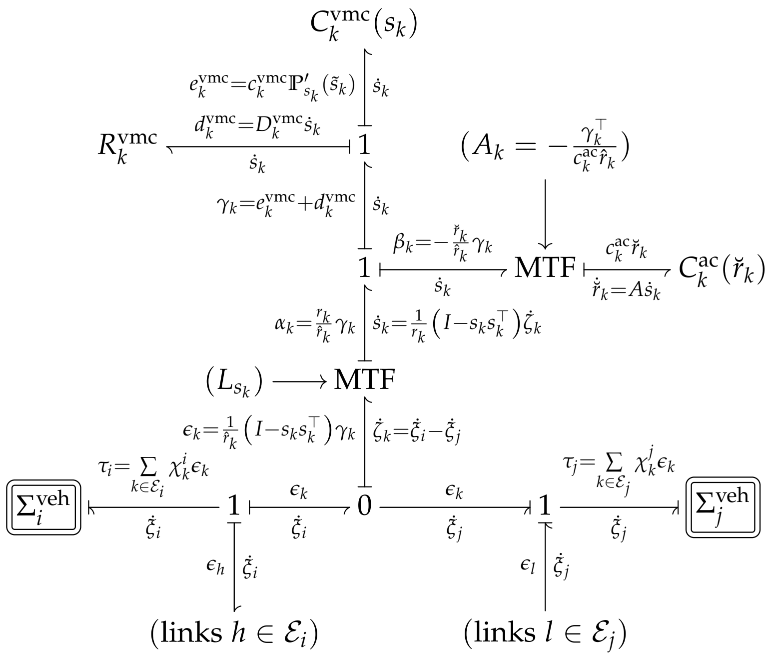

Figure 5.8: Bondgraph model of a control link k between two vehicles, given a direction measurement s_k and using adaptive compensation to handle the unknown distance r_k.

The key modification from the prior design in Subsection 5.3.1 (c.f. Figure 5.4) is the addition of the central 1-junction, which introduces a branch to the adaptive compensation on the right. The virtual effort γ_k from the virtual mechanical coupling is modified by the correction β_k that accounts for the energy discrepancy associated with $\check{r}_k$. This results in the virtual effort α_k that is transformed by the lower MTF to produce the implemented control term ϵ_k described by (5.22). The power associated with β_k is drawn from the energy H_k^{ac} reserved in the storage element C_k^{ac}, via the upper-right MTF which implements the transform A_k. Note that as $\gamma_k \to 0$, the transform of this MTF will close off the power flow from C_k^{ac}; this provides the insight that $\check{r}_k$ may not converge to zero if the vehicles converge to the desired formation first.

5.4.2 Control using Distance Measurements

For a distance measurement r_k (5.5) between two vehicles, knowledge of the direction s_k (5.6) is required in order to compute the distance Jacobian L_{r_k} (5.9) for the control term ϵ_k (5.17). I will address this with a similar approach to that used for direction measurements in Subsection 5.4.1; however, the different measurement structure means that the result is not entirely analogous. Most notably, rather than introducing a substitute variable for the unknown direction s_k, I will use an adaptive variable $\hat{\zeta}_k \in \mathbb{R}^3$ that is substituted for the full relative position ζ_k.

Denote $\breve{\zeta}_k := \hat{\zeta}_k - \zeta_k$ as the error in the substitute variable, and define

$$\hat{L}_{r_k} := \frac{\hat{\zeta}_k^\top}{r_k}. \tag{5.24}$$

Analogously to the case of a direction measurement, I propose the realisable control term

$$\epsilon_k := \hat{L}_{r_k}^\top \gamma_k \tag{5.25}$$

in the place of (5.17). Using

$$\alpha_k := L_{r_k}^\top \gamma_k = \frac{\zeta_k}{r_k}\gamma_k$$

to denote the ideal control force, the error in the implemented effort is given by

$$\beta_k := \epsilon_k - \alpha_k = \frac{\breve{\zeta}_k}{r_k}\gamma_k.$$

To adaptively compensate for the energy discrepancy associated with this error, I use the Hamiltonian

$$H_k^{\mathrm{ac}} := \frac{1}{2}\breve{\zeta}_k^\top c_k^{\mathrm{ac}} \breve{\zeta}_k,$$

where $c_k^{\mathrm{ac}} > 0$ is a scalar constant. This Hamiltonian is associated with an effort

$$e_k^{\mathrm{ac}} := \frac{\partial H_k^{\mathrm{ac}}}{\partial \breve{\zeta}_k} = c_k^{\mathrm{ac}} \breve{\zeta}_k$$

and a flow equal to $\dot{\breve{\zeta}}_k$. Define

$$A_k := \frac{\gamma_k}{c_k^{\mathrm{ac}} r_k} \in \mathbb{R} \tag{5.26}$$

as the transform such that $\beta_k = A_k e_k^{\mathrm{ac}}$, and let the dynamics of the adaptive variable $\hat{\zeta}_k$ be given by

$$\dot{\hat{\zeta}}_k = \dot{\zeta}_k + A_k \dot{\zeta}_k. \tag{5.27}$$

With this choice, it is straightforward to verify that the power associated with the error β_k is precisely accounted for by the Hamiltonian H_k^{ac}:

$$\begin{aligned} \langle \beta_k \mid \dot{\zeta}_k \rangle = \langle A_k e_k^{\mathrm{ac}} \mid \dot{\zeta}_k \rangle &= \langle e_k^{\mathrm{ac}} \mid A_k \dot{\zeta}_k \rangle \\ &= \langle e_k^{\mathrm{ac}} \mid \dot{\breve{\zeta}}_k \rangle. \end{aligned}$$

Note that the dynamics (5.27) are implementable if, as for the adaptive control of direction measurements in Subsection 5.4.1, neighbouring vehicles can communicate estimates of their own velocity.

The behaviour of the adaptive variable $\hat{\zeta}_k$ plays a key role in the performance of the adaptive control scheme for distance measurements. In practice, a simple modification to the dynamics (5.27) can be employed to significantly improve the system's behaviour. The key idea is that by numerically differentiating the distance measurement r_k, one can extract further information about the direction s_k through the relationship $\dot{r}_k = s_k^\top \dot{\zeta}_k$. The modification takes the form of an additional term in the dynamics (5.27), applying a periodic correction that is guaranteed to reduce the error $\breve{\zeta}_k$. Instead of (5.27), I propose the dynamics

$$\begin{aligned}\dot{\hat{\zeta}}_k &= \dot{\zeta}_k + A_k\dot{\zeta}_k - \delta_k^0 \frac{\dot{\zeta}_k^\top \breve{\zeta}_k \dot{\zeta}_k}{2\|\dot{\zeta}_k\|^2} \\ &= \dot{\zeta}_k + A_k\dot{\zeta}_k - \delta_k^0 \frac{(\dot{\zeta}_k^\top \hat{\zeta}_k - \dot{r}_k r_k)\dot{\zeta}_k}{2\|\dot{\zeta}_k\|^2}.\end{aligned} \tag{5.28}$$

Here, δ_k^0 denotes a Dirac delta function with a deadzone around $\|\dot{\zeta}_k\| = 0$, to prevent the correction from being applied when it is undefined. That is,

$$\delta_k^0(\dot{\zeta}_k) := \begin{cases} 0 & \text{if } \|\dot{\zeta}_k\| < c_k^\delta \\ \delta(t, c_k^t) & \text{otherwise,} \end{cases}$$

where $c_k^\delta > 0$ is a small positive constant, and $\delta(t, c_k^t)$ denotes a periodic Dirac delta function consisting of a Dirac delta impulse every $c_k^t > 0$ seconds, i.e.

$$\delta(t, c_k^t) := \begin{cases} 1 & t = a_\delta c_k^t \text{ for some positive integer } a_\delta \\ 0 & \text{otherwise.} \end{cases}$$

To analyse the switching system resulting from the modified dynamics (5.28), I consider the energy change in the system due to the new term, over a cycle of c_k^t seconds. This is given by the integral of the associated power, i.e.

$$\int_{t_0}^{t_0+c_k^t} \left\langle c_k^{\mathrm{ac}} \breve{\zeta}_k \,\middle|\, -\delta_k^0 \frac{\dot{\zeta}_k^\top \breve{\zeta}_k \dot{\zeta}_k}{2\|\dot{\zeta}_k\|^2} \right\rangle \mathrm{d}t = -\frac{c_k^{\mathrm{ac}}}{2\|\dot{\zeta}_k\|^2} \left(\dot{\zeta}_k^\top \breve{\zeta}_k\right)^2 \Big|_{t=t_\delta} \tag{5.29}$$

if $\|\dot{\zeta}_k\| \geq c_k^\delta$, and zero otherwise. Note that the power integral degenerates into an algebraic expression evaluated at the instant t_δ where the periodic Dirac delta is active. Since (5.29) is non-positive, the resulting switched system remains passive and its stability can be analysed in the standard manner. Simulation results have verified that the modified dynamics (5.28) significantly improve the behaviour of the system.

In Figure 5.9 I present the bondgraph diagram for an adaptive control link using a distance measurement. The right-hand branch from the central 1-junction represents the adaptive compensation that is introduced to the basic control architecture from Figure 5.4. Due to the dimension of the unknown variable s_k, this adaptive compensation is incorporated in the space of relative positions, rather than the sensor space as was done for direction measurements (c.f. Figure 5.8). The energy H_k^{ac} used to drive the adaptive compensation is stored in C_k^{ac}. The upper-right 0-junction dissipates part of the power exchanged with this Hamiltonian via the resistive element

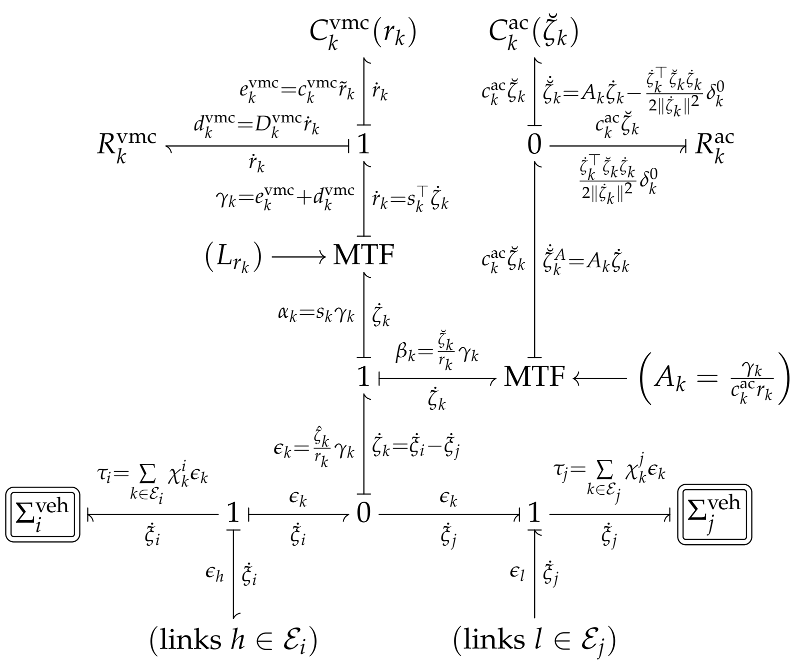

Figure 5.9: Bondgraph model of a control link k between two vehicles, using a distance measurement r_k and an adaptive variable $\hat{\zeta}_k \in \mathbb{R}^3$.

$\mathbb{R}_k^{\mathrm{ac}}$; this is the power given in (5.29) that is associated with the modification to the dynamics of $\dot{\breve{\zeta}}_k$ (5.28). The remainder of the power exchanged with H_k^{ac} is passed from the 0-junction through the right-hand MTF, which applies the transform A_k (5.26), to account for the energy discrepancy associated with the error β_k in the implemented control.

5.4.3 Stability Analysis

The passivity of the adaptive control schemes presented in Subsections 5.4.1 and 5.4.2 enables stability analysis to be performed for a network of vehicles that is composed of both sensor modalities (note that one can also include measurements for which the basic virtual mechanical coupling from Section 5.3 can be directly implemented). Before proceeding to the stability analysis, I summarise the scenario considered and introduce some helpful notation.

Scenario 5.4.1. Consider a connected network of N vehicles with M links between them. The i'th vehicle has a state $(\xi_i, \dot{\xi}_i)$ and dynamics described by (5.2) and (5.3). The set of all links is denoted $\mathcal{E}$, and the set of links attached to vehicle i is denoted $\mathcal{E}_i$. Suppose that each link $k \in \mathcal{E}$ is associated with a partial measurement $y_k(\zeta_k)$ of the relative position (5.4), and that these measurements are well-defined and smooth for $\zeta_k \in \mathbb{R}^3 \setminus \{0\}$. Furthermore, suppose that the first $M_s \geq 0$ links are associated with a direction measurement s_k (5.6) (see Subsection 5.4.1), the next $M_r \geq 0$ links with a distance measurement r_k (5.5) (see Subsection 5.4.2), and the remaining M_z

links with a measurement $z_k(\zeta_k)$ for which the measurement Jacobian (5.7) is known[2] (Section 5.3). Let $\mathcal{E}_s$ denote the set of links associated with direction measurements, with $\mathcal{E}_r$ and $\mathcal{E}_z$ denoted similarly. Let $\mathring{y}_k$ denote a target stationary value for the partial relative position measurement y_k, with the error denoted by $\tilde{y}_k$ as in (5.11). Suppose that each direction measurement is associated with an adaptive variable $\hat{r}_k \in \mathbb{R}_{>0}$, and that each distance measurement is associated with an adaptive variable $\hat{\zeta}_k \in \mathbb{R}^3$. The dynamics of $\hat{r}_k$ are described by (5.23), while those of $\hat{\zeta}_k$ are given by (5.27). The control input τ_i for each vehicle is described by (5.12), with ϵ_k defined by (5.22) for a link $k \in \mathcal{E}_s$, (5.25) for $k \in \mathcal{E}_r$, and (5.17) otherwise. The effort γ_k is given by (5.16). Denote $\xi := (\xi_1^\top, \ldots, \xi_N^\top)^\top$ and $\tau := (\tau_1^\top, \ldots, \tau_N^\top)^\top$. Let $\zeta := (\zeta_1^\top, \ldots, \zeta_M^\top)^\top$ and define y, $\mathring{y}$, $\tilde{y}$ and γ analogously. Similarly define r_s and $\hat{r}$ for $k \in \mathcal{E}_s$ with $\check{r} := \hat{r} - r_s$, as well as ζ_r and $\hat{\zeta}$ for $k \in \mathcal{E}_r$ with $\check{\zeta} := \hat{\zeta} - \zeta_r$. Denote $Z := \{\zeta \mid \tilde{y}(\zeta) = 0\}$ as the set of desired relative positions, with $\Xi := \{\xi \mid \zeta(\xi) \in Z\} \subset \mathbb{R}^{3\times N}$. $\diamond$

From the bondgraph diagrams, one can see that the total energy in the system is given by the Hamiltonian

$$H^{\text{total}}(\xi, \dot{\xi}, \hat{r}, \hat{\zeta}) := T(\dot{\xi}) + H^{\text{vmc}}(\zeta(\xi)) + H^{\text{ac}}(\zeta(\xi), \hat{r}, \hat{\zeta}), \tag{5.30}$$

where:

$$\begin{aligned} T(\dot{\xi}) &:= \sum_{i=1}^{N} T_i(\dot{\xi}_i), \\ H^{\text{vmc}}(\zeta) &= \sum_{k=1}^{M} H_k^{\text{vmc}}(y_k(\zeta_k)), \\ H^{\text{ac}}(\zeta, \hat{r}, \hat{\zeta}) &= \sum_{k\in\mathcal{E}_s} H_k^{\text{ac}}(\hat{r}_k - \|\zeta_k\|) + \sum_{k\in\mathcal{E}_r} H_k^{\text{ac}}(\hat{\zeta}_k - \zeta_k). \end{aligned}$$

Similarly, by summing the power dissipated from the system as shown in the bondgraphs, one finds that the time-derivative of the total energy is

$$\frac{\mathrm{d}}{\mathrm{d}t} H^{\text{total}} := -\sum_{i=1}^{N} \dot{\xi}_i^\top D_i \dot{\xi}_i - \sum_{k=1}^{M} \dot{y}_k^\top D_k^{\text{vmc}} \dot{y}_k - \sum_{k\in\mathcal{E}_r} \delta_k^0 \frac{c_k^{\text{ac}}(\check{\zeta}_k^\top \dot{\zeta}_k)^2}{2\|\dot{\zeta}_k\|^2}. \tag{5.31}$$

The stability analysis will be performed with aid of a construction I term the *network MTF*. This terminology is chosen to reflect the fact that the network MTF describes the transform between the variables in the sensor space associated with the virtual mechanical couplings, and those in $\mathbb{R}^3$ that are associated with the relative positions of pairs of vehicles. In this regard, the network MTF is analogous to the generalised rigidity matrix described in Section 4.2.

[2] An example of such a measurement is the relative height obtained from pressure sensors, for which $L_{z_k} = (0, 0, 1)$.

Definition 5.4.2. (**Network MTF**) Denote,

$$J_i(\xi) := \begin{bmatrix} -\tilde{\chi}^i_1 L_{y_1}^\top & \vdots & \cdots & \vdots & -\tilde{\chi}^i_M L_{y_M}^\top \end{bmatrix}^\top,$$

where $\tilde{\chi}^i_k$ is equal to χ^i_k (as defined for (5.12)) if $k \in \mathcal{E}_i$, and is 0 otherwise. The *network MTF* for the formation is defined as

$$J(\xi) := \begin{bmatrix} J_1(\xi) & \vdots & \cdots & \vdots & J_N(\xi) \end{bmatrix}.$$

Similarly, using (5.21), (5.24) and $\hat{L}_{z_k} := L_{z_k}$, denote

$$\hat{J}_i := \begin{bmatrix} -\tilde{\chi}^i_1 \hat{L}_{y_1}^\top & \vdots & \cdots & \vdots & -\tilde{\chi}^i_M \hat{L}_{y_M}^\top \end{bmatrix}^\top,$$

and define the *implemented network MTF* as

$$\hat{J} := \begin{bmatrix} \hat{J}_1 & \vdots & \cdots & \vdots & \hat{J}_N \end{bmatrix}. \qquad \diamond$$

With the construction of the network MTF one has the easily verified relationship $\dot{y} := J\dot{\xi}$. In the case where the Jacobians are known (as in Section 5.3), the dual relationship $\tau = -J^\top \gamma$ also holds (here, the sign change is simply due to the choice of directions for positive power flow through the associated bonds, as seen in Figure 5.4). That is, J represents the power transform between the space of the physical formation and the combined sensor space:

$$\begin{aligned} \langle \tau \mid \dot{\xi} \rangle &= \langle -J^\top \gamma \mid \dot{\xi} \rangle = \langle -\gamma \mid J\dot{\xi} \rangle \\ &= \langle -\gamma \mid \dot{y} \rangle. \end{aligned} \tag{5.32}$$

For the adaptive control architectures presented in this section, the control forces are determined by the implemented network MTF rather than the true state, giving the relationship $\tau = -\hat{J}^\top \gamma$. In this case, the relationship (5.32) fails to hold, i.e. $\langle \tau \mid \dot{\xi} \rangle \neq \langle -\gamma \mid \dot{y} \rangle$. This observation reflects the energy mismatch, across the full network, that is accounted for by the adaptive Hamiltonians H^{ac}_k. Stability of the system is guaranteed by the passivity property enforced by the design paradigm. Local convergence analysis relies on showing that, at least in a neighbourhood of the desired formation, the presence of the adaptive Hamiltonians H^{ac}_k does not destroy the energy shaping provided by the measurement Hamiltonians H^{vmc}_k. To show local asymptotic stability, I require the following rank assumption on J.

Assumption 5.4.3. Let

$$R := \sum_{k=1}^{M} \operatorname{rank}(L_{y_k}),$$

assume that $R \leq 3N$, and also assume

$$\inf_{\xi \in \Xi} \sigma_R(J(\xi)) > \rho_1 > 0,$$

where $\sigma_R(J(\xi))$ denotes the R'th largest singular value of J. $\diamond$

Theorem 5.4.4. *Consider Scenario 5.4.1, where the full state of the system is described by* $(\xi, \hat{r}, \hat{\zeta}, \dot{\xi}, t)$*, and the total energy* H^{total} *is given by* (5.30)*. Assume that* Z *is nonempty and compact. Define* J *and* $\hat{J}$ *as in Definition 5.4.2. Suppose that Assumptions 5.3.2 and 5.4.3 hold.*

Then, there exists an open set $\mathcal{A} \subset (\mathbb{R}^{3N}, \mathbb{R}^{M_s}, \mathbb{R}^{3M_r}, \mathbb{R}^{3N}, \mathbb{R})$ *about* $(\Xi, r_s, \zeta_r, 0, \mathbb{R})$ *such that* $(\xi, \dot{\xi}) \to (\Xi, 0)$*, for all initial conditions* $(\xi(0), \hat{r}(0), \hat{\zeta}(0), \dot{\xi}(0), 0) \in \mathcal{A}$*.*

Proof Note that the time-derivative (5.31) of the total Hamiltonian H^{total} (5.30) is negative semi-definite, despite the switching associated with δ_k^0, and that all physical variables (i.e. $\xi, \dot{\xi}$) remain continuous. It follows that $\|\dot{\xi}\|$ is bounded and hence that trajectories exist for all time. Let $H^{\text{link}} := H^{\text{vmc}} + H^{\text{ac}}$, and note that H^{link} is well-defined and smooth (with respect to $(\zeta, \hat{r}, \hat{\zeta})$) everywhere except when some $r_k = 0$ on the exceptional set $\mathcal{W}$.

Clearly, ϵ_k ((5.17), (5.22) and (5.25)) is undefined if $r_k = 0$ or $\hat{r}_k = 0$. From Assumption 5.3.2, $H^{\text{vmc}}(\zeta(\xi)) < \kappa_1$ implies that $r_k > r_{\min}$ for all $k \in \mathcal{E}$, where $r_{\min} > 0$ is some common lower bound. Define

$$\kappa_2 := \min_{k \in \mathcal{E}_s} \inf_{r_k \geq r_{\min}} H_k^{\text{ac}}(\hat{r}_k - r_k)|_{\hat{r}_k = 0} > 0.$$

Choose a positive constant $\kappa_3 < \min(\kappa_1, \kappa_2)$. On the set where $H^{\text{link}} \leq \kappa_3$, there is a positive lower bound on both r_k and $\hat{r}_k$, for all k. This implies that H^{link} is well-defined and smooth on this set, and that the control terms also remain well-defined. Therefore, there exists a positive constant $\kappa_4 \leq \kappa_3$ such that the only critical points of $H^{\text{link}}(\zeta(\xi), \hat{r}, \hat{\zeta})$ in

$$\mathcal{A}_0 := \{(\xi, \hat{r}, \hat{\zeta}) \in (\mathbb{R}^{3N}, \mathbb{R}^{M_s}, \mathbb{R}^{3M_r}) \mid H^{\text{link}}(\zeta(\xi), \hat{r}, \hat{\zeta}) < \kappa_4\}$$

are those in $(\Xi, \mathbb{R}^{M_s}, \mathbb{R}^{3M_r})$.

Let $\check{J} := \hat{J} - J$, and note that $\hat{J} = J + \check{J}$. Since all $\|\check{r}_k\|$ (for $k \in \mathcal{E}_s$) and $\|\check{\zeta}_k\|$ (for $k \in \mathcal{E}_r$) are continuous near $\hat{r} = r$ and $\hat{\zeta} = \zeta$ respectively, and are upper bounded by the energy in the system, for any positive value ρ_2 there exists a positive bound $\kappa_5 \leq \kappa_4$ such that $H^{\text{ac}} < \kappa_5$ ensures $\|\check{J}\|_F < \rho_2$. Note that on $\mathcal{A}_0$, J is smooth with respect to ξ and $\|\partial J / \partial \xi\|_F$ is upper bounded due to the positive lower bound on all r_k. Since $\sigma_R(J) > \rho_1$ (by Assumption 5.4.3), it follows that for any $\rho_3 > 0$ there exists $b_2 > 0$ such that

$$\inf_{\xi' \in \Xi} \|\xi - \xi'\| < b_2$$

implies $\sigma_R(J) > \rho_1 - \rho_3$. Furthermore, since Ξ is equivalent to the set of critical points of $H^{\text{vmc}}(\zeta(\xi))$ in $\mathcal{A}_0$ (on which H^{vmc} is smooth), for any such b_2 there exists positive

$\kappa_6 \leq \kappa_5$ such that $H^{\text{vmc}} < \kappa_6$ implies

$$\inf_{\xi' \in \Xi} \|\xi - \xi'\| < b_2.$$

It follows that one can choose ρ_2, ρ_3, κ_6 such that $H^{\text{link}} < \kappa_6$ implies $\sigma_R(\hat{J}) > 0$, i.e. $\hat{J}$ is a sufficiently small perturbation of J. More precisely, since the non-zero singular values of J are the positive square-roots of the eigenvalues of the normal matrix $J^\top J$, one can apply [Horn and Johnson, 1990, Corollary 6.3.4].

Define $\mathcal{A} \subset (\mathbb{R}^{3N}, \mathbb{R}^{M_s}, \mathbb{R}^{3M_r}, \mathbb{R}^{3N}, \mathbb{R})$ as the set of points $(\xi, \hat{r}, \hat{\zeta}, \dot{\xi}, t)$ such that $H^{\text{total}} < \kappa_6$. Note that the extension of the state to include velocity $\dot{\xi}$ and time t does not compromise the analysis performed on $\mathcal{A}_0$. Firstly, the energy functions T and H^{link} rely on independent state variables. Furthermore, when $\delta_k^0 \neq 0$, more energy will be dissipated (as seen from (5.31)) than in the case $\delta_k^0 = 0$; hence, the state resulting from switching cannot be further from the critical points of H^{link}.[3]

Let

$$g(\dot{\xi}) := \sum_{i=1}^{N} \dot{\xi}_i^\top D_i \dot{\xi}_i.$$

Considering the trajectories of a system initialised in $\mathcal{A}$, observe that $g(\dot{\xi})$ is uniformly continuous since τ (and hence $\ddot{\xi}$) is bounded. Since the quantity of energy

$$\int_0^t g(\dot{\xi}(x))\mathrm{d}x$$

is non-decreasing as $t \to \infty$ and is upper bounded by H^{total}, it converges to a finite limit. From Barbalat's lemma [Khalil, 2002, Lemma 8.2], one has that $g(\dot{\xi}) \to 0$ and thus $\dot{\xi} \to 0$. It follows that the system converges in finite time to a set $\mathcal{A}_1 \subseteq \mathcal{A}$ on which $\|\dot{\zeta}_k\| < c_k^\delta$ for all $k \in \mathcal{E}$, and hence that the switching ceases. Noting that the third time-derivative of ξ is bounded on $\mathcal{A}_1$ and applying Barbalat's lemma again, one has $\ddot{\xi} \to 0$. It then follows from (5.2) and (5.3) that $\tau \to 0$. Observe that $\sigma_R(\hat{J}) = \sigma_R(J + \breve{J}) > 0$ will hold for all points in $\mathcal{A}_1$. This implies (since $R \leq 3N$ by assumption) that $\hat{J}^\top$ will effectively be a full rank map from the tangent space

$$T_y\mathcal{Y} := \prod_{k=1}^{M} T_{y_k}\mathcal{Y}_k,$$

which has dimension R. Recalling that $\tau = -\hat{J}^\top \gamma$, and noting the smoothness of γ and τ on $\mathcal{A}_1$, it follows that $\gamma \to 0$. Hence, $y \to \hat{y}$ for all initial conditions in $\mathcal{A}$. ∎

[3] The advantage of the adjustment in (5.28) is that it enables the system trajectory to bypass undesired equilibria by extracting energy from the adaptive Hamiltonian and allowing the shaping of the measurement Hamiltonian to dominate.

5.4.4 Discussion and Simulations

In this subsection, I provide further discussion concerning the practical implementation of the proposed control architecture, and I present simulation results to support the developed theory for the adaptive control scheme. The simulated scenario is identical to the one in Subsection 5.3.3, only without the true relative states being known. The behaviour observed in the simulations is quite similar, illustrating that the adaptive control scheme typically has little impact on performance.

Recall the formation control task simulated in Subsection 5.3.3, where vehicle 1 measures the direction to each other vehicle, and vehicle 2 measures the distance to each other vehicle. Figures 5.10 and 5.11 show a typical result using the proposed adaptive control scheme. The initial positions of the vehicles are the same as for the simulation in Subsection 5.3.3, while the adaptive control variables $\hat{r}_k$ and $\hat{\zeta}_k$ are initialised to random values within $0.3 \times \|\zeta_k\|$ of the true values. For this simulation, the reset modification $\hat{\zeta}_k$ (5.28) is applied at every control step.

The trajectory of each vehicle is plotted in Figure 5.10(a). Figure 5.10(b) compares the total energy of the system with the total energy reserved for adaptive compensation. One can observe from this graph that the adaptive variables do not necessarily approach the true values, but all other energy in the system converges zero. Consequently, convergence to the desired formation is still achieved. The errors in the relative states with respect to the desired formation are shown in Figures 5.11(a) (for direction measurements) and 5.11(b) (for distance measurements).

This simulation has been run forty times using the same random initialisation as for the prior case in Subsection 5.3.3 (see Appendix E for the Matlab code). Similar behaviour was observed in all cases except one, where the formation converged to an undesired equilibrium (see the plot of trajectories in Figure 5.12(a) and the plot of energy in Figure 5.12(b)). This outcome is possible (outside of a local region of attraction) due to errors in the adaptive compensation variables, which may occasionally conspire to neutralise the gradient of the Hamiltonian associated with the virtual coupling. In this case, the relative velocities are able to converge to zero and prevent further evolution of the adaptive variable. A similar issue is encountered with classical observers that estimate full relative positions based on partial position information; typically, they require a *persistency of excitation* property (see e.g. Bras et al. [2015]) in order to guarantee convergence to the true value. A practical method of resolving this issue is to incorporate a small amount of noise in the control term; note that such a disturbance is often naturally introduced into the system by the environment.

It is of interest to give some consideration to the practical implementation of the proposed control scheme. Suppose that each vehicle is equipped with an inertial measurement unit (IMU) that provides knowledge of its orientation in an inertial frame. The partial relative position measurements can be obtained by a camera on vehicle 1 and a time-of-flight sensor on vehicle 2 (with the IMU data being used to de-rotate bearings measured by the onboard camera). The vehicle velocities are more difficult to measure, but estimates can be acquired by dead-reckoning with the IMU

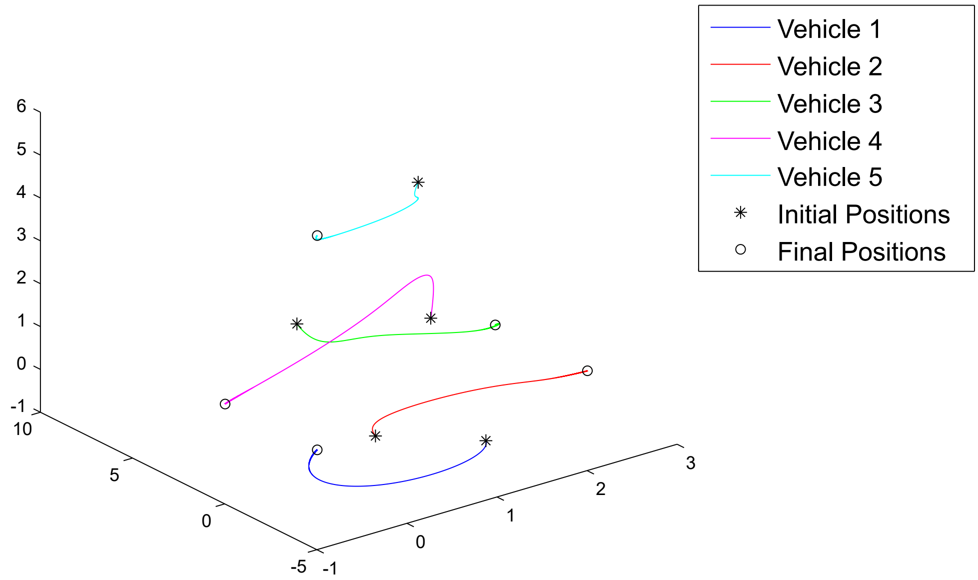

(a) The positions of each vehicle in the network, starting at the points marked with asterisks and ending at those marked with circles.

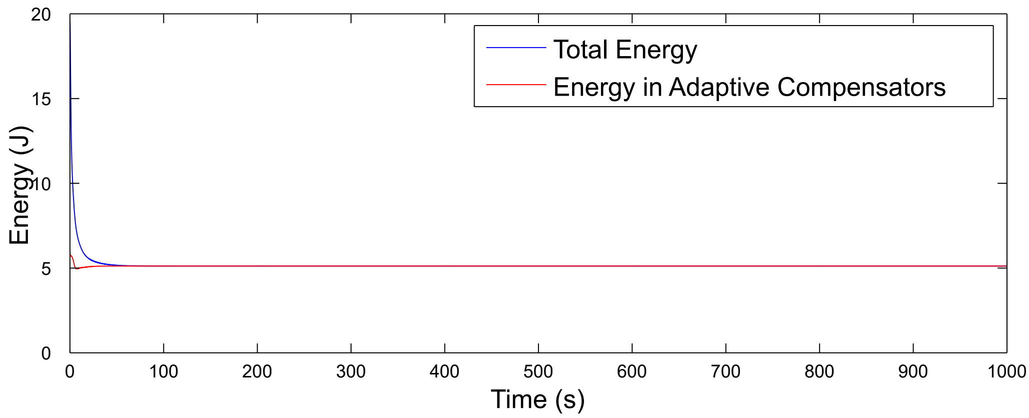

(b) Plot of the total energy in the network, and the total energy associated with the adaptive compensation scheme.

Figure 5.10: Simulation results for the proposed passivity-based formation control scheme, using adaptive compensation to account for the unknown information in the measurement Jacobians. The goal formation is achieved by regulating directions from vehicle 1 and distances from vehicle 2.

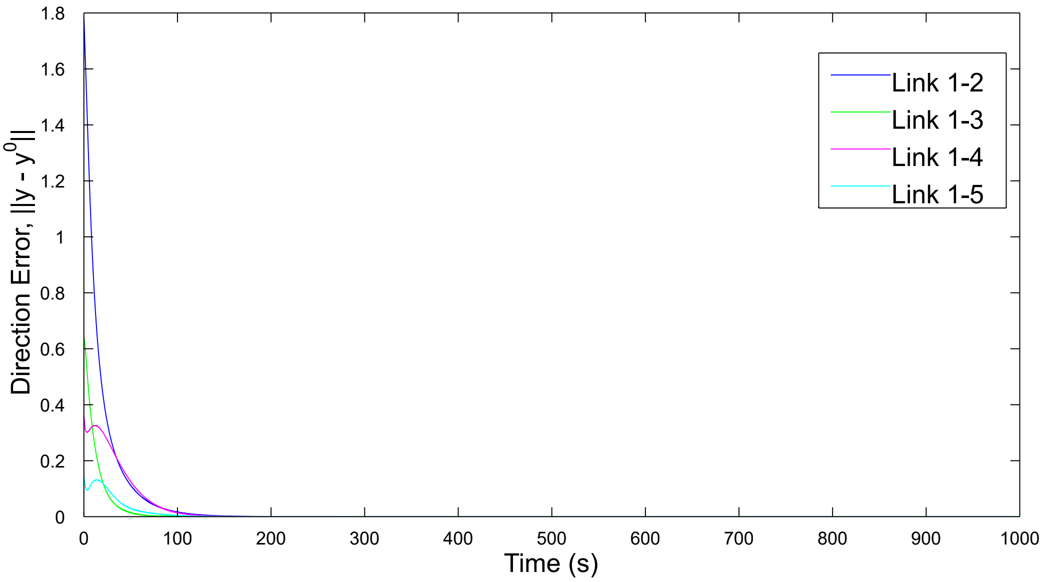

(a) Plot of the error in the regulated directions between vehicles.

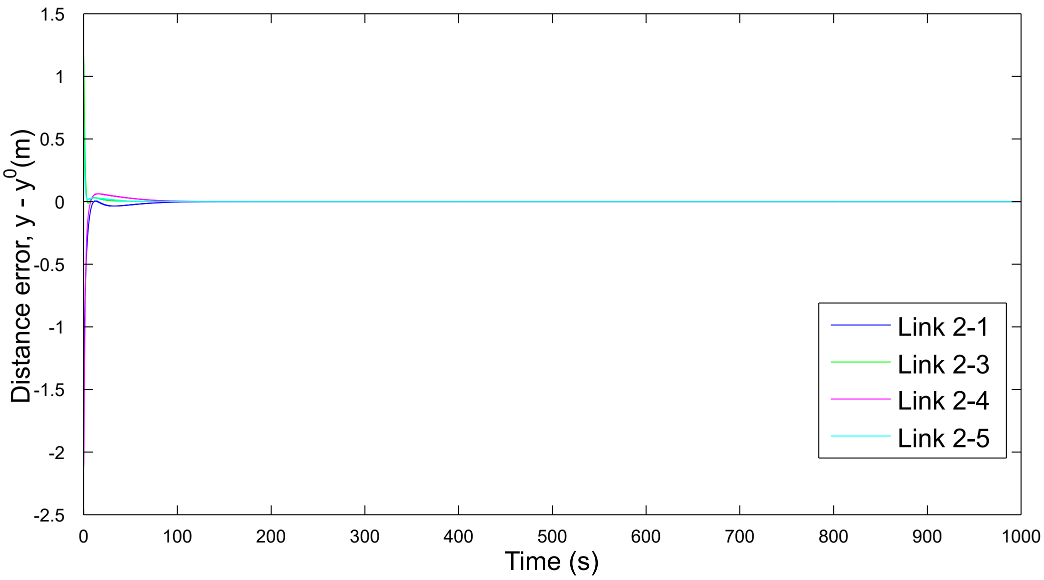

(b) Plot of the error in the regulated distances between vehicles.

Figure 5.11: Simulation results for the proposed passivity-based formation control scheme, using adaptive compensation to account for the unknown information in the measurement Jacobians. The goal formation is achieved by regulating directions from vehicle 1 and distances from vehicle 2. Here, the goal measurement $\mathring{y}$ is written y^0.

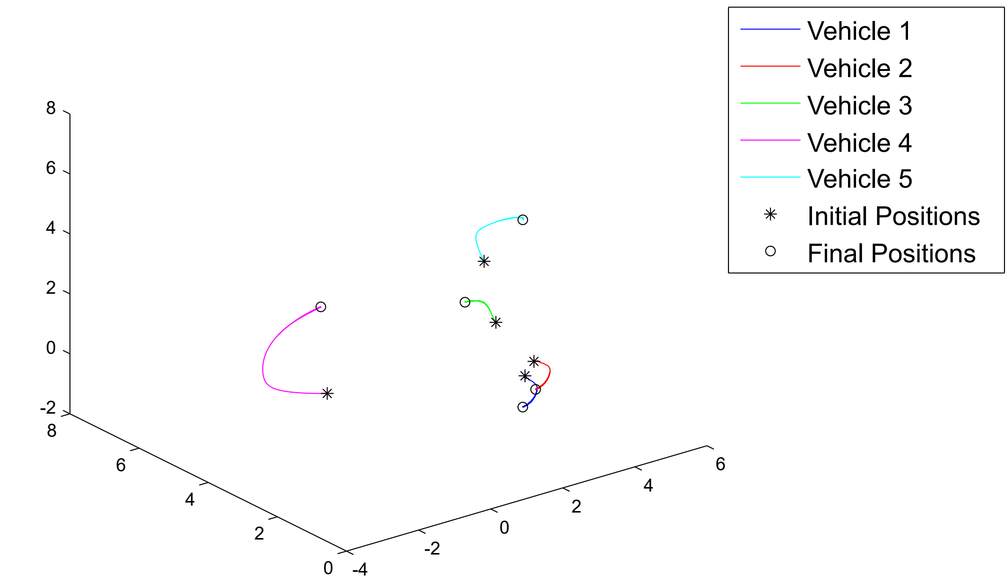

(a) The positions of each vehicle in a simulation that converges to an undesired equilibrium. Vehicles start at the points marked with asterisks and end at those marked with circles.

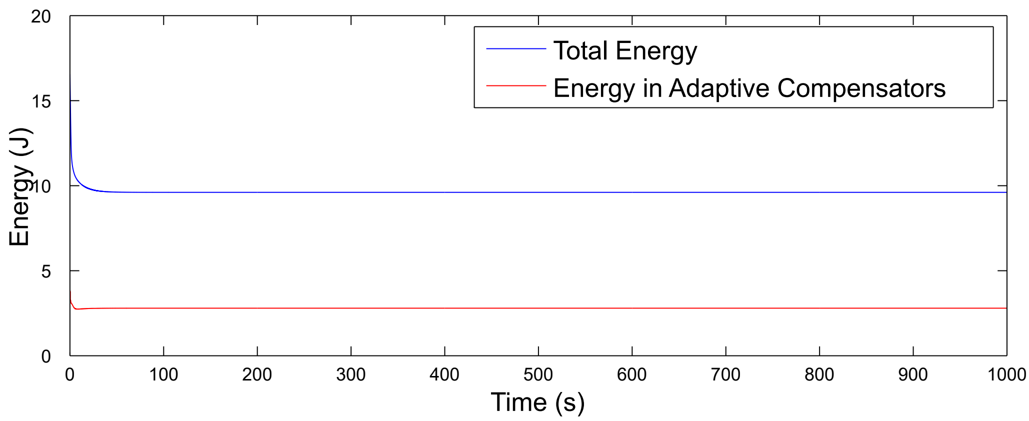

(b) The total energy in the network and the total energy in the adaptive compensation scheme, for a simulation that converges to an undesired equilibrium.

Figure 5.12: Simulation results for the proposed passivity-based formation control scheme, using adaptive compensation to account for the unknown information in the measurement Jacobians. In this case the initial state lies outside the region of attraction and the vehicles converge to an undesired equilibrium.

measurements or using visual flow techniques. The accuracy of these estimates is not likely to have a significant effect on the position regulation, since they are only employed in the damping terms and the dynamics of the adaptive variables. Given basic communication capabilities between neighbours, vehicles 1 and 2 can compute the control terms associated with each link and pass these on to the other vehicles as necessary. This is a very lightweight sensor arrangement that leaves vehicles 3, 4, and 5 entirely free of relative position sensors, thereby saving resources of weight and power for other mission objectives. I am not aware of any formation control schemes in the literature that are directly applicable to such a generic configuration where different sensors are available to each vehicle.

The proposed controller will be particularly well-suited to scenarios where GPS signals are unreliable or intermittent, such as suburban environments where the formation may regularly transition between indoor and outdoor areas. The relative position measurements supplied by the onboard sensors are likely to enable greater accuracy for regulation of the formation (compared to that enabled by GPS), and drift in the velocity estimates can be corrected by the GPS data when it is available. It should be noted that the necessity of information about the inertial frame and the relative velocities is not a particular shortcoming of the proposed approach; rather, it is a consequence of the problem's formulation and its difficulty. In the current literature, formation control using partial measurements commonly relies on either reference agents as employed by Franchi et al. [2012a], or stationary references as used by Cao et al. [2011]. In practice, there is no reason why similar strategies could not be incorporated into the proposed framework, to obtain the necessary estimates of relative state. The most appropriate approach will be dependent upon the particular situation and sensor capabilities at hand.

5.5 Conclusions and Future Work

This chapter has considered a passivity-based approach to the task of achieving a desired static formation with dynamic agents in $\mathbb{R}^3$. The bondgraph modelling formalism leads to a highly modular control architecture while enforcing strict energy consistency throughout the design. A primary focus in the control task is the use of generic *partial* measurements of relative position. In particular, for the important cases of direction and distance measurements between agents, I have shown how an adaptive compensation technique can be incorporated into the framework in order to account for the energy discrepancy associated with the unknown component of the relative state. The main result relies on the passivity of the system to provide conditions for local asymptotic stability of the desired formation. Typical performance of the control scheme has been illustrated by simulation results.

The modularity of the framework, and the passivity-based analysis, suggests that the control architecture can be readily extended to address a variety of additional considerations. In the proposed architecture, virtual springs and dampers are applied on the sensor errors (with respect to the desired formation) in order to drive the control terms for the vehicles. Energy shaping of the Hamiltonians can be used to derive alternative control laws that achieve other desirable behaviour, such as collision avoidance between vehicles. Further extensions may be inspired by existing energy-based techniques in the literature. The concept of *variable springs*, as studied in Stramigioli and Duindam [2001], could be applied in order to allow time-varying formations via a desired reference velocity $\mathring{y}_k(t)$ in the tangent space of the measurements. An interesting question introduced by this possibility is how the desired trajectories should be determined. One idea is to consider the energy reserved in the measurement Hamiltonians as a measure of the formation's proximity to the desired state. Since this energy is known, it could be incorporated into the evaluation of a suitable set-point such that the system remains in the basin of attraction as the desired formation varies with time. Alternatively, a similar strategy to that of Franchi et al. [2012b] might be used to develop a haptic control interface for a pilot, or to handle time-varying network topologies.

Another extension of the proposed design that has clear practical motivation is the incorporation of other vehicle models. In particular, it would be interesting to investigate models of nonholonomic or underactuated vehicles. While underactuated vehicles can typically be given a local controller that will mimic the point-mass dynamics I have considered, mismatches in the vehicle models could conceivably introduce energy that compromises the system's passivity. The passive control of underactuated vehicles (such as quadrotors) using the bondgraph formalism has not, to my knowledge, been studied in the literature. Furthermore, the modular architecture makes my proposed formation control framework particularly well-suited to the inclusion of multiple different types of vehicle, since in principle the desired control reference can simply be passed into an alternative vehicle model in Figure 5.4 (this modification would be analogous to the way in which different sensor modalities can be included).

Chapter 6

Conclusion

In this chapter, I bring my research on sensor-based formation control to a conclusion. I begin with a brief summary of my contributions in Section 6.1. With this perspective, avenues for future research are discussed in Section 6.2. Note that conclusions for individual chapters have already been provided; thus, the discussion here will only focus on future work that builds upon material from multiple preceding chapters.

6.1 Summary

The research in this thesis addresses the task of sensor-based formation control, where a collection of autonomous agents use partial relative state measurements to achieve a desired configuration. In Chapter 3, I introduced a generalised rigidity framework that can be used to model a wide variety of agent networks that are not readily addressed by existing rigidity-based techniques in the formation control literature. In particular, this framework accommodates agents that lie in different and possibly non-Euclidean state-spaces, along with state constraints that are described by fixing the value of a general output map that can be used to model the available sensor modalities. A new concept of *path-rigidity* was also introduced.

Chapter 4 builds upon the generalised rigidity framework and extends several fundamental structural results concerning the property of *infinitesimal rigidity* to the generalised scenario. With the aid of a new notion of *robust rigidity*, the generalised rigidity framework enables existing approaches to network localisation and formation control problems to be extended to far more general settings.

Although rigidity theory is a popular method of controlling kinematic agents, energy-based approaches are very well-suited for the control of dynamic agents. In Chapter 5, I employed the bondgraph modelling formalism to develop a passivity-based formation control architecture for dynamic agents in $\mathbb{R}^3$. To enable true *sensor-based* formation control, where only *partial* relative position measurements are available from onboard sensors, I illustrated how adaptive compensation can be integrated into the control architecture whilst preserving strict passivity of the system. Unlike many other approaches in the literature, the resulting control scheme permits a general arrangement of both range and bearing sensors, without requiring the use of special *beacon agents* to act as references for the other vehicles.

6.2 Future Work

The passivity-based control architecture presented in Chapter 5 was developed prior to the generalised rigidity framework discussed in the earlier chapters. A major focus for future work is the application of the generalised rigidity theory to the passivity-based control approach. By combining these two tools, one should be able to accommodate dynamic agent models (as in the passivity-based framework) that lie in generic state-spaces (as enabled by the rigidity framework), with an arbitrary sensor configuration. One might also extend other results from energy-based control to this setting, such as adaptive compensation for unknown variables or the piloting of a passive formation as by Franchi et al. [2012b].

An interesting outcome of my research is that rigidity theory appears to be very closely related to the passivity-based control system; indeed, the *network MTF* constructed in Definition 5.4.2 is analogous to the generalised rigidity matrix from Remark 4.2.3. This suggests that stability analysis for a much more general passivity framework (involving other agent states and output maps) can be readily performed using the existing tools provided in this thesis. The rank condition in Assumption 5.4.3 ensures the network MTF is surjective onto the tangent space of the output map. Thus, if such a formation is infinitesimally rigid with respect to a specified symmetry then it will be *minimally* infinitesimally rigid (see Remark 4.4.7). Furthermore, I believe the rank condition can be relaxed for an infinitesimally rigid formation (such that *minimal* rigidity is not necessary) by applying the insight used to prove Theorem 4.4.1; that is, by considering a subset of sensor modalities for which the network MTF is (locally) surjective onto the tangent space of the resulting output space. Additional insight into the relationship between the stability of the kinematic system considered in Section 4.4.1 and a general form of the dynamic system studied in Chapter 5 might be possible through similar analysis techniques to those of Sun and Anderson [2015]. The extension to dynamic agents in this work was achieved via a parametrised Hamiltonian system, for which the bondgraph modelling formalism should be very well-suited.

A desirable extension of the passivity framework is to enable dynamic agents to be manoeuvred through space while preserving state constraints. I believe the orbit structure provided by the rigidity framework can play a key role in this task. If the orbit is a curved submanifold of the state-space (e.g. rotations in Euclidean space), then it is necessary to introduce a control term that applies a Coriolis force to the agents, to preserve the formation. Since an infinitesimally rigid formation is a regular submanifold of the state-space, the control input τ can be decomposed into a component $\tau_{\mathcal{F}}$ that steers the agents along the submanifold, and an orthogonal component $\tau_{\mathcal{X}}$ that keeps the agent configuration in this submanifold. For a given value of $\tau_{\mathcal{F}}$ specified by a control algorithm, it should be straightforward to compute the corresponding value of $\tau_{\mathcal{X}}$ via Lagrangian mechanics. It may be possible to acquire further insight by relating these dynamics to the group action describing the system's symmetry.

Appendix A

Summary of Group Theory

Group theory (Hall [2003]) has emerged as a fundamental tool for the study of robotics, due to its role in representing and manipulating coordinate frames. In my research, group theory also plays a key role in describing the symmetries of a formation, and the ways in which a global transformation may be applied to a given state. In this section, I will briefly revise some basic properties of topological groups and Lie groups, before introducing some Lie groups that are of particular interest for my work.

Definition A.1. ([Hall, 2003, Definition A.1]) A *group* $\mathbf{G}$ is a nonempty set for which there is a binary *group operation* $\cdot$ that maps any two elements $G_1, G_2 \in \mathbf{G}$ of the group to another element $G_1 \cdot G_2 \in \mathbf{G}$ of the group. In addition, the group operation must satisfy the following properties:

(i) (**Associativity**) For all $G_1, G_2, G_3 \in \mathbf{G}$, one has $(G_1 \cdot G_2) \cdot G_3 = G_1 \cdot (G_2 \cdot G_3)$.

(ii) (**Identity element**) There exists a unique element $\iota \in \mathbf{G}$ such that $\iota \cdot G = G \cdot \iota = G$ for all $G \in \mathbf{G}$.

(iii) (**Inverse element**) For each $G \in \mathbf{G}$, there exists a unique element $G^{-1} \in \mathbf{G}$ such that $G \cdot G^{-1} = G^{-1} \cdot G = \iota$. $\diamond$

Definition A.2. ([Singh, 2013, Definition 12.1.1]) A *topological group* $\mathbf{G}$ is a topological space that possesses a group structure, and for which the group operation $\cdot : \mathbf{G} \times \mathbf{G} \to \mathbf{G}$ and the inverse map $\mathbf{G} \to \mathbf{G}, G \mapsto G^{-1}$ are continuous (where $\mathbf{G} \times \mathbf{G}$ is given the product topology). $\diamond$

Definition A.3. ([Hall, 2003, Definition C.4]) A *Lie group* $\mathbf{G}$ is a smooth (C^∞) manifold that possesses a group structure, and for which the group operation $\cdot : \mathbf{G} \times \mathbf{G} \to \mathbf{G}$ and the inverse map $\mathbf{G} \to \mathbf{G}, G \mapsto G^{-1}$ are smooth (C^∞) functions (where $\mathbf{G} \times \mathbf{G}$ is given the product topology). $\diamond$

Definition A.4. ([Hall, 2003, Definition C.5, Definition 2.36]) The *Lie algebra* $\mathfrak{g}$ of a Lie group $\mathbf{G}$ is the tangent space at the identity of $\mathbf{G}$ (i.e. $T_\iota \mathbf{G}$), for which a binary *Lie* *bracket*[1] $[\cdot,\cdot] : \mathfrak{g} \times \mathfrak{g} \to \mathfrak{g}$ is defined with the following properties:

(i) (**Bilinearity**) For all $g_1, g_2, g_3 \in \mathfrak{g}$ and all scalars a, b, one has $[ag_1 + bg_2, g_3] = a[g_1, g_3] + b[g_2, g_3]$ and $[g_3, ag_1 + bg_2] = a[g_3, g_1] + b[g_3, g_2]$.

(ii) (**Skew-symmetry**) For all $g_1, g_2 \in \mathfrak{g}$, one has $[g_1, g_2] = -[g_2, g_1]$.

(iii) (**Jacobi identity**) For all $g_1, g_2, g_3 \in \mathfrak{g}$, one has

$$[g_1, [g_2, g_3]] + [g_3, [g_1, g_2]] + [g_2, [g_3, g_1]] = 0. \qquad \diamond$$

Definition A.5. ([Singh, 2013, Definition 13.1.1]) For a topological group (resp. Lie group) $\mathbf{G}$, a *left group action* (resp. *left Lie group action*) $\Phi : \mathbf{G} \times \mathcal{M} \to \mathcal{M}$ on a topological space (resp. smooth manifold) $\mathcal{M}$ is a continuous (resp. smooth) function satisfying the following properties:

(i) (**Identity**) For all $x \in \mathcal{M}$, one has $\Phi(\iota, x) := x$, where $\iota \in \mathbf{G}$ is the group identity.

(ii) (**Compatibility**) For all $G_1, G_2 \in \mathbf{G}$ and $x \in \mathcal{M}$, one has $\Phi(G_1 \cdot G_2, x) = \Phi(G_1, \Phi(G_2, x))$. $\diamond$

A *right group action* can be defined analogously, but only left group actions are used in this thesis. Note that a group's action on itself can be defined by the group operation. Some useful terminology for the discussion of groups is outlined below.

Definition A.6. ([Hall, 2003, Definition A.7]) A *subgroup* $\mathbf{H}$ of a group $\mathbf{G}$ is a subset of $\mathbf{G}$ that is by itself a group under the inherited group operation $\cdot$ defined for $\mathbf{G}$. In this case, $\mathbf{G}$ is said to be an *overgroup* of $\mathbf{H}$. $\diamond$

Definition A.7. ([Hall, 2003, Definition A.14]) A *normal subgroup* $\mathbf{H}$ of a group $\mathbf{G}$ is a subgroup of $\mathbf{G}$ such that $G \cdot H \cdot G^{-1} \in \mathbf{H}$ for all $G \in \mathbf{G}, H \in \mathbf{H}$. $\diamond$

Definition A.8. ([Singh, 2013, Definition 13.1.3]) The *stabiliser* $\operatorname{stab} \Phi_x \subseteq \mathbf{G}$ of a group action $\Phi : \mathbf{G} \times \mathcal{M} \to \mathcal{M}$ at a point $x \in \mathcal{M}$ is defined as the set $\{G \in \mathbf{G} \mid \Phi(G, x) = x\}$. $\diamond$

In the remainder of this appendix, I describe several groups that are of particular interest for my study of formation control. These include the Special Orthogonal group commonly used to represent rotations, the Special Euclidean group used to represent rigid-body transforms, and less common groups that permit scaling of a formation. Note that all groups discussed here have matrix representations; the group operations are naturally defined by matrix multiplication, the identity of the group is given by the matrix identity, and the inverse of an element is given by the matrix inverse.

[1] Note that the structure of the Lie bracket is not used in this thesis but has been included here for completeness.

A.1 The (Special) Orthogonal group

The *Orthogonal group* of dimension n, written $\mathrm{O}(n)$, is the set of $n \times n$ orthogonal matrices; i.e. the rows and columns of a matrix $Q \in \mathrm{O}(n)$ are unit vectors and the determinant of Q is ± 1. An important property of the Orthogonal group is that $Q^{-1} = Q^\top$ for all $Q \in \mathrm{O}(n)$. The *Special Orthogonal group* $\mathrm{SO}(n)$ is a normal subgroup of the Orthogonal group that consists of the $n \times n$ orthogonal matrices for which the determinant is $+1$. The Special Orthogonal group is commonly used to represent the orientation of a coordinate frame, with the columns describing unit vectors in the direction of the axes. The group $\mathrm{O}(n)$ is not normally used for this purpose since matrices of determinant -1 correspond to reflected coordinates (i.e. unconventional left-hand frames). The Special Orthogonal group can also be used to describe a *rotation* of a coordinate frame; a rotation $R_1 \in \mathrm{SO}(n)$ of an orientation $R_2 \in \mathrm{SO}(n)$ is given by the group action $\Phi(R_1, R_2) := R_1 R_2 \in \mathrm{SO}(n)$ (the angles of the rotation are such that $R_1 I_n = R_1$, where I_n is the $n \times n$ identity matrix). Note that although $\mathrm{SO}(n)$ can act on $\mathrm{O}(n)$ in this natural manner (resulting in an element of $\mathrm{O}(n)$), the reverse is not true since the result might not be an element of $\mathrm{SO}(n)$.

Both $\mathrm{O}(n)$ and $\mathrm{SO}(n)$ can be used to describe transformations of a vector $x \in R^n$, via the group action $\Phi(Q, x) := Qx$ (for $Q \in \mathrm{O}(n)$ or $Q \in \mathrm{SO}(n)$). Elements of $\mathrm{SO}(n)$ describe the rotation of a point in Euclidean space about the origin, while elements of $\mathrm{O}(n)$ may additionally include a reflection through the origin.

A.2 The (Special) Euclidean group

The *Euclidean group* $\mathrm{E}(n)$ is the set of $(n+1) \times (n+1)$ matrices of the form

$$X := \begin{pmatrix} Q & \xi \\ 0_n^\top & 1 \end{pmatrix},$$

where $Q \in \mathrm{O}(n)$, $\xi \in \mathbb{R}^n$, and $0_n \in \mathbb{R}^n$ denotes the n-vector of zeroes. It is commonly used to describe rigid-body transforms of a vector $x \in \mathbb{R}^n$; i.e. transforms consisting of a rotation Q about the origin (with a possible reflection through the origin) followed by a translation of ξ. The result is computed by expressing the vector in homogeneous coordinates $\bar{x} := (x^\top, 1)^\top$ and using matrix multiplication for the group action; i.e. the transformed vector $\Phi(X, x)$ is given in homogeneous coordinates by,

$$\overline{\Phi(X, x)} := X\bar{x}.$$

The *Special Euclidean group* $\mathrm{SE}(n)$ is defined analogously, but with $R \in \mathrm{SO}(n)$ in the place of $Q \in \mathrm{O}(n)$ to disallow reflections. The group $\mathrm{SE}(n)$ is frequently used to describe a coordinate frame, consisting of an orientation $R \in \mathrm{SO}(n)$ and an origin ξ expressed in another frame of reference.

A.3 The (Special) Similarity group

For this research, I introduce the *Similarity group* $\mathrm{S}(n)$ to consider the possibility of *scaling* a formation, in addition to applying rigid-body transformations (as with rotations, the scaling is centred at the origin). An element $S \in \mathrm{S}(n)$ is represented in matrix form by

$$S := \begin{pmatrix} Q & \xi \\ 0_n^\top & \frac{1}{\rho} \end{pmatrix},$$

where $Q \in \mathrm{O}(n)$ is a rotation matrix (with a possible reflection), $\xi \in \mathbb{R}^n$ represents a translation, and $\rho \in \mathbb{R}_{>0}$ is the scaling factor. It is straightforward to verify that this defines a group, with matrix multiplication as the group operation.

The group action of $\mathrm{S}(n)$ on a state $x \in \mathbb{R}^n$ can be defined using matrix multiplication on the homogeneous vector $\bar{x} := (x^\top, 1)^\top$. Let $\mathbb{RP}^n$ denote the real projective space and let $\lfloor v \rfloor := \{w \in \mathbb{R}^{n+1} \mid \exists \lambda > 0 : w = \lambda v\}$ be the equivalence class of a vector $v \in \mathbb{R}^{n+1}$. Define $\mathbb{RP}^n_+ := \{\lfloor v \rfloor \mid v^\top \vec{e}_{n+1} > 0\} \subset \mathbb{RP}^n$ (where $\vec{e}_{n+1} := (0_n^\top, 1)^\top$), and let $\chi(x) := \lfloor \bar{x} \rfloor \in \mathbb{RP}^n_+$ be the bijective map that identifies a position $x \in \mathbb{R}^n$ with the equivalence class $\lfloor \bar{x} \rfloor \in \mathbb{RP}^n_+$. The group action $\Phi : \mathrm{S}(n) \times \mathbb{R}^n \to \mathbb{R}^n$ can now be described by

$$\Phi(S, x) := \chi^{-1}(\lfloor S\bar{x} \rfloor).$$

Note that this construction is equivalent to the definition

$$\Phi(S, x) := \rho(Qx + \xi).$$

The *Special Similarity group* $\mathrm{SS}(n)$ is analogous, but with Q restricted to the *Special* Orthogonal group $\mathrm{SO}(n)$.

A.4 The (Scaled) Translations group

Another group considered in this work is that of *Scaled Translations*, denoted $\mathrm{ST}(n)$. This group corresponds to translating a formation and then scaling it, without applying a rotation or a reflection. It can be derived from the Similarity group by fixing $Q = I_n$, and it inherits the same group operation and group action on $\mathbb{R}^n$. If the scaling factor is restricted to 1, the resulting group $\mathrm{T}(n)$ consists only of translations.

A.5 Subgroup Relations and Invariant Sensor Modalities

In Figure A.1, I illustrate the relations between the groups discussed above. An arrow $\mathbf{G} \hookleftarrow \mathbf{H}$ is used to indicate that $\mathbf{H}$ is a subgroup of $\mathbf{G}$. Sensor modalities written underneath each group are invariant to the associated group action (see the examples in Section 3.2.2). Note that if a sensor modality is invariant to a group $\mathbf{G}$, then it is also invariant to all subgroups of $\mathbf{G}$. Observe that the measurements involving states in $\mathrm{SE}(n)$ cannot be invariant to groups that apply a reflection, since there is no natural group action.

$$
\begin{tikzcd}
\boxed{\begin{array}{c}\mathrm{S}(n)\\ \text{Angles } (\mathbb{R}^n)\end{array}} & \boxed{\begin{array}{c}\mathrm{E}(n)\\ \text{Distances } (\mathbb{R}^n)\end{array}} \arrow[l, hook] & \boxed{\mathrm{O}(n)} \arrow[l, hook] \\
\boxed{\begin{array}{c}\mathrm{SS}(n)\\ \text{Bearings in BFF } (\mathrm{SE}(n))\end{array}} \arrow[u, hook] & \boxed{\begin{array}{c}\mathrm{SE}(n)\\ \text{Relative positions in BFF } (\mathrm{SE}(n))\end{array}} \arrow[u, hook] \arrow[l, hook] & \boxed{\mathrm{SO}(n)} \arrow[u, hook] \arrow[l, hook] \\
\boxed{\begin{array}{c}\mathrm{ST}(n)\\ \text{Inertial directions } (\mathbb{R}^n)\end{array}} \arrow[u, hook] & \boxed{\begin{array}{c}\mathrm{T}(n)\\ \text{Inertial relative positions } (\mathbb{R}^n)\end{array}} \arrow[u, hook] \arrow[l, hook] &
\end{tikzcd}
$$

Figure A.1: Relation between various groups discussed in this thesis, with arrows pointing from subgroups to overgroups. Some invariant sensor modalities of interest are written underneath each group. The relevant state-space for these measurements is written in parentheses. The acronym *BFF* stands for *body-fixed-frame*.

Appendix B

Classical Rigidity Theory

Rigidity theory (Jackson [2007]) has played a key role in the existing formation control literature. In particular, it provides insight into whether a desired rigid formation can be enforced by only regulating a specific set of relative distances between the agents. The slightly stronger property of *infinitesimal rigidity* offers further insight concerning infinitesimal deviations from the desired formation, and can therefore be used to study the system's behaviour in a local neighbourhood. In this section, I will briefly review the well-established techniques employed in classical rigidity analysis, which provide some background for the more general theory developed in Chapters 3 and 4 of this thesis.

Consider a collection of N agents, where the i'th agent has position $x_i \in \mathbb{R}^d$ (with $d \geq 2$). Suppose M pairs of agents have *distance* or *range* constraints between them, indexed by k. That is, each value of k is associated with a unique unordered pair of agents i and j. To avoid duplicity (since the edge (i, j) is identical to that of (j, i)) I will arbitrarily assume $i < j$ throughout this thesis. Let $r_k := \|x_i - x_j\| \in \mathbb{R}_{\geq 0}$ denote the distance between the pair of agents i and j, with $r := (r_1, \ldots, r_M)^\top \in \mathbb{R}^M$. To formalise this scenario, it is useful to model the network using a graph (see Godsil and Royle [2001] for background graph theory).

Definition B.9. An *agent network* is encoded by a undirected graph $\mathcal{G} := (\mathcal{V}, \mathcal{E})$, where the N vertices (or nodes) $i \in \mathcal{V}$ correspond to the agents and the M edges $k \in \mathcal{E}$ correspond to the distance constraints between them. ◇

The advantage of modelling the network as a graph is that it enables the structure of the network to be encoded as a matrix. The use of an *undirected* graph is justified by the observation that the distance between two agents is symmetric (i.e. $\|x_i - x_j\| = \|x_j - x_i\|$).

Definition B.10. Two agents $i, j \in \mathcal{V}$ are *neighbours* if there is an edge $k = (i, j) \in \mathcal{E}$ connecting them. ◇

The following definitions formalise the classical notion of rigidity for agent networks.

Definition B.11. A *configuration* of an agent network $\mathcal{G}$ is the full system state $x := (x_1^\top, \ldots, x_N^\top)^\top \in \mathbb{R}^{dN}$. ◇

Definition B.12. (Jackson [2007]) A *framework* is an agent network combined with a specific configuration, i.e. $(\mathcal{G}, x)$. $\diamond$

Definition B.13. (Jackson [2007]) Two frameworks $(\mathcal{G}, x^a)$ and $(\mathcal{G}, x^b)$ with distances $r_k^a(x_i^a, x_j^a)$ and $r_k^b(x_i^b, x_j^b)$ are *equivalent* if $r_k^a = r_k^b$ for all $k \in \mathcal{E}$. $\diamond$

Definition B.14. (Jackson [2007]) Two frameworks $(\mathcal{G}, x^a)$ and $(\mathcal{G}, x^b)$ are *congruent* if $\|x_i^a - x_j^a\| = \|x_i^b - x_j^b\|$ for all $i, j \in \mathcal{V}$. $\diamond$

Definition B.15. (Jackson [2007]) A framework $(\mathcal{G}, x)$ is *globally rigid* if all equivalent frameworks $(\mathcal{G}, x')$ are congruent. If this (only) holds for $x' \in \mathcal{U}_x$, where $\mathcal{U}_x$ is an open neighbourhood of x, then the framework $(\mathcal{G}, x)$ is *locally rigid*. $\diamond$

The notion of minimal rigidity is also of interest for certain applications.

Definition B.16. A locally rigid framework $(\mathcal{G}, x)$ with $\mathcal{G} := (\mathcal{V}, \mathcal{E})$ is *minimally rigid* if there does *not* exist a subgraph $\mathcal{G}' := (\mathcal{V}, \mathcal{E}')$ with $\mathcal{E}' \subset \mathcal{E}$ (a proper subset) such that $(\mathcal{G}', x)$ is a locally rigid framework. $\diamond$

I now introduce the classical notion of infinitesimal rigidity, using the following definitions.

Definition B.17. (Jackson [2007]) For a given framework $(\mathcal{G}, x)$ with $x \in \mathbb{R}^{dN}$, the *rigidity matrix* $R(x) := (\mathrm{d}/\mathrm{d}x) r^\top r$ is an $M \times dN$ matrix with the (k, i)'th $1 \times d$ block entry given by $(x_i - x_j)^\top$ (i.e. with the (k, j)'th block entry being $(x_j - x_i)^\top$). $\diamond$

Definition B.18. A (first order) *infinitesimal variation* of a configuration $x \in \mathbb{R}^{dN}$ is any tangent vector $\Delta_x \in \mathbb{R}^{dN}$. $\diamond$

Definition B.19. (Jackson [2007]) A (first order) *infinitesimal motion* of a framework $(\mathcal{G}, x)$ is an infinitesimal variation Δ_x such that, for all $k \in \mathcal{E}$, the relative distance r_k remains unchanged. That is,

$$R(x)\Delta_x := 0. \qquad \diamond$$

Definition B.20. (Asimow and Roth [1979]) A framework $(\mathcal{G}, x)$ is *infinitesimally rigid* if the only infinitesimal motions are rigid-body transforms (i.e. correspond to the action of elements in the Lie algebra $\mathfrak{se}(d)$ of the Special Euclidean group $\mathrm{SE}(d)$). $\diamond$

My study of rigidity will also employ the following result concerning the rank of a smooth map.

Lemma B.21. *Let $\mathcal{M}$ and $\mathcal{N}$ be smooth finite-dimensional manifolds, and let $f : \mathcal{M} \to \mathcal{N}$ be a smooth map. For any point $x \in \mathcal{M}$, there exists an open neighbourhood $\mathcal{U}_x$ such that* $\operatorname{rank} \mathrm{D}f(x') \geq \operatorname{rank} \mathrm{D}f(x)$ *for all $x' \in \mathcal{U}_x$.*

Proof Let $r := \operatorname{rank} \mathrm{D}f(x)$. This implies that $\mathrm{D}f(x)$ contains an $r \times r$ submatrix (constructed by removing particular rows and columns) with nonzero determinant. By the continuity of $\mathrm{D}f(x)$ and the determinant, this submatrix will remain full rank in an open neighbourhood $\mathcal{U}_x$ of x, and hence $\operatorname{rank} \mathrm{D}f(x') \geq r$ for $x' \in \mathcal{U}_x$. ■

Appendix C

Port-Hamiltonian Theory

In this appendix I provide a brief review of port-Hamiltonian theory (Duindam et al. [2009]), which has found successful application to formation control problems by e.g. Franchi et al. [2012b]; Vos et al. [2016]. Port-Hamiltonian theory was originally developed as a framework for modelling complex systems whose state variables lie in multiple physical domains. For example, a system might involve the interconnection of thermodynamic, electrical, mechanical or hydraulic components. The port-Hamiltonian framework provides an elegant method of describing the interactions between such components in terms of the energy flow through *ports*; this can be achieved in a generic manner regardless of the particular domain of the state variables. The idea is that power can be decomposed into a *flow* vector, denoted $f \in \mathcal{V} := \mathbb{R}^m$, and a dual *effort* vector, denoted $e \in \mathcal{V}^*$. The *power* is then described by the duality product $\langle e \mid f \rangle := e^\top f$. The total energy in a component is described by a Hamiltonian $H(x,t) \geq 0$, which depends on the component's state $x \in \mathbb{R}^n$ and (possibly) the time $t \in \mathbb{R}_{\geq 0}$. The system is then described by the following equations:

$$\dot{x} = (J(x,t) - D(x,t)) \frac{\partial H^\top(x,t)}{\partial x} + g(x,t)u(t) \tag{C.1a}$$

$$y = g^\top(x,t) \frac{\partial H^\top(x,t)}{\partial x}. \tag{C.1b}$$

Here, $u(t) \in \mathbb{R}^m$ is an input (typically an effort, such as the force driving a vehicle) and $y \in \mathbb{R}^m$ is the resulting output (typically a flow, such as the velocity of a vehicle). Thus, the power exchanged with the component through the port is $\langle u \mid y \rangle$. The relationship between the port variables and the system state is described by the matrix $g(x,t) \in \mathbb{R}^{n\times m}$. The matrix $J(x,t) = -J^\top(x,t) \in \mathbb{R}^{n\times n}$ is skew-symmetric and represents the symplectic structure of the state-space, while the matrix $D(x,t) = D^\top(x,t) \in \mathbb{R}^{n\times n}$ is positive-definite and determines the energy dissipation in the system.

The primary advantage of the port-Hamiltonian framework is that it makes the *passivity* property of the system quite transparent. A system is termed *passive* (with respect to the input u and output y) if the energy in the system, as described by the energy function H, satisfies the relationship $\dot{H} \leq \langle u \mid y \rangle$ (i.e. all increases in the energy of the system are supplied by the power input). Note that if no power is supplied to the system, then $\dot{H} \leq 0$. The process of *passivity-based control* exploits this property to analyse the trajectories of the system; in particular, to argue that the state of the system cannot possess more energy than the sum of the initial energy and the total quantity of introduced energy. This implies that states of minimum energy are not unstable. Furthermore, if the system is *strictly passive* (i.e. $\dot{H}$ is negative definite) then the system state under zero input will converge to a (possibly local) minima of H. This idea is analogous to Lyapunov analysis (see Khalil [2002]), and in practice the energy H is very often used as a Lyapunov function.

In general, a port-Hamiltonian system of the form in (C.1) is not passive. However, if the system is of the following time-invariant form,

$$\dot{x} = (J(x) - R(x))\,\frac{\partial H^\top(x)}{\partial x} + g(x)u(t)$$

$$y = g^\top(x)\frac{\partial H^\top(x)}{\partial x}$$

then passivity is well-known to be guaranteed (see e.g. Fujimoto and Sugie [2001]).

A common strategy for passivity-based control is to augment the physical energy V in the system (i.e. the kinetic energy and the potential energy) with an additional nonnegative *virtual* potential energy U, and to define $H := V + U$. This technique is known as *energy shaping*, and the idea is to shape the function H such that its minima correspond to a desired system state. Achieving the desired stability of the physical system is then a matter of applying a control input that mimics the effect of the virtual effort $-\frac{\partial U}{\partial x}$ (note that this control input is *not* the variable u; it is already modelled in the energy function H).

Appendix D

Bondgraph Diagrams

In this appendix I provide an introduction to bondgraph diagrams (Borutzky [2006]), which provide a graphical formalism for the representation of port-Hamiltonian systems (see Appendix C). In particular, they offer an elegant method of visualising the power flows between various subcomponents of the system, along with the associated mathematical relationships; thus, they are a valuable and convenient tool for the design and stability analysis of the system. A key feature of the bondgraph formalism is that it guarantees the modelled system is energy-consistent; that is, all energy introduced to the system or dissipated from it is clearly represented in the diagram.

Bondgraph models represent systems as a composition of several basic elements, which are interconnected via *bonds* between the *power ports* of each element (i.e. the input and output connections). The notation for a bond between two elements, labelled A and B, is shown in Figure D.1. As described by the port-Hamiltonian theory in the previous subsection, the power $\langle e \mid f \rangle = e^\top f$ through each bond is composed of an *effort* vector $e \in \mathbb{R}^m$ and a *flow* vector $f \in \mathbb{R}^m$. The half-arrow points in the direction of positive power flow through the bond; in Figure D.1, positive power flows from element B to element A. It is conventional for the half-arrow to be drawn on the lower side of a horizontal bond (as in the diagram) or on the right-hand side of a vertical bond; this indicates which side the flow variable (f) is written (with the effort e written on the opposite side). The vertical stroke at the end of the bond indicates the *causality* relation between the elements, i.e. which element applies the effort to the other (note that the causality bar is completely unrelated to the half-arrow, i.e. they may appear at the same or different ends of the bond). In Figure D.1, the causality bar shows that the effort e is an output of element A and an input of element B. Consequently, the associated flow f is an output of element B and an input of element A. The elements with which bondgraph models are constructed, and the ways in which they may be interconnected, are outlined below.

- *Source* or *Sink*: Sources supply power to the system, while Sinks draw power

$$A \;\underset{f}{\overset{e}{\leftharpoondown\!\!\relbar\!\!\relbar\!\!\relbar\!\!\dashv}}\; B$$

Figure D.1: A single power bond between two elements, A and B.

from it. In their basic form, these elements fix either the *effort* or *flow* of the attached bond, and are represented by Se or Sf respectively (these symbols are short for *Source: effort* and *Source: flow*). A typical example is a battery that applies a voltage (effort) to the system. Since the output of an Se element is always an effort, the causality bar is always on the far end of any attached bonds; similarly, Sf elements have the flow as an output and the causality bar must therefore be placed on their end of the bond. The setpoint of the power variable may be modulated based on other state variables, in which case the symbol is prefixed by M (e.g. MSe).

- *Storage*: This element represents the storage of energy in the system. The stored energy is described by an associated Hamiltonian $H(x)$ that is a function of a time-varying state $x(t)$. In a capacitative storage element, such as a spring, the element is denoted by a C and the derivative of the state ($\dot{x}$) is a flow variable[1]. The time-derivative of the energy storage function is

$$\frac{\mathrm{d}}{\mathrm{d}t}H := \frac{\partial H}{\partial x}\dot{x}.$$

  In this case, the storage element applies an effort $e := \frac{\partial H}{\partial x}$ to the system and the causality bar will be on the far end of the attached bond. The alternative is to have an inductive storage element, denoted by an I, where the derivative of the state is an effort variable, and the resulting output is a flow. This case may, for example, correspond to a mass for which the kinetic energy depends on the velocity.

- *Resistors*: These elements irreversibly dissipate energy from the system, and are represented by the symbol R. The causality assigned to the attached bonds depends upon the type of resistor. For a mechanical vehicle overcoming air resistance, the dissipated power is typically of the form $\langle Df \mid f \rangle$ (where f is a flow and D is a positive coefficient). In this case, the resistor applies an effort to the system and the causality bar belongs on the far end of the bond from the resistive component. Of course, if the dissipated power takes the form $\langle e \mid De \rangle$ where the effort e is the input, then the causality bar will go on the end attached to the resistive element.

- *Transformers* and *Gyrators*: These elements represent a reversible transformation of power, typically between only two power bonds. They are illustrated in Figure D.2. Transformer elements are denoted TF, and possess at least one port with an output effort causality and at least one port with an input effort causality. They specify a linear relationship between the output effort and the input effort, with a dual relationship defined between the associated flows. Gyrators, which are denoted GY, have the same causality on all ports (i.e. either each port has effort as the output, or each port has flow as the output). The output

[1] In this thesis I have assumed all storage elements to have the common *integral* causality, rather than the unusual *derivative* causality (Borutzky [2006]).

$$\begin{tikzcd} & M \arrow[d] & \\ A \arrow[r, "e_A := M^\top e_B", "f_A"'] & MTF \arrow[r, "e_B", "f_B := M f_A"'] & B \end{tikzcd}$$

$$\begin{aligned} \langle e_A \mid f_A \rangle &= \langle M^\top e_B \mid f_A \rangle \\ &= \langle e_B \mid M f_A \rangle \\ &= \langle e_B \mid f_B \rangle \end{aligned}$$

(a) Relationship of power variables for a Transformer, modulated by a matrix signal $M \in \mathbb{R}^{m \times m}$.

$$\begin{tikzcd} & M \arrow[d] & \\ A \arrow[r, "e_A", "f_A := M^\top e_B"'] & MGY \arrow[r, "e_B", "f_B := M e_A"'] & B \end{tikzcd}$$

$$\begin{aligned} \langle e_A \mid f_A \rangle &= \langle e_A \mid M^\top e_B \rangle \\ &= \langle M e_A \mid e_B \rangle \\ &= \langle f_B \mid e_B \rangle \end{aligned}$$

(b) Relationship of power variables for a Gyrator with flow as the output, modulated by a matrix signal $M \in \mathbb{R}^{m \times m}$.

Figure D.2: Bondgraph notation and energy relations for Transformers and Gyrators.

variables are again a linear function of the input variable from the other port. For both transformers and gyrators, the linear relationship may be modulated, in which case the symbol is prefixed by M and the modulating input signal is indicated with a normal arrow as shown in Figure D.2. Importantly, the power input must be equivalent to the power output at any instance in time. This leads to the relationships given below the corresponding diagrams in Figure D.2.

- 0-*junctions* and 1-*junctions*: These junctions provide a means of interconnecting multiple bonds in an energy consistent manner, i.e. such that the power flow into the junction (as indicated by the half-arrows on the bonds) matches the power flow out of it. Illustrations of these junctions are shown in Figure D.3. A 0-junction indicates that the effort associated with each bond is the same, while the flows into the junction sum to zero (i.e. after accounting for the positive direction of the bonds). Similarly, a 1-junction indicates that the flow associated with each bond is the same, while the efforts sum to zero. This leads to the mathematical relationships outlined in Figure D.3. Precisely one of the bonds must have the causality bar on the side of a 0-junction, while all but one bond must have the causality bar on the side of a 1-junction.

$$\begin{tikzcd} A \arrow[r, maps to, "e_A:=e", "f_A"'] & 0 \arrow[d, "e_C:=e"', "f_C:=f_A+f_B"] & B \arrow[l, maps to, "e_B:=e"', "f_B"] \\ & C & \end{tikzcd}$$

$$\begin{aligned} \langle e_C \mid f_C \rangle &= \langle e \mid f_A + f_B \rangle \\ &= \langle e_A \mid f_A \rangle + \langle e_B \mid f_B \rangle \end{aligned}$$

(a) Relationship of power variables for a 0-junction.

$$\begin{tikzcd} A \arrow[r, "e_A", "f_A:=f"'] & 1 \arrow[d, "e_C:=e_A+e_B"', "f_C:=f"] & B \arrow[l, "e_B"', "f_B:=f"] \\ & C & \end{tikzcd}$$

$$\begin{aligned} \langle e_C \mid f_C \rangle &= \langle e_A + e_B \mid f \rangle \\ &= \langle e_A \mid f_A \rangle + \langle e_B \mid f_B \rangle \end{aligned}$$

(b) Relationship of power variables for a 1-junction.

Figure D.3: Bondgraph notation and energy relations for 0-junctions and 1-junctions.

Appendix E

Simulation Code

In this appendix I provide the simulation code for the passivity-based formation controllers in Chapter 5. Note that this code includes a flag for random initialisation (as opposed to the specific initialisation used for the simulations presented in this thesis), and a flag for the use of adaptive compensation. The code was run using Matlab R2013a developed by MathWorks (website: `https://au.mathworks.com/products/matlab`).

```
% Simulation for vehicles trying to achieve a goal configuration using
% partial measurements of relative position
%
% By Geoff Stacey
%
% Last modified 05/1/2016

function Formation_Simulation

    %close all;

    % Settings --------------------------------------------------------------%

    % This code has been run many times with randomly generated initialisation
    % parameters. To produce the particular results presented in the thesis,
    % set the following flag to 0.
    random_initialisation = 0;

    % To run the simulation with the true Jacobian (i.e. without the adaptive
    % compensation) set the following flag to 0.
    adaptive_compensation = 1;

    % Randomisation Parameters ----------------------------------------------%

    % Parameters for random initialisation
    rand_pos = 3; % maximum distance of initial positions from goal positions
    eta_r = 0.3;    % maximum error in initial distance and position estimates
    eta_zeta = 0.3; % as a fraction of the true values

    % Simulation Parameters -------------------------------------------------%
    t_step_sim = 0.001; % time step of simulation
    t_step_control = 0.01; % time step of controller
    end_time = 1000; % duration of the simulation
```

```
mass = 1; % mass of each vehicle
gain_s = 3; % gain for direction measurements
gain_r = 2; % gain for distance measurements
gain_hat_r = 1; % gain for adaptive distance variable
gain_hat_zeta = 1; % gain for adaptive position variable

c_Delta = 0.0001; % threshold for periodic correction of adaptive position
% variable for distance links

d = 1; % vehicle damping
d_r = 1; % damping on distance coupling
d_s = 1; % damping on direction coupling

% Shorthand Declarations -------------------------------------------------%
I3 = [1, 0, 0; 0, 1, 0; 0, 0, 1];

% Initialisation ---------------------------------------------------------%

% The desired formation is generated by the following goal positions for
% each agent, relative to the first and reading across
goal_q = [0, 0, 0;
          3, 0, 0;
          3, 5, 0;
          0, 5, 0;
          0, 0, 5];

q_size = size(goal_q);
n = q_size(1); % Number of agents

% Error in initial positions
if random_initialisation == 0 % Use fixed values

    % Values used in the simulation
    rand_q = [ 1.6530   -2.3122   -1.9468    1.9666    0.8042;
              -1.2082    0.0678    1.1151   -1.6831   -1.6792;
              -0.8994   -0.4683    0.6286    0.7986    0.7526];

    % Use these values for simulation that fails to converge with adaptive
    % compensation
    %    rand_q = [  1.8129   -0.9117    1.7832   -1.6997    0.3299;
    %                0.8976    0.9262   -0.1630   -2.0443    0.5343;
    %                1.2909    1.6585   -0.2255    0.7592    0.8393];

else % Use random values
    rand_q = zeros(q_size);
    for i = 1 : n
        rand_q(i, :) = ball_noise(rand_pos);
    end
    rand_q = transpose(rand_q);
end

% Initial positions of the agents
q = transpose(goal_q) + rand_q;
```

```
star_q = transpose(goal_q);

link_r = [2, 1; % Vehicles between which there is a distance link
          2, 3;
          2, 4;
          2, 5];

link_s = [1, 2; % Vehicles between which there is a direction link
          1, 3;
          1, 4;
          1, 5];

r_size = size(link_r);
s_size = size(link_s);

mr = r_size(1); % Number of distance links
ms = s_size(1); % Number of direction links

star_r = zeros(1, mr);
star_s = zeros(3, ms);

hat_r = zeros(1, ms);
hat_zeta = zeros(3, mr);

% Initialisation of goal values and estimates ----------------------------%

% Error in initial position estimates
if random_initialisation == 0 % Use fixed values

    % Values used in the simulation
    rand_hat_z = [ 0.1069   -0.0608    0.0747   -0.1892;
                   0.1052    0.0880   -0.1804    0.0325;
                  -0.0944   -0.1910    0.1319   -0.0541];

    % Use these values for simulation that fails to converge with adaptive
    % compensation
    %     rand_hat_z = [ -0.0374   -0.2007   -0.1292    0.0869;
    %                     0.0788    0.1578   -0.2197   -0.0816;
    %                     0.1601   -0.0233    0.1023   -0.0712];

else % Use random values
    rand_hat_z = zeros(3, mr);
    for i = 1 : mr
        rand_hat_z(:,i) = ball_noise(eta_zeta);
    end
end

for i = 1 : mr
    % Set desired distance
    star_r(i) = magnitude(squeeze(star_q(:,link_r(i,1))) - ...
        squeeze(star_q(:,link_r(i,2))));

    % Set initial position estimates
    hat_zeta(:,i) = (squeeze(q(:,link_r(i,1))) - ...
```

```
        squeeze(q(:,link_r(i,2)))) + ...
        magnitude(squeeze(q(:,link_r(i,1))) - ...
        squeeze(q(:,link_r(i,2)))) * squeeze(rand_hat_z(:,i));
end

% Error in initial distance estimates
if random_initialisation == 0 % Use fixed values

    % Values used in the simulation
    rand_hat_r = [  -0.1216   -0.2628   -0.1211   -0.2722];

    % Use these values for simulation that fails to converge with adaptive
    % compensation
    %     rand_hat_r =  [ -0.0061   -0.1841    0.2375   -0.2405];

else % Use random values
    rand_hat_r = zeros(1, ms);
    for i = 1 : ms
        rand_hat_r(i) = 2 * rand(1) * eta_r - eta_r;
    end
end

for i = 1 : ms
    % Set desired directions
    star_s(:,i) = (squeeze(star_q(:,link_s(i,1))) - ...
        squeeze(star_q(:,link_s(i,2)))) / ...
        magnitude(squeeze(star_q(:,link_s(i,1))) - ...
        squeeze(star_q(:,link_s(i,2))));

    % Set initial distance estimates
    hat_r(i) = magnitude(squeeze(q(:,link_s(i,1))) - ...
        squeeze(q(:,link_s(i,2)))) + ...
        magnitude(squeeze(q(:,link_s(i,1))) - ...
        squeeze(q(:,link_s(i,2)))) * (rand_hat_r(i));
end

% Variable Declarations --------------------------------------------------%

v = zeros(3,n); % velocity
a = zeros(3,n); % acceleration

% data for plots
q_plot = zeros(3, n, end_time / t_step_control); % position data
error_r = zeros(mr, end_time / t_step_control + 1); % distance error data
error_s = zeros(ms, end_time / t_step_control + 1); % direction error data
total_energy = zeros(1, end_time / t_step_control + 1); % total energy data
ac_energy = zeros(1, end_time / t_step_control + 1); % adaptive compension
% energy data

% Main Simulation Loop ---------------------------------------------------%
for step_count = 0 : end_time / t_step_sim
    % physical state update
    v = v + a * t_step_sim;
    q = q + v * t_step_sim;
```

```
% Control Loop -------------------------------------------------------%
if rem(step_count * t_step_sim, t_step_control) == 0

    % data entry number for this iteration
    data_entry = step_count / t_step_control * t_step_sim + 1;
    % record the positions
    q_plot(:, :, data_entry) = q;

    tau = zeros(3,n); % initialise the control input variable

    % Distance Links -------------------------------------------------%

    for ind = 1 : mr

        i = link_r(ind,1);
        j = link_r(ind,2);

        zeta = squeeze(q(:,i)) - squeeze(q(:,j)); % relative position
        dot_zeta = squeeze(v(:,i)) - squeeze(v(:,j)); % relative
        % velocity

        r = magnitude(zeta); % distance
        s = zeta / r; % direction

        Lr = transpose(s); % true distance Jacobian
        Ls = (1 / r) * (I3 - s * transpose(s)); % true image Jacobian

        dot_r = Lr * dot_zeta; % distance derivative
        dot_s = Ls * dot_zeta; % direction derivative

        % effort from distance-based virtual coupling
        gamma = (gain_r * (r - star_r(ind)) + d_r * dot_r);

        % update the adaptive position variable
        if (transpose(dot_zeta) * dot_zeta > c_Delta)
            % use the correction term
            hat_zeta(:,ind) = squeeze(hat_zeta(:,ind)) + ...
                t_step_control * (dot_zeta + ...
                (gamma / (gain_hat_zeta * r) - ... % transform A
                transpose(dot_zeta) * (squeeze(hat_zeta(:,ind)) - ...
                zeta) / (2 * transpose(dot_zeta) * dot_zeta)) * ...
                dot_zeta);                        % correction term
        else
            % don't use the correction term
            hat_zeta(:,ind) = squeeze(hat_zeta(:,ind)) + ...
                t_step_control * (dot_zeta + ...
                (gamma / (gain_hat_zeta * r)) * ... % transform A
                dot_zeta);
        end

        % implemented Jacobian
        hat_Lr = transpose(squeeze(hat_zeta(:,ind))) / r;
        % control input from the link
```

```
        if adaptive_compensation == 0
            er = transpose(Lr * gamma); % Use true Jacobian
        else
            er = transpose(hat_Lr * gamma); % Use implemented Jacobian
        end

        tau(:,i) = squeeze(tau(:,i)) - er - (d * squeeze(v(:,i)));
        tau(:,j) = squeeze(tau(:,j)) + er - (d * squeeze(v(:,j)));

        % record the distance error
        error_r(ind, data_entry) = (r - star_r(ind));

        total_energy(1, data_entry) = total_energy(1, data_entry) + ...
            0.5 * gain_r * (r - star_r(ind)) * (r - star_r(ind));
        ac_energy(1, data_entry) = ac_energy(1, data_entry) + ...
            0.5 * gain_hat_zeta * ...
            transpose(hat_zeta(:, ind) - zeta) * ...
            (hat_zeta(:, ind) - zeta);
    end

    % Direction Links ------------------------------------------------%

    for ind = 1 : ms

        i = link_s(ind,1);
        j = link_s(ind,2);

        zeta = squeeze(q(:,i)) - squeeze(q(:,j));% relative position
        dot_zeta = squeeze(v(:,i)) - squeeze(v(:,j)); % relative
        % velocity

        r = magnitude(zeta); % distance
        s = zeta / r; % direction

        Lr = transpose(s); % true distance Jacobian
        Ls = (1 / r) * (I3 - s * transpose(s)); % true image Jacobian

        dot_r = Lr * dot_zeta; % distance derivative
        dot_s = Ls * dot_zeta; % direction derivative

        % effort from direction-based virtual coupling
        gamma = (gain_s * (I3 - s * transpose(s)) * ... % projection
            (s - squeeze(star_s(:,ind))) + d_s * dot_s);

        % adaptive distance variable
        hat_r(ind) = squeeze(hat_r(ind)) + t_step_control * ...
            (dot_r - ...
            transpose(gamma) / (gain_hat_r * hat_r(ind)) * dot_s);

        hat_Ls = (1 / hat_r(ind)) * (I3 - s * transpose(s));
        % implemented image
        % Jacobian

        % control input from the link
```

```
            if adaptive_compensation == 0
                es = Ls * gamma; % Use true Jacobian
            else
                es = hat_Ls * gamma; % Use implemented Jacobian
            end

            tau(:,i) = squeeze(tau(:,i)) - es - (d * squeeze(v(:,i)));
            tau(:,j) = squeeze(tau(:,j)) + es - (d * squeeze(v(:,j)));

            % Record the direction error
            error_s(ind, data_entry) = ...
                magnitude(s - squeeze(star_s(:,ind)));

            total_energy(1, data_entry) = total_energy(1, data_entry) + ...
                0.5 * gain_s * transpose(s - squeeze(star_s(:, ind))) * ...
                (s - squeeze(star_s(:, ind)));
            ac_energy(1, data_entry) = ac_energy(1, data_entry) + ...
                0.5 * gain_hat_r * (hat_r(ind) - r) * (hat_r(ind) - r);
        end

        % Vehicles -------------------------------------------------------%

        for ind = 1 : n
            a(:,ind) = squeeze(tau(:,ind)) / mass;
            total_energy(1, data_entry) = total_energy(1, data_entry) + ...
                0.5 * mass * transpose(v(:, ind)) * v(:, ind);
        end

        % Add the energy from the adaptive compension to the total energy
        if adaptive_compensation ~= 0
            total_energy(1, data_entry) = total_energy(1, data_entry) + ...
                ac_energy(1, data_entry);
        end

    end

end

% Data Plots -------------------------------------------------------------%
time = t_step_control * [0 : end_time / t_step_control];

% plot distance errors
figure;
hold off;
plot(time, squeeze(transpose(error_r(1, :))), 'b');
hold on;
plot(time, squeeze(transpose(error_r(2, :))), 'g');
plot(time, squeeze(transpose(error_r(3, :))), 'm');
plot(time, squeeze(transpose(error_r(4, :))), 'c');
legend('Link 2-1', 'Link 2-3', 'Link 2-4', 'Link 2-5');
figure;
hold off;

% plot direction errors
```

```
    plot(time, squeeze(transpose(error_s(1, :))), 'b');
    hold on;
    plot(time, squeeze(transpose(error_s(2, :))), 'g');
    plot(time, squeeze(transpose(error_s(3, :))), 'm');
    plot(time, squeeze(transpose(error_s(4, :))), 'c');
    legend('Link 1-2', 'Link 1-3', 'Link 1-4', 'Link 1-5');
    figure;
    hold off;

    % plot energy
    plot(time, squeeze(transpose(total_energy(1, :))), 'b');
    hold on;
    if adaptive_compensation == 0
        legend('Total Energy');
    else
        plot(time, squeeze(transpose(ac_energy(1, :))), 'r');
        legend('Total Energy', 'Energy in Adaptive Compensators');
    end
    figure;
    hold off;

    % plot positions
    for ind = 1 : n
        if ind == 1
            c = 'b';
            elseif ind == 2
            c = 'r';
            elseif ind == 3
            c = 'g';
            elseif ind == 4
            c = 'm';
            elseif ind == 5
            c = 'c';
        end
        h(1, ind) = plot3(squeeze(q_plot(1,ind,:)), ...
            squeeze(q_plot(2,ind,:)),squeeze(q_plot(3,ind,:)),c);

        hold on;
        h(2, ind) = plot3(squeeze(q_plot(1,ind,1)), ...
            squeeze(q_plot(2,ind,1)),squeeze(q_plot(3,ind,1)),'*k');

        h(3, ind) = plot3(squeeze(q_plot(1,ind, ...
            step_count / t_step_control * t_step_sim + 1)), ...
            squeeze(q_plot(2,ind, ...
            step_count / t_step_control * t_step_sim + 1)), ...
            squeeze(q_plot(3,ind, ...
            step_count / t_step_control * t_step_sim + 1)),'ok');
    end
    legend([h(1, 1), h(1, 2), h(1, 3), h(1, 4), h(1, 5), h(2, 1), h(3, 5)], ...
        {'Vehicle 1', 'Vehicle 2', 'Vehicle 3', 'Vehicle 4', 'Vehicle 5', ...
        'Initial Positions', 'Final Positions'});
end

% compute the magnitude of a vector
```

```
function [mag] = magnitude(vect)
    sumsquared = 0;
    for i = 1 : length(vect)
        sumsquared = sumsquared + vect(i)^2;
    end
    mag = sumsquared^0.5;
end

% generate a random point in a sphere of a given radius
function [rand_noise] = ball_noise(radius)
    x = normrnd(0,1);
    y = normrnd(0,1);
    z = normrnd(0,1);
    u = rand(1);
    rand_noise = radius * nthroot(u, 3) / ...
        sqrt(x * x + y * y + z * z) * [x, y, z];
end
```

Bibliography

Abraham, R.; Marsden, J. E.; and Ratiu, T., 1988. *Manifolds, Tensor Analysis, and Applications*. Springer-Verlag New York Inc., 2nd edn. (cited on page 77)

Absil, P.-A.; Mahony, R.; and Sepulchre, R., 2008. *Optimization Algorithms on Matrix Manifolds*. Princeton University Press. (cited on pages 66, 67, and 93)

Anderson, B. D. O.; Yu, C.; Fidan, B.; and Hendrickx, J. M., 2008. Rigid graph control architectures for autonomous formations. *IEEE Control Systems Magazine*, 28, 6 (December 2008), 48–63. (cited on pages 1, 5, 22, 29, 31, 38, 61, 68, and 69)

Antonelli, G. and Chiaverini, S., 2006. Kinematic control of platoons of autonomous vehicles. *IEEE Trans. on Robotics*, 22, 6 (December 2006), 1285–1292. (cited on pages 1, 18, and 35)

Arcak, M., 2007. Passivity as a design tool for group coordination. *IEEE Trans. on Automatic Control*, 52, 8 (August 2007), 1380–1390. (cited on page 27)

Asimow, L. and Roth, B., 1978. The rigidity of graphs. *Trans. of the American Mathematical Society*, 245 (November 1978), 279 – 289. (cited on pages 32, 45, 61, 62, 66, and 83)

Asimow, L. and Roth, B., 1979. The rigidity of graphs, II. *Journal of Mathematical Analysis and Applications*, 68, 1 (March 1979), 171 – 190. (cited on pages 8, 32, 61, 62, 66, 68, 83, and 130)

Aspnes, J.; Eren, T.; Goldenberg, D. K.; Morse, A. S.; Whiteley, W.; Yang, Y. R.; Anderson, B. D. O.; and Belhumeur, P. N., 2006. A theory of network localization. *IEEE Trans. on Mobile Computing*, 5, 12 (December 2006), 1663–1678. (cited on pages 21, 31, and 61)

Balch, T. and Arkin, R. C., 1998. Behavior-based formation control for multirobot teams. *IEEE Trans. on Robotics and Automation*, 14, 6 (December 1998), 926–939. (cited on pages 4, 18, and 29)

Baldwin, G.; Mahony, R.; and Trumpf, J., 2009. A nonlinear observer for 6 DOF pose estimation from inertial and bearing measurements. In *Proc. IEEE Int. Conf. on Robotics and Automation* (Kobe, Japan, May 2009). (cited on page 26)

Bayezit, İ. and Fidan, B., 2013. Distributed cohesive motion control of flight vehicle formations. *IEEE Trans. on Industrial Electronics*, 60, 12 (December 2013), 5763–5772. (cited on page 25)

Beard, R. W.; Lawton, J.; and Hadaegh, F. Y., 2001. A coordination architecture for spacecraft formation control. *IEEE Trans. on Control Systems Technology*, 9, 6 (November 2001), 777–790. (cited on pages 1 and 29)

Borutzky, W., 2006. Bond graph modelling and simulation of mechatronic systems an introduction into the methodology. In *Proc. European Conf. on Modelling and Simulation* (Bonn, Germany, May 2006). (cited on pages 88, 133, and 134)

Bras, F. L.; Hamel, T.; Mahony, R.; and Samson, C., 2015. Observer design for position and velocity bias estimation from a single direction output. In *Proc. IEEE Conf. on Decision and Control* (Osaka, Japan, December 2015). (cited on pages 26 and 112)

Cao, M.; Yu, C.; and Anderson, B. D. O., 2011. Formation control using range-only measurements. *Automatica*, 47, 4 (April 2011), 776–781. (cited on pages 3, 23, 86, and 116)

Chaumette, F. and Hutchinson, S., 2006. Visual servo control I: Basic approaches. *IEEE Robotics & Automation Magazine*, 13, 4 (December 2006), 82–90. (cited on pages 2, 6, 26, 30, 86, and 91)

Chaumette, F. and Hutchinson, S., 2007. Visual servo control II: Advanced approaches. *IEEE Robotics & Automation Magazine*, 14, 1 (March 2007), 109–118. (cited on pages 2, 6, 26, 30, 86, and 91)

Chen, Y. Q. and Wang, Z., 2005. Formation control: a review and a new consideration. In *Proc. IEEE/RSJ Int. Conf. on Intelligent Robots and Systems* (Edmonton, Alberta, Canada, August 2005). (cited on pages 1 and 85)

Cheviron, T.; Hamel, T.; Mahony, R.; and Baldwin, G., 2007. Robust nonlinear fusion of inertial and visual data for position, velocity and attitude estimation of UAV. In *Proc. IEEE Int. Conf. on Robotics and Automation* (Roma, Italy, April 2007). (cited on page 26)

Comport, A. I.; Mahony, R.; and Spindler, F., 2011. A visual servoing model for generalised cameras: Case study of non-overlapping cameras. In *Proc. IEEE Int. Conf. on Robotics and Automation* (Shanghai, China, May 2011). (cited on page 27)

Connelly, R., 2005. Generic global rigidity. *Discrete & Computational Geometry*, 33, 4 (April 2005), 549–563. (cited on page 32)

Consolini, L.; Morbidi, F.; Prattichizzo, D.; and Tosques, M., 2008. Leader-follower formation control of nonholonomic mobile robots with input constraints. *Automatica*, 44, 5 (May 2008), 1343–1349. (cited on pages 2 and 17)

Corke, P. and Mahony, R., 2009. Sensing and control on the sphere. In *Proc. 14th Int. Symposium of Robotics Research* (Lucerne, Switzerland, September 2009). (cited on page 91)

Corke, P. I. and Hutchinson, S. A., 2001. A new partitioned approach to image-based visual servo control. *IEEE Trans. on Robotics and Automation*, 17, 4 (August 2001), 507–515. (cited on page 27)

Cortés, J., 2009. Global and robust formation-shape stabilization of relative sensing networks. *Automatica*, 45, 12 (December 2009), 2754–2762. (cited on page 21)

Crassidis, J. L.; Markley, F. L.; and Cheng, Y., 2007. Survey of nonlinear attitude estimation methods. *Journal of Guidance, Control, and Dynamics*, 30, 1 (January 2007), 12–28. (cited on page 26)

Cui, R.; Ge, S. S.; How, B. V. E.; and Choo, Y. S., 2010. Leader-follower formation control of underactuated autonomous underwater vehicles. *Ocean Engineering*, 37, 17-18 (December 2010), 1491–1502. (cited on page 17)

Das, A. K.; Fierro, R.; Kumar, V.; Ostrowski, J. P.; Spletzer, J.; and Taylor, C. J., 2002. A vision-based formation control framework. *IEEE Trans. on Robotics and Automation*, 18, 5 (October 2002), 813–825. (cited on pages 1, 2, 3, 4, 16, and 29)

Desai, J. P., 2002. A graph theoretic approach for modeling mobile robot team formations. *Journal of Robotic Systems (now called: Journal of Field Robotics)*, 19, 11 (November 2002), 511–525. (cited on page 24)

Dimarogonas, D. V. and Johansson, K. H., 2008. On the stability of distance-based formation control. In *Proc. IEEE Conf. on Decision and Control* (Cancun, Mexico, December 2008). (cited on page 21)

Dörfler, F. and Francis, B., 2009. Formation control of autonomous robots based on cooperative behavior. In *Proc. European Control Conference* (Budapest, Hungary, August 2009). (cited on pages 5, 22, 62, 79, and 80)

Dörfler, F. and Francis, B., 2010. Geometric analysis of the formation problem for autonomous robots. *IEEE Trans. on Automatic Control*, 55, 10 (October 2010), 2379–2384. (cited on pages 5, 8, 23, and 62)

Duindam, V.; Macchelli, A.; Stramigioli, S.; and Bruyninckx, H., 2009. *Modeling and Control of Complex Physical Systems: The Port-Hamiltonian Approach*. Springer Science & Business Media. (cited on pages 28, 93, 103, and 131)

Duistermaat, J. J. and Kolk, J. A. C., 2000. *Lie Groups*. Springer-Verlag Berlin Heidelberg. (cited on page 83)

Eren, T., 2011. Cooperative localization in wireless ad hoc and sensor networks using hybrid distance and bearing (angle of arrival) measurements. *EURASIP Journal on Wireless Communications and Networking*, 2011, 72 (August 2011). (cited on pages 21, 32, 76, and 83)

Eren, T., 2012. Formation shape control based on bearing rigidity. *Int. Journal of Control*, 85, 9 (September 2012), 1361 – 1379. (cited on pages 23, 24, and 25)

Eren, T.; Belhumeur, P. N.; Anderson, B. D. O.; and Morse, A. S., 2002. A framework for maintaining formations based on rigidity. In *Proc. IFAC World Congress* (Barcelona, Spain, July 2002). (cited on page 22)

Fink, J.; Michael, N.; Kim, S.; and Kumar, V., 2011. Planning and control for cooperative manipulation and transportation with aerial robots. *Int. Journal of Robotics Research*, 30, 3 (March 2011), 324–334. (cited on page 1)

Franchi, A.; Masone, C.; Grabe, V.; Ryll, M.; Bülthoff, H. H.; and Robuffo Giordano, P., 2012a. Modeling and control of UAV bearing formations with bilateral high-level steering. *Int. Journal of Robotics Research*, 31, 12 (November 2012), 1504–1525. (cited on pages 3, 5, 9, 23, 24, 30, 32, 86, and 116)

Franchi, A.; Secchi, C.; Son, H. I.; Bülthoff, H. H.; and Robuffo Giordano, P., 2012b. Bilateral teleoperation of groups of mobile robots with time-varying topology. *IEEE Trans. on Robotics*, 28, 5 (October 2012), 1019–1033. (cited on pages 2, 3, 6, 9, 28, 30, 85, 89, 117, 120, and 131)

Fujimoto, K.; Sakurama, K.; and Sugie, T., 2003. Trajectory tracking control of port-controlled Hamiltonian systems via generalized canonical transformations. *Automatica*, 39, 12 (December 2003), 2059–2069. (cited on page 29)

Fujimoto, K. and Sugie, T., 2001. Canonical transformation and stabilization of generalized Hamiltonian systems. *Systems & Control Letters*, 42, 3 (March 2001), 217–227. (cited on pages 29 and 132)

Fujita, M.; Kawai, H.; and Spong, M. W., 2007. Passivity-based dynamic visual feedback control for three-dimensional target tracking: Stability and L_2-gain performance analysis. *IEEE Trans. on Control Systems Technology*, 15, 1 (January 2007), 40–52. (cited on pages 6, 27, 30, and 86)

Godsil, C. and Royle, G., 2001. *Algebraic Graph Theory*. Springer-Verlag New York, Inc. (cited on pages 21 and 129)

Goldstein, H., 1980. *Classical Mechanics*. Addison-Wesley Publishing Company, 2nd edn. (cited on page 88)

Gortler, S. J.; Gotsman, C.; Liu, L.; and Thurston, D. P., 2013. On affine rigidity. *Journal of Computational Geometry*, 4, 1 (2013), 160–181. (cited on pages 21 and 32)

Hall, B. C., 2003. *Lie Groups, Lie Algebras, and Representations: An Elementary Introduction*. Springer-Verlag New York, Inc. (cited on pages 123 and 124)

Hatanaka, T.; Igarashi, Y.; Fujita, M.; and Spong, M. W., 2012. Passivity-based pose synchronization in the three dimensions. *IEEE Trans. on Automatic Control*, 57, 2 (February 2012), 360–375. (cited on pages 2, 3, 28, and 85)

Hendrickson, B., 1992. Conditions for unique graph realizations. *SIAM Journal on Computing*, 21, 1 (February 1992), 65–84. (cited on page 64)

Hendrickx, J. M.; Anderson, B. D. O.; Delvenne, J.-C.; and Blondel, V. D., 2007. Directed graphs for the analysis of rigidity and persistence in autonomous agent systems. *Int. Journal of Robust and Nonlinear Control*, 17, 10-11 (July 2007), 960–981. (cited on pages 5, 24, and 35)

Hong, Y.; Chen, G.; and Bushnell, L., 2008. Distributed observers design for leader-following control of multi-agent networks. *Automatica*, 44, 3 (March 2008), 846–850. (cited on page 17)

Horn, R. A. and Johnson, C. R., 1990. *Matrix Analysis*. Cambridge University Press. (cited on page 111)

Horn, R. A. and Johnson, C. R., 1991. *Topics in Matrix Analysis*. Cambridge University Press. (cited on pages 73 and 74)

Hua, M.-D.; Hamel, T.; Morin, P.; and Samson, C., 2013. Introduction to feedback control of underactuated VTOL vehicles. *IEEE Control Systems Magazine*, 33, 1 (February 2013), 61–75. (cited on page 89)

Hutchinson, S.; Hager, G.; and Corke, P., 1996. A tutorial on visual servo control. *IEEE Trans. on Robotics and Automation*, 12, 5 (October 1996), 651–670. (cited on pages 2, 6, 26, 30, 86, and 91)

Ihle, I.-A. F.; Arcak, M.; and Fossen, T. I., 2006. Passivity-based designs for synchronized path following. In *Proc. IEEE Conf. on Decision and Control* (San Diego, CA, USA, December 2006). (cited on page 27)

Jackson, B., 2007. Notes on the rigidity of graphs. In *Levico Conference Notes*. (cited on pages 31, 39, 44, 45, 69, 129, and 130)

Ji, M. and Egerstedt, M., 2007. Distributed coordination control of multiagent systems while preserving connectedness. *IEEE Trans. on Robotics*, 23, 4 (August 2007), 693–703. (cited on pages 3 and 21)

Johnson, E. N.; Calise, A. J.; Sattigeri, R.; Watanabe, Y.; and Madyastha, V., 2004. Approaches to vision-based formation control. In *Proc. IEEE Conf. on Decision and Control* (Atlantis, Paradise Island, Bahamas, December 2004). (cited on pages 16, 86, and 101)

Juan, S. H. and Tur, J. M. M., 2008. Tensegrity frameworks: Static analysis review. *Mechanism and Machine Theory*, 43, 7 (July 2008), 859–881. (cited on pages 20 and 31)

Khalil, H. K., 2002. *Nonlinear Systems*. Prentice Hall, 3rd edn. (cited on pages 77, 96, 111, and 132)

Krick, L.; Broucke, M. E.; and Francis, B. A., 2009. Stabilization of infinitesimally rigid formations of multi-robot networks. *Int. Journal of Control*, 82, 3 (March 2009), 423 – 429. (cited on pages 1, 5, 8, 22, 31, 39, 45, 61, 62, 65, 66, 79, 80, and 97)

LAMAN, G., 1970. On graphs and rigidity of plane skeletal structures. *Journal of Engineering Mathematics*, 4, 4 (October 1970), 331–340. (cited on pages 22 and 32)

LAWTON, J. R. T.; BEARD, R. W.; AND YOUNG, B. J., 2003. A decentralized approach to formation maneuvers. *IEEE Trans. on Robotics and Automation*, 19, 6 (December 2003), 933–941. (cited on pages 18 and 82)

LEE, J. M., 2013. *Introduction to Smooth Manifolds*. Springer Science+Business Media New York, 2nd edn. (cited on page 34)

LEONARD, N. E. AND FIORELLI, E., 2001. Virtual leaders, artificial potentials and coordinated control of groups. In *Proc. IEEE Conf. on Decision and Control* (Orlando, Florida, USA, December 2001). (cited on pages 6, 17, 27, 29, 85, and 86)

LEWIS, M. A. AND TAN, K.-H., 1997. High precision formation control of mobile robots using virtual structures. *Autonomous Robots*, 4, 4 (October 1997), 387–403. (cited on pages 4, 17, and 29)

LI, N. H. M. AND LIU, H. H. T., 2008. Formation UAV flight control using virtual structure and motion synchronization. In *Proc. American Control Conf.* (Seattle, Washington, USA, June 2008). (cited on page 17)

LI, Z.; DUAN, Z.; CHEN, G.; AND HUANG, L., 2010. Consensus of multiagent systems and synchronization of complex networks: A unified viewpoint. *IEEE Trans. on Circuits and Systems*, 57, 1 (January 2010), 213–224. (cited on page 19)

LIU, B.; CHU, T.; WANG, L.; AND XIE, G., 2008. Controllability of a leader-follower dynamic network with switching topology. *IEEE Trans. on Automatic Control*, 53, 4 (May 2008), 1009–1013. (cited on page 17)

MAHONY, R.; HAMEL, T.; AND PFLIMLIN, J.-M., 2008. Nonlinear complementary filters on the special orthogonal group. *IEEE Trans. on Automatic Control*, 53, 5 (June 2008), 1203–1218. (cited on pages 26 and 89)

MAHONY, R. E. AND STRAMIGIOLI, S., 2012. A port-Hamiltonian approach to image-based visual servo control for dynamic systems. *Int. Journal of Robotic Research*, 31, 11 (September 2012), 1303–1319. (cited on pages 6, 27, 30, and 86)

MAO, G.; FIDAN, B.; AND ANDERSON, B. D. O., 2007. Wireless sensor network localization techniques. *Computer Networks*, 51, 10 (July 2007), 2529–2553. (cited on pages 21, 76, and 83)

MASTELLONE, S.; STIPANOVIC, D. M.; GRAUNKE, C. R.; INTLEKOFER, K. A.; AND SPONG, M. W., 2008. Formation control and collision avoidance for multi-agent non-holonomic systems: Theory and experiments. *Int. Journal of Robotics Research*, 27, 1 (January 2008), 107–126. (cited on page 85)

Michael, N.; Fink, J.; and Kumar, V., 2011. Cooperative manipulation and transportation with aerial robots. *Autonomous Robots*, 30, 1 (January 2011), 73–86. (cited on page 1)

Monteiro, S. and Bicho, E., 2010. Attractor dynamics approach to formation control: Theory and application. *Autonomous Robots*, 29, 3-4 (November 2010), 331–355. (cited on page 18)

Murray, R. M.; Åström, K. J.; Boyd, S. P.; Brockett, R. W.; and Stein, G., 2003. Future directions in control in an information-rich world. *IEEE Control Systems Magazine*, 23, 2 (April 2003), 20–33. (cited on page 29)

Nair, S. and Leonard, N. E., 2007. Stable synchronization of rigid body networks. *Networks and Heterogeneous Media*, 2, 4 (December 2007), 595–624. (cited on page 28)

Ögren, P.; Fiorelli, E.; and Leonard, N. E., 2004. Cooperative control of mobile sensor networks: Adaptive gradient climbing in a distributed environment. *IEEE Trans. on Automatic Control*, 49, 8 (August 2004), 1292–1302. (cited on pages 1 and 27)

Oh, K.-K. and Ahn, H.-S., 2011. Formation control of mobile agents based on inter-agent distance dynamics. *Automatica*, 47, 10 (October 2011), 2306–2312. (cited on pages 5, 22, and 61)

Oh, K.-K.; Park, M.-C.; and Ahn, H.-S., 2015. A survey of multi-agent formation control. *Automatica*, 53 (March 2015), 424–440. (cited on pages 1 and 85)

Olfati-Saber, R., 2006. Flocking for multi-agent dynamic systems: Algorithms and theory. *IEEE Trans. on Automatic Control*, 51, 3 (March 2006), 401–420. (cited on pages 2, 3, 20, 33, 37, and 47)

Olfati-Saber, R.; Fax, J. A.; and Murray, R. M., 2007. Consensus and cooperation in networked multi-agent systems. *Proceedings of the IEEE*, 95, 1 (January 2007), 215–233. (cited on pages 4, 19, 21, and 29)

Olfati-Saber, R. and Murray, R. M., 2002a. Distributed cooperative control of multiple vehicle formations using structural potential functions. In *Proc. IFAC World Congress* (Barcelona, Spain, July 2002). (cited on page 27)

Olfati-Saber, R. and Murray, R. M., 2002b. Distributed structural stabilization and tracking for formations of dynamic multi-agents. In *Proc. IEEE Conf. on Decision and Control* (Las Vegas, Navada, USA, December 2002). (cited on page 22)

Olfati-Saber, R. and Murray, R. M., 2002c. Graph rigidity and distributed formation stabilization of multi-vehicle systems. In *Proc. IEEE Conf. on Decision and Control* (Las Vegas, Navada, USA, December 2002). (cited on pages 22 and 31)

Patwari, N.; Ash, J. N.; Kyperountas, S.; III, A. O. H.; Moses, R. L.; and Correal, N. S., 2005. Locating the nodes: Cooperative localization in wireless sensor networks. *IEEE Signal Processing Magazine*, 22, 4 (July 2005), 54–69. (cited on page 21)

Porfiri, M.; Roberson, D. G.; and Stilwell, D. J., 2007. Tracking and formation control of multiple autonomous agents: A two-level consensus approach. *Automatica*, 43, 8 (August 2007), 1318–1328. (cited on pages 3 and 19)

Rehbinder, H. and Ghosh, B. K., 2003. Pose estimation using line-based dynamic vision and inertial sensors. *IEEE Trans. on Automatic Control*, 48, 2 (February 2003), 186–199. (cited on page 2)

Ren, W. and Beard, R. W., 2004a. Decentralized scheme for spacecraft formation flying via the virtual structure approach. *Journal of Guidance, Control and Dynamics*, 27, 1 (January-February 2004), 73–82. (cited on pages 4, 17, and 85)

Ren, W. and Beard, R. W., 2004b. Formation feedback control for multiple spacecraft via virtual structures. *IEE Proc.-Control Theory and Applications*, 151, 3 (May 2004), 357–368. (cited on page 17)

Ren, W.; Beard, R. W.; and Atkins, E. M., 2007. Information consensus in multivehicle cooperative control. *IEEE Control Systems Magazine*, (April 2007), 71–82. (cited on pages 4, 19, 21, and 29)

Reynolds, C. W., 1987. Flocks, herds and schools: a distributed behavioral model. *Computer Graphics*, 21, 4 (July 1987), 25–34. (cited on pages 3, 15, and 33)

Sarlette, A.; Bonnabel, S.; and Sepulchre, R., 2010. Coordinated motion design on Lie groups. *IEEE Trans. on Automatic Control*, 55, 5 (May 2010), 1047–1058. (cited on pages 2, 3, and 19)

Sarlette, A.; Sepulchre, R.; and Leonard, N. E., 2007. Autonomous rigid body attitude synchronization. In *Proc. IEEE Conf. on Decision and Control* (New Orleans, LA, USA, December 2007). (cited on page 28)

Sarlette, A.; Sepulchre, R.; and Leonard, N. E., 2009. Autonomous rigid body attitude synchronization. *Automatica*, 45, 2 (February 2009), 572–577. (cited on page 28)

Schreck, P. and Mathis, P., 2006. Geometrical constraint system decomposition: A multi-group approach. *Int. Journal of Computational Geometry & Applications*, 16, 5-6 (December 2006), 431–442. (cited on pages 20 and 32)

Secchi, C.; Franchi, A.; Bülthoff, H. H.; and Robuffo Giordano, P., 2012. Bilateral teleoperation of a group of UAVs with communication delays and switching topology. In *Proc. IEEE Int. Conf. on Robotocis and Automation* (St. Paul, MN, USA, May 2012). (cited on pages 4 and 28)

SERVATIUS, B. AND WHITELEY, W., 1999. Constraining plane configurations in computer-aided design: Combinatorics of directions and lengths. *SIAM Journal on Discrete Mathematics*, 12, 1 (1999), 136–153. (cited on page 20)

SINGH, T. B., 2013. *Elements of Topology*. Taylor and Francis Group, LLC. (cited on pages 32, 34, 41, 50, 51, 54, 55, 123, and 124)

STACEY, G. AND MAHONY, R., 2013. A port-Hamiltonian approach to formation control using bearing measurements and range observers. In *Proc. IEEE Conf. on Decision and Control* (Florence, Italy, December 2013). (cited on page 85)

STACEY, G. AND MAHONY, R., 2016. A passivity-based approach to formation control using partial measurements of relative position. *IEEE Trans. on Automatic Control*, 61, 2 (February 2016), 538–543. (cited on pages 6, 61, and 85)

STACEY, G.; MAHONY, R.; AND CORKE, P., 2013. A bondgraph approach to formation control using relative state measurements. In *Proc. European Control Conf.* (Zürich, Switzerland, July 2013). (cited on page 85)

STACEY, G.; MAHONY, R.; AND TRUMPF, J., 2016. Generalised rigidity and path-rigidity for agent formations. In *Proc. Int. Symposium on Mathematical Theory of Networks and Systems* (Minneapolis, Minnesota, USA, July 2016). (cited on page 31)

STRAMIGIOLI, S. AND DUINDAM, V., 2001. Variable spatial springs for robot control applications. In *Proc. IEEE/RSJ Int. Conf. on Intelligent Robots and Systems* (Maui, Hawaii, USA, October-November 2001). (cited on pages 29 and 117)

SU, H.; WANG, X.; AND LIN, Z., 2009. Flocking of multi-agents with a virtual leader. *IEEE Trans. on Automatic Control*, 54, 2 (February 2009), 293–307. (cited on page 20)

SUMMERS, T. H.; YU, C.; DASGUPTA, S.; AND ANDERSON, B. D. O., 2011. Control of minimally persistent leader-remote-follower and coleader formations in the plane. *IEEE Trans. on Automatic Control*, 56, 12 (December 2011), 2778–2792. (cited on page 25)

SUN, Z. AND ANDERSON, B. D. O., 2015. Rigid formation control systems modelled by double integrators: System dynamics and convergence analysis. In *Proc. Australian Control Conference* (Gold Coast, Australia, November 2015). (cited on pages 5, 23, and 120)

SUN, Z.; MOU, S.; ANDERSON, B. D. O.; AND CAO, M., 2016. Exponential stability for formation control systems with generalized controllers: A unified approach. *Systems & Control Letters*, 93 (July 2016), 50–57. (cited on pages 5, 8, 22, 62, and 80)

TANNER, H. G.; PAPPAS, G. J.; AND KUMAR, V., 2004. Leader-to-formation stability. *IEEE Trans. on Robotics and Automation*, 20, 3 (June 2004), 443–455. (cited on pages 4 and 16)

Thorpe, M. F. and Duxbury, P. M., 1999. *Rigidity Theory and Applications*. Kluwer Academic/Plenum Publishers, New York. (cited on pages 20 and 31)

Turpin, M.; Michael, N.; and Kumar, V., 2012. Decentralized formation control with variable shapes for aerial robots. In *Proc. IEEE Int. Conf. on Robotocs and Automation* (St. Paul, MN, USA, May 2012). (cited on page 85)

van der Schaft, A. J. and Maschke, B. M., 2013. Port-Hamiltonian systems on graphs. *SIAM Journal on Control and Optimization*, 51, 2 (March 2013), 906–927. (cited on pages 6, 29, and 85)

Vasconcelos, J. F.; Cunha, R.; Silvestre, C.; and Oliveira, P., 2010. A nonlinear position and attitude observer on SE(3) using landmark measurements. *Systems and Control Letters*, 59, 3-4 (March-April 2010), 155–166. (cited on pages 26 and 29)

Vidal, R.; Shakernia, O.; and Sastry, S., 2003. Formation control of nonholonomic mobile robots with omnidirectional visual servoing and motion segmentation. In *Proc. IEEE. Int. Conf. on Robotics and Automation* (Taipei, Taiwan, September 2003). (cited on page 16)

Vos, E.; Scherpen, J. M. A.; and van der Schaft, A. J., 2014. Equal distribution of satellite constellations on circular target orbits. *Automatica*, 50, 10 (October 2014), 2641–2647. (cited on pages 1 and 29)

Vos, E.; van der Schaft, A. J.; and Scherpen, J. M. A., 2016. Formation control and velocity tracking for a group of nonholonomic wheeled robots. *IEEE Trans. on Automatic Control*, 61, 9 (September 2016), 2702–2707. (cited on pages 2, 6, 29, 85, 86, and 131)

Wang, J. and Xin, M., 2013. Integrated optimal formation control of multiple unmanned aerial vehicles. *IEEE Trans. on Control Systems Technology*, 21, 5 (September 2013), 1731–1744. (cited on page 18)

Wang, Y.; Yan, W.; and Li, J., 2012. Passivity-based formation control of autonomous underwater vehicles. *IET Control Theory and Applications*, 6, 4 (March 2012), 518–525. (cited on page 28)

Yu, C.; Anderson, B. D. O.; Dasgupta, S.; and Fidan, B., 2009. Control of minimally persistent formations in the plane. *SIAM Journal on Control and Optimization*, 48, 1 (February 2009), 206–233. (cited on page 25)

Yu, C.; Hendrickx, J. M.; Fidan, B.; Anderson, B. D. O.; and Blondel, V. D., 2007. Three and higher dimensional autonomous formations: Rigidity, persistence and structural persistence. *Automatica*, 43, 3 (March 2007), 387–402. (cited on pages 5, 24, and 35)

Zelazo, D.; Franchi, A.; Allgöwer, F.; Bülthoff, H. H.; and Robuffo Giordano, P., 2012. Rigidity maintenance control for multi-robot systems. In *Robotics: Science and Systems Conf.* (Sydney, Australia, July 2012). (cited on page 23)

Zelazo, D.; Franchi, A.; Bülthoff, H. H.; and Robuffo Giordano, P., 2015. Decentralized rigidity maintenance control with range measurements for multi-robot systems. *Int. Journal of Robotics Research*, 34, 1 (January 2015), 105–128. (cited on pages 3, 5, 9, 23, 30, 39, 61, 64, 69, and 86)

Zelazo, D.; Franchi, A.; and Robuffo Giordano, P., 2014. Rigidity theory in $SE(2)$ for unscaled relative position estimation using only bearing measurements. In *Proc. European Control Conf.* (Strasbourg, France, June 2014). (cited on pages 5, 21, 32, and 62)

Zhao, S. and Zelazo, D., 2016. Bearing rigidity and almost global bearing-only formation stabilization. *IEEE Trans. on Automatic Control*, 61, 5 (May 2016), 1255–1268. (cited on pages 3, 5, 24, 32, and 86)